

VOL. 673 NO. 2 JULY 8, 1994

THIS ISSUE COMPLETES VOL. 673

JOURNAL OF

CHROMATOGRAPHY A

INCLUDING ELECTROPHORESIS AND OTHER SEPARATION METHODS

EDITORS

U.A.Th. Brinkman (Amsterdam)

R.W. Giese (Boston, MA)

J.K. Haken (Kensington, N.S.W.)

L.R. Snyder (Orinda, CA)

EDITORS, SYMPOSIUM VOLUMES,

E. Heftmann (Orinda, CA), Z. Deyl (Prague)

EDITORIAL BOARD

D.W. Armstrong (Rolla, MO)

W.A. Aue (Halifax)

P. Boček (Brno)

A.A. Boulton (Saskatoon)

P.W. Carr (Minneapolis, MN)

N.H.C. Cooke (San Ramon, CA)

V.A. Davankov (Moscow)

G.J. de Jong (Weesp)

Z. Deyl (Prague)

S. Dilli (Kensington, N.S.W.)

Z. El Rassi (Stillwater, OK)

H. Engelhardt (Saarbrücken)

F. Erni (Basle)

M.B. Evans (Hatfield)

J.L. Glajch (N. Billerica, MA)

G.A. Guiochon (Knoxville, TN)

P.R. Haddad (Hobart, Tasmania)

I.M. Hais (Hradec Králové)

W.S. Hancock (Palo Alto, CA)

S. Hjertén (Uppsala)

S. Honda (Higashi-Osaka)

Cs. Horváth (New Haven, CT)

J.F.K. Huber (Vienna)

K.-P. Hupe (Waldbronn)

J. Janák (Brno)

P. Jandera (Pardubice)

B.L. Karger (Boston, MA)

J.J. Kirkland (Newport, DE)

E. sz. Kováts (Lausanne)

K. Macek (Prague)

A.J.P. Martin (Cambridge)

L.W. McLaughlin (Chestnut Hill, MA)

E.D. Morgan (Keele)

J.D. Pearson (Kalamazoo, MI)

H. Poppe (Amsterdam)

F.E. Regnier (West Lafayette, IN)

P.G. Righetti (Milan)

P. Schoenmakers (Amsterdam)

R. Schwarzenbach (Dübendorf)

R.E. Shoup (West Lafayette, IN)

R.P. Singhal (Wichita, KS)

A.M. Siouffi (Marseille)

D.J. Strydom (Boston, MA)

N. Tanaka (Kyoto)

S. Terabe (Hyogo)

K.K. Unger (Mainz)

R. Verpoorte (Leiden)

Gy. Vigh (College Station, TX)

J.T. Watson (East Lansing, MI)

B.D. Westerlund (Uppsala)

EDITORS, BIBLIOGRAPHY SECTION

Z. Deyl (Prague), J. Janák (Brno), V. Schwarz (Prague)

ELSEVIER

JOURNAL OF CHROMATOGRAPHY A

INCLUDING ELECTROPHORESIS AND OTHER SEPARATION METHODS

Scope. The *Journal of Chromatography A* publishes papers on all aspects of **chromatography, electrophoresis** and related methods. Contributions consist mainly of research papers dealing with chromatographic theory, instrumental developments and their applications. In the *Symposium volumes*, which are under separate editorship, proceedings of symposia on chromatography, electrophoresis and related methods are published. *Journal of Chromatography B: Biomedical Applications*—This journal, which is under separate editorship, deals with the following aspects: developments in and applications of chromatographic and electrophoretic techniques related to clinical diagnosis or alterations during medical treatment; screening and profiling of body fluids or tissues related to the analysis of active substances and to metabolic disorders; drug level monitoring and pharmacokinetic studies; clinical toxicology; forensic medicine; veterinary medicine; occupational medicine; results from basic medical research with direct consequences in clinical practice.

Submission of Papers. The preferred medium of submission is on disk with accompanying manuscript (see *Electronic manuscripts* in the Instructions to Authors, which can be obtained from the publisher, Elsevier Science B.V., P.O. Box 330, 1000 AH Amsterdam, Netherlands). Manuscripts (in English; *four* copies are required) should be submitted to: Editorial Office of *Journal of Chromatography A*, P.O. Box 681, 1000 AR Amsterdam, Netherlands, Telefax (+31-20) 5862 304, or to: The Editor of *Journal of Chromatography B: Biomedical Applications*, P.O. Box 681, 1000 AR Amsterdam, Netherlands. Review articles are invited or proposed in writing to the Editors who welcome suggestions for subjects. An outline of the proposed review should first be forwarded to the Editors for preliminary discussion prior to preparation. Submission of an article is understood to imply that the article is original and unpublished and is not being considered for publication elsewhere. For copyright regulations, see below.

Publication information. *Journal of Chromatography A* (ISSN 0021-9673): for 1994 Vols. 652–682 are scheduled for publication. *Journal of Chromatography B: Biomedical Applications* (ISSN 0378-4347): for 1994 Vols. 652–662 are scheduled for publication. Subscription prices for *Journal of Chromatography A*, *Journal of Chromatography B: Biomedical Applications* or a combined subscription are available upon request from the publisher. Subscriptions are accepted on a prepaid basis only and are entered on a calendar year basis. Issues are sent by surface mail except to the following countries where air delivery via SAL is ensured: Argentina, Australia, Brazil, Canada, China, Hong Kong, India, Israel, Japan, Malaysia, Mexico, New Zealand, Pakistan, Singapore, South Africa, South Korea, Taiwan, Thailand, USA. For all other countries airmail rates are available upon request. Claims for missing issues must be made within six months of our publication (mailing) date. Please address all your requests regarding orders and subscription queries to: Elsevier Science B.V., Journal Department, P.O. Box 211, 1000 AE Amsterdam, Netherlands. Tel.: (+31-20) 5803 642; Fax: (+31-20) 5803 598. Customers in the USA and Canada wishing information on this and other Elsevier journals, please contact Journal Information Center, Elsevier Science Inc., 655 Avenue of the Americas, New York, NY 10010, USA, Tel. (+1-212) 633 3750, Telefax (+1-212) 633 3764.

Abstracts/Contents Lists published in Analytical Abstracts, Biochemical Abstracts, Biological Abstracts, Chemical Abstracts, Chemical Titles, Chromatography Abstracts, Current Awareness in Biological Sciences (CABS), Current Contents/Life Sciences, Current Contents/Physical, Chemical & Earth Sciences, Deep-Sea Research: Part B: Oceanographic Literature Review, Excerpta Medica, Index Medicus, Mass Spectrometry Bulletin, PASCAL-CNRS, Referativnyi Zhurnal, Research Alert and Science Citation Index.

US Mailing Notice. *Journal of Chromatography A* (ISSN 0021-9673) is published weekly (total 52 issues) by Elsevier Science B.V., (Sara Burgerhartstraat 25, P.O. Box 211, 1000 AE Amsterdam, Netherlands). Annual subscription price in the USA US\$ 4994.00 (US\$ price valid in North, Central and South America only) including air speed delivery. Second class postage paid at Jamaica, NY 11431. **USA POSTMASTERS:** Send address changes to *Journal of Chromatography A*, Publications Expediting, Inc., 200 Meacham Avenue, Elmont, NY 11003. Airfreight and mailing in the USA by Publications Expediting.

See inside back cover for Publication Schedule. Information for Authors and information on Advertisements.

© 1994 ELSEVIER SCIENCE B.V. All rights reserved.

0021-9673 94/\$07.00

No part of this publication may be reproduced, stored in a retrieval system or transmitted in any form or by any means, electronic, mechanical, photocopying, recording or otherwise, without the prior written permission of the publisher, Elsevier Science B.V., Copyright and Permissions Department, P.O. Box 521, 1000 AM Amsterdam, Netherlands.

Upon acceptance of an article by the journal, the author(s) will be asked to transfer copyright of the article to the publisher. The transfer will ensure the widest possible dissemination of information.

Special regulations for readers in the USA – This journal has been registered with the Copyright Clearance Center, Inc. Consent is given for copying of articles for personal or internal use, or for the personal use of specific clients. This consent is given on the condition that the copier pays through the Center the per-copy fee stated in the code on the first page of each article for copying beyond that permitted by Sections 107 or 108 of the US Copyright Law. The appropriate fee should be forwarded with a copy of the first page of the article to the Copyright Clearance Center, Inc., 27 Congress Street, Salem, MA 01970, USA. If no code appears in an article, the author has not given broad consent to copy and permission to copy must be obtained directly from the author. The fee indicated on the first page of an article in this issue will apply retroactively to all articles published in the journal, regardless of the year of publication. This consent does not extend to other kinds of copying, such as for general distribution, resale, advertising and promotion purposes, or for creating new collective works. Special written permission must be obtained from the publisher for such copying.

No responsibility is assumed by the Publisher for any injury and/or damage to persons or property as a matter of products liability, negligence or otherwise, or from any use or operation of any methods, products, instructions or ideas contained in the materials herein. Because of rapid advances in the medical sciences, the Publisher recommends that independent verification of diagnoses and drug dosages should be made.

Although all advertising material is expected to conform to ethical (medical) standards, inclusion in this publication does not constitute a guarantee or endorsement of the quality or value of such product or of the claims made of it by its manufacturer.

Ⓢ The paper used in this publication meets the requirements of ANSI NISO Z39.48-1992 (Permanence of Paper).

Printed in the Netherlands

CONTENTS

(Abstracts/Contents Lists published in *Analytical Abstracts*, *Biochemical Abstracts*, *Biological Abstracts*, *Chemical Abstracts*, *Chemical Titles*, *Chromatography Abstracts*, *Current Awareness in Biological Sciences (CABS)*, *Current Contents/Life Sciences*, *Current Contents/Physical, Chemical & Earth Sciences*, *Deep-Sea Research/Part B: Oceanographic Literature Review*, *Excerpta Medica*, *Index Medicus*, *Mass Spectrometry Bulletin*, *PASCAL-CNRS*, *Referativnyi Zhurnal*, *Research Alert* and *Science Citation Index*)

REVIEW

- Purification of lipases, phospholipases and kinases by heparin-Sepharose chromatography
by A.A. Farooqui, H.-C. Yang and L.A. Horrocks (Columbus, OH, USA) (Received March 4th, 1994) 149

REGULAR PAPERS

Column Liquid Chromatography

- Adsorption and separation of proteins on composite anion exchangers with poly(N-diethylaminoethylacrylamide) bonded phases
by A.E. Ivanov and V.P. Zubov (Moscow, Russian Federation) (Received February 23rd, 1994) 159
- Separation of ribonucleotides, ribonucleosides, deoxyribonucleotides, deoxyribonucleosides and bases by reversed-phase high-performance liquid chromatography
by J. Zhao, B. Todd and G.H. Fleet (Kensington, Australia) (Received March 14th, 1994) 167
- Determination of barium and strontium in calcium-containing matrices using high-performance chelation ion chromatography
by P. Jones, M. Foulkes and B. Paull (Plymouth, UK) (Received March 17th, 1994) 173

Gas Chromatography

- Pair-wise interactions by gas chromatography. IV. Interaction free enthalpies of solutes with trifluoromethyl-substituted alkanes
by K.S. Reddy, R. Cloux and E. Kováts (Lausanne, Switzerland) (Received February 28th, 1994) 181
- Matrix effects during standard addition quantitation of a trace volatile impurity in a drug substance sample
by J.J. Sun and D.A. Roston (Skokie, IL, USA) (Received February 14th, 1994) 211

Supercritical Fluid Chromatography

- Large-rim-tethered permethyl-substituted β -cyclodextrin polysiloxanes for use as chiral stationary phases in open tubular column chromatography
by G. Yi, J.S. Bradshaw, B.E. Rossiter, A. Malik, W. Li, H. Yun and M.L. Lee (Provo, UT, USA) (Received February 25th, 1994) 219
- Capillary supercritical fluid chromatography-Fourier transform infrared spectroscopy study of triglycerides and the qualitative analysis of normal and "unsaturated" cheeses
by M. Kaplan, G. Davidson and M. Poliakoff (Nottingham, UK) (Received February 17th, 1994) 231

Electrophoresis

- Correlation between zone velocity and current in automated single capillary isotachopheresis-zone electrophoresis
by N.J. Reinhoud, U.R. Tjaden and J. van der Greef (Leiden, Netherlands) (Received March 8th, 1994) 239
- Automated on-capillary isotachopheretic reaction cell for fluorescence derivatization of small sample volumes at low concentrations followed by capillary zone electrophoresis
by N.J. Reinhoud, U.R. Tjaden and J. van der Greef (Leiden, Netherlands) (Received March 7th, 1994) 255
- Capillary electrophoresis of some tetracycline antibiotics
by S. Croubels and W. Baeyens (Ghent, Belgium), C. Dewaele (Nazareth, Belgium) and C. Van Peteghem (Ghent, Belgium) (Received March 22nd, 1994) 267

(Continued overleaf)

Contents (continued)

Determination of alkali and alkaline earth metals in real samples by capillary ion analysis
by Q. Yang, M. Jimidar, T.P. Hamoir, J. Smeyers-Verbeke and D.L. Massart (Brussels, Belgium) (Received March
8th, 1994) 275

SHORT COMMUNICATIONS

Column Liquid Chromatography

1-Thio- β -D-galactose as a chiral derivatization agent for the resolution of D,L-amino acid enantiomers
by A. Jegorov and J. Tříska (České Budějovice, Czech Republic) and T. Trnka (Prague, Czech Republic) (Received
January 13th, 1994) 286

Simultaneous determination of cobalt and nickel by reversed-phase high-performance liquid chromatography with diethyl-
dithiocarbamic acid
by V. González Rodríguez, J.M. Castro Romero, J.M. Fernández Solís, J. Pérez Iglesias and H.M. Seco Lago
(Ferrol, Spain) (Received February 27th, 1994) 291

Gas Chromatography

Capillary gas chromatography method for the analysis of the *trans* isomers of ceralure, a medfly attractant
by A.B. DeMilo, J.D. Warthen, Jr. and B.A. Leonhardt (Beltsville, MD, USA) (Received April 6th, 1994) 295

Electrophoresis

Capillary electrophoresis coupled on-line with flame photometric detection
by C.E. Sānger-van de Griend and Ch.E. Kientz (Rijswijk, Netherlands) and U.A.Th. Brinkman (Amsterdam,
Netherlands) (Received April 14th, 1994) 299

ERRATUM 303

AUTHOR INDEX 304



ELSEVIER

Journal of Chromatography A, 673 (1994) 149–158

JOURNAL OF
CHROMATOGRAPHY A

Review

Purification of lipases, phospholipases and kinases by heparin-Sepharose chromatography

Akhlaq A. Farooqui*, Hsiu-Chiung Yang, Lloyd A. Horrocks

Department of Medical Biochemistry, Ohio State University, Hamilton Hall, Room 479, 1645 Neil Avenue, Columbus, OH 43210, USA

(First received December 27th, 1993; revised manuscript received March 4th, 1994)

Abstract

Heparin interacts with lipases, phospholipases and kinases. Immobilized heparin can be used for the purification of diacylglycerol and triacylglycerol lipases, phospholipases A₂ and C and protein and lipid kinases. The use of heparin-Sepharose is an important development in analytical and preparative techniques for the separation and isolation of lipases, phospholipases and kinases.

Contents

1. Introduction	149
2. Interactions of heparin with lipases	150
3. Interactions of heparin with phospholipases	151
4. Interactions of heparin with protein and lipid kinases	152
5. Attachment of heparin to solid supports	153
6. Assay of heparin in heparin-Sepharose samples	153
7. Purification of lipases, phospholipases, lysophospholipases and kinases by heparin-Sepharose chromatography	154
7.1. Purification of lipases	154
7.2. Purification of phospholipases A ₂	154
7.3. Purification of phospholipase C	154
7.4. Purification of protein kinase C and casein kinase II	155
7.5. Purification of diacylglycerol kinase and phosphatidylinositol 4-kinase	155
8. Advantages and disadvantages of heparin-Sepharose chromatography	156
9. Conclusions	156
10. Acknowledgement	157
11. References	157

1. Introduction

In recent years heparin-Sepharose chromatog-

raphy has revolutionized the purification of enzymes and macromolecules. This method utilizes the specific and electrostatic interactions of heparin with enzymes, growth factors, receptors and blood coagulation factors [1–3]. The general

* Corresponding author.

scheme of heparin-Sepharose chromatography involves the covalent attachment of heparin to Sepharose. A crude tissue preparation is then applied to the column; only those enzymes and macromolecules that specifically interact with heparin are retained on the column while the other proteins having no affinity for heparin are washed out. The retained enzymes and macromolecules can be eluted from the column either by adding an excess of heparin to the equilibrating buffer or by using substances such as salts or denaturants [2]. Theoretically, the success of heparin-Sepharose chromatography depends largely upon how closely the conditions used in the experiment mimic the native or biological interactions.

Heparin-Sepharose chromatography has been useful for the purification of lipases, phospholipases and kinases [4–13]. These enzymes, along with glycosaminoglycans, play an important role in cell division, cell differentiation and signal transduction [14,15]. The purpose of this review is to discuss the use of heparin-Sepharose for the purification of lipases, phospholipases and kinases. It is hoped that this discussion will promote further studies on the uses of heparin-Sepharose in analytical and preparative biochemistry and will result in the development of procedures for better understanding of heparin-enzyme interactions and evaluation of heparin-enzyme binding constants.

Heparin is a linear, naturally occurring, highly sulfated glycosaminoglycan with anticoagulant and antilepemic properties [16]. It is characterized by the presence of 2-acetamido-2-deoxy- α -D-glucopyranosyl and α -D-glucopyranosyl-uronic acid residues containing various proportions of O-sulfate, N-sulfate and acetyl groups. In the disaccharide repeating units of heparin, glucuronic acid and D-glucosamine are linked by α -1,4-glycosidic linkages [2]. Heparin exists in a wide range of molecular masses (5000–40 000). It is highly charged and appears to occur entirely in mast cells. Heparin has many structural features in common with heparan sulfate except it is more highly sulfated and contains a large proportion of iduronic acid. Because of its unique structure and surface charge distribution,

heparin is able to interact strongly with many enzymes and macromolecules in two ways: a positive, cooperative binding and a specific binding [16,17]. In positive, cooperative binding, heparin binds to a protein at different sites, and the affinity shown at each individual interacting site contributes to the overall affinity of the heparin for its protein ligand. An example of a positive, cooperative interaction is that between heparin and a lipoprotein particle with several apolipoprotein molecules [18,19]. In specific binding of heparin to protein, other glycosaminoglycans cannot substitute for heparin in its binding nor in exerting a biological activity. An example of a specific heparin protein interaction is the binding between heparin and antithrombin III [2].

When a protein is bound to heparin, its biological activity is either enhanced or decreased; when the heparin is then removed, the original activity of the protein is restored. This restorative property plays an important role in the purification of enzymes and growth factors by heparin-Sepharose chromatography, and also in the evaluation of heparin-enzyme equilibrium constants and other quantitative features of protein-heparin reactions. Effects of heparin on lipases, phospholipases and kinases are shown in Table 1.

2. Interactions of heparin with lipases

Two triacylglycerol lipases are released into the bloodstream after intravenous injections of heparin [20]. Lipoprotein lipase, released from extrahepatic tissues, is required for the removal of both chylomicron and very low-density lipoprotein triacylglycerol from plasma. This enzyme is inhibited by sodium chloride and requires a specific apolipoprotein for optimal activity. A second enzyme that is released from the liver is hepatic triacylglycerol lipase. This enzyme differs from lipoprotein lipase in that there is no requirement for an apoprotein cofactor, and 1 M NaCl stimulates rather than inhibits the enzymic activity.

Rat lipoprotein lipase is markedly stimulated

Table 1
Effects of heparin on lipases, phospholipases and lipid and protein kinases

Enzyme	Effect
Diacylglycerol kinase	Inhibition [12]
Phosphatidyl inositol 4-kinase	Inhibition [35]
Protein kinase C	Inhibition [32]
Casein kinase II	Inhibition [30]
Nuclear kinase	Inhibition [67]
β -Adrenergic receptor kinase	Inhibition [34]
Protein kinase A	Inhibition [32]
Myosin II heavy chain kinase A	Activation [31]
Tyrosine protein kinase	Inhibition [32]
Lipoprotein lipase	Inhibition [22]
Triacylglycerol lipase (Plasma)	Activation [43]
Triacylglycerol lipase (Brain)	Inhibition [23]
Diacylglycerol lipase	Inhibition [4]
Lysophospholipase	Inhibition [4]
Monoacylglycerol lipase	No effect [4]
Phospholipase A ₂ (pancreas)	Inhibition [24]
Phospholipase A ₂ (synovial fluid)	No effect [25]
Phospholipase A ₂ (brain, M_r 110 000)	No effect [26]
Phospholipase A ₂ (brain, M_r 39 000)	Inhibition [26]

by heparin, perhaps by binding of the enzyme to chylomicrons. Heparin has no effect on the stability of the enzyme nor on its activity once the enzyme–chylomicron complex is formed. It has been proposed that heparin functions as a specific ligand that acts as an allosteric modifier of lipoprotein lipase and alters the kinetics of substrate–enzyme interactions [21]. In contrast, milk lipoprotein lipase is strongly inhibited by heparin [22].

Hepatic triacylglycerol lipase participates in the clearance of chylomicron remnants and in conversion of high-density lipoprotein subfractions (HDL2 into HDL3). Like lipoprotein lipase, this enzyme is also stimulated by heparin [11]. Mammalian brain triacylglycerol lipase is strongly inhibited by heparin. At 5 μ g/ml, heparin produces 50% inhibition of enzymic activity [23]. Heparin also inhibits bovine brain diacylglycerol lipase in a concentration-dependent manner. It has no effect on monoacylglycerol lipase, whereas lysophospholipase is partially inhibited (Fig. 1). The inhibition of diacylglycerol lipase by heparin is quite specific

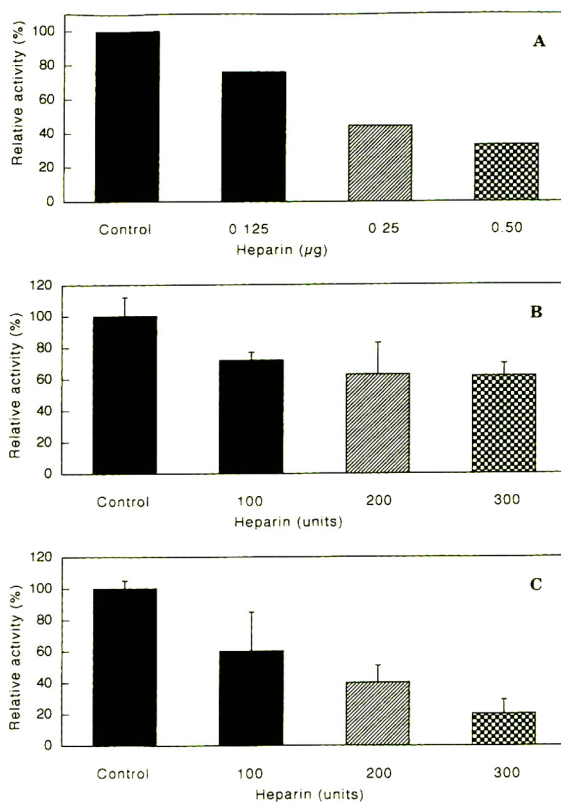


Fig. 1. Effect of heparin on triacylglycerol lipase, lysophospholipase and diacylglycerol lipase. (A) Milk triacylglycerol lipase [22], (B) bovine brain lysophospholipase [4] and (C) bovine brain diacylglycerol lipase [4].

because other glycosaminoglycans do not affect the enzymic activity [4].

3. Interactions of heparin with phospholipases

Heparin markedly inhibits the activity of porcine pancreatic phospholipase A₂ [24]. It has been suggested that interactions of porcine pancreatic phospholipase A₂ are electrostatic, and Ca²⁺, which is required for optimal activity of phospholipases A₂, is not required for heparin binding to pancreatic phospholipase A₂. Based on circular dichroism and fluorescence probe studies, the conformation of the amino-terminus region of pancreatic phospholipase A₂ is important in heparin binding [24]. This region of

pancreatic phospholipase A_2 contains Arg, His and Lys. These amino acids may play an important role in the binding of pancreatic phospholipase A_2 to heparin. Synovial fluid phospholipase A_2 , which resembles pancreatic enzyme in its kinetic properties, also binds to heparin, but its catalytic activity is not affected [25].

Glycosaminoglycans affect the activities of bovine brain cytosolic phospholipases A_2 [26]. Heparin and other glycosaminoglycans markedly inhibit phospholipase A_2 of M_r 39 000, whereas phospholipase A_2 of M_r 110 000 is not affected by heparin or other glycosaminoglycans (Fig. 2). Inhibition of phospholipase A_2 of M_r 39 000 by heparin and other glycosaminoglycans was reversed with protamine sulfate and histone. This suggests that at least some interactions of

heparin with this phospholipase A_2 are electrostatic. Rat liver lysosomal phospholipases A_1 and A_2 are also inhibited by heparin [27]. The mechanism of inhibition of lipases and phospholipases is not known. However, three possibilities should be carefully considered. Heparin may bind directly to the amino-terminus of lipases and phospholipases (which is rich in basic amino acids), blocking the interfacial recognition site by steric hindrance. Another possibility is that the conformation of the interfacial recognition site may be altered by the binding of heparin to another site on the enzymes. Finally, heparin is known to bind phospholipids [28] and may interfere with the interaction between enzyme and substrate.

4. Interactions of heparin with protein and lipid kinases

Protein kinases are classified into several groups. Cyclic nucleotide-dependent kinases are active only with ATP as the phosphate donor and preferentially phosphorylate basic proteins such as histone *in vitro*. Cyclic nucleotide-independent protein kinases utilize GTP as well as ATP as the phosphate donor and prefer acidic proteins such as casein and phosvitin. Heparin is a potent inhibitor of phosvitin and casein kinases but has no effect on histone kinase [29–31]. For casein kinase the nature of inhibition is competitive (inhibitor constant, $K_i = 1.4$ nM). The inhibition is not reversed by ATP. However, in rabbit smooth muscle cells, protein kinases are markedly inhibited by heparin [32]. Dictyostelium myosin II heavy-chain kinase A is stimulated by heparin [31], whereas protein kinase C is strongly inhibited in a dose-dependent manner [32]. The nature of inhibition is non-competitive with respect to ATP ($K_i = 0.2$ μ M). The molecular size of heparin is a critical determinant for inhibition of protein kinase C and other protein kinases [32]. Very-low-molecular-mass fractions of heparin (M_r 600–20 000) have no effect on the activities of protein kinases, but high-molecular-mass heparin (*ca.* 40 000) produces maximal inhibition. Heparin also inhibits formation of

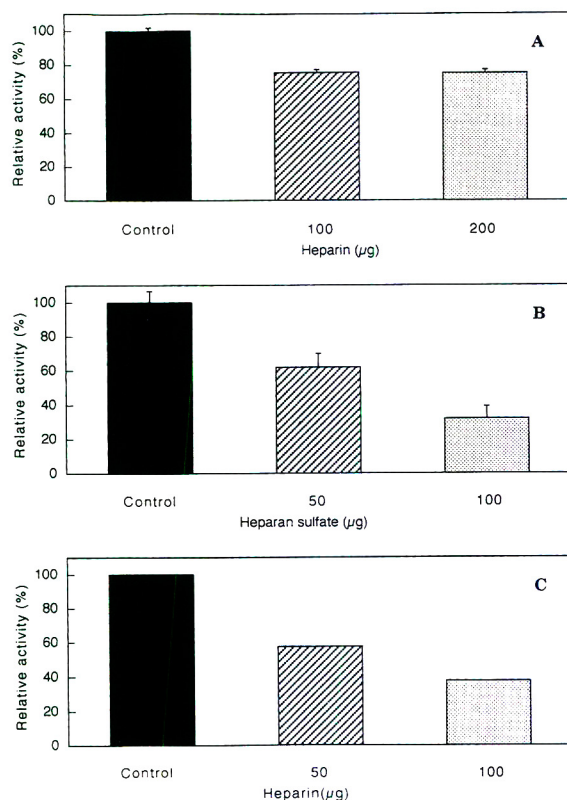


Fig. 2. Effect of heparin and heparan sulfate on phospholipases A_2 . (A) Bovine brain phospholipase A_2 , M_r 39 000 [26], (B) bovine brain phospholipase A_2 , M_r 39 000 [26] and (C) pancreatic phospholipase A_2 [24].

c-fos mRNA in control vascular smooth muscle cells but does not inhibit serum stimulation of c-fos mRNA in protein kinase down-regulated vascular smooth muscle cells. Thus, heparin may selectively inhibit protein kinase C-dependent but not protein kinase C-independent stimulation of gene expression [33].

β -Adrenergic receptor kinase is also inhibited by heparin in a concentration-dependent manner [34]. In this system, heparin is a competitive inhibitor with respect to rhodopsin. Fibroblast growth factor receptor kinase has an essential heparin-binding domain that markedly affects its kinase activity [3]. One of the early cellular events induced by the binding of growth factors to their respective receptors is the stimulation of phospholipases A₂ and C. These enzymes hydrolyze membrane phospholipids and generate second messengers, arachidonate, eicosanoids, diacylglycerol and inositol 1,4,5-trisphosphate [14,15]. The messengers are required for normal cell function.

Lipid kinases (phosphatidylinositol 4-phosphate kinase and diacylglycerol kinases) are also inhibited by heparin in a dose-dependent manner [12,35,36]. The effects of heparin on these enzymes may be involved in the mechanism of oncogene-induced cell transformation.

5. Attachment of heparin to solid supports

The ideal matrix for the attachment of heparin should be hydrophilic, inert, rigid, spherical and stable to chemical and microbial degradation. Sepharose is the trade name (Pharmacia, Uppsala, Sweden) of the beaded agarose (a linear polysaccharide consisting of alternating residues of D-galactose and 3,6-anhydro-L-galactose). This matrix has been used extensively for the coupling of heparin [2]. The major requirements for the immobilization of heparin to matrix are the synthesis of a stable linkage between the matrix and heparin and, perhaps more importantly, retention of specific heparin-binding characteristics of the immobilized heparin. Heparin has been coupled to Sepharose, Affi-Gel, poly-

acrylamide and Toyopearl gel by several procedures described elsewhere in detail [2,37–39]. Several factors affect the coupling of heparin to the matrix. They are the pH of the coupling buffer, temperature, reaction time and amount of reacted heparin.

Success of the purification of lipases, phospholipases and kinases depends upon the following requirements: (1) the protein to be isolated should bind in a reversible way to heparin with an affinity such that it can be retained on the heparin-Sepharose while the other proteins are washed away; (2) the enzymes should interact with heparin-Sepharose with an affinity allowing their elution by the free ligand or by other non-denaturing agents; and (3) accompanying proteins should not bind to the matrix, but, if retained, should not be eluted from it under the conditions used for the desired protein.

6. Assay of heparin in heparin-Sepharose samples

The heparin content of heparin-Sepharose can be estimated by determining the hexosamine, uronic acid, and sulfate contents of the gel. With this method the above heparin constituents in the reaction mixture are determined prior to coupling and are compared to the free heparin that is left in the supernatant and washing after coupling. The difference is taken as the amount of heparin bound to Sepharose [2]. The amount of heparin in heparin-Sepharose can also be determined potentiometrically by the titration of heparin carboxyl groups [40]. Some investigators have used the dye-binding interactions of o-toluidine blue to colorimetrically or fluorimetrically quantitate unbound heparin before and after coupling [41]. The amount of heparin covalently bound to Sepharose can also be determined by assessing the interference by heparin in the Bradford dye-binding assay for proteins [42]. This method is extremely sensitive, rapid, and inexpensive, and it is capable of distinguishing between heparin and other polysaccharides.

7. Purification of lipases, phospholipases, lysophospholipases and kinases by heparin-Sepharose chromatography

Lipases, phospholipases and kinases have been successfully purified by heparin-Sepharose column chromatography (Table 2). Heparin-Sepharose is packed into a column and washed with 4 to 6 bed volumes of the desired buffer. Crude preparations of lipolytic enzymes or kinases are dialyzed against the equilibrating buffer and applied to the heparin-Sepharose column at a flow-rate of 0.2 ml/min. Enzymes that interact with immobilized heparin are retained and all other proteins are washed out. The retained enzymes can be eluted from the column with a gradient of NaCl or heparin.

7.1. Purification of lipases

Lipoprotein lipase and hepatic triacylglycerol lipase from human plasma bind tightly to heparin-Sepharose, but can be eluted with a linear gradient of sodium chloride. This procedure resulted in a 7400-fold purification of lipoprotein lipase with 95% recovery of enzymic activity. Hepatic triacylglycerol lipase was purified 6500-fold with 48% recovery under similar conditions by heparin-Sepharose chromatography [5]. The elution profile and fold purification of canine hepatic triacylglycerol lipase [43]

Table 2

Lipases, phospholipases and kinases purified by heparin-Sepharose chromatography

Enzyme	Fold purification
Diacylglycerol lipase [4]	10
Triacylglycerol lipase [5]	6250
Lipoprotein lipase [5]	7430
Phospholipase A ₂ [7]	17
Phospholipase A ₂ [48]	4
Phospholipase A ₂ [47]	61
Phospholipase A ₂ [46]	3
Phospholipase C [13]	7
Phospholipase C [11]	17
Phospholipase C [11]	9
Diacylglycerol kinase [12]	3
Diacylglycerol kinase [12]	7

was similar to that of the human plasma triacylglycerol lipase. Bovine brain diacylglycerol lipases have also been purified by heparin-Sepharose chromatography. About 60 to 65% of the protein was washed out while diacylglycerol lipase was completely retained. The enzyme appeared as a sharp peak when the column was washed with 0.5 M NaCl [4]. Heparin-Sepharose chromatography yielded a 4-fold purification with 75% recovery over the previous step [44].

7.2. Purification of phospholipases A₂

Heparin-Sepharose chromatography has been used extensively for the purification of rabbit and bovine platelet phospholipases A₂ [8,45,46]. Some phospholipases A₂ were retained on the heparin-Sepharose column; others were washed out [8,45,46]. In rabbit platelets the heparin binding form of phospholipase A₂ had a molecular mass of 14 000 and reacted with antihuman phospholipase A₂ monoclonal antibody of M_r 14 000. The phospholipase A₂ activity found in the heparin unbound fraction did not appreciably react with the above antibody [8,45,46]. Heparin-Sepharose chromatography gave a 3-fold purification of phospholipase A₂ with 70% recovery of enzymic activity. Similarly, pancreatic phospholipase A₂ can also be separated into heparin-bound and heparin-unbound fractions [32]. A phosphatidylserine-hydrolyzing phospholipase A₂ has been purified by heparin-Sepharose chromatography from cultured mast cells. In this case, heparin-Sepharose chromatography yielded a 61-fold purification with 83% recovery of enzymic activity [47]. Heparin-Sepharose chromatography of human monocytic cell cytosolic phospholipase A₂ resulted in a 4-fold purification of this enzyme [48].

7.3. Purification of phospholipase C

Heparin-Sepharose chromatography has been useful for the purification of phospholipase C from several sources. Heparin-Sepharose chromatography gave a 5-fold purification of human platelet phospholipase C with 73% recovery of enzymic activity [49]. Similarly, bovine liver [10],

spleen [50], and iris sphincter muscle [11] phospholipases C have been purified by this procedure. In all cases heparin-Sepharose chromatography resulted in good purification and yield of enzymic activity (Fig. 3).

7.4. Purification of protein kinase C and casein kinase II

Protein kinase C and casein kinase II can be purified by heparin-Sepharose chromatography [51,52]. Heparin-Sepharose chromatography yielded a 17-fold purification of bovine kidney protein kinase C with a recovery of 42% [51]. Similarly, casein kinase II was completely retained on a heparin-Sepharose column and was eluted with 0.5 M NaCl. This step resulted in an increase of specific activity with 55% yield of enzymic activity.

7.5. Purification of diacylglycerol kinase and phosphatidylinositol 4-kinase

Diacylglycerol kinases and phosphatidylinositol 4-kinases were retained on heparin-Sepharose and heparin-acrylamide columns [12,35,36]. They can be eluted from heparin-Sepharose with a linear gradient of NaCl. Heparin-Sepharose

chromatography of diacylglycerol kinase preparations resulted in two peaks designated as diacylglycerol kinase I and diacylglycerol kinase II [12]. Phosphatidylinositol 4-kinase also bound to a heparin-acrylamide column and could be eluted by a linear NaCl gradient. This procedure resulted in a 15-fold purification with 81% recovery of enzymic activity [36].

An important feature of heparin-Sepharose chromatography is the resolution of multiple forms (isozymes) of lipases, phospholipases and kinases. It is not possible to separate the multiple forms of the above enzymes by ion-exchange and hydrophobic chromatographies. Multiple forms of phospholipases A₂ [7], phospholipase C [13,53–55], diacylglycerol kinase [12] and protein kinase C [51] can be separated easily from crude extracts using heparin-Sepharose chromatography. This suggests that multiple forms of these enzymes have different affinities for heparin. Heparin-Sepharose chromatography can also be used as an alternative to equilibrium dialysis for the direct determination of enzyme-heparin affinity constants [56].

Heparin-Sepharose columns can be regenerated for reuse by washing the gel alternatively with a 10 × bed volume of high pH (8.5) and low pH (5.0) buffers containing 0.5 M NaCl. The

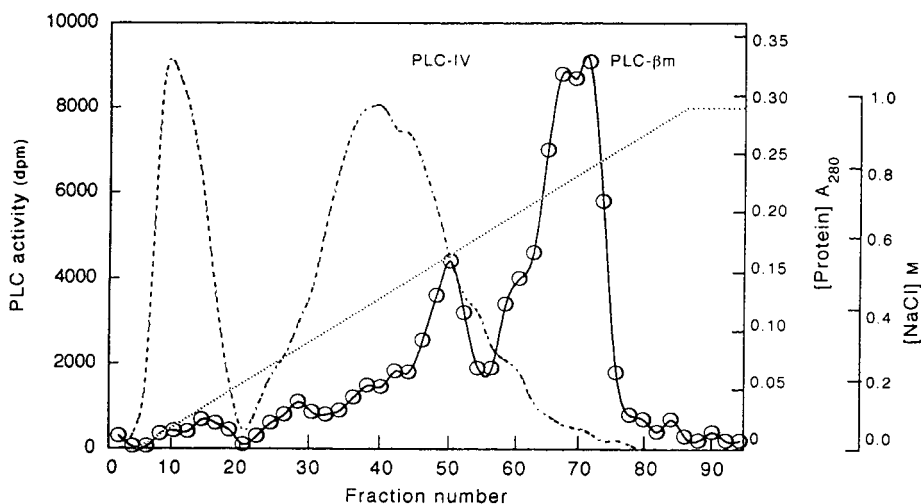


Fig. 3. Separation of multiple forms of rabbit brain phospholipase C by heparin-Sepharose chromatography. ○ = Phospholipase C (PLC) activity; broken line = A_{280} ; dotted line = NaCl. Data taken from ref. 13.

addition of 6 M urea or guanidine hydrochloride to the washing buffer removes all proteins from the heparin-Sepharose columns.

8. Advantages and disadvantages of heparin-Sepharose chromatography

Heparin has a stable structure, and its functional groups can be easily coupled to Sepharose, Affi-Gel or polyacrylamide. The immobilized heparin can interact reversibly with many enzymes and proteins [2]. The swollen heparin-Sepharose is stable for at least two years at 4°C in the presence of 0.02% merthiolate [57]. Heparin-Sepharose can be sterilized by autoclaving at pH 7.0 at 120°C. It has excellent flow properties and packs well into columns. Because of its polymeric and polyanionic properties, the immobilized heparin has a very high binding capacity, and this allows the use of a small bed volume. As a result, enzymes are eluted from the column in small volumes with very high activities. The elution of lipases, phospholipases or kinases from heparin-Sepharose columns by heparin or other polyanionic polysaccharides gives sharper peaks than elution by a salt gradient.

Heparin is a general ligand that inhibits a variety of biological reactions. Some of these interactions are specific; others are electrostatic. The presence of negatively charged groups on heparin results in retention of many positively charged proteins on the heparin-Sepharose column. Thus, electrostatic interactions can modify the efficiency of the protein separation process. These interactions can be eliminated by packing the column in high-ionic-strength buffer and eluting it with either heparin or other glycosaminoglycans. Trehalose phosphate synthetase and hyaluronidase have been successfully eluted from a heparin-Sepharose column by heparin and hyaluronic acid, respectively [58,59]. Under high ionic strength the elution of specifically bound proteins can also be achieved by using low concentrations of denaturants. In some cases this procedure has resulted in the elution of proteins

that interact with heparin by specific interactions.

Another major disadvantage of heparin-Sepharose chromatography is its lack of specificity. It is not possible to obtain homogeneous preparations of lipases, phospholipases or kinases in a single step. Furthermore, the chemical modification of heparin or the matrix during coupling can introduce additional binding sites. Blocking of these sites, as well as prior knowledge of the isoelectric points of the enzymes to be purified and their behavior on ion-exchange columns, are required in order to select the appropriate spacer and buffer for optimal elution of enzymic activities.

9. Conclusions

The unique structure and surface charge distribution of heparin allow it to interact with lipases, phospholipases, lysophospholipases and kinases in a specific manner (Fig. 4). These interactions inhibit or stimulate activities of the

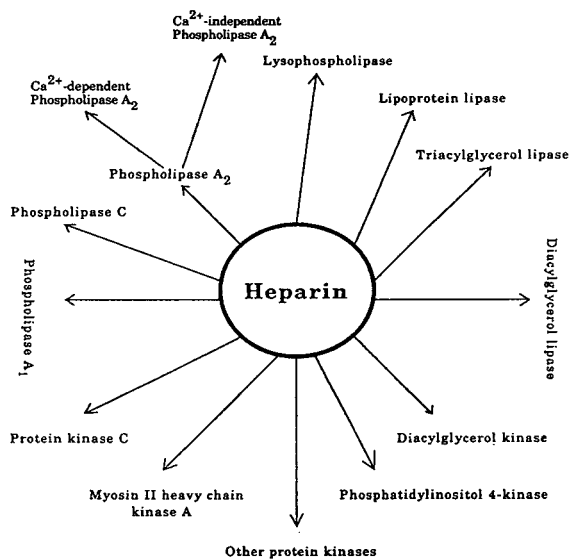


Fig. 4. Interactions of lipases, phospholipases and kinases with heparin.

above enzymes. The crucial question, whether these interactions occur *in vivo* and play some role in the regulation of lipases, phospholipases, lysophospholipases and kinases, cannot be answered at this time because our knowledge of heparin–enzyme interactions is incomplete. However, it is possible that in the plasma membrane, heparan sulfate, a glycosaminoglycan similar to heparin in structure, and other glycosaminoglycans may serve to anchor lipases, phospholipases and kinases from cytosol to the plasma membrane and regulate signal transduction, cell proliferation, cell differentiation and cell division [14,15]. Tyrosine kinase and phospholipases A₂ and C are linked to epidermal and fibroblast growth factors (FGFs) [15,60]. FGFs bind heparin, which potentiates or inhibits specific actions on different cell types [61,62]. Heparin also protects the FGF from proteolytic degradation [62,63]. Based on these studies, it has been suggested that heparin or heparan sulfate, along with protein kinases, may be involved in translocation and regulation of lipases and phospholipases [26]. Heparin has also been shown to possess anti-cancer activity. It may cause tumor regression and inhibit metastasis [64]. Recent studies have also indicated that heparin suppresses local immune response leading to tissue destruction. In fact, heparin reduces glomerulosclerosis, whereas the administration of protamine accelerates the development of this pathology [65,66]. There is a growing body of evidence to indicate that heparin–enzyme interactions are important in connective tissues and in the circulatory system [16]. This suggests that heparin and other glycosaminoglycans play important roles in cellular metabolism *in vivo*. *In vitro*, heparin–protein interactions can be used successfully for the isolation and characterization of lipases, phospholipases and kinases.

10. Acknowledgement

Supported by research grants NS-10165 and NS-29441 from the National Institutes of Health, US Public Health Service.

11. References

- [1] A.A. Farooqui, *J. Chromatogr.*, 184 (1980) 335.
- [2] A.A. Farooqui and L.A. Horrocks, *Adv. Chromatogr.*, 23 (1984) 127.
- [3] M. Kan, F. Wang, J. Xu, J.W. Crabb, J. Hou and W.L. McKeehan, *Science*, 259 (1993) 1918.
- [4] A.A. Farooqui, W.A. Taylor and L.A. Horrocks, *Biochem. Biophys. Res. Commun.*, 122 (1984) 1241.
- [5] C.-F. Cheng, A. Bensadoun, T. Bersot, J.S.T. Hsu and K.H. Melford, *J. Biol. Chem.*, 260 (1985) 10720.
- [6] J. Peinado-Onsurbe, C. Soler, M. Soley, M. Llobera and I. Ramirez, *Biochim. Biophys. Acta*, 1125 (1992) 82.
- [7] M. Hayakawa, I. Kudo, M. Tomita and K. Inoue, *J. Biochem.*, 103 (1988) 263.
- [8] D.K. Kim, I. Kudo, Y. Fujimori, H. Mizushima, M. Masuda, R. Kikuchi, K. Ikizawa and K. Inoue, *J. Biochem.*, 108 (1990) 903.
- [9] S. Higashi, T. Kobayashi, I. Kudo and K. Inoue, *J. Biochem.*, 103 (1988) 442.
- [10] K. Shaw and J.H. Exton, *Biochemistry*, 31 (1992) 6347.
- [11] C.-J. Zhou, R.A. Akhtar and A.A. Abdel-Latif, *Biochem. J.*, 289 (1993) 401.
- [12] Q. Chen, N. Klemm and I. Jeng, *J. Neurochem.*, 60 (1993) 1212.
- [13] H.R. Carter, M.A. Wallace and J.N. Fain, *Biochim. Biophys. Acta*, 1054 (1990) 119.
- [14] Y. Nishizuka, *Science*, 258 (1992) 607.
- [15] A.A. Farooqui, Y. Hirashima and L.A. Horrocks, in N.G. Bazan, G. Toffano and M. Murphy (Editors), *Neurobiology of Essential Fatty Acids*, Plenum Press, New York, 1992, pp. 11–25.
- [16] M.-C. Bourin and U. Lindahl, *Biochem. J.*, 289 (1993) 313.
- [17] F. Zhou, T. Hook, J.A. Thompson and M. Hook, *Adv. Exp. Med. Biol.*, 313 (1992) 141.
- [18] M. Gigli, G. Ghiselli, G. Torri, A. Naggi and V. Rizzo, *Biochim. Biophys. Acta*, 1167 (1993) 211.
- [19] D. Gómez-Coronado, G.T. Sáez, M.A. Lasunción and E. Herrera, *Biochim. Biophys. Acta*, 1167 (1993) 70.
- [20] P.E. Fielding, V.G. Shore and C.J. Fielding, *Biochemistry*, 13 (1974) 4318.
- [21] R.L. Patten and C.H. Hollenberg, *J. Lipid Res.*, 10 (1969) 374.
- [22] I. Posner and J. DeSanctis, *Arch. Biochem. Biophys.*, 253 (1987) 475.
- [23] J. Le Petit, O. Nobili and J. Boyer, *Pharmacol. Biochem. Behav.*, 24 (1986) 1543.
- [24] M.B. Diccianni, L.R. McLean, W.D. Stuart, M.J. Mistry, C.M. Gil and J.A.K. Harmony, *Biochim. Biophys. Acta*, 1082 (1991) 85.
- [25] T.P. Parks, S. Lukas and A.F. Hoffman, *Adv. Exp. Med. Biol.*, 275 (1990) 55.
- [26] H.-C. Yang, A.A. Farooqui and L.A. Horrocks, *Biochem. J.*, 299 (1994) 91.

- [27] W.B. Weglicki, R.C. Ruth, K. Owens, H.D. Griffin and B.M. Waite, *Biochim. Biophys. Acta*, 150 (1973) 145.
- [28] S.L. Drake, D.J. Klein, D.J. Mickelson, T.R. Oegama, L.T. Furcht and J.B. McCarthy, *J. Cell Biol.*, 117 (1992) 1331.
- [29] P.H. Mäenpää, *Biochim. Biophys. Acta*, 498 (1977) 294.
- [30] G.M. Hathaway, T.H. Lubben and J.A. Traugh, *J. Biol. Chem.*, 255 (1980) 8038.
- [31] Q.G. Medley, W.L. Bagshaw, T. Truong and G.P. Côté, *Biochim. Biophys. Acta*, 1175 (1992) 7.
- [32] J.-M. Herbert and J.-P. Maffrand, *Biochim. Biophys. Acta*, 1091 (1991) 432.
- [33] L.A. Pukac, M.E. Ottlinger and M.J. Karnovsky, *J. Biol. Chem.*, 267 (1992) 3707.
- [34] J.L. Benovic, W.C. Stone, M.G. Caron and R.J. Lefkowitz, *J. Biol. Chem.*, 264 (1989) 6707.
- [35] C. Cochet and E.M. Chambaz, *Biochem. J.*, 237 (1986) 25.
- [36] G.H. Jenkins, G. Subrahmanyam and R.A. Anderson, *Biochim. Biophys. Acta*, 1080 (1991) 11.
- [37] R.L. Schnaar, *Anal. Biochem.*, 143 (1984) 1.
- [38] H. Sasaki, A. Hayashi, H. Kitagaki-Ogawa, I. Matsumoto and N. Seno, *J. Chromatogr.*, 400 (1987) 123.
- [39] S.R. Narayanan, S.V. Kakodkar and L.J. Crane, *Anal. Biochem.*, 188 (1990) 278.
- [40] M.Ya. Varshavskaya, A.L. Klivanov, V.S. Goldmacher and V.P. Torchilin, *Anal. Biochem.*, 95 (1979) 449.
- [41] P.K. Smith, A.K. Mallia and G.T. Hermanson, *Anal. Biochem.*, 109 (1980) 466.
- [42] M.Y. Khan and S.A. Newman, *Anal. Biochem.*, 187 (1990) 124.
- [43] P.H. Frost, V.G. Shore and R.J. Havel, *Biochim. Biophys. Acta*, 712 (1982) 71.
- [44] A.A. Farooqui, K.W. Rammohan and L.A. Horrocks, *Ann. N.Y. Acad. Sci.*, 559 (1989) 25.
- [45] D.K. Kim, P.G. Suh and S.H. Ryu, *Biochem. Biophys. Res. Commun.*, 174 (1991) 189.
- [46] D.K. Kim, I. Kudo and K. Inoue, *Biochim. Biophys. Acta*, 1083 (1991) 80.
- [47] M. Murakami, I. Kudo, M. Umeda, A. Matsuzawa, M. Takeda, M. Komada, Y. Fujimori, K. Takahashi and K. Inoue, *J. Biochem.*, 111 (1992) 175.
- [48] W. Rehfeldt, K. Resch and M. Goppelt-Struebe, *Biochem. J.*, 293 (1993) 255.
- [49] J.J. Baldassare, P.A. Henderson and G.J. Fisher, *Biochemistry*, 28 (1989) 6010.
- [50] Y. Homma, Y. Emori, F. Shibasaki, K. Suzuki and T. Takenawa, *Biochem. J.*, 269 (1990) 13.
- [51] H. Nakanishi and J.H. Exton, *J. Biol. Chem.*, 267 (1992) 16347.
- [52] J.S. Sanghera, L.A. Charlton, H.B. Paddon and S.L. Pelech, *Biochem. J.*, 283 (1992) 829.
- [53] H. Kawaguchi and H. Yasuda, *Circ. Res.*, 62 (1988) 1175.
- [54] A. Faber and I. Aviram, *Biochim. Biophys. Acta*, 1128 (1992) 8.
- [55] Y. Banno, T. Nakashima, T. Kumada, K. Ebisawa, Y. Nonomura and Y. Nozawa, *J. Biol. Chem.*, 267 (1992) 6488.
- [56] D.J. Winzor, *J. Chromatogr.*, 597 (1992) 67.
- [57] A.A. Farooqui, unpublished results.
- [58] A.D. Elbein and M. Mitchell, *Arch. Biochem. Biophys.*, 168 (1975) 369.
- [59] P.N. Srivastava and A.A. Farooqui, *Biochem. J.*, 183 (1979) 531.
- [60] N. Hack, B.L. Margolis, A. Ullrich, J. Schlessinger and K.L. Skorecki, *Biochem. J.*, 275 (1991) 563.
- [61] S. Vannucchi, F. Pasquali, G. Fiorelli, P. Bianchini and M. Ruggiero, *FEBS Lett.*, 263 (1990) 137.
- [62] D. Gospodarowicz and J. Cheng, *J. Cell. Physiol.*, 128 (1986) 475.
- [63] G. Neufeld, D. Gospodarowicz, L. Dodge and D.K. Fujii, *J. Cell. Physiol.*, 131 (1987) 131.
- [64] A. Górski, M. Wasik, M. Nowaczyk and G. Korczak-Kowalska, *FASEB J.*, 5 (1991) 2287.
- [65] D.R. Coombe, C.R. Parish, I.A. Ramshaw and J.M. Snowden, *Int. J. Cancer*, 39 (1987) 82.
- [66] T. Saito, E. Sumithran, E.F. Glasgow and R.C. Atkins, *Kidney Int.*, 32 (1987) 691.
- [67] D.L. Friedman, N.J. Kleiman and F.E. Campbell, Jr., *Biochim. Biophys. Acta*, 847 (1985) 165.



ELSEVIER

Journal of Chromatography A, 673 (1994) 159–165

JOURNAL OF
CHROMATOGRAPHY A

Adsorption and separation of proteins on composite anion exchangers with poly(N-diethylaminoethylacrylamide) bonded phases[☆]

Alexander E. Ivanov*, Vitali P. Zubov

Shemyakin and Ovchinnikov Institute of Bioorganic Chemistry, Russian Academy of Sciences, Miklukho-Maklaya 16/10, 117871 Moscow V-437, Russian Federation

(First received May 9th, 1993; revised manuscript received February 23rd, 1994)

Abstract

Composite anion exchangers for chromatography of proteins were prepared by chemical adsorption of poly(*p*-nitrophenyl acrylate) on γ -aminopropylsilicas followed by coupling of the esters to 2-diethylaminoethylamine. Separation of standard proteins (bovine serum albumin and ovalbumin) on these anion exchangers established their enhanced selectivity and milder desorption conditions as compared with polyethyleneiminesilicas and DEAE-Toyopearl 650M. Frontal analysis was used to evaluate the maximum binding capacity for ovalbumin adsorption on the new packing, which was found to be 13 mg/ml and so nearly half those observed with polyethyleneiminesilicas of comparable pore diameter. The possible role of the excluded volume of the attached polymer is discussed with respect to the adsorptivity of the composite ion exchangers.

1. Introduction

Since polyethyleneimine-coated silicas were developed by Regnier and co-workers [1,2] for use as packings in the anion-exchange chromatography of proteins, attempts have been made to design other polymer-coated silicas for the same purpose. Apart from variations with polyethyleneimine coatings [3,4] and use of DEAE-dextran as the bonded phase [5], the synthetic approach of Müller [6] seems to be most interesting because it ensures the formation of end-

grafted polyelectrolyte chains with maximum motional freedom and, therefore, the best adaptivity towards the absorbing proteins. Better separation properties of such “tentacle-like” composite sorbents as compared with the traditional ion exchangers based on cross-linked polymers were reported [6]. However, under overloading conditions the tentacle-type anion exchangers gradually lose their protein adsorption capacity [7]. This might be related to the peculiar behaviour of end-grafted chains or their leakage during the desorption stages.

The stability of the coating and the reproducibility of the loading capacities may be improved, in principle, by the preparation of bonded phases composed of multivalently attached macromolecules. On the other hand, the multivalently attached polymeric chains will have

* Corresponding author.

[☆] Presented at the 17th International Symposium on Column Liquid Chromatography, Hamburg, May 9–14, 1993. The proceedings of this symposium were published in *J. Chromatogr. A*, Vols. 660 + 661 (1994).

less mobility and thus may give a diminished effect of tentacles.

In previous papers [8,9], we described the chemical adsorption of poly(*p*-nitrophenyl acrylate) (PNPA) as a method for the preparation of multivalently attached polymeric phases. Ester functions of the chemically adsorbed PNPA can be coupled to various primary amines and yield bonded phases composed of *N*-substituted polyacrylamides. If 2-diethylaminoethylamine is used for such a synthesis, an adsorbent with DEAE functions is formed with a chemical structure almost identical with that explored by Müller [6]. However, the arrangement of the grafted chains is different in our case and may lead to a different behaviour of separated solutes.

In this work we examined the separation properties of a composite anion-exchanger prepared by the PNPA method and compared them with those of polyethyleneiminesilica (PEI-silica) and DEAE-Toyopearl 650M, a wide-pore cross-linked polymer. We also considered some features of the chemical adsorption of PNPA on γ -aminopropylsilicas as they can help to elucidate the structure of the new bonded phases. To characterize its interaction with proteins, the adsorption isotherm was obtained and the maximum capacity was evaluated for ovalbumin binding.

2. Experimental

2.1. Materials

MPS-2000 VGKh wide-pore glass (WPG) with particle diameter 50–150 μm and mean pore diameter 2100 Å, manufactured by GOZ VNII NP (Nizhny Novgorod, Russian Federation) was washed with 6 *M* hydrochloric acid and distilled water and fractionated by sedimentation. Ultimately, the fraction with particle diameter 50–100 μm was collected and dried. Silica gel XWP-1500 with particle diameter 16–23 μm and mean pore diameter 1500 Å was a gift from Diagen (Hilden, Germany). Monospher (MS) non-porous silica beads with particle diameter $1.4 \pm 0.1 \mu\text{m}$ were a gift from Professor K.K. Unger

(Johannes Gutenberg-Universität, Mainz, Germany). DEAE-Toyopearl 650M was obtained from Tosoh (Akasaka, Tokyo, Japan).

Poly(*p*-nitrophenyl acrylate) (PNPA) $\bar{M}_w = 42\,000$, $\bar{M}_w/\bar{M}_n = 3.3$ (\bar{M}_w = mass-average molecular mass; \bar{M}_n = number-average molecular mass), was prepared by free-radical polymerization of the monomer in dry benzene with azobisisobutyronitrile as initiator at 70°C with nitrogen bubbling for 20 h. γ -Aminopropyltriethoxysilane was purchased from Fluka (Buchs, Switzerland). Dimethyl sulphoxide (DMSO) was supplied by Sigma (St. Louis, MO, USA). Tris-hydroxymethylaminomethane (Tris) was obtained from Gerbu (Gaiberg, Germany). 2-Diethylaminoethylamine was purchased from Fluka. Other chemicals (solvents and salts) of analytical-reagent grade were supplied by Reakhim (Moscow, Russian Federation) benzene and toluene being distilled.

Bovine serum albumin (BSA), fraction 5, was obtained from Boehringer-Mannheim (Vienna, Austria) and ovalbumin from Serva (Heidelberg, Germany).

2.2. Chemical modification of silicas

All silicas were chemically modified with γ -aminopropyltriethoxysilane and analysed as described previously [8]. The amino group contents were 38, 210 and 150 $\mu\text{mol g}^{-1}$ for MS-NH₂, WPG-NH₂ and XWP-NH₂, respectively. Amino-propylsilicas were treated with PNPA solution as described previously [8], washed with DMSO and suspended in a 2% solution of 2-diethylaminoethylamine in DMSO. After 2 days of periodic shaking at room temperature, the deposits of silicas were washed with distilled water and incubated in 0.5 *M* ammonium acetate (pH 9.0) for 1 week. Ultimately, the prepared sorbents were washed with distilled water and stored as wet cakes at room temperature in 0.02% sodium azide solution.

2.3. PNPA isotherm measurements

Isotherms of the polymer adsorption were obtained by means of a probe isolation from the

reaction media. From 0.05 to 0.1 g of aminopropylsilica was incubated in 1–10 ml of 0.05–3% (w/v) PNPA solution in DMSO for 2 days with moderate shaking at 25°C, the molar ratio of ester to aminopropyl groups being not less than 3. Samples of 5 mg of the PNPA-silica were isolated from the reaction medium, washed with DMSO and acetone, dried under vacuum, weighed and treated with concentrated aqueous ammonia solution (25°C, 24 h). The *p*-nitrophenolate concentration in the supernatant was determined by UV spectrophotometry ($\lambda_{\max} = 405$ nm, $\epsilon_{\max} = 15\,300$ l mol⁻¹ cm⁻¹) and the specific *p*-nitrophenyl ester group content in the PNPA-silicas was then calculated.

2.4. Ovalbumin isotherm measurements

The adsorption isotherm of ovalbumin was obtained by recording the breakthrough curves of ovalbumin (A_{280}) applied in a frontal mode to the thermostated column (25°C, 1.5 cm × 1 cm I.D.) packed with anion exchanger based on XWP-1500 silica (DEAE-PA-silica) at various concentrations of the protein dissolved in 0.02 M Tris-HCl buffer (pH 7.8). The saturation of the column was judged at the point where 10% of the feedstock absorbance was detected in the effluent. The amount of adsorbed protein was then calculated by multiplying the volume pumped by the concentration. The flow-rate in frontal experiments was 0.5 ml min⁻¹.

2.5. Analytical chromatography of proteins

Ovalbumin and bovine serum albumin [0.5 mg each in 0.5 ml of 0.02 M Tris-HCl buffer (pH 7.8)] was applied to a glass MS-PC 10/20 Whatman column (3.9 cm × 1 cm I.D.) equipped with a thermostated water jacket (25°C) and packed with the anion exchanger. For sample application a V-7 valve (Pharmacia, Uppsala, Sweden) connected to a 0.5-ml polyethylene tubing loop was used. A linear gradient of sodium chloride was formed by an Ultrograd 11300 gradient mixer (LKB, Bromma, Sweden) and an NP-1 peristaltic pump (Analytical Apparatus SKB, Kiev, Ukraine). A Holochrome HMD HPLC detector (Gilson, Villiers-le-Bel, France) con-

nected to a Mettler (Zurich, Switzerland) GA17 recorder was used to detect absorbing fractions during chromatographic procedures.

The resolution (R_s) was calculated as $2(t_2 - t_1)/(\Delta t_1 + \Delta t_2)$, where t_1 and t_2 are the retention times and Δt_1 and Δt_2 are the peak widths at the baseline in minutes.

3. Results and discussion

3.1. Bonded-phase synthesis: chemical adsorption of PNPA to aminopropylsilicas

Chemical adsorption of PNPA to aminopropylsilicas proceeds via formation of amide bonds between the polymer and moieties of the immobilized silane [8]. Many ester functions, however, remain unreacted and held by segments of the fixed macromolecular coils. These segments, loops and tails form a diffuse interface which is dense enough to prevent adsorption of proteins on the surface of silica [8]. To characterize the structure of the polymeric bonded phases, the adsorption isotherms were obtained for PNPA binding to non-porous aminopropyl Monospher silica gel (MS-NH₂) and wide-pore aminopropyl-glass (PG-NH₂) from solution in DMSO (Fig. 1a).

The plateau value of PNPA adsorption to PG-NH₂ exceeds that for MS-NH₂ by a factor of 8. This may be ascribed to the larger surface area and higher aminopropyl group content in the porous glass carrier as compared with non-porous silica. Indeed, the positions and shapes of the two isotherms differ only slightly from each other if the amount of polymer adsorbed is expressed as the *p*-nitrophenyl ester group content divided by the initial content of aminopropyls (Fig. 1b). Apparently, the pore structure of glass does not seriously hinder the transport of reactive PNPA molecules into the depth of particles, so that the adsorption mechanisms are closely related on the two carriers. Theoretically, this phenomenon may be explained by the high ratio of the mean pore diameter of glass (2000 Å) to the hydrodynamic radius of polymer coil, the latter being evaluated as 80 Å [10]. One can

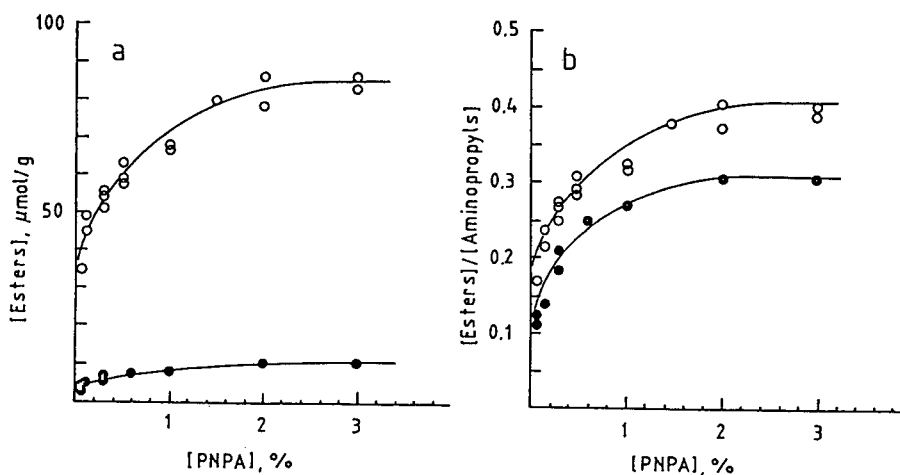


Fig. 1. Isotherms for poly(*p*-nitrophenyl acrylate) chemical adsorption on (○) aminopropylsilylated wide-pore glass and (●) non-porous silica.

expect, therefore, almost free diffusion of the polymer through the pores, concurrently with its chemical adsorption on the aminopropyl-glass surface.

The ester group content in the resultant composites increases with increasing PNPA concentration from 0 to 10 mg ml^{-1} and levels off at higher concentrations. The shape of the isotherms indicates the permeability of the adsorbed PNPA layer, which is assumed to be diffuse with flexible loops and tails. These findings correspond well with the conclusions of theories developed by Barford and co-workers [11,12] which predict more extended polymer profiles, as a function of adsorbate concentration, for a non-equilibrium mechanism of polymer adsorption rather than for the equilibrium mechanism.

Further, according to the above-mentioned theories, the density of segments plotted against the distance from the surface exhibits a slower decrease for neutral polymers than polyelectrolytes. One can expect, therefore, longer loops and tails in the PNPA adsorbed layers rather than in the adsorbed layers of PEI. Hence the effect of tentacles on protein separations seems to be more probable with PNPA- than with PEI-coated sorbents.

3.2. Analytical chromatography of proteins

For testing proteins by anion-exchange chromatography, composite sorbents with DEAE functions (DEAE-PA-silica and -glass) were prepared by the PNPA method from 20- μm particle size XWP-silica (average pore diameter 1500 Å) and from 80- μm particle size wide-pore glass (average pore diameter 2000 Å). The particles used were large enough to be packed into the Whatman standard glass column, which allows the use of low-pressure peristaltic pumping. The separation profiles obtained for commercial samples of ovalbumin and bovine serum albumin are shown in Fig. 2b and c. A typical separation performed with commercial DEAE-Toyopearl 650M, a cross-linked vinyl polymer [13], is given for comparison in Fig. 2a.

The better separation and sharper peaks observed for the DEAE-PA-silica are possibly due to its smaller particles and their narrow size distribution as compared with the Toyopearl material. However, the separation carried out with DEAE-PA-glass having larger particles (50–100 μm) is also better, as demonstrated in Fig. 2c.

The differences in the retention behaviour of the proteins indicates some other mechanism of

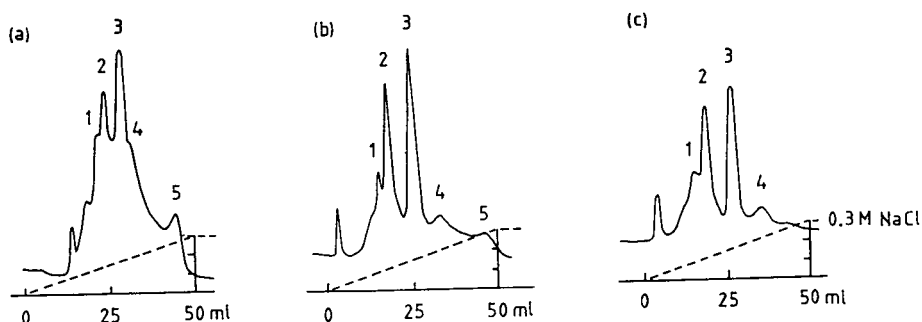


Fig. 2. Analytical separations of ovalbumin (peaks 1 and 2) and bovine serum albumin (peaks 3, 4 and 5) on 3.9 cm \times 1 cm I.D. columns packed with (a) DEAE-Toyopearl 650M, (b) DEAE-PA-silica and (c) DEAE-PA-glass. Starting buffer, 0.02 M Tris-HCl (pH 7.8); sample, 0.5 mg of each protein in 0.5 ml of the starting buffer; elution, gradient from 0 to 0.3 M NaCl in the starting buffer; flow-rate, 1.1 ml min⁻¹; gradient time, 45 min. Proteins were detected by UV absorbance at 280 nm.

their adsorption, which contributes to the improved protein separation. Indeed, the main peak of ovalbumin elutes at 0.11 M NaCl concentration and the albumin peak at 0.16 M NaCl, the resolution factor being 1.4.

With a use of DEAE-Toyopearl 650M as a packing, ovalbumin elutes at 0.14 M NaCl and albumin at 0.19 M NaCl with $R_s < 0.8$, so that the better resolution of proteins on DEAE-PA sorbents is accompanied by milder desorption conditions.

The described effects are similar to those reported by Müller [6] for tentacle-like anion exchangers (DMA type). We believe that the diffuse structure of the polymer coating displaying many tails ensures an analogous improved function of DEAE-PA sorbents.

When compared with PEI-silicas, DEAE-PA-silica again shows a capability for better resolution. Vanecek and Regnier [3] studied the separation of albumin and ovalbumin on a series of PEI-silicas and obtained an optimum resolution factor of 1.40 on a 5 cm \times 0.41 cm I.D. stainless-steel column with 10- μ m PEI-LiChrospher Si 4000 with a 40-min gradient of sodium acetate.

DEAE-PA-silica of 20- μ m particle size packed into a 3.9 cm \times 1 cm I.D. column by the conventional low-pressure technique ensures comparable resolution factors for the same pair of proteins as listed in Table 1. It is noteworthy that PEI-silicas release the proteins at higher ionic

strength than do DEAE-PA-silicas. Desorption of ovalbumin and albumin from PEI-silica requires 0.30 and 0.38 M sodium acetate, respectively, in 0.02 M Tris-CH₃COOH buffer (pH 8.0) [2].

The significantly milder desorption conditions observed for DEAE-PA-silicas prompted us to study the adsorption isotherm of ovalbumin in order to detect the possible deviations from the literature data for PEI-silicas and to evaluate the maximum loading capacity of the sorbent.

3.3. Adsorption isotherm

To obtain the adsorption isotherm, the dynamic load capacities (DLC) of DEAE-PA-silica were measured by frontal analysis at various concentrations of ovalbumin (Fig. 3). It was reported by Janzen *et al.* [7] that DLC may

Table 1
Resolution of bovine serum albumin and ovalbumin on DEAE-PA-silica at various flow-rates and gradient times

Flow-rate (ml min ⁻¹)	Gradient time (min)	R_s
0.6	90	2.0
0.7	45	1.4
1.2	45	1.4
1.4	22	1.2

R_s = resolution; for calculation, see Experimental. Column size and chromatographic conditions as in Fig. 2.

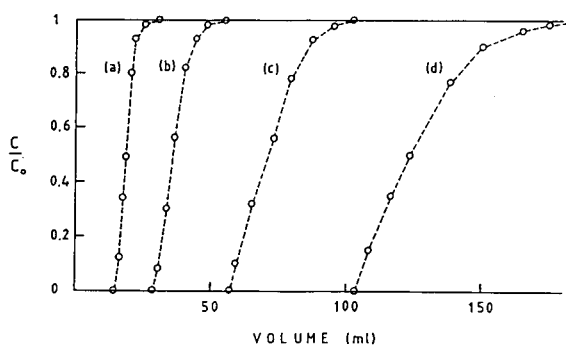


Fig. 3. Breakthrough curves of ovalbumin adsorption obtained on a 1.5 cm \times 1 cm I.D. column packed with DEAE-PA-silica at various concentrations of the protein: (a) 1; (b) 0.4; (c) 0.2; (d) 0.1 mg ml⁻¹.

depend on the number of repetitive loadings on the same column. In this study, after six consecutive steps of loading and desorption, DLC was found to change by only 4% at a concentration of ovalbumin of 1 mg ml⁻¹ and thus allowed the same packing to be used at least five times before it was replaced with a fresh portion of the sorbent. Moreover, virtually quantitative release of the protein (95–100%) was observed with DEAE-PA-silica and DEAE-PA-glass packings during the frontal experiments followed by a desorption step [0.5 M NaCl in 0.02 M Tris-HCl buffer (pH 7.8)].

The isotherm is illustrated in Fig. 4. Non-linearity of the Scatchard plot shows that the adsorption of ovalbumin strongly deviates from the course of the Langmuir isotherm, the same phenomenon having been observed earlier for adsorption of albumin on some PEI-silicas [7]. The maximum adsorption capacity was evaluated by extrapolation from a double reciprocal plot of the isotherm and equals 13 mg ml⁻¹ of the sorbent. This amount is half that reported for ovalbumin adsorbed on 1000 Å pore diameter PEI-silicas (26 mg ml⁻¹ for thin PEI coatings) [3].

Judging by the moderate protein capacity and milder desorption conditions, one may conclude that the synthesis based on PNPA chemical adsorption leads to an anion-exchange bonded phase exhibiting a sort of repellency towards proteins.

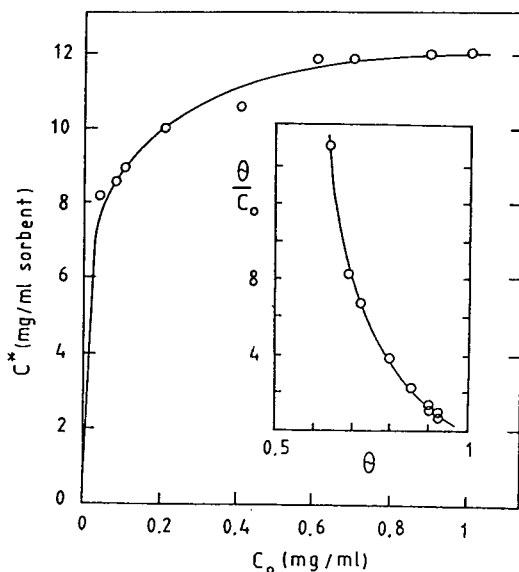


Fig. 4. Adsorption isotherm of ovalbumin on DEAE-PA-silica. The inset shows the Scatchard plot of the isotherm, where θ is the degree of sorbent saturation by the protein and c_0 is the amount of the protein adsorbed.

As was mentioned above, neutral reactive PNPA macromolecules are not as tightly adsorbed on silica as polycations of PEI. This is the reason why the resultant polymeric phase has a larger excluded volume and may produce an entropic repulsion towards the approaching particles [14]. Although the electrostatic attraction overwhelms this effect by far, something like a "springing" mechanism of protein adsorption may be suggested for polymeric ion exchangers with flexible loops and tails. For PEI-silicas with heavily cross-linked oligomeric coatings, no such "springing" may be expected. The same holds true for cross-linked vinyl polymers such as Toyopearl. The retention and adsorption of proteins are stronger on these materials.

4. Conclusions

Chemically bonded phases composed of multivalently adsorbed poly(N-diethylaminoethylacrylamide) exhibit an improved selectivity of protein separation and milder desorption conditions as compared with cross-linked anion

exchangers, an effect observed previously with end-grafted polymers [6]. The maximum loading capacities of the novel sorbents are, however, lower than those in the literature for analogous sorbents of a comparable pore size. On the other hand, the diffuse structure of the multivalently adsorbed polymer ensures highly reproducible protein adsorption capacities and an apparent absence of irreversible protein binding. These characteristics seem to be valuable for both the analytical and preparative chromatography of proteins.

Acknowledgements

We express our sincere gratitude to Professor K.K. Unger (Johannes Gutenberg-Universität, Mainz, Germany) for presenting a sample of Monospher silica and to Dr. K. Henco (Diagen, Hilden, Germany) for the sample of XWP-1500 silica.

References

- [1] A.J. Alpert and F.E. Regnier, *J. Chromatogr.*, 185 (1979) 375.
- [2] G. Vanecek and F.E. Regnier, *Anal. Biochem.*, 109 (1980) 345.
- [3] G. Vanecek and F.E. Regnier, *Anal. Biochem.*, 121 (1982) 156.
- [4] M. Flashner, H. Ramsden and L.J. Crane, *Anal. Biochem.*, 135 (1983) 340.
- [5] X. Santarelli, D. Muller and J. Jozefonvicz, *J. Chromatogr.*, 443 (1988) 55.
- [6] W. Müller, *J. Chromatogr.*, 510 (1990) 133.
- [7] R. Janzen, K.K. Unger, W. Muller and M.T.W. Hearn, *J. Chromatogr.*, 522 (1990) 77.
- [8] A.E. Ivanov, L.V. Kozlov, B.B. Shojbonov, V.P. Zubov and V.K. Antonov, *Biomed. Chromatogr.*, 6 (1991) 90.
- [9] V.P. Zubov, A.E. Ivanov and V.V. Saburov, *Adv. Polym. Sci.*, 104 (1992) 135.
- [10] A.E. Ivanov, S.V. Belov and V.P. Zubov, *Vysokomol. Soed., Ser. A*, 35 (1993) 1320.
- [11] W. Barford, R.C. Ball and C.C.M. Nex, *J. Chem. Soc., Faraday Trans. 1*, 82 (1986) 3233.
- [12] W. Barford and R.C. Ball, *J. Chem. Soc., Faraday Trans. 1*, 83 (1987) 2515.
- [13] *Toyopearl —The Packings for Medium Performance Liquid Chromatography*, Tosoh, Tokyo.
- [14] J. Hermans, *J. Chem. Phys.*, 77 (1982) 2193.

Separation of ribonucleotides, ribonucleosides, deoxyribonucleotides, deoxyribonucleosides and bases by reversed-phase high-performance liquid chromatography

Jian Zhao, Bryan Todd, Graham H. Fleet*

Department of Food Science and Technology, University of New South Wales, P.O. Box 1, Kensington, N.S.W. 2033, Australia

(First received December 20th, 1993; revised manuscript received March 14th, 1994)

Abstract

A procedure is described for the separation of 21 purine and pyrimidine bases, ribonucleotides, ribonucleosides, deoxyribonucleotides and deoxyribonucleosides in a single chromatographic run by reversed-phase high-performance liquid chromatography using a Waters Resolve C₁₈ 5- μ m Radial-Pak cartridge and a gradient elution system. The method is fast, taking 35 min for one run. It has proved useful in analysing flavour-enhancing compounds of nucleic acid origin in yeast autolysates.

1. Introduction

We are interested in studying the products of DNA and RNA degradation that are formed during the autolysis of yeasts. Yeast autolysates containing these products have commercial applications in the food industry as flavour ingredients [1], while yeast autolysis and the degradation of nucleic acids during wine, champagne and beer fermentations can impact on the final quality of these beverages [2,3].

Many high-performance liquid chromatography (HPLC) procedures for separating individual classes of purine and pyrimidine compounds have been developed and these are well documented in the literature [4–6]. Generally,

anion-exchange chromatography is used for separating the highly charged nucleotides, while reversed-phase chromatography is used for separating the less charged nucleosides and bases. Recently, methods based on reversed-phase HPLC to separate mixtures of these compounds have been reported [7–12]. Although the published methods are successful in their respective applications, none of them can separate a mixture of ribonucleotides, ribonucleosides, deoxyribonucleotides, deoxyribonucleosides and bases in one chromatographic run. Some of the procedures have the additional disadvantage of requiring long analysis times.

We report, here, a reversed-phase HPLC procedure which is able to separate a mixture of 21 nucleotides, nucleosides and bases. The analysis is rapid, taking only 35 min for one run, and was used successfully for the analysis of RNA

* Corresponding author.

and DNA degradation products in yeast autolysates.

2. Experimental

2.1. Instrumentation

The HPLC system consisted of a Bio-Rad HPLC gradient processor system which included two Bio-Rad Model 1330 HPLC pumps and a Bio-Rad automation interface with an Apple Model IIe computer; a Waters U6K injector and a Waters Model 440 absorbance detector with two wavelengths of 245 and 280 nm. Retention times and peak areas or peak heights were measured with a Waters 745 data module.

2.2. Column

The column used was a Waters Resolve C₁₈ 5- μ m Radial-Pak cartridge (100 mm \times 8 mm I.D.) equipped with a Waters RCM-100 cartridge holder. Packing material of the cartridge was a silica-based reversed-phase C₁₈ HPLC matrix of 5- μ m spherical beads.

2.3. Chemicals and chromatographic standards

Potassium dihydrogenphosphate (analytical-reagent grade) was obtained from BDH (Sydney, Australia). Methanol (HPLC grade) was obtained from Waters–Millipore (Sydney, Australia). Standards of individual nucleotides, nucleosides and nucleic acid purine and pyrimidine bases (as listed in Table 1) were purchased from United States Biochemical Corporation (Cleveland, OH, USA).

Stock solutions of standards (1%, w/v) were made up by dissolving individual compounds in de-ionised water and were stored at -20°C . Working solutions of standards were made by diluting the stock solutions to 0.01% (w/v).

2.4. Preparation of solvents for HPLC elution

Solvent A was a solution of 0.02 M K₂HPO₄ with pH adjusted to 6.30 with concentrated

potassium hydroxide solution. Solvent B was a solution of methanol in distilled, de-ionised water (60%, v/v). Prior to use, the eluents were filtered through a membrane filter, pore size 0.45 μ m (Millipore, Sydney, Australia), and degassed by vacuum and sonification for 5 min.

2.5. Chromatographic conditions

Before injection of samples, the column was equilibrated with solvent A for 5 min at a flow-rate of 3 ml/min. This step served two purposes. Firstly, it washed out residuals from previous injections and secondly, it stabilised the baseline of the system for the next injection.

After injection of the sample (20 μ l), elution was started with 100% solvent A and 0% solvent B. The ratio of solvent B in the elution system was increased linearly from 0 to 40% over 18 min. Solvent B was then increased to 100% over 5 min and the column was then flushed with 100% solvent B for a further 2 min in order to remove strongly absorbed compounds. The system was automatically returned to its starting condition (*i.e.* 100% solvent A and 0% solvent B) over 5 min by computer control. The elution of one sample took 35 min with the solvent flow-rate being maintained at 3 ml/min throughout the program. The elution was performed at ambient temperature (25°C).

2.6. Autolysis of yeasts

Cells of *Saccharomyces cerevisiae* x2180 were grown in 0.5% yeast extract–5% glucose medium at 25°C for 48 h. Cells were harvested by centrifugation, washed, and suspended in 0.2 M sodium phosphate–citric acid buffer, pH 7.0. Autolysis was initiated by incubating the suspension at 40°C with orbital shaking at 200 rpm [13]. Samples were withdrawn daily and separated by centrifugation (5000 g for 5 min) into cell pellets and cell-free autolysate. The autolysate fraction was filtered through a 0.45- μ m pore-sized membrane filter (Millipore) and used in the HPLC without further treatment.

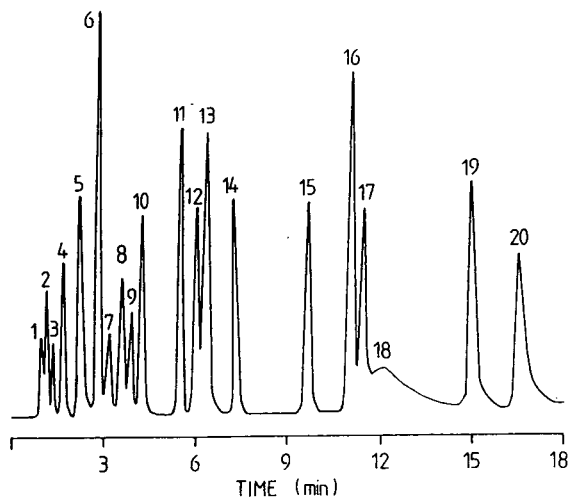


Fig. 1. Chromatogram of a standard mixture of nucleotides, nucleosides and purine and pyrimidine bases (0.01%, w/v, each). Injection volume, 20 μ l; detection wavelength, 254 nm. Peaks: 1 = 5'-CMP; 2 = 5'-UMP; 3 = 5'-dCMP; 4 = 5'-GMP; 5 = cytosine; 6 = uracil; 7 = 5'-dTMP; 8 = 5'-AMP; 9 = 5'-dGMP; 10 = cytidine; 11 = uridine; 12 = deoxycytidine; 13 = 5'-dAMP and thymine; 14 = guanine; 15 = guanosine; 16 = deoxyguanosine; 17 = thymidine; 18 = adenine; 19 = adenosine; 20 = deoxyadenosine. For conditions see Experimental section.

3. Results and discussion

Fig. 1 shows the separation of a mixture of standards comprising 21 individual ribonucleotides, ribonucleosides, deoxyribonucleotides, deoxyribonucleosides and bases. Peaks of the chromatogram were identified by matching their respective retention times with those of standard compounds injected individually. Out of the 21 components, 19 were separated, but 5'-dAMP and thymine did not separate and eluted together as one peak (peak 13). All the compounds were eluted within 18 min. A further 17 min were needed to wash the column and to return it to its initial conditions for the next injection. Nucleotides eluted in the first 7 min, followed by bases and nucleosides, as expected in a reversed-phase HPLC system. If a sample contains nucleotides, or one is interested in the analysis of nucleotides only, the analysis time can be shortened to about 25 min.

The retention times and capacity factors of the 21 compounds are presented in Table 1 and

Table 1

The retention times of 21 nucleotides, nucleosides and purine and pyrimidine bases as separated by HPLC on a Waters Resolve C₁₈ 5- μ m Radial-Pak cartridge

Component	Retention time (min) ^a	Capacity factor ^b
<i>Purine and pyrimidine bases</i>		
Ade	11.85 \pm 0.05	17.52
Cytosine	2.14 \pm 0.02	2.34
Guanine	7.07 \pm 0.03	10.05
Uracil	2.64 \pm 0.02	3.13
Thymine	6.45 \pm 0.05	9.08
<i>Nucleosides</i>		
Adenosine	14.68 \pm 0.05	21.94
Cytidine	3.94 \pm 0.03	5.16
Guanosine	9.55 \pm 0.04	13.92
Uridine	5.25 \pm 0.03	7.20
Deoxyadenosine	16.18 \pm 0.08	24.28
Deoxycytidine	5.73 \pm 0.03	7.95
Deoxyguanosine	10.81 \pm 0.05	15.89
Thymidine	11.26 \pm 0.05	16.59
<i>Nucleotides</i>		
5'-AMP	3.41 \pm 0.02	4.33
5'-CMP	1.00 \pm 0.02	0.56
5'-GMP	1.67 \pm 0.02	1.61
5'-UMP	1.15 \pm 0.02	0.80
5'-dAMP	6.10 \pm 0.03	8.53
5'-dCMP	1.34 \pm 0.02	1.10
5'-dGMP	3.65 \pm 0.02	4.70
5'-dTMP	3.04 \pm 0.02	3.75

^a The data indicate average retention times \pm variation taken from 10 analyses.

^b Capacity factor was calculated as $(t_R - t_0)/t_0$, where t_R is the retention time of solute and t_0 is the retention time of a non-retaining compound (calculated as system void volume/flow-rate); $t_0 = 0.64$ min.

showed high degrees of reproducibility. For compounds eluted in the first few minutes, deviations of retention times were less than 0.03 min. Compounds eluting at later times showed slightly greater deviations, but these were not more than 0.05 min, except for deoxyadenosine, which came out last.

An important factor influencing the separation was control of pH in solvent A, which must be kept at pH 6.30 \pm 0.05. Deviation from this value resulted in overlapping of some peaks. Increasing the flow-rate to 4 ml/min or decreas-

ing it to 0.5 ml/min did not improve peak resolution; the latter had the adverse effect of causing peak broadening. It is unfortunate that the system did not resolve 5'-dAMP and thymine. To resolve these two compounds, it was necessary to elute with solvent A adjusted to pH 6.5. However, under this condition resolution of several other components was lost due to peak overlapping (e.g. 5'-AMP, 5'-dGMP).

Fig. 2 shows the resolution of nucleic acid degradation products in an autolysate of the yeast, *Saccharomyces cerevisiae*. The majority of peaks in the chromatogram were readily identified

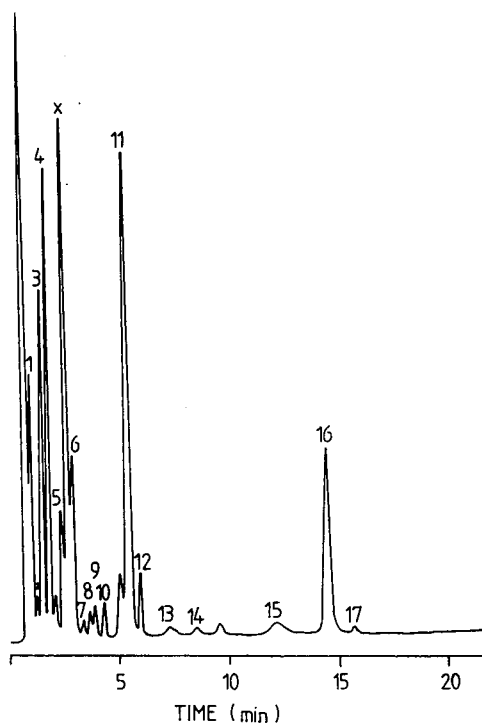


Fig. 2. Chromatogram of an autolysate sample; the autolysate was taken from a sample after cells of *Saccharomyces cerevisiae* had been autolysed at 40°C for 10 days at pH 7.0. Injection volume, 20 μ l; detection wavelength, 254 nm; Peaks: 1 = 5'-CMP; 2 = 5'-UMP; 3 = 5'-dCMP; 4 = 5'-GMP; 5 = cytosine; 6 = uracil; 7 = 5'-dTMP; 8 = 5'-AMP; 9 = 5'-dGMP; 10 = cytidine; 11 = uridine; 12 = deoxycytidine; 13 = guanine; 14 = guanosine; 15 = adenine; 16 = adenosine; 17 = deoxyadenosine. For conditions see Experimental section.

by comparing their retention times with those of the standards. One of the major peaks (denoted as x) did not correspond to any component in the mixture of standards and could be 3'- or 2'-isomers of ribonucleotides.

There are several published methods which can separate ribonucleotides from ribonucleosides and bases [8,14,15]. Also, methods have been described for separation of mixtures of ribonucleotides and deoxyribonucleotides [16,17]. However, these methods cannot separate mixtures of ribonucleotides and ribonucleosides from deoxyribonucleotides and deoxyribonucleosides in one step. To deal with samples that contain all of these components, such as yeast autolysates, group separation has to be carried out first, which can be time-consuming. Methods are known which can separate ribonucleosides from deoxyribonucleosides [18-20], but they cannot separate nucleotides from nucleosides and bases and the above-mentioned disadvantage of group separation also applies to these methods.

The HPLC procedure presented in this paper is a new method that has the capacity to separate a mixture of 21 purine and pyrimidine bases, ribonucleotides, ribonucleosides, deoxyribonucleotides and deoxyribonucleosides. It is fast and retention times have good reproducibility. An additional advantage of the method is that sample preparation (membrane filtration) is simple and quantitative. There is no need for solvent extraction of the sample, as required by many other methods, which is tedious and contributes to poor reproducibility. It has been successfully used for analysing the degradation products of nucleic acid origin in yeast autolysates, and may be used for analysis of similar products in beer, wine and champagne. However, the present method cannot separate different isomers of nucleotides. Methods for such separation are described elsewhere [21]. For the present study, the primary interest is 5'-isomers of nucleotides, which have desirable flavour-enhancing properties [22]. Our study shows that 5'-isomer nucleotides are the major degradation products of nucleic acids during yeast autolysis.

References

- [1] G. Reed and T.W. Nagodawithana, *Yeast Technology*, Van Nostrand, New York, 2nd ed., 1991, p. 369.
- [2] C. Charpentier and M. Feuillat, in G.H. Fleet (Editor), *Wine Microbiology and Biotechnology*, Harwood Academic Publ., Chur, Switzerland, 1993, p. 225.
- [3] J.A. Thorn, *Brew. Dig.*, 46 (1971) 110.
- [4] M. Zakaria and P.R. Brown, *J. Chromatogr.*, 226 (1981) 267.
- [5] P.R. Brown, in P.R. Brown (Editor), *HPLC in Nucleic Acid Research*, Part I, Marcel Dekker, New York, 1984, p. 3.
- [6] A. Fallon, R.F.G. Booth and L.D. Bell, *Applications of HPLC in Biochemistry*, Elsevier, New York, 1987, p. 145.
- [7] R.A. Hartwick and P.R. Brown, *J. Chromatogr.*, 112 (1975) 651.
- [8] R.A. Hartwick, S.P. Assenza and P.R. Brown, *J. Chromatogr.*, 186 (1979) 647.
- [9] J. Boháček, *Anal. Biochem.*, 94 (1979) 237.
- [10] A.A. Miller, J.A. Benvenuto and T.L. Loo, *J. Chromatogr.*, 228 (1982) 165.
- [11] D.L. Ramos and A.M. Schoffstall, *J. Chromatogr.*, 261 (1983) 83.
- [12] H. Yokoi, T. Watanabe and H. Onishi, *Agric. Biol. Chem.*, 51 (1987) 3147.
- [13] W.N. Arnold, in W.N. Arnold (Editor), *Yeast Cell Envelopes: Biochemistry, Biophysics and Ultrastructure*, CRC Press, Cleveland, OH, 1981, p. 129.
- [14] A. Halfpenny and P.R. Brown, *Chromatographia*, 21 (1986) 317.
- [15] E. Nissinen, *Anal. Biochem.*, 106 (1980) 497.
- [16] E.J. Ritter and L.M. Bruce, *Biochem. Med.*, 21 (1979) 16.
- [17] M.B. Cohen, J. Maybaum and W. Sadée, *J. Chromatogr.*, 198 (1980) 435.
- [18] H.J. Breter, G. Seibert and R.K. Zahn, *J. Chromatogr.*, 140 (1977) 251.
- [19] S.P. Assenza, P.R. Brown and A.P. Goldberg, *J. Chromatogr.*, 277 (1983) 305.
- [20] R.P. Singhal and J.P. Landes, *J. Chromatogr.*, 485 (1988) 117.
- [21] A.A. Qureshi, N. Prentice and W.C. Burger, *J. Chromatogr.*, 170 (1979) 343.
- [22] A. Kuninaka, in R. Teranish, R.A. Flath and H. Sugisawa (Editors), *Flavour Research: Recent Advances*, Marcel Dekker, New York, 1981, p. 305.



ELSEVIER

Journal of Chromatography A, 673 (1994) 173–179

JOURNAL OF
CHROMATOGRAPHY A

Determination of barium and strontium in calcium-containing matrices using high-performance chelation ion chromatography

P. Jones*, M. Foulkes, B. Paull

Department of Environmental Sciences, University of Plymouth, Drake Circus, Plymouth PL4 8AA, UK

(First received February 1st, 1994; revised manuscript received March 17th, 1994)

Abstract

High-performance chelation ion chromatography involving dye-coated resins has been used to determine barium and strontium in samples of mineral water and milk powder containing several orders of magnitude higher levels of calcium and other alkali and alkaline earth metals. Detection limits of 0.03 mg dm^{-3} were achieved for both barium and strontium. The technique was used to determine both metals in a river water certified reference material and all results were compared to inductively coupled plasma optical emission spectroscopy producing overall good agreement between the two methods.

1. Introduction

There is a great deal of interest in the determination of barium and strontium in certain environmental and biological samples. The presence of either or both of the above often occurs in samples containing much larger concentrations of alkali and the other alkaline earth metals, which can cause problems in several commonly used analytical techniques.

When using traditional cation-exchange chromatography magnesium elutes first followed by calcium, strontium and finally barium [1]. Due to the longer retention time barium is often broad and therefore the sensitivity compared to the much sharper calcium and magnesium is greatly reduced. The presence of excess calcium or magnesium in the sample matrix can result in large peaks masking the signal for strontium and barium. Dilution of the sample prior to injection

could result in losing the signal for strontium and barium completely. Singh *et al.* [2] illustrated this problem by using a Dionex CS-2 cation-exchange column for the separation and determination of strontium from excess levels of sodium, calcium and magnesium in sub-surface waters. Under the conditions used, strontium eluted last from the column after sodium, calcium and magnesium and gave a broad asymmetrical peak resulting in poor sensitivity.

The determination of barium by other techniques has also given problems. The detection of barium in calcium-containing matrices using atomic absorption spectroscopy has been reported by Jaber and El-Issa [3]. Large interferences were reported due to the CaOH molecular species and solvent extraction to remove the calcium was needed prior to analysis. Jerrow *et al.* [4] illustrated the determination of barium in the presence of large amounts of alkali and alkaline earth metals by direct current plasma atomic emission spectroscopy and showed how

* Corresponding author.

magnesium in the sample greatly reduces the interference effects of calcium and strontium. However, they suggest strict guidelines of matrix matching should be followed if reliable results are to be obtained. The analysis of barium in complex matrices using spectrophotometric methods has been studied by Manna *et al.* [5] with Sulphonazo III used as a complexing agent. The presence of both calcium and strontium in wastewaters studied, resulted in major interferences and the method was concluded to be unsuitable for use with such samples.

A relatively new ion chromatography technique developed at Plymouth, high-performance chelation ion chromatography (HPCIC), has been evaluated for the determination of trace amounts of barium and strontium in environmental samples containing high levels of other alkali and alkaline earth metals, particularly calcium. HPCIC essentially involves chelating functional groups immobilised on a HPLC-grade resin. This can be achieved with chelating dyes which are used to impregnate the resin, producing chelating columns that have been shown to exhibit good separation efficiencies [6]. Retention of metal ions is a function of the relative magnitude of conditional stability constants and the order of retention of most groups of metals is found to be the reverse of that using simple cation-exchange chromatography. Therefore, with HPCIC, barium elutes first before strontium, followed by calcium and magnesium. As barium and strontium elute close to the solvent front, HPCIC produces not only very sharp peaks allowing for greater sensitivity for these two metals, but also baseline resolution completely clear of the massive peaks found in samples containing several orders of magnitude higher levels of calcium and magnesium. Salt ions such as sodium and potassium have very little affinity for the chelation sites of the impregnated resin and pass straight through the column. Therefore the ionic strength of the sample has little or no effect upon the separation.

Two samples of current interest were chosen to evaluate the technique. New proposed EC limits [7] for levels of barium in mineral waters

of 0.7 mg dm^{-3} require a rapid and sensitive method of analysis. Mineral waters often contain up to 300 mg dm^{-3} calcium combined with high levels of magnesium making the determination of low levels of barium and strontium difficult. The determination of strontium in skimmed milk powder was also carried out as the ratio of strontium to calcium of approximately 1:2000 also causes problems with other techniques.

2. Experimental

2.1. Instrumentation

The HPCIC post-column reaction system used is the same as illustrated by Challenger *et al.* [6]. A LKB 2150 HPLC titanium pump (Bromma, Sweden) was used to deliver the eluent. A Constametric model III pump (Laboratory Data Control, Riviera Beach, FL, USA) was used for post-column reagent (PCR) delivery. Injection of the sample was via a steel six-port injector (Rheodyne, Cotati, CA, USA) connected to a $100\text{-}\mu\text{l}$ PTFE sample loop. Post-column detection was achieved by the mixing of the eluent and the PCR at a zero-dead-volume T-piece followed by a $1.4 \text{ m} \times 0.3 \text{ mm}$ I.D. PTFE reaction coil. A spectral array detector (Dionex, Sunnyvale, CA, USA) set at 490 nm was used to detect the eluting metal complexes. A chart recorder (Labdata, Surrey, UK) was used to record the chromatograms.

A Varian Liberty 200 inductively coupled plasma optical emission spectrometry (ICP-OES) system (Melbourne, Australia) was used to compare results with the HPCIC technique. The wavelengths monitored were 407.771 for strontium and 455.403 for barium.

All reagents and samples were stored in acid-washed polypropylene bottles (BDH, Poole, UK).

2.2. Reagents

The reagents used were supplied by BDH except 4-(2-pyridylazo)resorcinol (PAR) and

zinc–ethylenediaminetetraacetic acid (Zn-EDTA) which were obtained from Fluka (Switzerland). Reagents were AnalaR grade unless stated otherwise. All solutions were prepared using distilled and deionised water from a Milli-Q system (Millipore, USA) and degassed using helium before use.

Potassium nitrate (1 M) containing 0.05 M lactic acid was used as the eluent, adjusted to the correct pH using dilute ammonia or nitric acid. The PCR used was a mixture of $2 \cdot 10^{-4}$ M Zn-EDTA, $1.2 \cdot 10^{-4}$ M PAR and 2 M ammonia. PAR alone is insensitive to alkaline earth metals, by adding Zn-EDTA a displacement reaction occurs [8]. The absorbance measured is due to Zn-PAR which has a λ_{max} of 490 nm. Flow-rates for both eluent and PCR were $1 \text{ cm}^3 \text{ min}^{-1}$.

Barium and strontium standards were prepared using barium nitrate and strontium nitrate (BDH).

2.3. Chelating column

The production of high-performance chelating columns is based upon the “dye-coating” techniques described by Jones and co-workers [9–12] in several recent papers. Chelating dye-stuffs are permanently immobilised upon HPLC-grade resins resulting in efficient chelating columns with a working lifetime of over 18 months. For the determination of barium and strontium in mineral waters methylthymol blue {3,3'-bis[N,N-di(carboxymethyl)-aminomethyl]thymol-sulphone-phthalein} (Sigma, UK) was used to impregnate 8.8- μm particle size, 120-Å pore size polystyrene-divinylbenzene neutral hydrophobic resin (Dionex). For the determination of strontium in skimmed milk powder phthalein purple (*o*-cresolphthalein - 3',3'' - bis - methyleneiminodiacetic acid) (Sigma) was used to modify the resin. The resins were impregnated and packed in 10×0.46 cm polyether ether ketone (PEEK) HPLC columns (Alltech, UK).

2.4. Samples

The bottled mineral waters chosen for analysis were used as bought, untreated except for being

thoroughly degassed with helium before being injected. The milk powder was ashed in a nickel crucible (1 g) using a Meker burner and dissolved into 10 cm^3 of dilute nitric acid with heating. The solution was neutralised using dilute ammonia and made up to 20 cm^3 immediately before being analysed.

3. Results and discussion

3.1. Choice of chelating column

Investigations into the dye-coating techniques of Jones and co-workers have resulted in the production of several types of high-performance chelating columns using triphenylmethane- or azo-based chelating dyes. The most efficient separations have been achieved using the triphenylmethane group of dyes to which methylthymol blue and phthalein purple belong. Both dyes contain two iminodiacetic acid functional groups which are the active chelating sites of the immobilised molecule. It is interesting to note that when different dyes containing the same functional coordinating group are compared on impregnated resins, significant differences in metal chelating ability are found. However, this is perhaps not too surprising, as small changes in the basicity of the iminodiacetic acid group could have a marked effect on the metal stability constants. The small variations in chelating ability between dyes can be very useful as there is a large number available, allowing chelating columns to be specifically designed for a particular separation. A good example is reported here, where a much greater degree of separation between strontium and calcium was achieved using the phthalein purple column compared to the methylthymol blue column. Therefore, the phthalein purple column was considered more suitable for samples with extremely high levels of calcium and thus used for the determination of strontium in milk powder. Although the order of separation and selectivity factor between metals remains constant for a particular impregnated dye, the conditional stability constant for a particular metal and

hence the speed of elution is markedly affected by pH. Thus, small changes in pH can be used to “fine tune” the separation.

3.2. Barium in mineral waters

Fig. 1 is a chromatogram showing the separation of four alkaline earth metals in 1 M KNO₃ at pH 7.9 using the methylthymol blue column. The chromatogram shows sharp peaks for barium and strontium eluting before and completely separate from both calcium and magnesium.

Eight brands of mineral waters were analysed. Three of these contained both barium and strontium and relatively high levels of calcium, so these were chosen for quantitative determinations. These were Evian, Highland Spring and Buxton mineral water. Fig. 2 shows a chromatogram of Highland Spring mineral water, a step down in the pH of the eluent was used after the

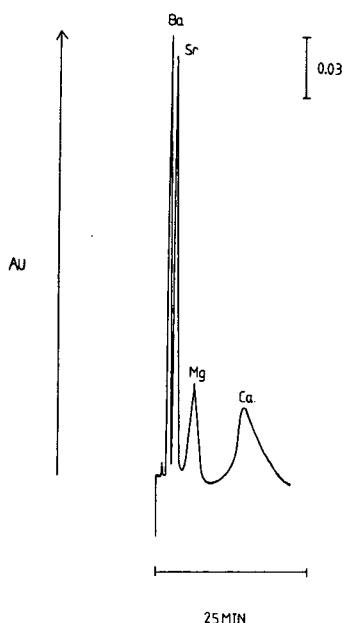


Fig. 1. Chromatogram showing the separation of four alkaline earth metals on a methylthymol blue-impregnated column. Sample: 100-mm³ injection of 10 mg dm⁻³ barium, strontium, magnesium and calcium. Eluent: 1 M KNO₃ with 0.05 M lactic acid (pH 7.9). PCR: $2 \cdot 10^{-4}$ M Zn-EDTA, $1.2 \cdot 10^{-4}$ M PAR and 2 M NH₃.

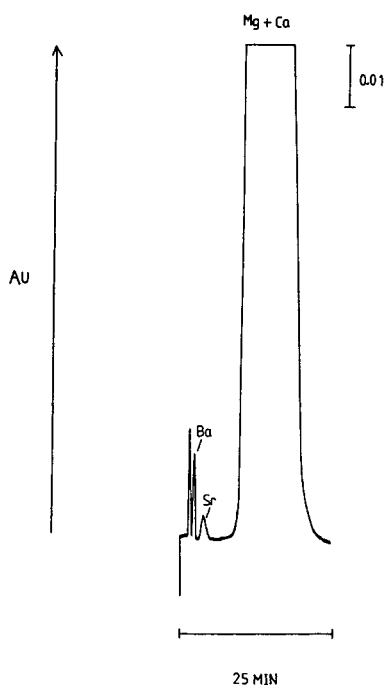


Fig. 2. Chromatogram showing the separation of barium and strontium from magnesium and calcium in Highland Spring mineral water on a methylthymol blue-impregnated column. Sample: 100-mm³ injection. Eluent: 1 M KNO₃ with 0.05 M lactic acid (pH 8.5, stepped down to pH 3.0 after 5 min). PCR as in Fig. 1.

elution of barium and strontium to sweep off calcium and magnesium, thus reducing analysis time. Highland Spring contained the highest levels of barium of the samples analysed, approximately half the proposed new limits. Determination of both barium and strontium was obtained through the method of standard additions to take into account any matrix effects which may affect the slope of the calibration graph. Five additions, ranging from 50 to 250 $\mu\text{g dm}^{-3}$ for barium and 100 to 500 $\mu\text{g dm}^{-3}$ for strontium were used. To produce a 500 $\mu\text{g dm}^{-3}$ strontium addition, 100 mm³ of a 500 mg dm⁻³ strontium standard was added to 100 cm³ of sample, resulting in negligible dilution of the original sample. Linear calibration curves for both metals were achieved using peak heights. Regression values were $r = 0.999$ for barium and $r = 0.998$ for strontium. The precision of the

method was determined with eight repeat injections of a mixed metal spike of 0.4 mg dm^{-3} barium and 0.8 mg dm^{-3} strontium added to Buxton mineral water containing 50 mg dm^{-3} calcium and 20 mg dm^{-3} magnesium, giving R.S.D. values of 3 and 10%, respectively. Using a 200-mm^3 sample loop detection limits of approximately 0.03 mg dm^{-3} for barium and strontium were achieved, calculated as twice the level of baseline noise. Table 1 shows the results from the analysis of a simulated river water certified reference material IAEA/W-4. Although the levels of calcium and magnesium in the river water, 10 and 4 mg dm^{-3} , were less than those found in mineral waters, the ratios of barium and strontium to calcium was still 1:200. The levels of barium and strontium determined compared well with the certified values. The relatively high R.S.D. values of 20% were a reflection of the fact that levels of both metals were close to the detection limits of the method. Fig. 3 shows a chromatogram of the certified reference material showing peaks for barium and strontium close to the limits of detection. ICP-OES was used to compare with all the results obtained using the HPCIC method. Table 2 compares the two sets of results and shows overall good agreement between the two methods.

3.3. Strontium in milk powder

Milk powder contains approximately $12\,000 \text{ mg dm}^{-3}$ calcium and only trace amounts of strontium, resulting in an extremely difficult sample matrix for most methods of analysis. The ashing and acid digestion of 1 g of sample produces a clear digest which was made up to 20 cm^3 , resulting in a 20-fold dilution before in-

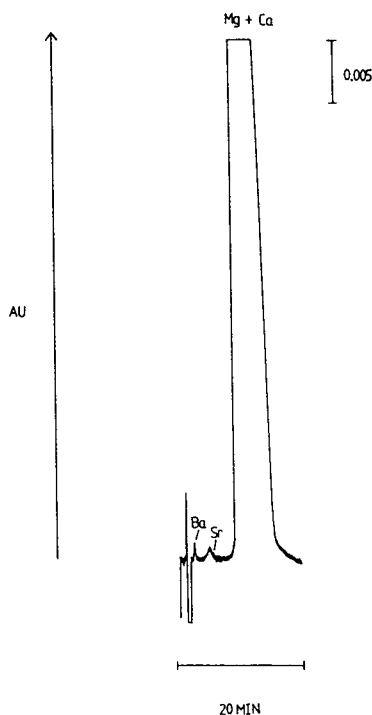


Fig. 3. Chromatogram showing the separation of barium and strontium from magnesium and calcium in fresh river water certified reference material on a methylthymol blue-impregnated column. Sample: 200-mm^3 injection. Eluent as in Fig. 2, PCR as in Fig. 1.

jections. Fig. 4 shows the separation of barium, strontium and calcium using the phthalein purple column at pH 9.8 in 1 M KNO_3 . Magnesium is completely retained at this pH. The chromatogram produced from the injection of the milk powder digest is shown in Fig. 5. In practice the calcium and magnesium can be swept off in a much shorter time using an acid wash. However, in this instance, the calcium peak was allowed to run the full time to show that the huge peak

Table 1
Determination of barium and strontium in simulated fresh water IAEA/W-4 certified standard reference material using HPCIC and ICP-OES

Metal ion	HPCIC	ICP-OES	Certified values
Ba(II)	0.05 (0.01)	0.041 (0.002)	0.052 (0.002)
Sr(II)	0.05 (0.01)	0.053 (0.003)	0.050 (0.003)

Values in mg dm^{-3} (\pm S.D.).

Table 2

Levels of barium and strontium determined in three bottled mineral waters using HPCIC compared with results achieved using ICP-OES

Mineral water	Metal ion	HPCIC	ICP-OES
Evian	Ba(II)	0.09 (0.01)	0.078 (0.003)
	Sr(II)	0.39 (0.01)	0.370 (0.005)
Buxton	Ba(II)	0.11 (0.02)	0.137 (0.015)
	Sr(II)	0.84 (0.07)	0.585 (0.023)
Highland Spring	Ba(II)	0.33 (0.04)	0.364 (0.016)
	Sr(II)	0.25 (0.08)	0.268 (0.010)

Values in mg dm^{-3} (\pm S.D.).

would cause serious problems with normal ion chromatography, where the order of elution would be reversed. The retention time for the large calcium peak is less than that for calcium shown in Fig. 4. This is due to the massive excess of calcium filling most of the chelation sites at the beginning of the column and thus speeding up the elution of the metal ions. This emphasises the requirement for close matrix matching of standards or standard addition.

For the reasons discussed above, standard addition was used to determine the levels of strontium present in the milk digest. The level of strontium found in the milk powder digest was

0.15 mg dm^{-3} which corresponds to 3.0 mg dm^{-3} in the actual milk powder. Barium was not quantitatively determined as after the 20-fold dilution of the milk powder the level present fell below the working detection limit with a 100-mm^3 sample loop. Linear results were achieved with a regression value of $r = 0.998$. ICP-OES was again used to compare methods, the results of which are shown in Table 3. Good agreement

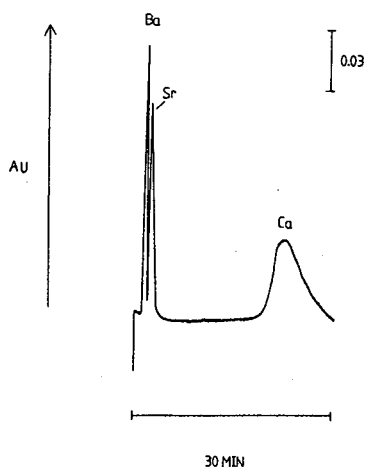


Fig. 4. Chromatogram showing the separation of three alkaline earth metals on a phthalein purple-impregnated column. Sample: 100-mm^3 injection of 5 mg dm^{-3} barium and strontium and 10 mg dm^{-3} calcium. Eluent: 1 M KNO_3 with 0.05 M lactic acid (pH 9.8). PCR as in Fig. 1.

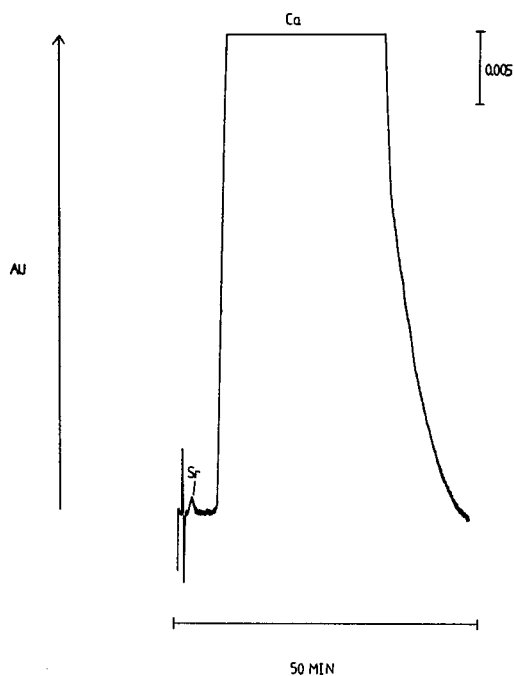


Fig. 5. Chromatogram showing the separation of strontium from calcium in milk powder digest on a phthalein purple-impregnated column. Sample: 100-mm^3 injection. Eluent: 1 M KNO_3 with 0.05 M lactic acid (pH 10.2). PCR as in Fig. 1.

Table 3
Determination of strontium in milk powder digest using HPCIC compared with results achieved using ICP-OES

Metal ion	HPCIC	ICP-OES
Ba(II)	ND ^a	0.027 (0.002)
Sr(II)	0.15 (0.03)	0.125 (0.005)

Values in mg dm⁻³ (± S.D.).

^a Below detection limit.

between the two methods was achieved, although the R.S.D. value for the chelation ion chromatography method was higher than those for ICP-OES, again reflecting the closeness of the signal to the detection limit in HPCIC compared to ICP-OES.

4. Conclusions

The HPCIC technique as outlined in this paper provides a quick and inexpensive solution to the determination of both barium and strontium in calcium- and magnesium-containing matrices. The results achieved for mineral waters and milk powder compared well with ICP-OES. The production of chelating columns is relatively simple and there is a large number of chelating dyes available to produce a range of separation characteristics, the most suitable of which can be chosen to suit a particular sample. The system can also be readily adapted to run as a on-line monitoring system and clearly will serve as a

useful alternative to atomic spectrophotometric techniques.

Acknowledgements

The authors wish to thank the Science and Engineering Research Council (SERC) for financial support and Dionex (UK) Ltd. for sponsorship through the CASE award scheme.

References

- [1] J.S. Fritz, D.T. Gjerde and C. Pohlandt, *Ion Chromatography*, Hüthig, Heidelberg, 1982, p. 156.
- [2] R.P. Singh, E.R. Pambid, P. Debayle and N.M. Abbas, *Analyst*, 116 (1991) 409–414.
- [3] A.M.Y. Jaber and M.Y.S. El-Issa, *Analyst*, 106 (1981) 939–943.
- [4] M. Jerrow, L. Marr and M. Cresser, *Analyst*, 116 (1991) 141–144.
- [5] F. Manna, F. Chimenti, A. Bolasco and A. Fulvi, *Talanta*, 39 (1992) 875–878.
- [6] O.J. Challenger, S.J. Hill, P. Jones and N.W. Barnett, *Anal. Proc.*, 29 (1992) 91–93.
- [7] *Chem. Br.*, 29 (1993) 855.
- [8] M.D. Arguello and J.S. Fritz, *Anal. Chem.*, 49 (1977) 1595–1598.
- [9] P. Jones and G. Schwedt, *J. Chromatogr.*, 482 (1989) 325–334.
- [10] P. Jones, O.J. Challenger, S.J. Hill and N.W. Barnett, *Analyst*, 117 (1992) 1447–1450.
- [11] O.J. Challenger, S.J. Hill and P. Jones, *J. Chromatogr.*, 639 (1993) 197–205.
- [12] B. Paull, M. Foulkes and P. Jones, *Analyst*, 119 (1994) in press.



ELSEVIER

Journal of Chromatography A, 673 (1994) 181–209

JOURNAL OF
CHROMATOGRAPHY A

Pair-wise interactions by gas chromatography

IV. Interaction free enthalpies of solutes with trifluoromethyl-substituted alkanes

K.S. Reddy, R. Cloux, E.sz. Kováts*

Laboratoire de Chimie Technique, Ecole Polytechnique Fédérale de Lausanne, CH-1015 Lausanne, Switzerland

(First received December 18th, 1993; revised manuscript received February 28th, 1994)

Abstract

Two polar-type liquids were used as stationary phases, one being a mono(trifluoromethyl) (MTF) and the other a tetrakis(trifluoromethyl) (TTF) derivative of the parent branched alkane, $C_{78}H_{158}$ (C78). Gas chromatographic data for about 160 molecular probes were measured on pure MTF and on C78–TTF mixtures at several temperatures. It was found that data on MTF are the same as data on a C78–TTF mixture with $\varphi_{TTF} = 0.25$, both melts having the same molar concentration of trifluoromethyl groups. Interaction free enthalpies were calculated from data measured on C78–TTF mixtures between the probe and a trifluoromethyl group, both at infinite dilution.

1. Introduction

The objective of this project described in detail in Part I [1], is the determination of interaction free enthalpies between solutes at infinite dilution and an interacting group also at infinite dilution in an alkane solvent. A series of interacting groups are proposed for characterizing different types of intermolecular forces such as dispersion- and polar-type interactions. The measuring system consists of a family of isosteric and isomorphous solvents, L, shown in Fig. 1, having molecules of the same size and form, and suitable for use as stationary phases in gas chromatography. The family includes a standard paraffin, A = C78 ($C_{78}H_{158}$), and a series of polar compounds, P, in which a methyl or an ethyl group is substituted for an interacting

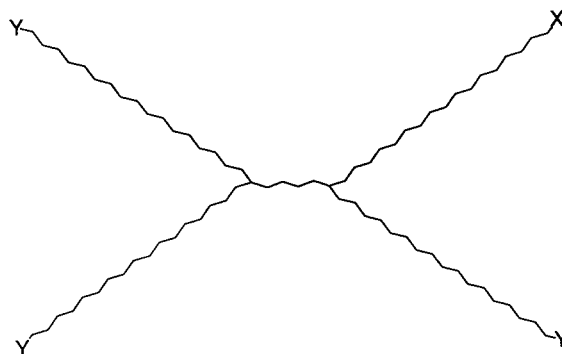


Fig. 1. Structure of the applied stationary phases: C78: X = Y = CH_3 ; MTF (monotrifluoromethyl): X = CF_3 , Y = CH_3 ; TTF (tetrakistrifluoromethyl): X = Y = CF_3 .

group, X. The synthesis of members of this family was reported in Part III [2]. With these stationary phases at hand, the method consists in measuring gas chromatographic data for a solute on a series of A–P mixtures at several tempera-

* Corresponding author.

tures, to convert these data into standard chemical potentials and to extrapolate the results to infinite dilution of the interacting group, $[X] \rightarrow 0$, with the aid of simple laws of regular mixtures [3,4]. In Part I the method was described in detail and was shown to give the desired data on the example of a stationary phase, P, having primary hydroxyl, POH, as an interacting group, X. The results have been shown (Part II) [5] to compare well with spectroscopic and calorimetric measurements of hydrogen bonding interactions.

In this paper we report the interaction free enthalpies of a series of chosen solutes at infinite dilution with an "alone-standing" trifluoromethylalkane "dissolved" in an alkane solvent. Such a group is thermostable and chemically inert. Bonded to an alkane chain, the group has a relatively high dipole moment (*ca.* 2.3 D [6]), hence it was hoped that such a stationary phase would measure the interaction of a solute with a permanent dipole [7–9]. It will be seen that the situation is more complicated and at present we cannot offer a satisfactory interpretation of the results.

Interaction free enthalpies between solutes and trifluoromethylalkane groups are considerably weaker than those between solutes and primary hydroxyl functions. Therefore, for this study we considered the question of whether a stationary phase substituted with more than one weakly interacting group, such as tetrakis(trifluoromethyl) (TTF) ($X = Y = CF_3$ in Fig. 1) may be applied for experimentation. In order to answer this question, data were measured on C78–TTF mixtures and the results were represented with the aid of Eq. 5 as a function of the composition. It will be shown that results on an appropriate C78–TTF mixture are very close to those measured on a pure mono(trifluoromethyl) (MTF) derivative ($X = CF_3$, $Y = CH_3$ in Fig. 1).

2. Theoretical

Detailed derivation of the necessary equations was given in Part I. A short summary of the essential equations is presented here for understanding the Experimental section and Table 6.

The molal Henry coefficient of a solute, g_j ,

can be calculated from the specific retention volume, $V_{g,j}$ (not reduced to 0°C) by using the equation

$$V_{g,j} = V_{N,j}/w_L = \mathcal{R}T/1000g_j \quad (1)$$

where $V_{N,j}$ is for the net retention volume at temperature T (K), w_L is the mass of the stationary liquid $L = A, P$ or $A-P$, in the column, and \mathcal{R} ($\text{cm}^3 \text{ atm mol}^{-1} \text{ K}^{-1}$; 1 atm = 101 325 Pa) is the universal gas constant. The standard chemical potential of a solute, j , with reference to the (ideal) gas phase is given by

$$\Delta\mu_j^L = RT \ln[g_j/(\text{atm kg mol}^{-1})] \quad (2)$$

By assuming that the partial molar heat capacity difference of the solute between the liquid and gas phase, $\Delta C_{P,j}^L$, is constant in the experimental temperature domain of *ca.* 100 K (Kirchhoff's approximation), the temperature dependence of the standard chemical potential can be described with adequate precision by

$$\Delta\mu_j^L = \Delta H_j^L - T \Delta S_j^L + \Delta C_{P,j}^L \left[T - T^\dagger - T \ln\left(\frac{T}{T^\dagger}\right) \right] \quad (3)$$

where ΔH_j^L and ΔS_j^L are the partial molar enthalpy and entropy difference, respectively, at the standard temperature T^\dagger . The standard chemical potential difference of a solute, j , in a liquid, L, with reference to the ideal dilute solution in the standard alkane, $A = C78$, is given by

$$\Delta\mu_j^L = \Delta\mu_j^L - \Delta\mu_j^A = \Delta H_j^L - T \Delta S_j^L + \Delta C_{P,j}^L \left[T - T^\dagger - T \ln\left(\frac{T}{T^\dagger}\right) \right] \quad (4)$$

If the liquid, L, is a regular mixture of A and P, then the standard chemical potential of the solute, j , as a function of the composition is given by the relationship

$$\Delta\mu_j^{A/P} = \varphi_P \Delta\mu_j^P + \varphi_A \varphi_P m_j^{A/P} \quad (5)$$

where φ_P is the volume fraction of P in the binary A–P mixture ($\varphi_A + \varphi_P = 1$) and $\Delta\mu_j^P$ is the standard chemical potential of the solute in pure P ($\varphi_P = 1$) with reference to A ($\varphi_P = 0$). In mixtures of the isosteric solvents, A and P, the

following relationship holds for the excess chemical potential $m_j^{A/P}$:

$$m_j^{A/P} = h_j - T s_j \quad (6)$$

If the specific volume of an A–P mixture can be given as a linear combination of those of the individual components (no excess volume on mixing), the relationship between the volume fraction, φ_P , and the molar concentration of the interacting group, $[X]$, is given by

$$\varphi_P = v_P[X]/1000n \quad (7)$$

where v_P (ml mol^{-1}) is the molar volume of P at temperature T and n is the number of interacting groups, X, in the molecule ($n = 1$ for MTF and $n = 4$ for TTF). Use of Eqs. 5 and 7 gives for the interaction free enthalpy of the solute j in the A–P mixture at ideal dilution

$$\begin{aligned} \Delta' \mu_j^{\text{idX}} &\equiv \left(\frac{\partial \Delta \mu_j^{A/P}}{\partial [X]} \right)_{T, [X]=0} \\ &= \left(\frac{\partial \Delta \mu_j^{A/P}}{\partial \varphi_P} \right)_{T, \varphi_P=0} \left(\frac{\partial \varphi_P}{\partial [X]} \right)_T \\ &= (\Delta \mu_j^P + m_j^{A/P}) v_P / 1000n \end{aligned} \quad (8)$$

Eq. 8 is the necessary relationship for calculating the interaction free enthalpy of the group X at infinite dilution with a solute also at infinite dilution, with reference to the alkane solvent. The meaning and use of Eq. 8 are illustrated in Fig. 2 on the example of three solutes, 6 = *n*-hexane, 7 = *n*-heptane and j = butyronitrile in mixtures of C78 and TTF. Note that in Fig. 2 chemical potentials are shown with reference to the gas phase (Δ) and not with reference to the dilute solution in C78 (Δ').

Chromatographic data for solutes other than *n*-alkanes were determined on the retention index scale. Let us recall that the retention index of a solute, j , is a measure of its standard chemical potential on a scale by the standard chemical potentials of the *n*-alkanes:

$$\begin{aligned} I &= 100 \frac{\Delta \mu_j^L - \Delta \mu_z^L}{\Delta \mu_{z+1}^L - \Delta \mu_z^L} + 100z \\ &= 100 \frac{\delta \mu_{j/z}^L}{\delta \mu_z^L} + 100z \end{aligned} \quad (9)$$

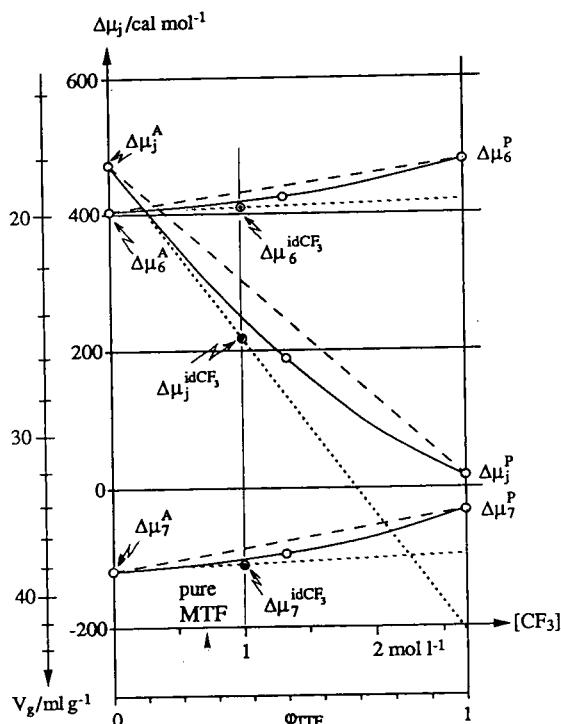


Fig. 2. Dependence of the standard chemical potential of a solute on composition in C78–TTF mixtures illustrated on the example of 6 = *n*-hexane, 7 = *n*-heptane and j = butyronitrile at 130°C. V_g is the specific retention volume, φ_{TTF} is the volume fraction of TTF and $[CF_3]$ is the molar concentration of trifluoromethyl groups in the liquid mixture applied as stationary phase. Reference state for all data: ideal gas in equilibrium with the stationary liquid. In Table 6 data are listed with reference to those in C78, *i.e.*, all data are equal to zero at $\varphi_{\text{TTF}} = [CF_3] = 0$.

where δ designates the difference between the standard chemical potential of two substances in the same solvent. In our mixtures of similar solvents the retention index can be given by the following approximation:

$$\Delta I_j^{A/P} = I_j^{A/P} - I_j^A = \varphi_P \Delta I_j^P + \varphi_A \varphi_P i_j^{A/P} \quad (10)$$

where

$$\Delta I_j^P = \Delta I_{130,j} + \Delta A_{T,j} \Delta T + \Delta A_{\text{TT},j} \Delta T^2 \quad (11)$$

and

$$i_j^{A/P} = A_{L,j} + A_{\text{LT},j} \Delta T \quad (12)$$

and the other symbols are as before. Using Eqs. 7 and 10, the retention index difference of a

solute at infinite dilution of the interacting group X in A is given by

$$\left(\frac{\partial \Delta I_j^{A/P}}{\partial [X]}\right)_{T,[X]=0} = (\Delta I_j^P + i_j^{A/P})v_P/1000n \quad (13)$$

Note that, as shown in ref. 1, the retention index of solute, j , in a hypothetical ideal mixture of A and P is given by

$$\begin{aligned} I_j^{A/idX} &= I_j^A + \left(\frac{\partial \Delta I_j^{A/P}}{\partial [X]}\right)_{T,[X]=0} \frac{[X]}{1 + [X]\kappa} \\ &= I_j^A + \Delta' I_j^{idX} \end{aligned} \quad (14)$$

with

$$\kappa = (\delta' \mu_z^{idX} - \delta' \mu_z^A) / \delta \mu_z^A \quad (15)$$

where $\delta' \mu_z^A$ and $\delta' \mu_z^{idX}$ are the values of the slope of the function $\delta \mu_z^{A/idX}([X])$ at $[X] = 0$ and 1 mol l^{-1} , respectively. In the case of C78–TTF mixtures, the value of κ is of the order of 0.02 l mol^{-1} , and consequently the value of the correcting factor in Eq. 14 is of the order of 0.98.

3. Experimental

3.1. Materials

Solutes were research-grade compounds from Fluka (Buchs, Switzerland). The preparation of the stationary liquids, 19,24-dioctadecyldotetracontane (C78) and 1,1,1-trifluoro-19,24-dioctadecyldotetracontane (MTF) was reported previously [2,10]. The stationary liquid TTF was prepared from dimethyl adipate (from Fluka) and 18,18,18-trifluorooctadecyl bromide (synthesized following ref. 11) in an analogous procedure to that described previously [10] as follows.

19,24-Bis(18,18,18-trifluorooctadecyl)-1,1,1,42,42,42-hexafluorodotetracontane-19,24-diol (TTF-diol)

In a 250-ml three-necked round-bottomed flask, Mg (2.40 g, 100 mmol) was covered with tetrahydrofuran (THF) (20 ml) in an argon atmosphere, then 1,2-dibromoethane (0.94 g, 5.0 mmol) was added (activation of Mg). When

evolution of ethylene had stopped, first a solution of 18,18,18-trifluorooctadecyl bromide (15.5 g, 40.0 mmol) in THF (40 ml) was added dropwise and the mixture was heated at reflux for 3.0 h. At this temperature, a solution of dimethyl adipate (1.57 g, 9.0 mmol) in THF (10 ml) was added dropwise (*ca.* 20 min.). The mixture was refluxed for a further 2.0 h and allowed to stand overnight at room temperature. After hydrolysis with saturated aqueous NH_4Cl (50 ml), the aqueous phase was extracted with cyclohexane (100 ml), the combined organic phase was dried (Na_2SO_4) and the solvent was removed in a rotary evaporator. The residue (13.85 g) was dissolved in cyclohexane (40 ml) and filtered on silica gel (100 g). With cyclohexane (600 ml) as eluent, a mixture of 1,1,1-trifluorooctadecane and 1,1,1,36,36,36-hexafluorohexatriacontane was eluted (3.13 g), then with cyclohexane–diethyl ether (50:50) (500 ml) 10.39 g of crude TTF-diol. The latter fraction was recrystallized from ethanol–cyclohexane (90:10) (300 ml) at 5°C to give 9.70 g (80%) of pure TTF-diol as a white powder, m.p. $44\text{--}45.5^\circ\text{C}$. IR (CCl_4 , CS_2): $\nu = 3620, 2920, 2860, 1465, 1390, 1255, 1145, 840, 720, 655 \text{ cm}^{-1}$. ^1H NMR (C^2HCl_3 , TMS): $\delta = 1.27$ (m, 126H), 1.55 (m, 12H), 2.06 ppm (m, 8 protons). ^{13}C NMR (C^2HCl_3 , TMS): $\delta = 21.84$ (q, $J = 2.7$), 23.52, 24.14, 28.71, 29.17, 29.35, 29.55, 29.68, 30.32, 33.76 (q, $J = 28$), 39.35, 74.40, 127.31 ppm (q, $J = 276 \text{ Hz}$).

19,24-Bis(18,18,18-trifluorooctadecyl)-1,1,1,42,42,42-hexafluorodotetracontane (TTF)

In a 250-ml round-bottomed flask equipped with a Dean–Stark trap, TTF-diol (9.62 g, 7.16 mmol) and *p*-toluenesulphonic acid monohydrate (0.14 g, 0.74 mmol) were dissolved in benzene (100 ml). The reaction mixture was heated at reflux for 3.0 h, then it was allowed to cool to room temperature and the acid was extracted with saturated aqueous NaHCO_3 (50 ml). The aqueous phase was extracted with hexane (50 ml), the combined organic phase was dried (Na_2SO_4) and the solvent was removed in a rotary evaporator. The residue (9.37 g) was dissolved in hexane (50 ml) and filtered on a

silica gel (100 g) column. With hexane (700 ml) were eluted 6.04 g of a mixture of 19,24-bis(18,18,18-trifluorooctadecyl)-1,1,1,42,42,42-hexafluorodotetraconta-A,B-dienes with A = 18 or 19 and B = 23 or 24. This TTF-dienes mixture was dissolved in cyclohexane (400 ml), transferred into a stainless-steel autoclave and 10% Pd-C (0.55 g) was added. The mixture was hydrogenated at 40°C and 10 bar H₂ pressure for 18 h. The catalyst was filtered on silica gel (20 g), then eluted with additional cyclohexane (100 ml). After removal of the solvent in a rotary evaporator, the crude TTF (6.04 g) was dissolved in a mixture of absolute ethanol (100 ml)-cyclohexane (40 ml) at 45°C and the product was crystallized at 5°C. The white crystalline powder was filtered, washed with a cold mixture of absolute ethanol (50 ml)-cyclohexane (20 ml) and finally dried in air to give 5.82 g (62%) of pure TTF, m.p. 54.5–57.5°C. IR (CCl₄, CS₂): $\nu = 2920, 2850, 1465, 1385, 1255, 1145, 840, 720, 655 \text{ cm}^{-1}$. ¹H NMR (C²HCl₃, TMS): $\delta = 1.27$ (m, 126H), 1.56 (m, 12H), 2.06 ppm (m, 8 protons). ¹³C NMR (C²HCl₃, TMS): $\delta = 21.88$ (q, $J = 2.8$), 26.81, 27.24, 28.75, 29.21, 29.40, 29.59, 29.66, 29.75, 30.21, 33.80 (q, $J = 28$), 33.85, 37.52, 127.34 ppm (q, $J = 276 \text{ Hz}$).

Densities

Densities were measured on samples of about 2 g with an ASTM Model 941/78 pycnometer from Schmizo (Zofingen, Switzerland) at 10 K intervals in the temperature range 80–200°C. Eq. 16 was fitted on the experimental points, cor-

rected for vacuum, by linear regression:

$$\begin{aligned} \ln \rho_L &= \ln M_L - \ln v_L \\ &= \ln \rho^\dagger - \alpha^\dagger \Delta T - B \Delta T^2 \end{aligned} \quad (16)$$

where ρ^\dagger is the density and α^\dagger is the isobaric coefficient of thermal expansion at the standard temperature $T^\dagger = 130.0 + 273.15 = 403.15 \text{ K}$ and $B = (1/2)(d\alpha/dT)$ [12]. Coefficients of Eq. 16 for the stationary liquids are listed in Table 1. Fig. 3 shows that the ratio of the molar volumes of the stationary phases C78–MTF and C78–TTF is reasonably near unity over the whole temperature range.

Support

For the preparation of the support, a batch of Chromosorb G HP from Supelco (Bellefonte, PA, USA) was sieved and the fraction with particle diameter 150–180 μm was deactivated

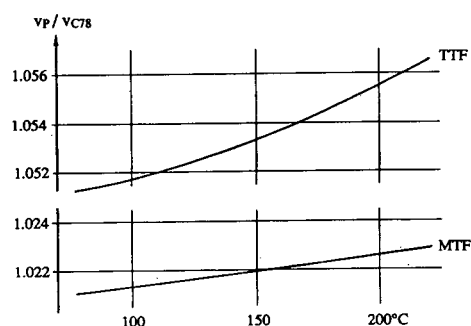


Fig. 3. Ratio of the molar volume of the P and C78 stationary phases as a function of temperature. P = MTF and TTF.

Table 1
Physical properties of the stationary phases

L	M.p.	<i>M</i>	ρ^\dagger	v^\dagger	$\alpha^\dagger \cdot 10^4$	$B \cdot 10^7$	σ	
Symbol	Formula	(°C)	(g mol ⁻¹)	(g cm ⁻³)	(cm ³ mol ⁻¹)	(K ⁻¹)	(K ⁻²)	
C78	C ₇₈ H ₁₅₈	69–75	1096.1	0.7714	1420.9	7.62	1.26	0.0004
MTF	C ₇₇ H ₁₅₅ CF ₃	69–74	1150.1	0.7922	1451.8	7.74	1.29	0.0007
TTF	C ₇₄ H ₁₄₆ (CF ₃) ₄	54–58	1312.0	0.8772	1495.7	7.92	2.54	0.0008
Δ_{95}				± 0.00009	± 0.17	± 0.34	± 0.93	

M = Molar mass; ρ^\dagger , α^\dagger and *B* = regression coefficient of Eq. 16 for the calculation of the density in the temperature range 80–210°C; v^\dagger = molar volume at the standard temperature $T^\dagger = 403.15 \text{ K}$. Data for C78 are from ref. 12.

by treatment with trimethyl(dimethyl-amino)silane (Fluka) at 250°C as described in ref. 1, where the preparation of column packings is also given. Columns (coiled Pyrex tubes, 330 cm × 0.40 cm I.D.) were weighed before and after packing; the mass difference gave the amount of stationary phase in the column. Column characteristics are given in Table 2. Columns were stored under argon. Two series of columns, (a) and (b), were prepared independently for each stationary liquid in order to estimate the importance of weighing errors.

3.2. Apparatus

Details of the gas chromatograph used for the determination of retention were presented previously [1,13]. In summary, a modified Packard-Becker (Delft, Netherlands) Model 439 gas chromatograph equipped with two thermal conductivity detectors was used. The temperature in the oven was measured with a Pt sensor (100 Ω; DIN 43710) and a measuring device from Systemtechnik (Lidingö, Sweden) Model S 1220. The Pt sensor was calibrated by the Eidg. Amt für Messwesen (Berne, Switzerland) between 0 and 400°C with a precision of ±0.1 K. The temperature gradient in the oven was measured with chromel–alumel thermocouples at eight points. The mean column temperature was calcu-

lated by considering the temperature gradient as described in ref. 14. IR spectra were recorded on a Perkin-Elmer (Norwalk, CT, USA) Model 684 spectrophotometer. ¹H NMR spectra were recorded at 200 MHz and ¹³C NMR spectra were measured at 50 MHz on a Model AC-P 200 spectrometer from Bruker (Spectrospin, Fällanden, Switzerland).

3.3. Retention data

Determination of retention data was described in detail previously [1,13]. In summary, the helium carrier flow was regulated with a Model 5850TR flow controller (Brooks, Veenendaal, Netherlands); flow-rates were measured by means of a soap-film flow meter; inlet and outlet pressures were measured with a Model 710B precision device (Heise, Bassweiler, Germany). Retention time was determined at the peak maximum with a Model 3396A integrator (Hewlett-Packard, Palo Alto, CA, USA). Neon was used for the determination of the hold-up time. Inlet pressures never exceeded 1.5 bar, and it was assumed that gas-phase imperfections were negligible. The overall reproducibility of the retention volume of neon was better than 1%. Retention data were measured at 20 K intervals between 90 and 210°C at experimental temperatures as near as possible to the envisaged nominal temperature. The experimental temperature did not change by more than 0.2 K during a working day. The first, last and the mid-day chromatograms of a working day were for a mixture of *n*-alkanes, C_zH_{2z+2}, always containing the alkanes with *z* = 5–10. Retention indices of all solutes were evaluated with the average net retention time of the alkanes if their individual values did not deviate by more than 1%. Otherwise, data for the working day were rejected.

Table 2
Characteristics of the chromatographic columns

Column	Series	100φ _p (%)	w _L (g)	P _L (%)
C78 ^a			2.101	6.81
MTF	(a)		1.771	6.13
	(b)		1.695	6.10
C78-TTF	(a)	50.0	1.946	6.04
	(b)	50.0	1.895	5.89
TTF	(a)		1.889	6.12
	(b)		1.819	5.97

φ_p = Volume fraction of the polar solvent in the A–P mixture at 130°C; w_L = mass of the stationary liquid in the column; P_L = mass percentage of L of the packing (100w_L/total mass).

^a Data reported in Table 6 were measured on this column.

Standard chemical potentials

After having measured all data on a given column, specific retention volumes of *n*-alkanes were converted into standard chemical potentials (see Eq. 2). With data determined near a given nominal temperature, the following average was

calculated:

$$\Delta\mu_z(\bar{T}_{\text{exp}}) = [\Delta\mu_z(T_{\text{exp},1}) + \dots + \Delta\mu_z(T_{\text{exp},n})]/n \quad (17)$$

where $T_{\text{exp},i}$ is the experimental temperature of the i th determination near a nominal temperature, n is the number of determinations and

$$\bar{T}_{\text{exp}} = (T_{\text{exp},1} + \dots + T_{\text{exp},n})/n \quad (18)$$

A quadratic regression was now fitted to every data set for an alkane measured on the same stationary liquid to give the dependence of the chemical potential on temperature, $\Delta\mu_z(T)$. Chemical potentials measured at \bar{T}_{exp} were then corrected to T_{nom} by using the first derivative of the quadratic regression.

Retention indices

Retention indices at nominal temperatures were calculated by an analogous iterative procedure. All successive calculations are based on these corrected data. They will be referred to as “experimental retention data”.

Retention data on MTF columns

Specific retention volumes of n -alkanes were determined on both series of MTF columns; they were systematically lower on columns of series (b) by about 1% (weighing error). Experimental standard chemical potentials were calculated for both series of columns for every alkane at every nominal temperature and the average of the data obtained on both columns was used for further calculations.

Correction for weighing errors on TTF and C78/TTF columns

On columns of series (a), data were determined at all temperatures. On columns of series (b), specific retention volumes of n -alkanes were determined at 90, 130 and 170°C only. Assuming that specific retention volumes differ on both series of columns owing to weighing errors by a factor $f = V_g^{(b)}/V_g^{(a)}$, the difference between the standard chemical potentials on the two columns is given by

$$RT \ln f = \Delta\mu_z^{(a)} - \Delta\mu_z^{(b)} \quad (19)$$

The best values of $RT \ln f$ were deduced from alkane data at the three temperatures, then data on column of series (a) were corrected by $0.5RT \ln f$. Values of $RT \ln f$ are given in Table 3.

3.4. Solution data for n -alkanes as a function of the factors T (temperature), L (composition of the liquid stationary phase) and Z (carbon number of the n -alkane)

C78–TTF: pentane–decane

Standard chemical potentials of n -alkanes, C_zH_{2z+2} with $z = 5–10$, were determined on two stationary phases ($\varphi = 0.5$ and 1) in the temperature range 90–210°C at 20 K intervals. Inclusion of data from ref. 1 for C78 gave a set of $6 \times 3 \times 7 = 126$ data points. The variance analysis of the influence of the factors T , L and Z on the standard chemical potentials of n -alkanes is shown in Table 4. The analysis refers to the description of the experimental space by Eq. 20 where $P_X^{(1)}$ is an orthogonal polynomial of the

Table 3
Average ratio of specific retention volumes on columns of series (a) and (b) [$f = V_g^{(b)}/V_g^{(a)}$] and the corresponding corrections to add to standard chemical potentials determined on columns of series (a)

L	f	$0.5RT \ln f$ (cal mol ⁻¹)						
		90°C	110°C	130°C	150°C	170°C	190°C	210°C
C78–TTF	0.992	-2.8	-2.9	-3.1	-3.2	-3.4	-3.5	-3.7
TTF	1.014	+4.9	+5.2	+5.5	+5.7	+6.0	+6.3	+6.6

Table 4

Analysis of variance of the set of 126 standard chemical potentials of the *n*-alkane solutes with $5 \leq z \leq 10$ in the temperature range 90–210°C at three compositions of the C78–TTF mixture

Source	<i>SQ</i>	ϕ	<i>V'</i>	<i>F</i>	Sign. (%)	$b_x^{(i)}$	Function
<i>X</i>	(<i>i</i>) ^a						
$\Delta\bar{\mu}$	(0)					22.0	$\Delta\mu_0^{+,A}$
<i>T</i>	(1)	68 516 332.2	1	id	$4.45 \cdot 10^5$	0.01	ΔS_0^A
	(2)	40 197.9	1	id	$2.61 \cdot 10^2$	0.01	$\Delta C_{P,0}^A$
	(res. <i>T</i> *)	1 430.1	4	357.5	2.32	20)	
<i>L</i>	(1)	181 025.0	1	id	$1.17 \cdot 10^3$	0.01	$\Delta\mu_0^{+,P}$
	(2)	3 908.9	1	id	$2.54 \cdot 10^1$	0.1	$m_0^{+,A/P}$
<i>TL</i>	(1,1)	439.8	1	id	2.85	10	ΔS_0^P
	(1,2)	466.9	1	id	3.03	10	$S_0^{A/P}$
	(2,1)	186.2	1	id	1.21	20	$\Delta C_{P,0}^P$
	(res. <i>TL</i> *)	573.1	9	63.7	0.41	–)	
1st res. ^a	($=\Sigma X^*$)	2 003.2	13	154.1			
<i>Z</i>	(1)	89 130 113.9	1	id	$7.18 \cdot 10^6$	0.01	$\delta\mu_z^{+,A}$
	(2)	14 911.3	1	id	$1.20 \cdot 10^3$	0.01	4.361
	(3)	65.6	1	id	$5.28 \cdot 10^1$	5	–0.220
	(res. <i>Z</i> **)	147.9	2	74.0	5.95	5)	
<i>TZ</i>	(1,1)	722 289.8	1	id	$5.82 \cdot 10^4$	0.01	δS_z^A
	(2,1)	4 374.4	1	id	$3.52 \cdot 10^2$	0.01	$\delta C_{P,z}^A$
	(res. <i>TZ</i> **)	666.8	28	23.8	1.92	5)	
<i>LZ</i>	(1,1)	9 717.1	1	id	$7.82 \cdot 10^1$	0.01	$\delta\mu_z^{+,P}$
	(2,1)	492.9	1	id	$3.97 \cdot 10^1$	0.01	$\delta m_z^{+,A/P}$
	(res. <i>LZ</i> **)	90.0	8	11.3	0.91	–)	
<i>TLZ</i>	(1,1,1)	13.6	1	id	1.10	–	δS_z^P
	(2,1,1)	6.7	1	id	0.54	–	$\delta C_{P,z}^P$
	(1,2,1)	92.5	1	id	7.45	1	$\delta S_z^{A/P}$
	(res. <i>TLZ</i> **)	275.4	57	4.8	0.39	–)	
2nd res. ^b	($=\Sigma X^{**}$)	1 180.1	95	12.4			

The source of variance is related to orthogonal terms in Eq. 20. $X^{(i)}$ is the systematic polynomial variation of $\Delta\mu$ on the effects *T* (temperature), *L* (composition of the liquid stationary phase, $100\varphi_{TTF} = 0.0, 50.0$ and 100.0%) and *Z* (carbon number of the solute). The subscripts in parentheses refer to the degree of the orthogonal polynomial: (1) linear; (2) quadratic; (3) cubic. *SQ* is the sum of squares, ϕ is the number of degrees of freedom and $V' = V(\text{res.}) + \nu_x V(X)$ is the combined variance to be analysed by Fisher's *F* (ν_x is the number of statistical units in one datum of the subset used for the evaluation of the effect). The coefficients $b_x^{(i)}$ in Eq. 20 are also listed along with the corresponding thermodynamic coefficients. The meaning of the symbols of thermodynamic functions are described in the text. The abbreviation "res." is for residual variance, "sign." is for significance level and "id." means that $V' = SQ/\phi$ is equal to the corresponding *SQ* ($\phi = 1$).

^a Sum of the residuals marked by one asterisk.

^b Sum of the residuals marked by two asterisks.

degree *i* related to the effect $X = T, L$ and Z and $b_x^{(i)}$ is the corresponding regression coefficient.

$$\begin{aligned} \Delta\mu_z^{A/P} = & b^{(0)} + b_z^{(1)} P_z^{(1)} + b_T^{(1)} P_T^{(1)} + b_{T,Z}^{(1,1)} P_T^{(1)} P_Z^{(1)} \\ & + b_T^{(2)} P_T^{(2)} + b_{T,Z}^{(2,1)} P_T^{(2)} P_Z^{(1)} + b_L^{(1)} P_L^{(1)} \\ & + b_{L,Z}^{(1,1)} P_L^{(1)} P_Z^{(1)} + b_{T,L}^{(1,1)} P_T^{(1)} P_L^{(1)} \\ & + b_{T,L,Z}^{(1,1,1)} P_T^{(1)} P_L^{(1)} P_Z^{(1)} + b_{T,L}^{(2,1)} P_T^{(2)} P_L^{(1)} \end{aligned}$$

$$\begin{aligned} & + b_{T,L,Z}^{(2,1,1)} P_T^{(2)} P_L^{(1)} P_Z^{(1)} + b_L^{(2)} P_L^{(2)} \\ & + b_{L,Z}^{(2,1)} P_L^{(2)} P_Z^{(1)} + b_{T,L}^{(1,2)} P_T^{(1)} P_L^{(2)} \\ & + b_{T,L,Z}^{(1,2,1)} P_T^{(1)} P_L^{(2)} P_Z^{(1)} \end{aligned} \quad (20)$$

It is seen that the residual variance in the subspace *TL* (1st res.) is higher than the residual variance deduced from the third-order effect *TLZ* (2nd res.). In fact, a higher error is intro-

duced by adjusting a new temperature or by working with a new column compared to the error between alkanes injected on a given column at exactly the same temperature. Consequently, effects in the *TL* subspace were tested against the “1st res.” and the remaining effects against the “2nd res.” (cf., the analogous variance analysis in ref. 1).

The results in Table 4 indicate that all the terms in Eq. 20 are significant with the exception of those underlined. In addition to the terms in Eq. 20, also the quadratic and cubic dependence of the standard chemical potential, $\Delta\mu_z^{A/P}$, on the carbon number were significant. The corresponding terms are not included in Eq. 20 in spite of the fact that the dependence of $\Delta\mu_z^{A/P}$ on carbon number, z , is not strictly linear. The relation of the coefficients $b_X^{(i)}$ to thermodynamic functions is listed in the last column in Table 4. This relationship was found by comparing coefficients in Eqs. 20 and 22. The latter equation was obtained by developing the relationship of Eq. 3 for $\Delta\mu_z^{A/P}$ around the standard temperature, T^\dagger , by introducing $\Delta T = T - T^\dagger$, and by approximating the logarithmic expression multiplying the partial molar heat capacity, ΔC_p , by the first term of its Taylor series and introducing a linear dependence on z for the functions $Y = H_z, S_z, C_{p,z}, h_z$ and s_z .

$$Y_z = Y_0 + z \delta Y_z \quad (21)$$

$$\begin{aligned} \Delta\mu_z^{A/P} = & \Delta\mu_0^{\dagger A} + z \delta\mu_z^{\dagger A} - \Delta T \Delta S_0^A - \Delta T z \delta S_z^A \\ & - \Delta T^2 \frac{\Delta C_{p,0}^A}{2T^\dagger} - \Delta T^2 z \frac{\delta C_{p,z}^A}{2T^\dagger} + \varphi_p (\Delta\mu_0^{\dagger P} + m_0^{\dagger A/P}) \\ & + \varphi_p z (\delta\mu_z^{\dagger P} - \delta\mu_z^{\dagger A} + \delta m_z^{\dagger A/P}) - \Delta T \varphi_p \Delta S_0^P \\ & - \Delta T \varphi_p z (\delta S_z^P - \delta S_z^A) - \Delta T^2 \varphi_p \frac{\Delta C_{p,0}^P}{2T^\dagger} \\ & - \Delta T^2 \varphi_p z \frac{\delta C_{p,z}^P - \delta C_{p,z}^A}{2T^\dagger} - \varphi_p^2 m_0^{\dagger A/P} \\ & - \varphi_p^2 z \delta m_z^{\dagger A/P} + \Delta T \varphi_p^2 s_0^A \\ & + \Delta T \varphi_p^2 z \delta s_z^{A/P} \quad (22) \end{aligned}$$

The visual arrangement of Eqs. 20 and 22 facilitates the identification of the corresponding coefficients. The non-significance of the three underlined terms in Eq. 22 is interpreted in terms of thermodynamic functions as follows. There is no difference between the entropy of the “methylene increment”, δS_z^P , on the stationary phase C78 and TTF (1st term) and the same is true for the partial molar heat capacity of a hypothetical “nullane”, $\Delta C_{p,0}^P$, (2nd term) and for the heat capacity of the “methylene increment”, $\delta C_{p,z}^P$, (3rd term).

C78

Retention index and thermodynamic data on C78 have been published previously [1]. New

Table 5
Retention indices and thermodynamic data of some solutes on the standard alkane C78

No.	Compound	n	Temperature range (°C)	Retention index (C78)			Thermodynamic data (C78)			
				I_{130}	$A_T \cdot 10$ (K ⁻¹)	σ	ΔH (cal mol ⁻¹)	ΔS (cal mol ⁻¹ K ⁻¹)	ΔC_p (cal mol ⁻¹ K ⁻¹)	σ (cal mol ⁻¹)
10.12	2,2-Dimethylhexane	15	90–170	719.9	+0.77	0.36	-7554	-18.180	+10.4	1.1
38.06	Iodobenzene	15	130–210	1078.9	+6.70	0.32	-9500	-18.533	+13.9	1.7
41.12	Benzyl alcohol	15	130–210	973.7	+4.29	0.37	-9389	-19.512	+10.6	2.1
41.13	2-Phenylethanol	15	130–210	1054.5	+4.83	0.31	-10164	-20.423	+14.3	1.7
41.16	Aniline	15	130–210	932.1	+6.98	0.59	-8423	-17.640	+8.0	3.3
41.17	Cyclohexylamine	15	130–210	860.2	+3.88	1.06	-8380	-18.432	+11.2	6.2

I_{130} is the retention index at the standard temperature, A_T is the temperature coefficient of retention index; thermodynamic functions are the coefficients of Eq. 3; other symbols are as in Table 6. 1 cal = 4.184 J.

Table 6

Retention indices and thermodynamic data for 160 solutes; data in C78–TTF mixtures where data derived for idCF₃ are also given and on pure MTF with reference to those in C78

Data in the reference alkane C78 (not listed) are given in ref. 1 and in Table 5 of this paper. The symbol *n* is the number of data points used for regression where points for pure C78 were taken from ref. 1 (*n*/3 for C78–TTF mixtures; *n*/2 for MTF). Constants and functions, *X*, preceded by Δ refer to those on C78, i.e., Δ*X* = *X* – *X* (in C78); Δ' values are derivatives with respect of concentration [CF₃]. Retention indices: *I*₁₃₀ is the retention index at the reference temperature *T*[†] = 130 + 273.15 K; for the meaning of the coefficients *A*, see Eqs. 11 and 12. Thermodynamic functions *H* and *S* are partial molar enthalpy and entropy at *T*[†] and *C*_p is the mean partial molar heat capacity in the temperature range indicated; for the meaning of the coefficients *h* and *s*, see Eq. 6. At the end of the Table additive corrections are listed to convert data (*A*) to those related to the partition coefficients *K*_D (see Eq. 30) and (*B*) to those where pressures are measured in units of bar (instead of atm). Errors: the symbol σ is the standard deviation around the regression and at the end of the Table are listed standard deviations of constants and functions in units of the standard deviation around the regression, *f* (coeff) = σ (coeff)/σ. Data with a superscript *s* are significant at the 10% significance level if tested against σ. Data with one asterisk are at the 20% significance level and those marked with two asterisks are under this limit. Note that linearity of the following thermodynamic functions of *n*-alkanes with carbon number was imposed by the regression function: Δ*H*, Δ*S*, Δ*C*_p, *h*, *s*, Δ'*H*, Δ'*S* and Δ'*C*_p.

No.	Compound	Temp. range (°C)	Retention index: C78 / TTF						C78 / MTF				
			TTF - C78		Mixture		id([CF ₃]=1) - C78		n MTF - C78				
			Δ <i>I</i> ₁₃₀	$\frac{10 \times}{\Delta \Delta T}$ (K ⁻¹)	<i>A</i> _L	$\frac{10 \times}{A_{LT}}$ (K ⁻¹)	Δ <i>I</i> ₁₃₀	$\frac{10 \times}{\Delta \Delta T}$ (K ⁻¹)	Δ <i>I</i> ₁₃₀	$\frac{10 \times}{\Delta \Delta T}$ (K ⁻¹)			
HYDROCARBONS													
<i>n</i> -Alkanes													
00.05	Pentane	90-210	21							14			
00.06	Hexane	90-210	21							14			
00.07	Heptane	90-210	21							14			
00.08	Octane	90-210	21							14			
00.09	Nonane	90-210	21							14			
00.10	Decane	90-210	21							14			
00.11	Undecane	150-210	12							8			
00.12	Dodecane	150-210	12							8			
00.13	Tridecane	150-210	12							8			
00.14	Tetradecane	150-210	12							8			
<i>Isoalkanes</i>													
10.01	2,2-Dimethylbutane	90-170	15 +	3.8	-0.53	+ 1.7	+0.04**	+ 2.1	-0.17	0.24	10 + 1.4	+0.10**	0.32
10.02	2,3-Dimethylbutane	90-170	15 +	2.8	-0.38	- 1.4**	-0.59**	+ 0.5	-0.36	0.82	10 + 0.7	+0.10	0.15
10.03	2,2-Dimethylpentane	90-170	15 +	4.7	-0.42	+ 1.1	-0.10**	+ 2.2	-0.18	0.33	10 + 1.5	-0.02**	0.41
10.04	2,3-Dimethylpentane	90-170	15 +	2.3	-0.31	- 1.5*	-0.54*	+ 0.3	-0.32	0.47	10 + 0.9	+0.15**	0.53
10.05	2,4-Dimethylpentane	90-170	15 +	4.0	-0.59	- 1.8*	-1.07	+ 0.8	-0.62	0.48	10 + 1.3	-0.19	0.08
10.06	2,3-Dimethylhexane	90-170	15 +	2.6	-0.31	- 1.6 ^s	-0.66	+ 0.3	-0.36	0.37	10 + 0.7	+0.14	0.13
10.07	2,4-Dimethylhexane	90-170	15 +	4.0	-0.30 ^s	- 0.4**	-0.39**	+ 1.4	-0.25	0.44	10 + 1.5	+0.09 ^s	0.18
10.08	3,4-Dimethylhexane	90-170	15 +	2.1	-0.28	- 1.9	-0.14**	- 0.0	-0.16	0.25	10 + 0.9	+0.18*	0.41
10.09	2,2,3-Trimethylbutane	90-170	15 +	7.1	+0.16*	+ 2.1	+0.51 ^s	+ 3.5	+0.28	0.29	10 + 3.4	+0.25 ^s	0.51
10.10	2,2,4-Trimethylpentane	90-170	15 +	7.0	-0.02**	+ 1.6	+0.06**	+ 3.2	+0.04	0.26	10 + 2.8	+0.28	0.38
10.11	2,3,4-Trimethylpentane	90-170	15 +	3.4	+0.11**	+ 0.0**	+0.21**	+ 1.6	+0.13	0.35	10 + 1.2	+0.32	0.33

No.	Thermodynamic data : C78 / TTF									C78 / MTF				
	TTF - C78			Mixture		id([CF ₃]=1) - C78			σ	MTF - C78			σ	
	ΔH (cal mol ⁻¹)	ΔS (cal mol ⁻¹ K ⁻¹)	ΔC_p	\bar{h}_i (cal mol ⁻¹)	s (cal mol ⁻¹ K ⁻¹)	ΔH (cal mol ⁻¹)	ΔS (cal mol ⁻¹ K ⁻¹)	ΔC_p		ΔH (cal mol ⁻¹)	ΔS (cal mol ⁻¹ K ⁻¹)	ΔC_p		(cal mol ⁻¹)
HYDROCARBONS														
<i>n-Alkanes</i>														
00.05	+	49	-0.026	- 1.9	- 236	-0.412	- 69	-0.161	-0.8	4.8	- 69	-0.113	-1.7	4.4
00.06	+	61	-0.026	- 1.7	- 230	-0.412	- 65	-0.166	-0.8	4.5	- 62	-0.107	-1.6	4.2
00.07	+	72	-0.026	- 1.6	- 225	-0.412	- 60	-0.171	-0.7	4.5	- 56	-0.101	-1.5	4.9
00.08	+	83	-0.026	- 1.5	- 219	-0.412	- 56	-0.176	-0.7	4.1	- 49	-0.095	-1.3	5.3
00.09	+	94	-0.026	- 1.4	- 214	-0.412	- 52	-0.181	-0.7	4.9	- 43	-0.089	-1.2	4.6
00.10	+	106	-0.026	- 1.3	- 208	-0.412	- 47	-0.186	-0.6	4.3	- 36	-0.083	-1.0	5.2
00.11	+	117	-0.026	- 1.2	- 202	-0.412	- 43	-0.191	-0.6	3.6	- 29	-0.077	-0.9	3.1
00.12	+	128	-0.026	- 1.1	- 197	-0.412	- 39	-0.195	-0.5	4.5	- 23	-0.071	-0.8	3.5
00.13	+	139	-0.026	- 1.0	- 191	-0.412	- 34	-0.200	-0.5	4.3	- 16	-0.065	-0.6	2.7
00.14	+	151	-0.026	- 0.8	- 185	-0.412	- 30	-0.205	-0.5	4.6	- 10	-0.059	-0.5	2.9
<i>Isoalkanes</i>														
10.01	-	104	-0.369	+ 2.1	- 249	-0.424	-128	-0.286	+0.6	1.0	- 62	-0.082*	+2.9*	1.8
10.02	-	52*	-0.273	+ 6.1 ^s	- 364	-0.754	-154	-0.381	+2.0	3.5	- 53	-0.073	+4.5	0.8
10.03	-	72	-0.310	+ 3.2	- 271	-0.501	-126	-0.297	+1.0	1.5	- 84	-0.144	+2.7*	2.1
10.04	-	19	-0.226	+ 4.8	- 331	-0.689	-132	-0.346	+1.6	1.5	- 40	-0.048**	+3.1**	2.7
10.05	-	98	-0.382	+ 3.0 ^s	- 443	-0.961	-202	-0.502	+0.8	1.9	-113	-0.218	-1.3	0.4
10.06	-	11**	-0.224	+ 2.7	- 346	-0.739	-137	-0.369	+0.8	1.5	- 33	-0.042 ^s	+1.7	0.7
10.07	-	27	-0.235	+ 2.3*	- 306	-0.622	-126	-0.324	+0.7	1.9	- 51	-0.074	+0.1**	0.9
10.08	-	0**	-0.202	+ 0.1**	- 239	-0.482	- 94	-0.267	-0.1	1.8	- 26**	-0.025**	+2.5*	2.1
10.09	+	23**	-0.044**	- 0.5**	- 148 ^s	-0.187**	- 43	-0.077	-0.2	2.0	- 43*	-0.019**	-0.9**	2.6
10.10	-	8	-0.137	+ 1.5**	- 232	-0.406	- 87	-0.196	+0.4	1.9	- 32*	-0.006**	+3.3 ^s	2.0
10.11	+	56	-0.042**	+ 3.4	- 187	-0.326 ^s	- 50	-0.141	+1.2	1.5	- 6**	+0.029**	+6.8	1.7

(Continued on p. 192)

Table 6 (continued)

No.	Compound	Temp. range (°C)	Retention index : C78 / TTF									C78 / MTF		
			n TTF - C78			Mixture		id([CF ₃]=1) - C78 σ				n MTF - C78		σ
			ΔI_{130}	$\frac{10 \times}{\Delta A_T}$ (K ⁻¹)	A_L	$\frac{10 \times}{A_{LT}}$ (K ⁻¹)	ΔI_{130} (l mol ⁻¹)	$\frac{10 \times}{\Delta A_T}$ (K ⁻¹)	ΔI_{130}	$\frac{10 \times}{\Delta A_T}$ (K ⁻¹)	ΔI_{130}	$\frac{10 \times}{\Delta A_T}$ (K ⁻¹)		
10.12	2,2-Dimethylhexane	90-170	15 +	4.1	-0.32	- 0.3**	-0.13**	+ 1.4	-0.17	0.36	10 +	0.9	+0.18*	0.39
<i>1-Alkenes</i>														
11.06	1-Hexene	90-170	15 +	4.7	-0.09**	- 1.0**	+0.51 ^s	+ 1.4	+0.17	0.36	10 +	0.8*	-0.12**	0.40
11.07	1-Heptene	90-170	15 +	5.6	+0.04**	- 0.3**	+0.79	+ 1.9	+0.32	0.26	10 +	1.6	+0.08**	0.42
11.08	1-Octene	90-170	15 +	5.5	+0.00**	- 0.0**	+0.62	+ 2.1	+0.25	0.25	10 +	1.2	+0.04**	0.32
11.09	1-Nonene	90-170	15 +	6.0	+0.01**	+ 0.8**	+0.57	+ 2.6	+0.24	0.29	10 +	1.5	+0.13*	0.38
11.10	1-Decene	90-170	15 +	5.8	+0.07**	+ 1.1	+0.35	+ 2.6	+0.18	0.19	10 +	1.3	+0.25	0.35
<i>1-Alkynes</i>														
12.05	1-Pentyne	90-170	15 +	19.3	+0.12**	+ 4.8	+1.44	+ 9.1	+0.67	0.81	10 +	7.3	+0.19*	0.44
12.06	1-Hexyne	90-170	15 +	19.3	-0.02**	+ 3.4	+0.89	+ 8.6	+0.40	0.38	10 +	6.4	-0.17**	0.80
12.07	1-Heptyne	90-170	15 +	19.9	+0.05**	+ 4.2	+0.95	+ 9.2	+0.46	0.30	10 +	6.6	-0.03**	0.62
12.08	1-Octyne	90-170	15 +	20.2	-0.02**	+ 4.0	+0.77	+ 9.2	+0.36	0.29	10 +	6.3	+0.03**	0.42
12.09	1-Nonyne	90-170	15 +	20.6	-0.13**	+ 4.1	+0.87	+ 9.4	+0.36	0.37	10 +	6.4	+0.05**	0.44
12.10	1-Decyne	90-170	15 +	20.5	-0.02**	+ 3.6	+0.85	+ 9.2	+0.39	0.34	10 +	6.4	+0.17*	0.48
<i>Alkynes</i>														
13.01	2-Hexyne	90-170	15 +	13.5	-0.48**	- 0.4**	-1.02**	+ 4.9	-0.53	1.20	10 +	3.8	-0.34	0.46
13.02	3-Hexyne	90-170	15 +	7.7	-1.04 ^s	+ 1.1**	+1.30 ^s	+ 3.3	+0.13	0.90	10 +	2.8	-0.08**	0.37
13.03	4-Octyne	90-170	15 +	9.9	-0.38**	- 0.3**	+0.36**	+ 3.6	+0.02	0.50	10 +	2.5	-0.23	0.10
<i>Monocyclic hydrocarbons</i>														
14.05	Cyclopentane	90-170	15 -	6.6	-0.65**	- 5.8	-1.38	- 4.7	-0.81	0.65	10 -	2.0	-0.51 ^s	1.06
14.06	Cyclohexane	90-170	15 -	6.1	-0.33**	- 3.4	-0.54**	- 3.6	-0.36	0.59	10 -	1.6	-0.12**	0.78
14.07	Cycloheptane	90-170	15 -	7.3	-0.21**	- 3.3	-0.18**	- 4.0	-0.18	0.45	10 -	1.9	+0.01**	0.58
14.08	Cyclooctane	90-170	15 -	7.5	-0.05**	- 3.2	+0.06**	- 4.1	-0.03	0.44	10 -	3.3	+0.73	0.74
14.10	Cyclodecane	130-210	15 -	7.0	-0.10**	+ 0.9	-0.23**	- 3.5	-0.02	0.47	10 -	3.7	+0.70	0.49
<i>Bicyclic hydrocarbons</i>														
15.01	cis-Hydrindane	130-210	15 -	7.9	-0.03**	- 3.5	+0.20**	- 4.0	-0.06	0.33	10 -	1.8	+0.12**	0.29
15.02	trans-Hydrindane	130-210	15 -	7.1	+0.06**	- 3.3	+0.20**	- 3.8	+0.06	0.43	10 -	0.9	-0.23	0.20
15.03	cis-Decalin	130-210	15 -	6.9	-0.22**	- 3.3	+0.08**	- 3.5	-0.16	0.30	10 +	1.1	-0.69	0.39
15.04	trans-Decalin	130-210	15 -	6.0	-0.06**	- 2.5	+0.09**	- 2.7	-0.15	0.38	10 -	0.1	-0.56	0.37
<i>Methylcyclohexanes (MCH)</i>														
16.01	Methylcyclohexane	90-170	15 -	3.3	-0.31**	+ 0.2**	-0.38**	- 1.2	-0.27	0.65	10 -	0.5*	+0.17**	0.53

No.	Thermodynamic data : C78 / TTF										C78 / MTF			
	TTF - C78			Mixture		id([CF ₃]=1) - C78			σ	MTF - C78			σ	
	ΔH	ΔS	ΔC _P	f _i	s	ΔH	ΔS	ΔC _P		ΔH	ΔS	ΔC _P		
	(cal mol ⁻¹)	(cal mol ⁻¹ K ⁻¹)		(cal mol ⁻¹)	(cal mol ⁻¹ K ⁻¹)	(cal mol ⁻²)	(cal mol ⁻² K ⁻¹)		(cal mol ⁻¹)	(cal mol ⁻¹ K ⁻¹)	(cal mol ⁻¹)			
10.12	- 33	-0.244	+ 1.7 ^s	- 254	-0.489	-108	-0.276	+0.5	1.1	- 59	-0.108 ^s	+1.8 [*]	2.3	
<i>I-Alkenes</i>														
11.06	- 12 ^{**}	-0.137 ^s	- 0.9 ^{**}	- 108 ^{**}	-0.118 ^{**}	- 43	-0.091	-0.4	2.7	- 98	-0.183	-0.5 ^{**}	2.4	
11.07	+ 21 ^{**}	-0.078 ^s	- 1.3 ^{**}	- 57 ^{**}	+0.003 ^{**}	- 13	-0.027	-0.5	1.8	- 59	-0.081 [*]	-2.2 ^{**}	2.0	
11.08	+ 25 [*]	-0.097	- 0.0 ^{**}	- 93 [*]	-0.097 ^{**}	- 27	-0.076	-0.0	1.7	- 55	-0.092 ^s	-0.6 ^{**}	1.7	
11.09	+ 33 [*]	-0.103	+ 0.5 ^{**}	- 109 [*]	-0.140 ^{**}	- 31	-0.097	+0.1	1.9	- 34 [*]	-0.043 ^{**}	-1.3 ^{**}	1.9	
11.10	+ 59	-0.069 ^s	+ 0.6 ^{**}	- 152	-0.255	- 39	-0.132	+0.1	1.3	- 2 ^{**}	+0.022 ^{**}	-1.4 ^{**}	1.7	
<i>I-Alkynes</i>														
12.05	- 111 ^s	-0.169 ^{**}	+ 5.2 ^{**}	+ 52 ^{**}	+0.370 ^{**}	- 4	+0.119	+2.0	5.6	- 99	-0.089 ^{**}	+1.6 ^{**}	2.6	
12.06	- 138	-0.267	+ 2.6 ^{**}	- 59 ^{**}	+0.077 ^{**}	- 59	-0.034	+0.9	2.5	-167	-0.269 ^s	-2.5 ^{**}	4.5	
12.07	- 119	-0.246	+ 1.5 ^{**}	- 69 ^{**}	+0.036 ^{**}	- 58	-0.047	+0.5	1.8	-130	-0.194 ^s	-1.4 ^{**}	3.3	
12.08	- 124	-0.288	+ 1.9 [*]	- 103 ^s	-0.067 ^{**}	- 75	-0.107	+0.6	1.7	-107	-0.156	+0.3 ^{**}	2.4	
12.09	- 140	-0.354	+ 2.0 ^{**}	- 87 [*]	-0.041 ^{**}	- 76	-0.127	+0.7	1.9	- 99	-0.145 ^s	+0.3 ^{**}	2.5	
12.10	- 105	-0.296	+ 1.5 [*]	- 79 ^s	-0.044 ^{**}	- 63	-0.113	+0.5	1.9	- 68	-0.077 ^{**}	-1.5 ^{**}	2.9	
<i>Alkynes</i>														
13.01	- 166	-0.435	+ 3.1 ^{**}	- 461 ^s	-0.987 [*]	-228	-0.515	+0.8	7.0	-170	-0.327	-1.3 ^{**}	2.3	
13.02	- 227	-0.651	+ 2.3 ^{**}	+ 19 ^{**}	+0.216 ^{**}	- 74	-0.152	+0.8	5.7	-104	-0.180	+1.8 ^{**}	1.9	
13.03	- 89 ^s	-0.338	+ 2.3 ^{**}	- 149 [*]	-0.242 ^{**}	- 88	-0.215	+0.7	2.8	-119	-0.240	+1.0	0.4	
<i>Monocyclic hydrocarbons</i>														
14.05	- 33 ^{**}	-0.339	- 1.5 ^{**}	- 487	-1.125	-203	-0.569	-0.9	4.1	-164	-0.378	-2.9 ^{**}	5.9	
14.06	+ 49 ^s	-0.151	- 2.5 ^{**}	- 305	-0.652	-105	-0.322	-1.1	2.8	- 72 [*]	-0.153 [*]	-2.8 ^{**}	3.9	
14.07	+ 96	-0.089 [*]	- 2.1 ^{**}	- 227	-0.478	- 61	-0.242	-0.9	2.3	- 33 ^{**}	-0.078 ^{**}	-1.9 ^{**}	3.0	
14.08	+ 144	-0.011 ^{**}	- 1.0 ^{**}	- 179 ^s	-0.376 [*]	- 28	-0.181	-0.5	2.6	+131	+0.302	-4.4 [*]	3.2	
14.10	+ 145	-0.060 ^{**}	- 1.8 ^{**}	- 245	-0.541	- 55	-0.268	-0.8	2.0	+112 [*]	+0.242 ^{**}	-4.4 ^s	2.1	
<i>Bicyclic hydrocarbons</i>														
15.01	+ 116 ^s	-0.104 ^{**}	+ 0.8 ^{**}	- 158	-0.336	- 32	-0.205	+0.2	1.8	- 83 ^s	-0.213	+0.2	0.9	
15.02	+ 167 ^s	+0.040 ^{**}	- 0.3 ^{**}	- 155 [*]	-0.323 [*]	- 11	-0.144	-0.2	2.5	- 12 ^{**}	-0.037 ^{**}	-1.0 ^{**}	1.6	
15.03	+ 78 [*]	-0.214 [*]	+ 1.0 ^{**}	- 173	-0.388	- 53	-0.269	+0.2	1.6	-123 [*]	-0.317 ^s	+0.7 ^{**}	1.8	
15.04	+ 68 ^{**}	-0.221 [*]	+ 1.7 ^{**}	- 182	-0.395	- 59	-0.270	+0.5	1.7	-175	-0.438	+2.1 [*]	1.6	
<i>Methylcyclohexanes (MCH)</i>														
16.01	+ 36 ^{**}	-0.179 ^s	+ 3.0 ^{**}	- 319	-0.649	-112	-0.324	+0.9	3.6	- 17 ^{**}	-0.022 ^{**}	+1.9 ^{**}	2.7	

(Continued on p. 194)

Table 6 (continued)

No.	Compound	Temp. range (°C)	Retention index : C78 / TTF							C78 / MTF			
			n TTF - C78		Mixture		id([CF ₃]=1) - C78 σ			n MTF - C78		σ	
			ΔI_{130}	$\frac{10 \times \Delta A_T}{(K^{-1})}$	A_L	$\frac{10 \times A_{LT}}{(K^{-1})}$	ΔI_{130}	$\frac{10 \times \Delta A_T}{(K^{-1})}$	σ	ΔI_{130}	$\frac{10 \times \Delta A_T}{(K^{-1})}$		
							(l mol ⁻¹)	(K ⁻¹)					
16.02	cis-1,2-Di MCH	90-170	15 -	2.4	-0.16**	- 0.4**	+0.09**	- 1.1	-0.03	0.52	10 + 0.4**	+0.13**	0.77
16.03	trans-1,2-Di MCH	90-170	15 -	1.0**	-0.09**	- 0.1**	-0.10**	- 0.4	-0.07	0.60	10 + 0.0**	+0.22**	0.85
16.04	cis-1,4-Di MCH	90-170	15 -	1.6*	-0.19**	- 0.5**	+0.11**	- 0.8	-0.04	0.62	10 + 0.1**	+0.12**	0.76
16.05	trans-1,4-Di MCH	90-170	15 -	0.2**	-0.21**	- 0.7**	+0.05**	- 0.4	-0.06	0.60	10 + 0.8*	+0.27*	0.71
<i>Cyclohexenes</i>													
17.01	Cyclohexene	90-170	15 -	1.5*	-0.53*	- 0.5**	-0.33**	- 0.8	-0.33	0.67	10 - 0.5 ^s	-0.15 ^s	0.29
17.02	1,3-Cyclohexadiene	90-170	15 +	8.5	-0.22**	+ 0.6**	+0.78*	+ 3.4	+0.24	0.63	10 + 3.2	+0.39	0.47
17.03	1,4-Cyclohexadiene	90-170	15 +	6.3	-0.49*	- 1.3**	+0.30**	+ 1.9	-0.06	0.57	10 + 1.5 ^s	-0.07**	0.99
<i>Alkylbenzenes</i>													
18.00	Benzene	90-170	15 +	25.5	+0.25**	+ 4.1*	+1.25*	+11.2	+0.66	1.10	10 + 7.6	+0.39*	1.01
18.01	Toluene	90-170	15 +	27.5	+0.10**	+ 3.1*	+0.89**	+11.6	+0.47	0.96	10 + 7.5	+0.30**	0.91
18.02	Ethylbenzene	90-170	15 +	25.4	-0.02**	+ 2.8*	+0.71**	+10.7	+0.35	0.84	10 + 6.9	+0.25	0.86
<i>Miscellaneous</i>													
19.01	Adamantane	130-210	15 -	10.8	-0.48	- 5.6	-0.74 ^s	- 6.0	-0.56	0.45	10 - 3.5	-0.43	0.41
19.02	Naphthalene	130-210	15 +	43.3	-0.33**	+ 3.9	-0.31**	+17.2	+0.06	0.79	10 +10.7	-0.09**	0.84
19.03	Azulene	130-210	15 +	39.5	+0.92	- 8.8	+2.54	+11.7	+1.41	1.18	10 + 8.6	+0.28**	1.61
<i>ALKANE DERIVATIVES</i>													
<i>1-Fluoroalkanes</i>													
20.05	1-Fluoropentane	90-170	15 +	36.1	-0.38**	+ 6.8	-0.04**	+16.2	-0.02	0.52	10 +10.3	-0.21**	1.28
20.06	1-Fluorohexane	90-170	15 +	36.6	-0.31**	+ 5.9	-0.33**	+16.1	-0.11	0.39	10 +10.3	-0.10**	0.91
20.07	1-Fluorooctane	90-170	15 +	36.1	-0.27**	+ 3.7	-0.39*	+15.1	-0.12	0.30	10 +10.1	-0.01**	0.55
<i>1,1,1-Trifluoroalkanes</i>													
21.08	1,1,1-Trifluorooctane	90-170	15 +	56.8	-0.09**	+18.6	-0.99	+28.5	-0.17	0.56	10 +17.8	+0.00**	0.54
21.10	1,1,1-Trifluorodecane	90-170	15 +	57.3	-0.07**	+19.3	-1.11 ^s	+29.0	-0.20	0.73	10 +18.2	-0.02**	0.57
<i>1-Chloroalkanes</i>													
22.04	1-Chlorobutane	90-170	15 +	27.7	+0.18**	+ 4.8	+1.03	+12.4	+0.56	0.57	10 + 7.5	-0.35 ^s	0.69
22.05	1-Chloropentane	90-170	15 +	28.6	+0.58*	+ 6.3	+1.64	+13.3	+0.95	0.50	10 + 8.0	+0.12**	0.72
22.06	1-Chlorohexane	90-170	15 +	29.1	+0.36*	+ 6.8	+1.29	+13.7	+0.74	0.50	10 + 8.3	+0.02**	0.70
<i>1-Bromoalkanes</i>													

No.	Thermodynamic data : C78 / TTF										C78 / MTF			
	TTF - C78			Mixture		id([CF ₃]=1) - C78			σ	MTF - C78			σ	
	ΔH (cal mol ⁻¹)	ΔS (cal mol ⁻¹ K ⁻¹)	ΔC_P	h (cal mol ⁻¹)	s (cal mol ⁻¹ K ⁻¹)	ΔH (cal l mol ⁻²)	ΔS (cal l mol ⁻² K ⁻¹)	ΔC_P		ΔH (cal mol ⁻¹)	ΔS (cal mol ⁻¹ K ⁻¹)	ΔC_P		(cal mol ⁻¹)
16.02	+	70	-0.121 ^s	+ 5.3	- 211	-0.405 ^s	- 60	-0.215	+1.8	2.3	- 25**	-0.045**	+3.8**	3.6
16.03	+	67 ^s	-0.101*	+ 4.6 ^s	- 256	-0.508 ^s	- 77	-0.243	+1.6	3.1	- 3**	+0.002**	+5.2*	3.3
16.04	+	52**	-0.139*	+ 1.9**	- 203*	-0.384**	- 63	-0.213	+0.6	4.2	- 29**	-0.048**	-0.1**	4.4
16.05	+	31**	-0.165 ^s	+ 1.4**	- 214 ^s	-0.410*	- 74	-0.229	+0.4	3.6	- 6**	+0.021**	-0.3**	4.2
<i>Cyclohexenes</i>														
17.01	-	31**	-0.309	+ 2.9**	- 307	-0.622 ^s	-131	-0.358	+0.9	3.7	- 86	-0.186	+1.8*	1.2
17.02	-	73	-0.285	+ 4.7	- 86**	-0.058**	- 56	-0.120	+1.7	2.3	- 15**	+0.046**	-1.6**	2.8
17.03	-	98	-0.382	+ 2.8**	- 165*	-0.282**	- 99	-0.249	+0.9	3.5	- 88*	-0.168**	+1.6**	5.7
<i>Alkylbenzenes</i>														
18.00	-	147	-0.252	+ 6.2 ^s	- 17**	+0.165**	- 45	+0.009	+2.3	4.2	- 54**	+0.001**	+0.8**	5.8
18.01	-	189	-0.365	+ 4.1*	- 82**	-0.025**	- 87	-0.110	+1.5	3.7	- 69**	-0.049**	+0.9**	5.2
18.02	-	180	-0.398	+ 5.0 ^s	- 115**	-0.125**	- 99	-0.168	+1.8	3.0	- 67**	-0.063**	+1.4**	4.8
<i>Miscellaneous</i>														
19.01	+	60**	-0.305*	+ 1.1**	- 282	-0.689	-104	-0.425	+0.1	4.1	- 91**	-0.272*	-0.3**	2.0
19.02	-	310 ^s	-0.599*	- 1.3**	- 297*	-0.608*	-213	-0.417	-0.8	4.6	-162**	-0.276**	-1.2**	4.0
19.03	-	127 ^s	-0.199*	- 7.6*	+ 298*	+0.699*	+ 66	+0.193	-2.7	5.8	- 53**	-0.051**	-0.7**	7.3
ALKANE DERIVATIVES														
<i>1-Fluoroalkanes</i>														
20.05	-	386	-0.629	- 0.5**	- 317	-0.517	-234	-0.358	-0.4	1.3	-220	-0.336 ^s	-6.3**	6.4
20.06	-	363	-0.627	+ 0.5**	- 362	-0.661	-247	-0.421	-2.4	1.4	-186	-0.277 ^s	-3.4**	4.5
20.07	-	326	-0.611	+ 0.7**	- 342	-0.668	-232	-0.434	-0.0	1.9	-150	-0.223	-0.6**	3.0
<i>1,1,1-Trifluoroalkanes</i>														
21.08	-	491	-0.726	+ 5.3	- 617	-1.138	-371	-0.590	+1.6	1.8	-225	-0.302	+2.8**	2.6
21.10	-	473	-0.747	+ 6.2	- 638	-1.213	-376	-0.636	+1.9	2.6	-222	-0.313	+2.7**	2.8
<i>1-Chloroalkanes</i>														
22.04	-	181	-0.290	+ 2.6**	- 69**	+0.050**	- 74	-0.043	+0.9	2.8	-211	-0.384	+1.0**	3.9
22.05	-	92	-0.091*	+ 2.7*	+ 47**	+0.339 ^s	+ 1	+0.137	+1.1	2.3	-109	-0.142*	+2.8**	3.7
22.06	-	138	-0.234	+ 2.3**	- 31**	+0.139**	- 47	+0.004	+0.9	2.6	-127	-0.195 ^s	+2.7**	3.6
<i>1-Bromoalkanes</i>														

(Continued on p. 196)

Table 6 (continued)

No.	Compound	Temp. range (°C)	Retention index : C78 / TTF							C78 / MTF				
			n	TTF - C78		Mixture		id([CF ₃]=1) - C78 σ			n	MTF - C78		
				ΔI_{130}	$\frac{10 \times}{\Delta A_T}$ (K ⁻¹)	A _L	$\frac{10 \times}{A_{LT}}$ (K ⁻¹)	ΔI_{130} (l mol ⁻¹)	$\frac{10 \times}{\Delta A_T}$ (K ⁻¹)	σ		ΔI_{130}	$\frac{10 \times}{\Delta A_T}$ (K ⁻¹)	σ
23.03	1-Bromopropane	90-170	15 + 24.4	-0.25**	+ 3.4	+0.02**	+10.5	+0.00	0.44	10 + 7.9	-0.01**	0.49		
23.04	1-Bromobutane	90-170	15 + 24.9	-0.21**	+ 4.8	-0.21**	+11.2	-0.07	0.59	10 + 8.2	-0.03**	0.80		
23.05	1-Bromopentane	90-170	15 + 25.7	-0.05**	+ 6.2	-0.11**	+12.1	+0.04	0.56	10 + 7.8	-0.10**	0.78		
<i>1-Cyanoalkanes</i>														
24.02	Cyanoethane	90-170	15 +105.9	-0.35**	+35.6	-0.05**	+53.6	+0.29	0.63	10 +35.6	-0.60 ^s	1.06		
24.03	1-Cyanopropane	90-170	15 +102.6	-0.25**	+28.9	-0.71**	+49.8	+0.05	0.80	10 +31.8	-0.54	0.61		
24.04	1-Cyanobutane	90-170	15 +102.6	+0.06**	+28.6	-0.44**	+49.7	+0.27	0.77	10 +31.5	-0.34	0.28		
24.05	1-Cyanopentane	90-170	15 +102.8	+0.22**	+28.2	-0.52**	+49.6	+0.30	0.83	10 +31.5	-0.16 [*]	0.44		
<i>1-Nitroalkanes</i>														
25.02	Nitroethane	90-170	15 + 99.8	-0.31 [*]	+23.2	-1.55	+46.5	-0.32	0.56	10 +27.9	+0.06**	0.34		
25.03	1-Nitropropane	90-170	15 + 96.8	-0.11**	+21.3	-1.27	+44.7	-0.15	0.41	10 +27.1	-0.43	0.51		
25.04	1-Nitrobutane	90-170	15 + 95.6	-0.03**	+20.4	-1.50	+43.9	-0.21	0.34	10 +27.4	-0.49	0.34		
25.05	1-Nitropentane	90-170	15 + 95.6	-0.04**	+20.1	-1.41	+43.8	-0.18	0.51	10 +27.5	-0.37	0.37		
<i>1-Acetoxyalkanes</i>														
26.03	1-Acetoxypropane	90-170	15 + 59.9	-0.35 [*]	+12.4	-1.00	+27.3	-0.28	0.59	10 +18.1	-0.27	0.30		
26.04	1-Acetoxybutane	90-170	15 + 60.2	-0.27**	+13.2	-0.72 [*]	+27.8	-0.14	0.58	10 +17.9	-0.19	0.20		
26.05	1-Acetoxyptentane	90-170	15 + 59.9	-0.36 [*]	+13.5	-0.80 ^s	+28.1	-0.20	0.57	10 +17.8	-0.28	0.19		
<i>1-Alkanols</i>														
27.04	1-Butanol	90-170	15 + 41.0	-0.53 [*]	+10.6	-1.28	+19.5	-0.52	0.48	10 +15.9	-0.51	0.43		
27.05	1-Pentanol	90-170	15 + 41.7	-0.30**	+ 9.9	-0.71**	+19.5	-0.22	0.79	10 +15.3	-0.22	0.30		
27.06	1-Hexanol	90-170	15 + 41.8	-0.38**	+ 9.6	-0.81**	+19.4	-0.29	0.92	10 +14.9	-0.31	0.38		
27.07	1-Heptanol	90-170	15 + 42.3	-0.33**	+10.3	-0.79**	+19.9	-0.26	1.06	10 +15.2	-0.31	0.46		
<i>2-Alkanols</i>														
28.04	2-Butanol	90-170	15 + 40.2	-0.09**	+ 9.9	-0.36**	+19.0	-0.01	0.38	10 +14.8	-0.04**	0.40		
28.05	2-Pentanol	90-170	15 + 41.7	+0.09**	+11.7	+0.15**	+20.2	+0.26	0.29	10 +15.4	+0.08**	0.35		
28.06	2-Hexanol	90-170	15 + 42.0	+0.01**	+11.6	+0.07**	+20.3	+0.20	0.34	10 +15.2	-0.04**	0.36		
28.07	2-Heptanol	90-170	15 + 42.1	-0.07**	+11.2	-0.08**	+20.2	+0.11	0.45	10 +14.9	-0.12 [*]	0.30		
<i>2-Methyl-2-alkanols</i>														
29.04	2-Methyl-2-propanol	90-170	15 + 42.2	-0.91	+ 8.6	-0.36 ^s	+19.2	-0.32	0.22	10 +15.0	-0.39	0.25		
29.05	2-Methyl-2-butanol	90-170	15 + 39.9	-0.67	+ 5.8	-1.14	+17.3	-0.54	0.33	10 +13.1	-0.86	0.43		
29.06	2-Methyl-2-pentanol	90-170	15 + 40.7	-0.46	+ 6.6	-0.89	+17.9	-0.36	0.33	10 +13.1	-0.57	0.23		

No.	Thermodynamic data : C78 / TTF									C78 / MTF			
	TTF - C78			Mixture		id([CF ₃)=1) - C78			σ	MTF - C78			σ
	ΔH (cal mol ⁻¹)	ΔS (cal mol ⁻¹ K ⁻¹)	ΔC _P	f _i (cal mol ⁻¹)	s (cal mol ⁻¹ K ⁻¹)	ΔH (cal l mol ⁻²)	ΔS (cal l mol ⁻² K ⁻¹)	ΔC _P		ΔH (cal mol ⁻¹)	ΔS (cal mol ⁻¹ K ⁻¹)	ΔC _P	
23.03	- 242	-0.476	+ 1.8**	- 274	-0.473 ^s	-177	-0.315	+0.5	2.8	-146	-0.214	-0.5**	2.8
23.04	- 226	-0.455	- 2.4**	- 324	-0.594	-191	-0.356	-1.1	3.0	-149	-0.221 ^s	-3.8**	3.7
23.05	- 197	-0.399	- 4.9 ^s	- 306	-0.549	-175	-0.322	-2.0	2.8	-152	-0.244	-3.8**	3.4
<i>1-Cyanoalkanes</i>													
24.02	-1 076	-1.374	+ 2.1**	- 628	-0.867 ^s	-542	-0.601	+0.4	4.7	-550	-0.832	+8.4 ^s	4.5
24.03	-1 038	-1.431	+ 2.9**	- 729	-1.231	-578	-0.789	+ 0.6	5.1	-509	-0.801	+4.7 ^s	2.7
24.04	- 944	-1.254	+ 1.0**	- 639	-1.049	-514	-0.668	- 0.1	4.4	-447	-0.672	+2.8	0.9
24.05	- 911	-1.228	+ 4.4**	- 647	-1.092	-508	-0.682	+ 1.2	4.6	-402	-0.581	+3.5	1.7
<i>1-Nitroalkanes</i>													
25.02	-1 025	-1.418	+ 4.7 ^s	- 848	-1.561	-620	-0.914	+1.2	2.1	-331	-0.392	+2.2*	1.8
25.03	- 931	-1.282	+ 2.5*	- 746	-1.388	-555	-0.821	+0.4	2.0	-427	-0.661	-1.6**	2.1
25.04	- 895	-1.259	+ 3.0	- 752	-1.437	-549	-0.842	+0.6	1.6	-428	-0.682	+0.3**	1.8
25.05	- 881	-1.266	+ 3.7	- 733	-1.418	-540	-0.846	+0.8	1.8	-401	-0.631	+1.8**	2.0
<i>1-Acetoxyalkanes</i>													
26.03	- 601	-0.925	+ 5.7	- 573	-1.091	-395	-0.645	+1.7	2.6	-299	-0.459	-0.6**	1.4
26.04	- 569	-0.879	+ 4.3 ^s	- 513	-0.950	-363	-0.581	+1.2	2.5	-270	-0.407	+0.2**	1.1
26.05	- 587	-0.961	+ 5.4	- 528	-0.998	-377	-0.635	+1.6	2.0	-281	-0.453	+1.3*	0.9
<i>1-Alkanols</i>													
27.04	- 473	-0.829	+ 4.2	- 636	-1.259	-382	-0.701	+1.1	1.6	-344	-0.592	-1.0**	2.3
27.05	- 404	-0.690	+ 3.5*	- 487	-0.924	-304	-0.532	+1.0	2.9	-256	-0.402	+0.3**	1.7
27.06	- 414	-0.752	+ 4.3*	- 499	-0.973	-315	-0.579	+1.2	3.5	-263	-0.443	+1.9**	1.9
27.07	- 395	-0.726	+ 2.4**	- 494	-0.967	-308	-0.572	+0.5	3.5	-259	-0.435	+0.2**	2.6
<i>2-Alkanols</i>													
28.04	- 363	-0.519	+ 2.8**	- 412	-0.708	-256	-0.375	+0.8	2.7	-221	-0.292	+0.4**	2.4
28.05	- 334	-0.492	+ 3.3	- 317	-0.472	-212	-0.282	+1.0	1.6	-199	-0.252	+1.4**	1.9
28.06	- 337	-0.534	+ 3.9	- 330	-0.525	-220	-0.324	+1.2	1.5	-210	-0.300	+2.8	1.2
28.07	- 349	-0.597	+ 3.6	- 356	-0.607	-237	-0.384	+1.1	2.0	-221	-0.342	+2.5	1.0
<i>2-Methyl-2-alkanols</i>													
29.04	- 577	-0.995	+ 0.2**	- 409	-0.709	-333	-0.549	-0.3	1.5	-306	-0.495	+1.7*	1.3
29.05	- 495	-0.889	- 0.8**	- 551	-1.118	-364	-0.682	-0.7	1.4	-385	-0.738	+1.4**	2.5
29.06	- 437	-0.769	- 0.2**	- 492	-0.977	-321	-0.587	-0.5	1.5	-312	-0.567	+0.4**	1.3

(Continued on p. 198)

Table 6 (continued)

No.	Compound	Temp. range (°C)	Retention index : C78 / TTF						C78 / MTF				
			TTF - C78			Mixture		id([CF ₃]=1) - C78 σ			MTF - C78		σ
			ΔI_{130}	$\frac{10 \times}{\Delta A_T}$ (K ⁻¹)		A_L	$\frac{10 \times}{A_{LT}}$ (K ⁻¹)	ΔI_{130}	$\frac{10 \times}{\Delta A_T}$ (l mol ⁻¹)		ΔI_{130}	$\frac{10 \times}{\Delta A_T}$ (K ⁻¹)	
29.07	2-Methyl-2-hexanol	90-170	15 + 41.4	-0.50	+ 7.3	-1.07	+18.4	-0.44	0.46	10 +13.8	-0.71	0.21	
<i>1-Alkanethiols</i>													
30.04	1-Butanethiol	90-170	15 + 12.8	-1.28	- 5.1	-2.16	+ 3.1	-1.28	0.39	10 + 4.4	-0.30*	0.80	
30.05	1-Pentanethiol	90-170	15 + 13.5	-1.24	- 5.4	-2.24	+ 3.2	-1.29	0.28	10 + 3.9	-0.56	0.68	
30.06	1-Hexanethiol	90-170	15 + 14.9	-1.21	- 4.5	-2.30	+ 3.9	-1.30	0.22	10 + 4.1	-0.48	0.39	
<i>2-Alkanones</i>													
31.04	2-Butanone	90-170	15 + 72.7	-0.90	+14.1	-1.58	+32.9	-0.67	0.35	10 +22.9	-0.81	0.44	
31.05	2-Pentanone	90-170	15 + 72.2	-0.66	+14.2	-1.19	+32.7	-0.43	0.26	10 +21.7	-0.73	0.29	
31.06	2-Hexanone	90-170	15 + 73.2	-0.51	+14.3	-1.22	+33.1	-0.38	0.23	10 +21.4	-0.52	0.37	
31.07	2-Heptanone	90-170	15 + 73.9	-0.55	+15.1	-1.06	+33.7	-0.33	0.24	10 +21.5	-0.32	0.34	
<i>Aldehydes</i>													
32.05	Pentanal	90-170	15 + 63.9	-0.48	+12.6	-1.13	+28.9	-0.37	0.30	10 +18.8	-0.79	0.64	
32.06	Hexanal	90-170	15 + 64.5	-0.32	+14.0	-1.03	+29.7	-0.26	0.23	10 +18.7	-0.56	0.47	
32.07	Heptanal	90-170	15 + 64.5	-0.30	+14.1	-0.68	+29.7	-0.12	0.40	10 +17.0	-0.11**	0.33	
<i>Ethers</i>													
33.06	Dipropylether	90-170	15 + 16.1	-0.41	- 0.5**	-0.49	+ 5.9	-0.29	0.19	10 + 4.5	-0.21*	0.54	
33.08	Dibutylether	90-170	15 + 16.5	-0.44	+ 1.0	-0.61	+ 6.6	-0.34	0.19	10 + 4.5	-0.24	0.27	
<i>Primary amines</i>													
34.04	Butylamine	90-170	15 + 25.8	-0.54**	+11.8	-1.98 ^s	+14.2	-0.83	1.28	10 +10.4	-0.60*	1.27	
34.05	Pentylamine	90-170	15 + 26.9	-0.31**	+16.6	-2.15	+16.4	-0.79	1.18	10 +10.7	-0.60*	1.53	
34.06	Hexylamine	90-170	15 + 27.3	-0.20**	+21.0	-2.42	+18.2	-0.84	1.09	10 + 9.9	-0.44*	0.95	
<i>Secondary amines</i>													
35.04	Diethylamine	90-170	15 + 20.5	+0.80**	+ 8.4	+1.95 ^s	+11.0	+1.13	1.36	10 + 6.9	+0.24*	0.63	
35.06	Dipropylamine	90-170	15 + 13.5	-0.38**	+ 1.0	-0.35**	+ 5.5	-0.23	1.13	10 + 3.3	-0.41**	1.26	
<i>Tertiary amines</i>													
36.06	Triethylamine	90-170	15 + 11.1	-0.72	+ 4.0	-0.83	+ 5.7	-0.54	0.86	10 + 3.4	-0.37*	0.59	
<i>Halomethanes</i>													
37.01	Dichloromethane	90-170	15 + 27.8	+0.14**	+ 7.2	+0.01**	+13.3	+0.17	0.49	10 +10.9	-0.03**	0.82	
37.02	Trichloromethane	90-170	15 + 17.1	-0.01**	+ 4.7	-0.28**	+ 8.2	-0.04	0.49	10 + 7.6	-0.32**	1.26	

No.	Thermodynamic data : C78 / TTF										C78 / MTF			
	TTF - C78			Mixture		id([CF ₃]=1) - C78			σ	MTF - C78			σ	
	ΔH	ΔS	ΔC_P	f_i	s	ΔH	ΔS	ΔC_P		ΔH	ΔS	ΔC_P		
	(cal mol ⁻¹)	(cal mol ⁻¹ K ⁻¹)		(cal mol ⁻¹)	(cal mol ⁻¹ K ⁻¹)	(cal mol ⁻¹)	(cal mol ⁻¹ K ⁻¹)	(cal mol ⁻¹ K ⁻¹)	(cal mol ⁻¹)	(cal mol ⁻¹)	(cal mol ⁻¹ K ⁻¹)	(cal mol ⁻¹)		
29.07	- 442	-0.806	- 1.2**	- 520	-1.049	-335	-0.632	-0.9	1.4	-337	-0.631	+0.5**	1.3	
<i>1-Alkanethiols</i>														
30.04	- 332	-0.873	+ 5.1	- 638	-1.495	-360	-0.879	+1.3	2.8	-165	-0.318	+0.6**	4.7	
30.05	- 319	-0.862	+ 4.0	- 632	-1.498	-355	-0.882	+0.9	1.8	-209	-0.437	-2.1**	3.3	
30.06	- 309	-0.851	+ 2.4	- 643	-1.526	-357	-0.891	+0.3	1.2	-187	-0.394	-1.5**	1.7	
<i>2-Alkanones</i>														
31.04	- 869	-1.337	+ 2.5**	- 740	-1.435	-543	-0.891	+0.4	2.4	-476	-0.809	+0.4**	2.7	
31.05	- 800	-1.250	+ 2.3*	- 632	-1.210	-483	-0.789	+0.3	1.6	-433	-0.752	+2.2*	1.6	
31.06	- 760	-1.179	+ 1.4**	- 628	-1.215	-469	-0.771	+0.0	1.6	-374	-0.626	+2.3*	1.8	
31.07	- 769	-1.239	+ 2.4 ^s	- 602	-1.156	-464	-0.776	+0.4	1.7	-331	-0.525	-0.1**	2.0	
<i>Aldehydes</i>														
32.05	- 683	-1.067	+ 0.3**	- 594	-1.137	-432	-0.710	-0.3	1.8	-417	-0.752	+2.6**	3.5	
32.06	- 637	-0.988	- 0.6**	- 573	-1.084	-408	-0.665	-0.7	1.3	-355	-0.615	+2.4**	2.4	
32.07	- 627	-1.001	- 0.8**	- 505	-0.934	-382	-0.621	-0.7	2.1	-243	-0.362	-1.1**	1.7	
<i>Ethers</i>														
33.06	- 180	-0.429	- 0.6**	- 328	-0.664	-182	-0.390	-0.5	1.2	-144	-0.265	+3.0**	2.7	
33.08	- 164	-0.450	+ 0.7**	- 357	-0.743	-190	-0.435	-0.0	1.2	-141	-0.267	-1.3*	1.0	
<i>Primary amines</i>														
34.04	- 301	-0.630	+13.8	- 783	-1.621	-382	-0.784	+4.7	4.1	-292	-0.549	+2.5**	5.3	
34.05	- 249	-0.516	+11.8	- 853	-1.749	-388	-0.787	+3.9	4.2	-285	-0.541	+3.9**	4.8	
34.06	- 229	-0.482	+ 6.7	- 941	-1.929	-413	-0.841	+2.0	4.5	-241	-0.441	-2.5**	5.6	
<i>Secondary amines</i>														
35.04	+ 38**	+0.199**	+ 4.0**	+ 110**	+0.556**	+ 75	+0.331	+1.7	8.2	- 78	-0.049**	+0.5**	3.9	
35.06	- 137	-0.381	- 1.5**	- 311 ^s	-0.614*	-162	-0.359	-0.9	4.9	-174	-0.349 ^s	-2.4**	6.4	
<i>Tertiary amines</i>														
36.06	- 194	-0.539	+ 1.8**	- 456	-0.924	-236	-0.529	+0.3	3.5	-172	-0.339	-0.8**	4.1	
<i>Halomethanes</i>														
37.01	- 196	-0.269	+ 5.6	- 310	-0.491 ^s	-164	-0.223	+1.9	2.8	-183	-0.251 ^s	+2.3**	5.0	
37.02	- 123	-0.266	- 0.0**	- 342	-0.623	-161	-0.301	-0.2	2.5	-213	-0.373 ^s	-3.3**	7.3	

(Continued on p. 200)

Table 6 (continued)

No.	Compound	Temp. range (°C)	Retention index : C78 / TTF							C78 / MTF		
			n TTF - C78		Mixture		id([CF ₃]=1) - C78 σ			n MTF - C78		σ
			ΔI_{130}	$\frac{10 \times \Delta A_T}{(K^{-1})}$	A_L	$\frac{10 \times A_{LT}}{(K^{-1})}$	ΔI_{130} (l mol ⁻¹)	$\frac{10 \times \Delta A_T}{(K^{-1})}$	ΔI_{130}	$\frac{10 \times \Delta A_T}{(K^{-1})}$		
37.03	Tetrachloromethane	90-170	15 + 1.6 ^s	-0.48	- 3.2	-1.11	- 0.7	-0.61	0.36	10 - 0.9**	-0.50 ^s	1.02
37.04	CF ₂ Br ₂	90-170	15 + 7.8	-1.06	- 3.0 ^s	+0.70**	+ 1.8	-0.12	0.70	10 + 1.2 ^s	-0.02**	0.74
HALOBENZENES												
38.01	Fluorobenzene	90-170	15 + 35.9	-0.15**	+ 1.4**	+0.04**	+14.1	+0.08	0.48	10 + 9.8	+0.03**	0.87
38.02	Hexafluorobenzene	90-170	15 + 61.1	-0.40*	+ 9.9	+1.01	+26.9	+0.45	0.52	10 +16.9	+0.80	0.37
38.03	Trifluoromethylbenzene	90-170	15 + 57.5	-0.15**	+ 9.1	+0.17**	+25.2	+0.22	0.62	10 +15.7	-0.30**	1.04
38.04	Chlorobenzene	90-170	15 + 29.3	-0.22	- 1.5*	-0.54 ^s	+10.5	-0.20	0.39	10 + 7.5	+0.08**	0.55
38.05	Bromobenzene	90-170	15 + 26.5	-0.57*	- 1.6*	-0.70 ^s	+ 9.4	-0.40	0.43	10 + 6.0	+0.33	0.52
38.06	Iodobenzene	130-210	15 + 24.0	-0.46*	- 7.2	+0.74	+ 6.3	+0.18	0.32	10 + 3.9	+0.78	0.28
ALKYLPYRIDINES												
39.01	Pyridine	90-170	15 + 56.0	-0.66	+11.8	+0.29**	+25.7	+0.07	0.32	10 +17.7	-0.57 ^s	0.76
39.02	2-Picoline	90-170	15 + 49.2	-0.62	+ 8.7	+0.61	+21.9	+0.18	0.24	10 +15.0	-0.42 ^s	0.65
39.03	3-Picoline	90-170	15 + 62.0	-0.25**	+15.5	+0.74 ^s	+29.4	+0.43	0.47	10 +19.8	-0.33**	0.90
39.04	4-Picoline	90-170	15 + 63.7	-0.31**	+15.2	-0.66 ^s	+29.9	-0.12	0.42	10 +19.6	-0.60	0.52
39.05	2,3-Lutidine	130-210	15 + 54.9	+0.10**	+ 9.9	+1.21	+24.2	+0.79	0.37	10 +15.8	+0.20**	0.63
39.06	2,4-Lutidine	130-210	15 + 57.4	+0.20**	+ 8.4	+1.66	+24.9	+0.89	0.35	10 +15.1	+0.34	0.09
39.07	2,5-Lutidine	130-210	15 + 53.8	+0.36*	+ 8.8	+1.54	+23.3	+1.03	0.49	10 +15.9	+0.13**	0.71
39.08	2,6-Lutidine	130-210	15 + 44.2	-1.60	+ 7.2	+0.66*	+17.9	+0.18	0.56	10 +15.5	+0.22**	0.69
39.09	3,4-Lutidine	130-210	15 + 72.9	-0.33**	+18.7	+0.54**	+33.3	+0.69	0.58	10 +20.5	+0.26*	0.65
39.10	3,5-Lutidine	130-210	15 + 68.1	-0.17**	+19.4	-0.15**	+33.7	+0.29	0.49	10 +19.9	-0.14	0.17
39.11	2-Ethylpyridine	130-210	15 + 43.6	-0.42*	+ 5.8	+0.66	+18.4	+0.34	0.36	10 +13.7	-0.79	0.10
39.12	3-Ethylpyridine	130-210	15 + 57.9	-0.21**	+ 6.9	+0.74	+24.5	+0.43	0.31	10 +15.8	-0.35 ^s	0.51
39.13	4-Ethylpyridine	130-210	15 + 61.6	+0.48**	+13.1	+0.33**	+29.0	+0.38	0.49	10 +19.6	-0.69	0.52
39.14	2-Propylpyridine	130-210	15 + 40.6	-0.09**	+ 5.1	+1.13	+18.2	+0.35	0.40	10 +16.6	-1.64	0.67
39.15	4-Propylpyridine	130-210	15 + 60.7	+0.96	+12.1	+2.30	+26.9	+1.64	0.24	10 +18.9	+0.32*	0.81
39.16	2,3,6-Collidine	130-210	15 + 43.0	-0.15**	+ 6.9	+0.78	+19.2	+0.35	0.34	10 +13.9	-0.49	0.39
39.17	2,4,6-Collidine	130-210	15 + 45.8	-0.17**	+ 7.7	+0.74	+19.9	+0.49	0.34	10 +14.6	-0.52	0.84
39.18	4-tert-Butylpyridine	130-210	15 + 66.6	+0.00**	+17.2	-0.01**	+31.2	+0.38	0.21	10 +19.8	-0.36*	0.77
39.19	3-Chloropyridine	90-170	15 + 43.7	-0.71	+ 3.0	-0.23**	+17.6	-0.21	0.29	10 +12.4	-0.31	0.36
ORGANOSILICON COMPOUNDS												
40.01	Tetramethylsilane	90-170	15 + 2.8	-0.05**	- 0.2**	-0.53*	+ 2.2	-0.19	0.49	10 + 4.9	+0.82*	1.89

No.	Thermodynamic data : C78 / TTF										C78 / MTF			
	TTF - C78			Mixture		id([CF ₃] _j =1) - C78			σ	MTF - C78			σ	
	ΔH (cal mol ⁻¹)	ΔS (cal mol ⁻¹ K ⁻¹)	ΔC _p	f _i (cal mol ⁻¹)	s (cal mol ⁻¹ K ⁻¹)	ΔH (cal l mol ⁻²)	ΔS (cal l mol ⁻² K ⁻¹)	ΔC _p		ΔH (cal mol ⁻¹)	ΔS (cal mol ⁻¹ K ⁻¹)	ΔC _p		(cal mol ⁻¹)
37.03	- 75	-0.348	+ 3.0 ^s	- 420	-0.955	-188	-0.496	+0.8	1.9	-154	-0.362	+3.6 ^{**}	5.7	
37.04	- 266	-0.706	+ 5.4	- 66 ^{**}	-0.029 ^{**}	-119	-0.262	+1.8	2.8	- 89 ^s	-0.139 ^{**}	-1.9 ^{**}	4.4	
HALOBENZENES														
38.01	- 339	-0.574	- 1.0 ^{**}	- 230	-0.394 ^s	-192	-0.310	-0.6	2.4	-159	-0.215 ^s	-4.0 ^{**}	4.3	
38.02	- 595	-0.817	+ 1.5 ^{**}	- 173	-0.098 ^{**}	-239	-0.224	+0.4	2.1	- 51 ^s	+0.162	-1.8 ^{**}	2.2	
38.03	- 540	-0.802	+ 1.9 ^{**}	- 297 ^s	-0.450 [*]	-273	-0.369	+0.5	4.1	-281	-0.449	-0.4 ^{**}	6.0	
38.04	- 268	-0.556	+ 1.6 ^{**}	- 324	-0.690	-211	-0.439	+0.3	1.6	-113	-0.159 ^s	-2.3 ^{**}	2.9	
38.05	- 296	-0.697	+ 4.7	- 360	-0.795	-238	-0.540	+1.4	2.1	- 44	-0.021 ^{**}	-0.8 ^{**}	2.9	
38.06	- 219	-0.565	+ 0.6 ^{**}	- 38 ^{**}	-0.081 ^{**}	- 97	-0.243	+0.1	1.7	+ 64 ^{**}	+0.209 [*]	-1.5 ^{**}	1.3	
ALKYLPYRIDINES														
39.01	- 626	-1.067	+ 4.0	- 302	-0.446	-309	-0.465	-0.5	1.6	-350	-0.618	+5.6 ^s	2.8	
39.02	- 548	-0.989	+ 3.5	- 204	-0.256 ^s	-251	-0.392	+1.1	1.5	-288	-0.509	+5.4	2.1	
39.03	- 598	-0.974	+ 6.0	- 240	-0.261 [*]	-272	-0.359	+2.0	2.3	-313	-0.521	+7.4	2.5	
39.04	- 631	-1.028	+ 2.8 ^{**}	- 515	-0.945	-387	-0.634	+0.6	2.8	-370	-0.654	+3.5 [*]	2.6	
39.05	- 402	-0.596	- 0.3 ^{**}	- 116	-0.039	-163	-0.160	-0.2	2.5	-168 ^{**}	-0.206 ^{**}	-0.0 ^{**}	3.3	
39.06	- 458	-0.698	+ 0.9 ^{**}	- 31 ^{**}	+0.159 ^s	-150	-0.121	+0.3	0.9	-128	-0.116	-0.2 ^{**}	0.4	
39.07	- 316	-0.393 [*]	- 1.2 ^{**}	- 39 ^{**}	+0.139 ^{**}	-103	-0.021	-0.5	3.2	-181 [*]	-0.240 ^{**}	+1.0 ^{**}	3.3	
39.08	- 469	-0.885	- 3.3 [*]	- 179 ^s	-0.224 ^{**}	-219	-0.357	-1.5	2.7	-151 ^{**}	-0.164 ^{**}	+0.8 ^{**}	3.4	
39.09	- 547	-0.762	- 1.8 ^{**}	- 305	-0.403 ^s	-274	-0.324	-0.9	2.3	-228 ^s	-0.289 ^{**}	-1.4 ^{**}	3.0	
39.10	- 581	-0.889	+ 0.6 ^{**}	- 444	-0.734	-339	-0.498	-0.1	1.1	-285	-0.444	+0.1 ^{**}	0.8	
39.11	- 389	-0.688	- 0.3 ^{**}	- 179	-0.240	-190	-0.290	-0.3	1.1	-333	-0.649	+3.1	0.5	
39.12	- 543	-0.907	+ 1.3 ^{**}	- 181	-0.235 ^s	-239	-0.349	+0.3	1.3	-268	-0.463 ^s	+2.3 ^{**}	2.5	
39.13	- 545	-0.859	+ 3.4 ^{**}	- 298	-0.452 ^s	-277	-0.396	+1.0	3.0	-366	-0.669	+4.7 ^s	2.4	
39.14	- 467	-0.933	+ 4.5	- 86 ^{**}	-0.031 ^{**}	-186	-0.310	+1.5	2.0	-503	-1.073	+8.9	3.2	
39.15	- 227	-0.125 [*]	- 2.1	+ 102	+0.513	- 13	+0.228	-0.6	1.0	-160 ^{**}	-0.169 ^{**}	+1.8 ^{**}	3.7	
39.16	- 400	-0.753	+ 2.3 [*]	- 145	-0.162 ^{**}	-183	-0.289	+0.7	1.8	-265	-0.493	+3.5 ^s	1.8	
39.17	- 351	-0.597	+ 0.2 ^{**}	- 168	-0.203 ^{**}	-171	-0.241	-0.1	2.0	-299 ^s	-0.557 [*]	+2.1 ^{**}	3.7	
39.18	- 514	-0.777	- 0.8 ^{**}	- 392	-0.650	-300	-0.437	-0.6	1.1	-309 ^s	-0.525 [*]	+1.3 ^{**}	3.6	
39.19	- 509	-0.984	+ 2.1	- 319	-0.623	-288	-0.547	+0.4	1.0	-238	-0.422	+3.3	0.9	
ORGANOSILICON COMPOUNDS														
40.01	- 8 ^{**}	-0.108 ^{**}	+17.9	- 361	-0.713	-130	-0.287	+6.5	3.6	+ 76 ^{**}	+0.289 [*]	+13.2 ^s	7.6	

(Continued on p. 202)

data presented in Table 6 are summarized as follows.

(i) Determinations of thermodynamic quantities of all substances were based on data collected for *n*-alkanes. Sets of standard chemical potentials of *n*-alkanes were first examined by variance analysis referring to the polynomial approximation given in Eqs. 20 and 22. Based on the results of the variance analysis, final data were calculated by fitting Kirchhoff's approximation to the original data (see Eq. 4) by non-linear regression techniques. For the regression it was assumed that ΔH , ΔS , ΔC_p , h and s are linear functions of the carbon number, z , of the *n*-alkanes and that the composition dependence in C78–TTF mixtures is described by Eqs. 5 and 6. Data on the standard alkane, C78, were always calculated with the coefficients given in Table 4 in ref. 1.

(ii) For all solutes other than *n*-alkanes, retention indices were determined. Temperature and composition dependences of the retention indices were analysed by linear regression where smoothed data on C78 were included from Table 4 in ref. 1. For the calculation of thermodynamic data, experimental retention indices were converted point by point into standard chemical potentials with the aid of the tabulated *n*-alkane data. Eq. 4 was then fitted to the resulting data as for *n*-alkanes. As a consequence of this procedure, retention indices calculated with Eq. 9 (*i.e.*, by using the "best" thermodynamic data) and the retention indices calculated with the coefficients of Eqs. 10–12 (*i.e.*, by using the "best" data fitted on the retention index scale) may be slightly different.

(iii) Thermodynamic data of *n*-alkanes in the ideal solvent idCF_3 ($[\text{CF}_3] = 1 \text{ mol l}^{-1}$) were determined with the aid of the final regression described under (i). Using the resulting regression coefficients and the molar volume of TTF, the value of $\Delta \mu^{\text{idX}}$ was then calculated with Eq. 8 at 20 K intervals. Fitting Eq. 4 to the results, by assuming a linear dependence of ΔH , ΔS and ΔC_p on the carbon number z , gave the thermodynamic functions shown in Table 6.

(iv) Thermodynamic data for solutes other than *n*-alkanes in the ideal solvent idCF_3 were

individually calculated following the procedure described under (iii).

(v) For retention indices on idCF_3 , a combination of Eqs. 10, 11 and 12 was fitted to the retention index data set of a given solute to give the index as a function of temperature and composition on C78–TTF mixtures. The resulting regression coefficients were used in Eq. 13 to calculate the value of $\Delta \mu^{\text{idX}}$ at 20 K intervals in the experimental temperature range. The resulting data set was then used to determine the coefficients of the linear relationship listed in Table 6.

4. Results and discussion

Retention index and thermodynamic data for about 160 solutes are presented in Table 6 measured using C78–TTF mixtures and pure MTF. The solvent MTF contained one whereas TTF contained four trifluoromethyl (TF) groups in the molecule. The distance between TF groups can be increased at will in the melt of MTF by dilution with the standard alkane C78, contrary to the TTF melt. In fact, with C78–TTF mixtures ideally dilute TF solutions cannot be prepared as the four TF groups are in the same molecule. The study of the effect of this regroupment of the TF groups was the first objective of this project.

In future work, data on a stationary liquid containing TF groups will be determined at only one TF concentration in order to economize on experimental effort. Obviously, determination at only one concentration of the interacting group does not permit the calculation of the curvature of the relationship between chromatographic data and concentration of the interacting group and data at ideal dilution cannot be determined. Therefore, the question of the predictability of the curvature of the composition dependence was the second objective.

Concerning the correlation of data on the stationary phases MTF and TTF, based on experience with a primary alcohol-containing stationary phase (POH contains an OH group instead of CF_3), it was assumed that composition

dependence of solution data in C78–TTF mixtures could be described by the simple quadratic Eqs. 5 and 10. Therefore, experimental data were determined at only two compositions ($\varphi_{\text{TTF}} = 0.50$ and 1). These data, together with data on pure C78 ($\varphi_{\text{TTF}} = 0$), permitted the determination of the constants A_L , A_{LT} and \hat{h} , s necessary to calculate the constants i and m , respectively, at a given temperature (Eqs. 6 and 12). With these constants listed in Table 6, retention index differences ΔI were calculated for a mixture containing a 0.25 volume fraction of TTF. Certainly in this mixture the spatial distribution of the TF groups will be different from that in an MTF melt. However, if these interacting groups are distant enough in the TTF molecule, data in both liquids should be the same. As an example, in Fig. 4, retention index differences in the MTF melt determined at 130°C are plotted as a function of those found in the mixture. The correlation is excellent, the correlation coefficient being $r = 0.988$ with all data taken and without the four outliers (amines) $r = 0.990$. The data are represented by Eq. 31 (without outliers)

$$\Delta I_{130}^{\text{MTF}} = (0.82 \pm 0.17) + (0.994 \pm 0.013) \Delta I_{130}^{\text{C78/TTF}}(\varphi_{\text{TTF}} = 0.25) \quad (31)$$

The slope of the correlation line does not deviate from unity. The slight positive deviation of the intercept (less than 1 index unit) is the only difference between the two liquids.

In conclusion, mixtures of C78–TTF may be used to determine data representative of melts of the monosubstituted compound MTF. Consequently, it may be assumed that the initial slopes of the equation representing interaction energies as a function of the volume fraction of TTF are the same as those which would be found with data determined in C78–MTF mixtures. The latter system would give less precise data because of the weak interaction of the TF group with some solutes.

The curvature of the composition dependence of the retention data in terms of standard chemical potential is given by the constant m in Eq. 5. In Part I [1] it was shown that this constant could be given as a function of the standard chemical potentials $\Delta\mu_j^{\text{C78}}$ and $\Delta\mu_j^{\text{POH}}$ with the exception

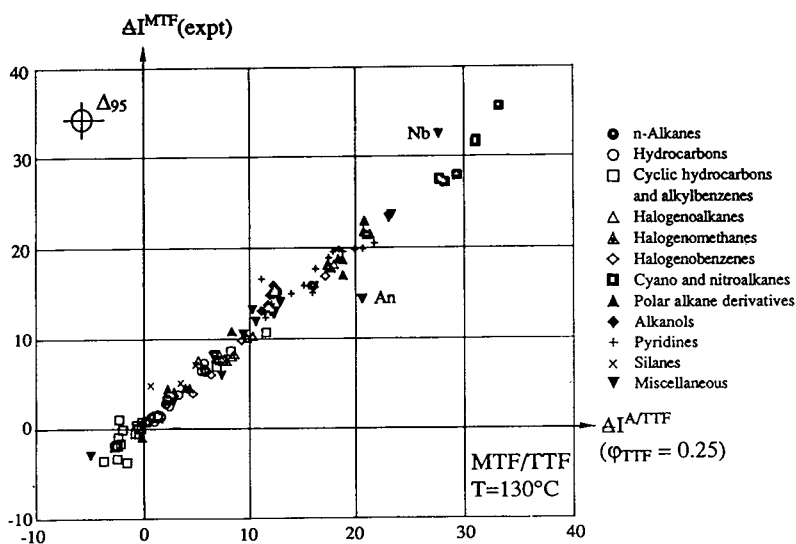


Fig. 4. Retention index differences on the MTF stationary liquid with reference of the standard alkane, C78, as a function retention index differences on a C78–TTF mixture with $\varphi_{\text{TTF}} = 0.25$. Both liquids contain the same molar concentration of TF groups. Outliers: Nb = nitrobenzene; An = aniline.

of the alcohols. The present data correlate without exception with the equation

$$m_j^{(e)} = a + b \Delta\mu_j^A + c \Delta\mu_j^{\text{TTF}} \quad (32)$$

where $a = -76 + 0.608 \Delta T$, $b = -0.00895 + 0.000063 \Delta T$, $c = 0.2757 - 0.00032 \Delta T$, $\Delta T = T - T^\dagger$ and $\sigma = \pm 25.1 \text{ cal mol}^{-1}$. As an illustration, in Fig. 5 are plotted constants $m_j^{(e)}$, estimated with Eq. 32, as a function of the constants calculated with data listed in Table 6 (h and s and use of Eq. 6).

Knowledge of the numerical values of the constants of Eq. 32 allows the estimation of the extent of curvature of the composition dependence. If working with a C78–TTF (or C78–MTF) mixture of known composition, φ_{TTF} , first the retention index of the compound in question is determined on this mixture and on the pure standard hydrocarbon. The index is now converted into standard chemical potentials by using data for *n*-alkanes listed in Table 6 to give $\Delta\mu_j^{\text{C78}}$ and $\Delta\mu_j^{\text{C78/TTF}}(\varphi_{\text{TTF}})$. Rearrangement of Eq. 5 gives

$$\Delta\mu_j^{\text{TTF}} = \frac{\Delta\mu_j^{\text{C78/TTF}}}{\varphi_{\text{TTF}}} - \varphi_{\text{C78}} m_j \quad (33)$$

Substitution of Eq. 33 in Eq. 32 gives after rearrangement

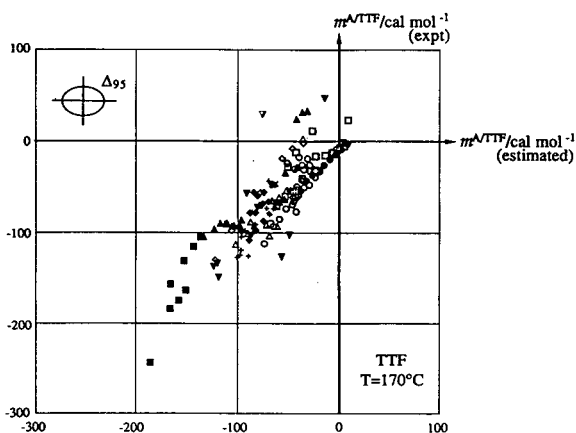


Fig. 5. Connection between experimental constants characterising the non-ideality of C78–TTF mixtures (constant m in Eq. 5) and those estimated with Eq. 32 at 170°C.

$$m_j^{(e)} = \frac{\varphi_{\text{TTF}}(a + b \Delta\mu_j^{\text{C78}}) + c \Delta\mu_j^{\text{C78/TTF}}}{\varphi_{\text{TTF}}(1 + c\varphi_{\text{C78}})} \quad (34)$$

Use of the measured values in Eq. 34 allows the estimation of $m_j^{(e)}$ and by use of Eq. 33 the values of $\Delta\mu_j^{\text{TTF}}$ can be calculated. The value of the derivative of $\Delta\mu_j^{\text{C78/TTF}}$ with respect to the volume fraction can now be calculated as follows:

$$\left(\frac{\partial \Delta\mu_j^{\text{C78/TTF}}}{\partial \varphi_{\text{TTF}}} \right)_{T, \varphi_{\text{TTF}}=0} = \Delta\mu_j^{\text{TTF}} + m_j^{(e)} \quad (35)$$

Finally, use of Eq. 8 permits the calculation of the standard chemical potential of the interaction at infinite dilution.

Fig. 6 illustrates the quality of the results when applying the proposed procedure. Data measured on MTF were considered as data measured on a C78–TTF mixture with $\varphi_{\text{TTF}} = 0.25$. With the aid of MTF data, the constant $m_j^{(e)}$ was estimated for each substance and the standard chemical potential of interaction was calculated with this estimated curvature. Estimated $\Delta\mu_j^{\text{idCF}_3}$ data are plotted as a function of data calculated with data measured on C78–TTF mixtures at 130°C.

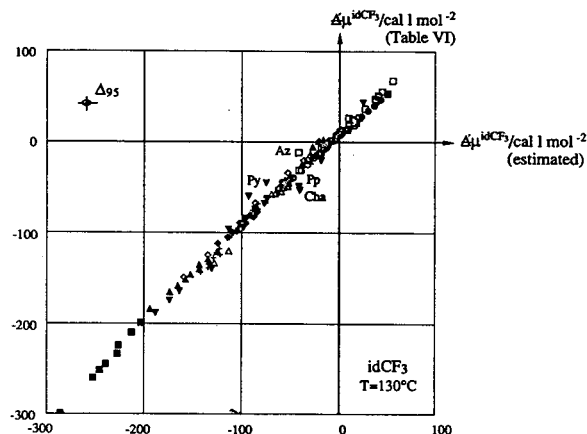


Fig. 6. Comparison of estimated and experimental standard chemical potential differences in an ideal TF solution ($[\text{CF}_3] = 1$). Estimated data were calculated from measurements on MTF with non-ideality given by Eq. 32. Outliers: Az = azulene; Py = pyrrolidine; Pp = piperidine; Cha = cyclohexylamine.

References

- [1] K.S. Reddy, J.-Cl. Dutoit and E.sz. Kováts, *J. Chromatogr.*, 609 (1992) 229.
- [2] R. Cloux, G. Défayes, K. Fóti, J.-Cl. Dutoit and E.sz. Kováts, *Synthesis*, (1993) 909.
- [3] J.H. Hildebrand and R.L. Scott, *The Solubility of Nonelectrolytes*, Reinhold, New York, 3rd ed., 1950.
- [4] E.A. Guggenheim, *Mixtures*, Oxford University Press, Oxford, 1952.
- [5] K.S. Reddy and E.sz. Kováts, *Chromatographia*, 34 (1992) 249.
- [6] R.C. Reid, J.M. Prausnitz and T.K. Sherwood, *The Properties of Gases and Liquids*, McGraw-Hill, New York, 3rd ed., 1977.
- [7] W.J.A. VandenHeuvel, E.O.A. Haachte and E.C. Horning, *J. Am. Chem. Soc.*, 83 (1961) 1513.
- [8] W. Ecknig, T. Kleinert and H. Kriegsmann, *J. Chromatogr.*, 147 (1978) 3.
- [9] J.A. Yancey, *J. Chromatogr. Sci.*, 23 (1985) 161.
- [10] G.A. Huber and E.sz. Kováts, *Anal. Chem.*, 45 (1973) 1155.
- [11] R. Cloux and E.sz. Kováts, *Synthesis*, (1992) 409.
- [12] G. Körösi and E.sz. Kováts, *J. Chem. Eng. Data*, 26 (1981) 323.
- [13] G. Défayes, D.F. Fritz, T. Görner, G. Huber, C. de Reyff and E.sz. Kováts, *J. Chromatogr.*, 500 (1990) 139.
- [14] D.F. Fritz, A. Sahil and E.sz. Kováts, *J. Chromatogr.*, 186 (1979) 63.



ELSEVIER

Journal of Chromatography A, 673 (1994) 211–218

JOURNAL OF
CHROMATOGRAPHY A

Matrix effects during standard addition quantitation of a trace volatile impurity in a drug substance sample

Jeffrey J. Sun*, Daryl A. Roston

Searle R & D, Product Development Analytical Department, Skokie, IL 60077, USA

(First received September 7th, 1993; revised manuscript received February 14th, 1994)

Abstract

Matrix effects during standard addition analysis were studied through the determination of trace amounts of butyric acid (a reagent in the synthesis of an experimental drug substance and a residual component affecting the drug quality). By studying the calibration curves with the same concentrations of added component (butyric acid) and different concentrations of drug matrix, it was found that the y -intercept in standard addition analysis is comprised of three factors: (1) y -intercept from a pure analyte calibration curve (without matrix substance), (2) matrix effect from the matrix substance and (3) analyte in the matrix substance. As the matrix effect was quantitatively determined, the absolute value (without matrix effect) of butyric acid in the drug sample could be obtained. Use of an internal standard greatly improved the linearity of the calibration curve and was necessary in this determination. The combination of internal standard and standard addition approaches yielded high accuracy in the determinations.

1. Introduction

One of the most important and difficult analytical problems in pharmaceutical analysis as well other types of chemical analysis is to determine trace amounts of residual components, such as impurities, solvents and reagents, in a large excess of sample matrix substances [1–4]. Standard addition is the most common and useful quantitative method for trace analysis [2,3]. It is widely used in gas chromatography (GC) [2,5], headspace determination [6,7], absorption measurement [8], potentiometric and polarographic measurements [9], etc. The basis for using the standard addition method is to eliminate or minimize matrix effects on the

quantitative results. A typical standard addition method is as follows: a series of sample solutions of the same concentration, which contain the analyte of interest, are spiked with increasing amounts of standards of the analyte. The instrumental response of these solutions are plotted *versus* the concentrations of added standards. A linear curve is obtained and extrapolated to the y -axis (see Fig. 1). The y -intercept K and slope A' are obtained ($y = A'x + K$). K is commonly accepted as the response of the analyte of interest. The concentration of the analyte (OX) is determined as K/A' .

A simple calibration curve of a series of standard solutions of a pure analyte is adequate for quantitation of the analyte without matrix substance. The linear equation $y = Ax + B$ is obtained from standard solutions, in which A is

* Corresponding author.

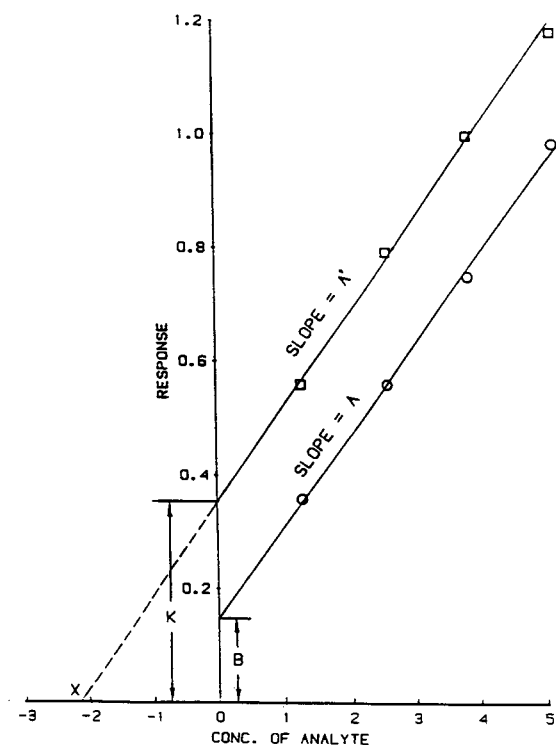


Fig. 1. Calibration curves with and without matrix substance.

the slope of the linear curve and B is the y -intercept (see Fig. 1). The unknown concentration of the analyte can be determined easily by this equation. The calibration curve does not pass through the origin (0) necessarily and, therefore, B cannot be neglected in quantitative analysis. The instrumental response from the analyte of unknown concentration is the sum of two parts: B and response from the analyte. B could be positive, negative or zero.

Compound SC-49483 [1,5-(butylimino)-1,5-dideoxy-D-glucitol tetrabutanoate] is an experimental drug substance being developed at Searle for the treatment of AIDS. Butyric acid is one of the reagents in synthesis. Because of its noxious smell, trace amounts of butyric acid in the drug will affect the drug quality. During the determination of residual butyric acid in drug substance samples by capillary GC, the problem of accurate quantitation was addressed and extensively studied. Internal standard and standard addition methods were studied and combined for

accurate determinations at ppm levels. The matrix effect from the drug was also studied and quantitatively determined. The present study has shown that K in standard addition analysis is comprised of three factors: (1) B from the pure analyte calibration curve (without matrix substance), (2) matrix effect from matrix substance and (3) analyte in the matrix substance. This paper has also shown the ways to determine matrix effects quantitatively and to determine the absolute value (without matrix effect) of trace components in a large amounts of matrix.

2. Experimental

2.1. Chemicals

The major drug component SC-49483 was synthesized by the Chemical Sciences Department of Searle Research and Development. Butyric acid, valeric acid and all other solvents were purchased from Aldrich (Milwaukee, WI, USA). The solvent methylene chloride was HPLC grade (99.9% pure).

2.2. Apparatus and conditions

All GC analyses were performed on a Hewlett-Packard HP 5890 gas chromatograph equipped with a flame ionization detector and an HP 7673 autosampler. A fused silicone capillary column DB-EEAP of 15 m \times 0.53 mm I.D. and 1 μ m thickness (J & W, Folsom, CA, USA) was used for analysis. A piece of 90 cm of phenylmethyl siloxane deactivated uncoated fused-silica tubing with 0.53 mm I.D. (J & W) was used for protection of major column. Carrier gas (helium) flow-rate was 5 ml/min, hydrogen and air flow-rates were 30 and 350 ml/min, respectively. The split ratio is 1:12. The GC conditions were as follows: the initial temperature was 110°C, held for 1 min, then raised at 8°C/min to 175°C, then raised at 70°C/min to 250°C, held for 10 min. The injection and detection temperatures were 180 and 260°C, respectively. All the data and chromatogram were recorded and processed with an in-house chromatographic data system.

2.3. Procedure for calibration curves with internal standard and drug matrix

A diluting solution (about 5 $\mu\text{g}/\text{ml}$) was made by accurately weighing about 5 mg valeric acid into a 1000-ml volumetric flask, filling with methylene chloride to the volume and shaking well. The concentration of valeric acid can be accurately calculated. This diluting solution was used for preparing all the calibration standards and drug samples. A stock solution of matrix sample (about 150 mg/ml) was made by accurately weighing about 1500 mg SC-49483 into a 10-ml volumetric flask, filling with diluting solution to the volume and shaking well until SC-49483 was completely dissolved. Then a series of calibration standards was made with five different concentrations of butyric acid and the same concentration of drug matrix (15 mg/ml, 1.00 ml stock solution of matrix sample solution in each of the standards). These standards were then injected into the GC system. The run was duplicated and the data were averaged. A calibration curve could be made by plotting the peak area ratio of butyric acid to valeric acid of these five standards *versus* the concentration of added butyric acid.

For quantitative determination of the matrix effect, five calibration curves were made with different matrix concentrations as 0, 15.07, 30.07, 45.05 and 60.02 mg/ml SC-49483 (see Table 3). The concentrations of added butyric acid for each of these calibration curves were the same, *viz.* 1.29, 2.58, 3.87, 5.16 and 6.45 $\mu\text{g}/\text{ml}$ (not listed in Table 3). The concentration of internal standard valeric acid was 4.37 $\mu\text{g}/\text{ml}$. The results in Table 3 are the average of two runs.

3. Results and discussion

3.1. Internal standard in the determination of butyric acid

Because of the nature of GC, especially under split injection mode, an internal standard can greatly improve the linearity of the calibration

curve for quantitation. The highest precision for quantitative chromatography is obtained by use of an internal standard because the uncertainties introduced by sample injection are avoided [10]. The internal standard approach is widely used in GC [11,15], headspace GC [12], GC–mass spectrometry [13], vapor measurement [14], liquid chromatography [16], etc. In the present analysis of trace amounts of butyric acid in the drug substance, the evaporation mode of the matrix substance is complicated. The evaporation rate of matrix substances and the exact split ratio of this vapor are unpredictable. Although an auto-sampler is used and the injected sample volume is constant, the amounts of butyric acid entering the separation column are different from injection to injection with the same sample solution. Therefore, an internal standard, valeric acid, was used since it has chemical properties similar to butyric acid and a suitable retention time. A chromatogram of butyric acid in drug matrix SC-49483 spiked with the internal standard valeric acid is shown in Fig. 2.

Tables 1 and 2 summarize the data for the responses of five concentrations of butyric acid, the internal standard valeric acid and respective peak area ratios. Table 1 was obtained from standards without drug matrix, Table 2 from

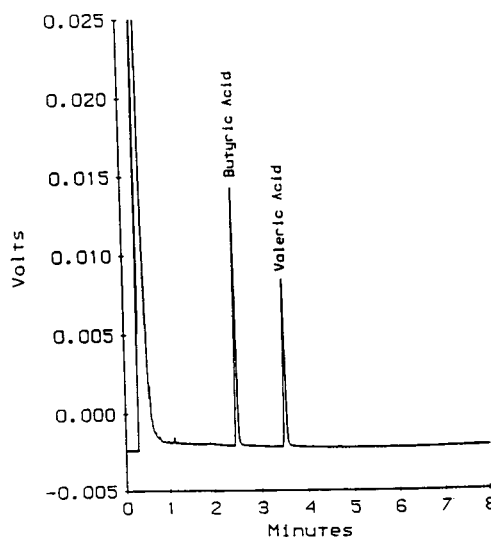


Fig. 2. Chromatogram of determination of butyric acid.

Table 1

Linearity without drug matrix

Concentration of butyric acid ($\mu\text{g/ml}$)	Peak area		Peak area ratio butyric acid/valeric acid
	Butyric acid ($t_R = 2.44$ min)	Valeric acid ($t_R = 3.46$ min) ^a	
1.91	0.0000653	0.0005057	0.12913
3.83	0.0000885	0.0003612	0.24502
5.74	0.0002163	0.0006028	0.35883
7.65	0.0001401	0.0002951	0.47475
9.56	0.0002223	0.0003790	0.58654
Average		0.0004338	
R.S.D. (%)		0.3058	
Correlation coefficient	0.8053		0.9999
y-Intercept	0.0003677		0.01537
Slope	0.00001912		0.05986

^a The concentration of valeric acid is 5.56 $\mu\text{g/ml}$.

standards with drug matrix. The internal standard significantly improved the linearity of the calibration curve for butyric acid with and without drug matrix. Without using internal standards, the linear correlation coefficients for butyric acid are 0.9212 and 0.8053, with and

without drug matrix, respectively. However, they are larger than 0.999 when using the internal standard valeric acid. It is obvious that use of an internal standard greatly improved the response linearity for butyric acid in the SC-49483 drug substance samples.

Table 2

Linearity with drug matrix SC-49483^a

Concentration of butyric acid ($\mu\text{g/ml}$)	Peak area		Peak area ratio butyric acid/valeric acid
	Butyric acid ($t_R = 2.44$ min)	Valeric acid ($t_R = 3.46$ min) ^b	
3.83	0.0003044	0.0004044	0.75272
5.74	0.0003948	0.0004547	0.86826
7.65	0.0005360	0.0005368	0.99851
9.56	0.0006228	0.0005527	1.12683
Average		0.0004996	
R.S.D. (%)		0.1333	
Correlation coefficient	0.9212		0.9996
y-Intercept	0.0002083		0.5087
Slope	0.00004065		0.06412

^a The concentration of SC-49483 is 15.024 mg/ml.

^b The concentration of valeric acid is 5.56 $\mu\text{g/ml}$.

3.2. Standard addition to minimize matrix effect

Previous authors have suggested that the standard addition method should be used to minimize errors when the difference in slopes of analyte calibration curves with and without sample matrix is larger than 5% [1]. Tables 1 and 2 compare slope values for butyric acid in a range of 1.91 to 9.56 $\mu\text{g/ml}$, with and without drug matrix. The slope value is 0.06412 and the linear correlation coefficient is 0.9997 with drug matrix, while it is 0.05986 without drug matrix. The difference between these two slopes is 7.1%, indicating that the standard addition method should be used for this analysis.

3.3. Quantitative determination of matrix effect

Although the matrix affects quantitative analysis, the quantitative study of matrix effects has not been reported. Usually, attempts are made to approximate the concentrations of analyte and matrix substance in standard addition analysis to minimize the matrix effects. In the present paper, a study was conducted to determine the

quantitative effects of the matrix substance in trace analysis.

Data in Table 3 and Fig. 3 show the information of calibration curves with different concentrations of drug matrix. The slopes of these calibration curves are different (7.2 to 11.1%) from the slope determined without matrix drug. The average of four slopes with drug matrix (concentrations from 15.07 to 60.02 mg/ml) is 0.1640 with 1.63% R.S.D. Although the matrix concentration increases 400%, the slopes of the calibration curves have only small changes in the range from 0.1616 to 0.1649. However, the y -intercept values exhibited marked changes from 0.1126 to 0.4615 as the matrix concentration increases. As shown in Table 3, the pure butyric acid calibration curve has an intercept of 0.01235, which means there was a chromatographic response at zero concentration of butyric acid although no peak was detected at this point. The response is not contributed by butyric acid but by unknown system factors. The zero-butyric acid response (y -intercept, 0.01235), of course, is also included in the y -intercepts of calibration curves with drug matrix since they are under the same experimental conditions. This is an im-

Table 3

Multiple calibration curve with different amounts of drug matrix

Matrix concentration (mg/ml of SC-49483)	Correlation coefficient	y -Intercept	Slope (ml/ μg)	Difference of slope (%) compared with pure butyric acid
0	0.9998	0.01235	0.1507	
15.07	0.9991	0.1126	0.1622	+ 7.6%
30.07	0.9980	0.2198	0.1616	+ 7.2%
45.05	0.9995	0.3403	0.1674	+ 11.1%
60.02	0.9919	0.4615	0.1649	+ 9.4%
Average ^a			0.1640	
S.D. ^a			0.00267	
R.S.D. (%) ^a			1.63	

The sample lot used in this table is different from the one used in Tables 1 and 2; therefore, the concentrations of butyric acid in these two sample lots are different. The concentrations of added butyric acid and internal standard valeric acid are described in the Experimental section.

^a Average, S.D. and R.S.D. are statistics of four slopes with different concentrations of drug matrix SC-49483.

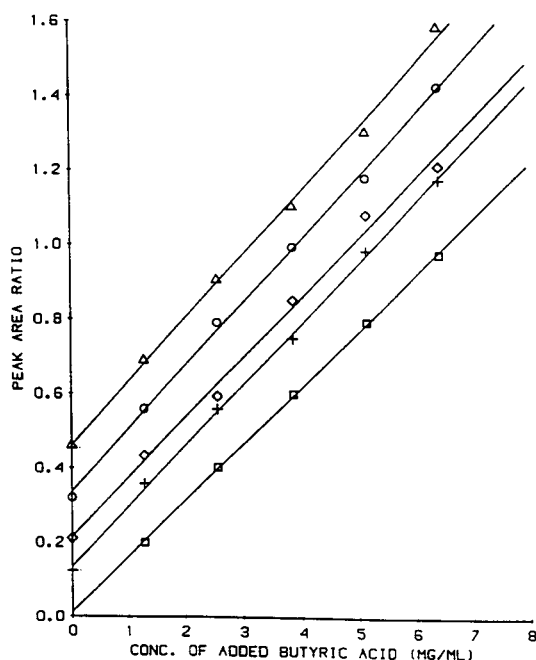


Fig. 3. Calibration curves with different concentrations of drug matrix including 0 (\square), 15.07 (+), 30.07 (\diamond), 45.05 (\circ) and 60.02 (Δ) mg/ml.

portant factor which should be considered in standard addition analysis.

Another factor, which is important but usually neglected in standard addition analysis, is the quantitative impact of the matrix concentration

on the analysis of the analyte. The y -intercept of the calibration curve with 15.07 mg/ml matrix concentration is 0.1126. The difference between 0.1126 and 0.01235 (y -intercept without matrix, see Fig. 3 and Table 3) is contributed by two factors: butyric acid in the drug substance and the matrix effect, which could be positive, negative or zero. Since butyric acid always exists in the drug samples, it is difficult to determine quantitative effects of matrix directly. An indirect method has to be used.

Data in Table 4 were used for studying the matrix effect quantitatively. Column 5 is analogous to the equation of K/A' (see Introduction). If the matrix effect is not considered, these values can be assumed to represent the concentration of butyric acid in the sample solution. The assumed unit concentrations of butyric acid in drug matrix ($\mu\text{g}/\text{mg}$) can be calculated by column 5/column 1 and are listed in column 6. The assumed unit concentration of butyric acid ($\mu\text{g}/\text{mg}$) increases as concentrations of drug matrix (mg/ml) increases. The increase is due to the matrix effects since the unit concentration of butyric acid in the drug matrix is constant in the same lot. The values in columns 5 and 6 are contributed by two factors: butyric acid in the drug substance and the matrix effect from the drug substance. A plot of assumed unit concentration *versus* matrix concentration was

Table 4

Matrix effect on chromatographic response

1: Matrix amounts (mg/ml of SC-49483)	2: y -Intercept	3: Difference of y -intercept with and without drug matrix	4: Slope (ml/ μg)	5: Column 3 divided by column 4 ($\mu\text{g}/\text{ml}$)	6: Assumed unit concentration of butyric acid ($\mu\text{g}/\text{mg}$)
0	0.01235				
15.07	0.1126	0.10025	0.1622	0.61806	0.0410
30.07	0.2198	0.20745	0.1616	1.28373	0.0427
45.05	0.3403	0.32795	0.1674	1.95908	0.0435
60.02	0.4615	0.44915	0.1649	2.72377	0.0454
y -Intercept ($\mu\text{g}/\text{ml}$)					0.0396
Slope ($\mu\text{g ml}/\text{mg}^2$)					0.0000934
Correlation coefficient					0.9895

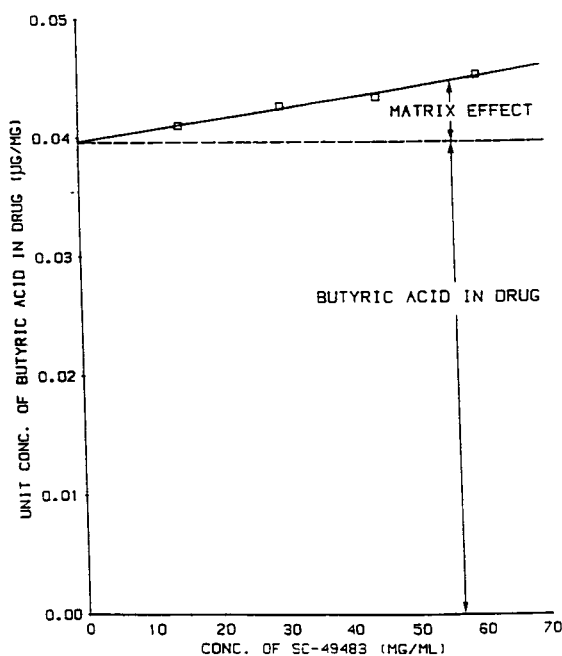


Fig. 4. Unit concentration ($\mu\text{g}/\text{mg}$) of butyric acid with different concentrations of drug matrix (mg/ml).

linear (Fig. 4). The intercept, slope and correlation coefficient were calculated and are also listed in column 6, Table 4. The value of intercept ($0.0396 \mu\text{g}/\text{mg}$) is the actual unit concentration of butyric acid in drug matrix SC-49483 since it is the value at zero concentration of drug matrix. Matrix effects no longer exist at this point. The higher assumed unit concentration of butyric acid observed with the higher concentration of drug matrix is due to the increased matrix effect, which has a positive quantity of 0.0000934 (slope) with a unit ($\mu\text{g}/\text{mg}$ per $\text{mg}/\text{ml} = \mu\text{g ml}/\text{mg}^2$). This means that $1 \text{ mg}/\text{ml}$ increase in concentration of drug matrix will result in $0.0000934 \mu\text{g}/\text{mg}$ increase in the experimentally determined butyric acid level. The matrix effects could be negative or zero. If it is negative, the assumed unit concentration of butyric acid would decrease as the concentration of matrix increases. If it is zero, the assumed unit concentration of butyric acid would not change as the concentration of the matrix changes.

The experiments detailed above illustrate the

impact of drug matrix concentration on butyric acid determination. It has been illustrated that K (see Introduction and Fig. 1) during standard addition analysis is comprised of three parts: (1) B from the pure butyric acid calibration curve (without drug matrix), (2) matrix effect from drug substance and (3) butyric acid in the drug substance.

3.4. Deviation in routine analysis due to matrix effect

It has been shown that the true value of butyric acid concentration in the matrix drug is accessible. However, it is not practical to analyze routine samples in this manner. It is much more practical in daily analysis to use one calibration curve for multiple samples under the same conditions, although some deviation in analysis will result.

The impact of the matrix concentration dependence illustrated in Table 4 and Fig. 4 on quantitative results can be understood by considering the following example. The deviation can be estimated according to the linear regression data (intercept and slope) in column 6 of Table 4. The slope is $0.0000934 (\mu\text{g ml}/\text{mg}^2)$, which means that a $1 \text{ mg}/\text{ml}$ increase of matrix concentration causes $(1 \times 0.0000934/0.0396 =)$ 0.24% deviation. For example, the deviation at $5.0 \text{ mg}/\text{ml}$ matrix concentration is about $(5 \times 0.0000934/0.0396 =)$ 1.2% higher. In daily analysis, it is difficult to weigh the sample so that it has exactly the same concentration as the matrix drug. But it can be weighed very close. For the concentration of matrix of $15.00 \text{ mg}/\text{ml}$, it is easy to weigh 140 to 160 mg sample for a 10-ml volumetric flask. The concentration would be within 14.0 to $16.0 \text{ mg}/\text{ml}$, and the error would be within $(\pm 1 \times 0.0000934/0.0396 =) \pm 0.24\%$, which is insignificant.

4. Conclusions

Matrix effects during standard addition analysis were extensively studied through the determination of trace amounts of butyric acid in the

matrix drug SC-49483. Both internal standard and standard addition are necessary for quantitation because of the nature of GC and matrix effect. Linearity is greatly improved by the use of internal standard. The difference of slopes with and without matrix drug is larger than 7%. The matrix effect was studied by calibration curves with different concentrations of matrix drug. The slopes have small changes when the concentration of matrix drug increased 400% from 15 to 60 mg/ml. The matrix effect of the drug substance was quantitatively analyzed and the true value of butyric acid concentration in the matrix drug was accurately determined. The deviation using one calibration curve for multiple samples in routine analysis was also discussed quantitatively.

5. References

- [1] J.E. Haky and T.M. Stickney, *J. Chromatogr.*, 321 (1985) 137.
- [2] R.W. Souter, *J. Chromatogr.*, 193 (1980) 207.
- [3] J. Novák, *Quantitative Analysis by Gas Chromatography*, Marcel Dekker, New York, 1975, p.138.
- [4] D.W. Foust and M.S. Bergren, *J. Chromatogr.*, 469 (1989) 161.
- [5] Y.K. Chan, P.T.S. Wong, G.A. Gengert and O. Kramar, *Anal. Chem.*, 51(1979)186.
- [6] J. Drozd and J. Novák, *J. Chromatogr.*, 136 (1977) 37.
- [7] J. Drozd and J. Novák, *J. Chromatogr.*, 152 (1978) 55.
- [8] D.A. Skoog, *Principles of Instrumental Analysis*, Saunders College Publ., Philadelphia, 1985, pp. 210, 279.
- [9] D.A. Skoog, *Principles of Instrumental Analysis*, Saunders College Publ., Philadelphia, 1985, p. 630.
- [10] D.A. Skoog, *Principles of Instrumental Analysis*, Saunders College Publ., Philadelphia, 1985, p. 694.
- [11] N.C. Shantha and R.G. Ackman, *J. Chromatogr.*, 533 (1990) 1.
- [12] C. B'Hymer, *J. Chromatogr.*, 438 (1988) 103.
- [13] A.E. Stafford, J. Corse and M. Lyman, *J. Chromatogr.*, 436 (1988) 93.
- [14] R.E. Schirmer, T.R. Pahl and D.W. Phelps, *Am. Ind. Hyg. Assoc. J.*, 45 (1984) 95.
- [15] M. Picer and N. Picer, *Ocean Sci. Engr.*, 8 (1983) 63.
- [16] I.D. Wilson, C.R. Bielby and E.D. Morgan, *J. Chromatogr.*, 236 (1982) 224.



ELSEVIER

Journal of Chromatography A, 673 (1994) 219–230

JOURNAL OF
CHROMATOGRAPHY A

Large-rim-tethered permethyl-substituted β -cyclodextrin polysiloxanes for use as chiral stationary phases in open tubular column chromatography

Guoliang Yi, Jerald S. Bradshaw*, Bryant E. Rossiter, Abdul Malik, Wenbao Li,
Hao Yun, Milton L. Lee

Department of Chemistry, Brigham Young University, Provo, UT 84602-4672, USA

(First received February 25th, 1994)

Abstract

3-O-(*p*-Allyloxybenzoyl)heptakis(2,6-di-O-methyl)- β -cyclodextrin, which was used for preparation of permethylated 3-O-(*p*-allyloxybenzoyl)- β -cyclodextrin (**4**), was produced in a 15% yield by a monoesterification of heptakis(2,6-di-O-methyl)- β -cyclodextrin. Heptakis[6-O-(*tert*.-butyl)dimethylsilyl]- β -cyclodextrin was regioselectively monoesterified with *p*-allyloxybenzoyl chloride or *p*-(*tert*.-butyl)benzoyl chloride to yield 2-O-(*p*-allyloxybenzoyl)heptakis[6-O-(*tert*.-butyl)dimethylsilyl]- β -cyclodextrin (**6**) or 2-O-[*p*-(*tert*.-butyl)benzoyl]heptakis[6-O-(*tert*.-butyl)dimethylsilyl]- β -cyclodextrin (**7**). Compound **6** was acylated to give tridecaacetate **8**, which was deprotected and methylated, to give 2^A-O-(*p*-allyloxybenzoyl)heptakis(3-O-acetyl-6-O-methyl)-2^B,2^C,2^D,2^E,2^F,2^G-hexa-O-acetyl- β -cyclodextrin (**10**). Both **6** and **7** were methylated, following by deprotection and methylation (on the 6-position), to give permethylated 2^A-O-(*p*-allyloxybenzoyl)- β -cyclodextrin (**15**) and permethylated 2^A-O-[*p*-(*tert*.-butyl)benzoyl]- β -cyclodextrin (**16**), respectively. Then, **16** was treated with lithium aluminum hydride to form monoalcohol, which was transformed into permethylated 2^A-O-(*p*-allyloxybenzyl)- β -cyclodextrin (**18**) by a nucleophilic substitution reaction. Four new permethyl- or per(methyl/acetyl)-substituted β -cyclodextrin-bound methylpolysiloxanes were prepared by a hydrosilylation reaction of the monoalkenyl-substituted β -cyclodextrin derivatives **4**, **10**, **15** and **18** with a specially prepared hydromethylpolysiloxane. The polymeric phases provide excellent enantiomeric separations of a variety of chiral solutes in open tubular column supercritical fluid chromatography and gas chromatography.

1. Introduction

Immobilized chiral stationary phases (CSPs) derived from cyclodextrin and a polysiloxane are of interest because they provide not only excellent chromatographic performance, but also high thermal stability, and they can be prepared in a reproducible manner. Recently, we developed a

new strategy to prepare cooperative copolymeric phases composed of cyclodextrin and hexasiloxane copolymeric parts [1]. These phases provided excellent resolution of a wide variety of chiral organic solutes in capillary supercritical fluid chromatography (SFC). We also reported the reproducible synthesis of new phases that have pendant cyclodextrin derivatives attached to a polysiloxane backbone by only one spacer group [2]. These latter phases provide superior

* Corresponding author.

separations in both SFC and gas chromatography (GC). Their performance appears to be better than phases prepared by Fischer *et al.* [3] and Schurig and co-workers [4–6] wherein the cyclodextrins were attached to the polysiloxane by an undetermined number of connecting groups.

Our reported cyclodextrin-bound polysiloxanes were prepared by the hydrosilylation reaction of a hydromethylpolysiloxane with permethylated 6-alkenyl-substituted β -cyclodextrins (**1a–1g**) that contained different substituents at the other 6-positions [2] (see Fig. 1). The chromatographic analysis of these phases indicates that the phase prepared from **1a** provided the best performance in both GC and SFC. The single connecting group in all these phases is tethered on the small rim of the cyclodextrin. In order to gain insight into the effect of the spacer position to chromatographic performance, four new permethyl- or per (methyl/acetyl)-substituted β -cyclodextrin polysiloxanes, wherein the cyclodextrins are attached through the 2- or 3-positions, have been synthesized. The synthetic routes to the monoalkenes needed for the hydrosilylation reaction are shown in Figs. 2 and 3, and their attachment to a polysiloxane is depicted in Fig. 4. These derivatives possess different spacers attached to different cyclodextrin positions, which provide new information for studies involving the chiral resolving abilities of cyclodextrin phases. These new cyclodextrin-containing phases provide enantiomeric resolution of a variety of chiral organic solutes in both capillary SFC and GC. Details of these chromatographic results will be reported later. This

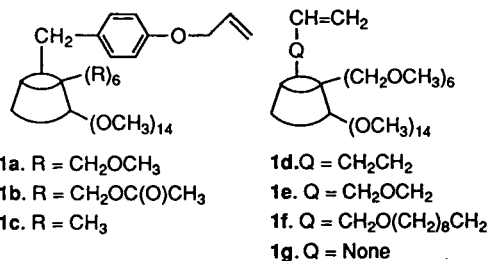


Fig. 1. Structures of persubstituted 6-O-alkenyl- β -cyclodextrins [2].

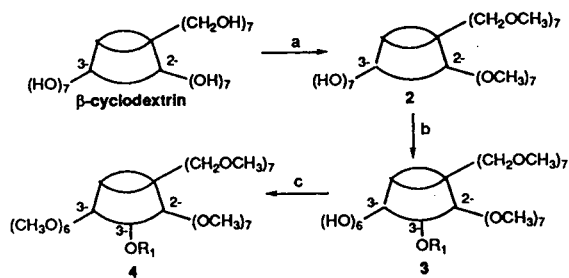


Fig. 2. Preparation of permethyl-substituted 3-O-(*p*-allyloxybenzoyl)- β -cyclodextrin **4**. a = (CH₃)₂SO₄, BaO, Ba(OH)₂, DMSO, DMF; b = *p*-allyloxybenzoyl chloride, pyridine; c = CF₃SO₃CH₃, 2,6-di-(*tert.*-butyl)-4-methylpyridine, CH₂Cl₂. R₁ = *p*-Allyloxybenzoyl.

paper reports the synthesis of these phases. Their utility in chromatography is shown by the separation of several racemic mixtures on three of the phases reported.

2. Experimental

Proton and carbon NMR spectra were recorded in C²HCl₃ at 200 MHz. β -Cyclodextrin (Aldrich) was dried with P₂O₅ under vacuum at 100°C for 24 h before use. Organic extracts were dried over anhydrous MgSO₄. Heptakis[6-O-(*tert.*-butyl) dimethylsilyl]- β -cyclodextrin (**5**) was prepared as reported [1].

2.1. Heptakis(2,6-di-O-methyl)- β -cyclodextrin (**2**) (Fig. 2)

A mixture of 46.7 g (0.24 mol) of BaO and 46.7 g (0.14 mol) of Ba(OH)₂ · 8H₂O was slowly added at room temperature to a stirred solution of β -cyclodextrin (22.7 g, 0.02 mol) and dimethyl sulfate (93.3 g, 0.98 mol) in 280 ml of dimethyl sulfoxide (DMSO)–dimethylformamide (DMF) (1:1). The mixture was stirred at room temperature for 7 days, and the solvent was removed by vacuum distillation. The residue was extracted five times by 200-ml portions of hot CHCl₃ and the extract solution was washed with water, dried and concentrated. The crude product was dried under vacuum at 60°C for 24 h to remove traces of DMSO and DMF, and then

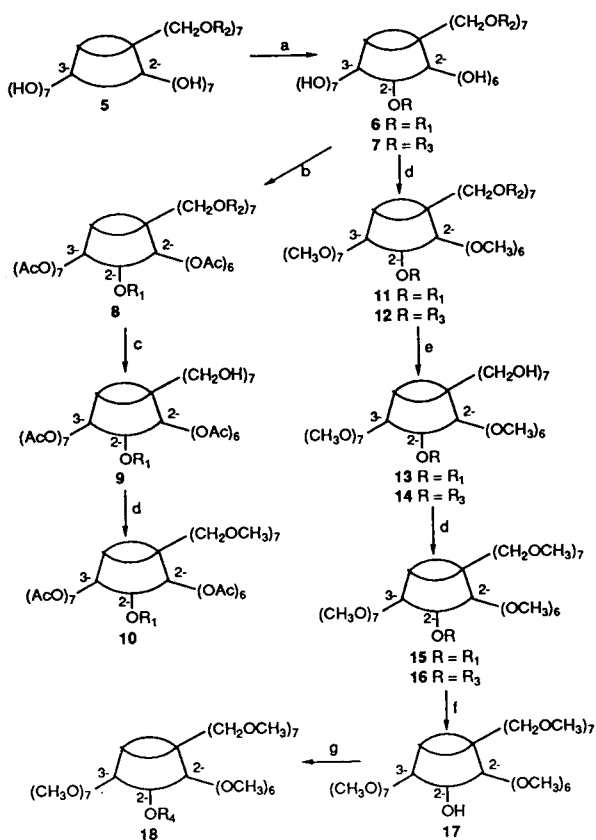


Fig. 3. Preparation of permethyl-substituted 2-O-alkenyl- β -cyclodextrins **10**, **15** and **18**. a = *p*-Allyloxybenzoyl chloride for **6** or *p*-*tert*-butylbenzoyl chloride for **7**, NEt₃, toluene; b = (CH₃CO)₂O, pyridine; c = BF₃·OEt₂, CH₂Cl₂; d = CF₃SO₃CH₃, 2,6-di-*tert*-butyl-4-methylpyridine, CH₂Cl₂; e = NH₄F, CH₃OH; f = LiAlH₄, diethyl ether (for **16**); g = NaH, *p*-allyloxybenzyl chloride. R₁ = *p*-Allyloxybenzoyl; R₂ = *tert*-butyldimethylsilyl; R₃ = *tert*-butylbenzoyl; R₄ = *p*-allyloxybenzyl.

subjected to column chromatography on silica gel (CH₃C₆H₅-C₂H₅OH, 20:1) to give crystalline **2** (14.7 g, 55%); m.p. 312–314°C (lit. [7,8] 312°C); $[\alpha]_{\text{D}}^{25} + 123.9^\circ$ ($c = 0.84$, CHCl₃) (lit. [7,8] 122°); ¹H NMR δ 5.05 (s, 7 H, OH), 4.95 (d, $J = 3.28$ Hz, 7 H), 3.90 (overlapping dd, $J_1 = 9.79$ Hz, $J_2 = 9.39$ Hz, 7 H), 3.81–3.30 (m, 70 H), 3.24 (dd, $J_1 = 3.28$ Hz, $J_2 = 9.79$ Hz, 7 H); ¹³C NMR δ 101.8, 84.1, 82.6, 73.7, 71.4, 70.8, 60.8, 59.4. Analysis for C₅₆H₉₈O₃₅: calculated: C, 50.52; H, 7.42; found: C, 50.69; H, 7.23.

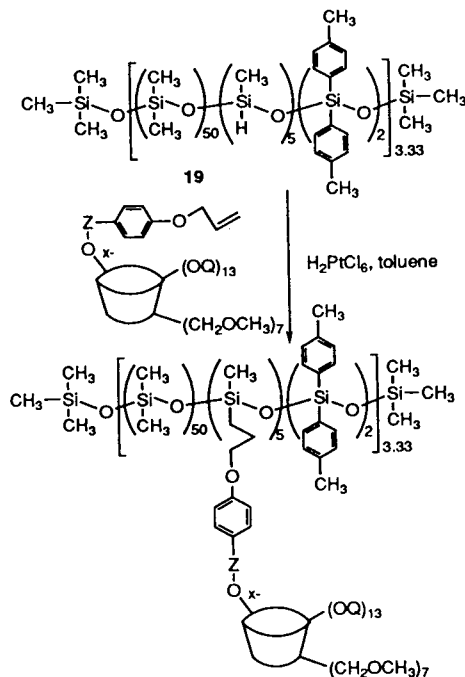


Fig. 4. Preparation of persubstituted β -cyclodextrin-bound polysiloxanes **20**–**23**.

2.2. 3-O-(*p*-Allyloxybenzoyl)heptakis(2,6-di-O-methyl)- β -cyclodextrin (**3**) (Fig. 2)

A solution of **2** (2.66 g, 2.0 mmol) and *p*-allyloxybenzoyl chloride (1.20 g, 6.0 mmol) in 100 ml of dry pyridine was stirred at 100°C for 2 days. Pyridine was removed by vacuum distillation. A solution of the residue in CHCl₃ was washed with water, dried and concentrated. Column chromatography (CHCl₃-CH₃OH, 100:1) of crude product gave 0.45 g (15%) of **3**; m.p. 273–275°C; $[\alpha]_{\text{D}}^{25} + 120.0^\circ$ ($c = 0.35$, CHCl₃); ¹H NMR δ 8.01 (d, $J = 8.82$ Hz, 2 H), 6.89 (d, $J = 8.82$ Hz, 2 H), 6.00 (m, 1 H), 5.45–5.22 (m, 4 H), 5.08 (s, 6 H, OH), 5.00–4.86 (m, 4 H), 4.82 (d, $J = 3.33$ Hz, 1 H), 4.71 (d, $J = 3.33$ Hz, 1 H), 4.53 (d, $J = 5.22$ Hz, 2 H), 4.05–2.98 (m, 83 H); ¹³C NMR δ 165.5,

Polymers	x-	Z	Q
20	3-	C=O	CH ₃
21	2-	C=O	CH ₃ CO
22	2-	C=O	CH ₃
23	2-	CH ₂	CH ₃

133.1, 133.0, 132.2, 124.1, 118.5, 118.4, 114.6, 102.2, 102.0, 101.8, 101.7, 101.6, 84.9, 84.8, 84.7, 84.5, 84.4, 84.3, 84.1, 84.0, 83.8, 82.8, 82.5, 82.3, 81.8, 81.6, 81.5, 79.9, 78.4, 73.6, 73.5, 72.8, 72.6, 72.3, 72.2, 72.1, 71.8, 71.6, 71.4, 70.9, 70.6, 70.4, 69.3, 69.1, 61.2, 60.9, 60.8, 60.7, 59.6, 59.5, 59.4, 59.3. Analysis for $C_{66}H_{106}O_{37}$: calculated: C, 53.15; H, 7.16; found: C, 53.30; H, 7.35.

2.3. 3^A -*O*-(*p*-Allyloxybenzoyl)heptakis(2,6-di-*O*-methyl)- $3^B, 3^C, 3^D, 3^E, 3^F, 3^G$ -hexa-*O*-methyl- β -cyclodextrin (**4**) (Fig. 2)

A solution of **3** (0.23 g, 0.15 mmol), 2,6-di-(*tert*-butyl)-4-methylpyridine (0.38 g, 1.9 mmol) and methyl trifluoromethanesulfonate (triflate) (0.23 g, 1.4 mmol) in 5 ml of CH_2Cl_2 was stirred in a capped PTFE tube at 80°C for 2.5 h. After being dried and concentrated the crude product was purified by column chromatography ($CHCl_3$ - CH_3OH , 100:1) to yield pure **4** (0.19 g, 79%); m.p. 243–244°C; $[\alpha]_D^{25} + 105.1^\circ$ ($c = 1.16$, $CHCl_3$); 1H NMR δ 8.04 (d, $J = 8.83$ Hz, 2 H), 6.91 (d, $J = 8.83$ Hz, 2 H), 6.04 (m, 1 H), 5.48–5.20 (m, 4 H), 5.17–5.05 (m, 4 H), 5.03 (d, $J = 3.30$, 1 H), 4.90 (d, $J = 3.30$, 1 H), 4.59 (d, $J = 5.24$ Hz, 2 H), 4.07–3.28 (m, 95 H), 3.18 (dd, $J_1 = 3.30$, $J_2 = 9.60$, 6 H); ^{13}C NMR δ 164.8, 133.1, 132.2, 124.4, 118.5, 114.4, 100.0, 99.8, 99.6, 99.3, 83.0, 82.9, 82.6, 82.5, 82.3, 82.2, 82.1, 82.0, 81.5, 81.3, 81.0, 80.8, 80.7, 79.2, 72.6, 72.0, 71.9, 71.7, 71.6, 71.4, 71.3, 71.2, 71.1, 71.0, 69.6, 69.3, 62.2, 62.0, 61.9, 61.8, 61.6, 60.0, 59.5, 59.4, 59.3, 59.1, 58.9, 58.7, 58.6. Analysis for $C_{72}H_{118}O_{37}$: calculated: C, 54.88; H, 7.55; found: C, 54.85; H, 7.92.

2.4. 2-*O*-(*p*-Allyloxybenzoyl)heptakis[6-*O*-(*tert*-butyl) dimethylsilyl]- β -cyclodextrin (**6**) (Fig. 3)

A mixture of **5** (5.0 g, 2.6 mmol), *p*-allyloxybenzoyl chloride (0.5 g, 2.6 mmol) and NEt_3 (0.31 g, 3.1 mmol) in 50 ml of toluene was stirred at room temperature for 24 h. The mixture was diluted with 50 ml of toluene and washed successively with cold 3% HCl, 5% aqueous $NaHCO_3$ and water. The organic layer

was dried and concentrated. The residue was chromatographed on silica gel ($CHCl_3$ - CH_3OH , 20:1) to produce pure compound **6** (1.12 g, 21%); m.p. 255–256°C; $[\alpha]_D^{25} + 105.8^\circ$ ($c = 3.91$, $CHCl_3$); 1H NMR δ 7.95 (d, $J = 8.85$ Hz, 2 H), 6.87 (d, $J = 8.85$ Hz, 2 H), 6.02 (m, 1 H), 5.70–5.15 (m, 15 H), 5.11 (d, $J = 3.28$ Hz, 1 H), 5.01–4.73 (m, 7 H), 4.54 (d, $J = 5.22$ Hz, 2 H), 4.26–3.25 (m, 41 H), 0.90 (s, 63 H), 0.05 (s, 42 H); ^{13}C NMR δ 166.8, 133.1, 133.0, 132.7, 132.4, 122.2, 118.5, 115.0, 103.2, 102.7, 102.6, 102.5, 102.1, 100.7, 82.5, 82.2, 74.7, 74.6, 74.3, 74.0, 73.8, 73.5, 73.3, 73.2, 73.0, 72.7, 69.3, 69.2, 62.1, 26.4, 26.3, 19.0, 18.8, 18.7, -4.6, -4.7, -4.8. Analysis for $C_{94}H_{176}O_{37}Si_7$: calculated: C, 53.89; H, 8.47; found: C, 53.87; H, 8.22.

2.5. 2-*O*-[*p*-(*tert*-Butyl)benzoyl]heptakis[6-*O*-(*tert*-butyl)dimethylsilyl]- β -cyclodextrin (**7**) (Fig. 3)

Cyclodextrin derivative **7** was prepared as **6** above from 9.7 g (5.0 mmol) of **5**, 1.0 g (5.0 mmol) of *p*-(*tert*-butyl)benzoyl chloride and 0.56 g (5.5 mmol) of NEt_3 to give 2.00 g (19%) of **7**; m.p. 264–266°C; $[\alpha]_D^{25} + 102.6^\circ$ ($c = 3.50$, $CHCl_3$); 1H NMR δ 7.97 (d, $J = 8.54$ Hz, 2 H), 7.43 (d, $J = 8.54$ Hz, 2 H), 5.50 (broad s, 13 H, OH), 5.39 (d, $J = 3.23$ Hz, 1 H), 5.00–4.75 (m, 7 H), 4.46–3.30 (m, 41 H), 1.29 (s, 9 H), 0.88 (s, 63 H), 0.05 (s, 42 H); ^{13}C NMR δ 166.2, 130.3, 127.8, 125.8, 102.6, 102.5, 102.4, 82.2, 77.6, 74.3, 74.1, 73.9, 73.6, 73.5, 73.3, 73.2, 73.0, 72.8, 72.7, 72.4, 62.2, 62.1, 35.5, 31.6, 26.7, 26.5, 26.4, 26.3, 26.1, 19.0, 18.8, 18.7, -4.6, -4.7, -4.8. Analysis for $C_{95}H_{180}O_{36}Si_7$: calculated: C, 54.46; H, 8.66; found C, 54.62; H, 8.49.

2.6. 2^A -*O*-(*p*-Allyloxybenzoyl)heptakis[3-*O*-acetyl-6-*O*-(*tert*-butyl)dimethylsilyl]- $2^B, 2^C, 2^D, 2^E, 2^F, 2^G$ -hexa-*O*-acetyl- β -cyclodextrin (**8**) (Fig. 3)

A solution of **6** (0.84 g, 0.40 mmol) in 30 ml of acetic anhydride and 30 ml of pyridine was stirred at 100°C for 4 h. The solvent was re-

moved under reduced pressure and the residue was dissolved in CHCl_3 . The solution was washed with water twice, dried and concentrated. The crude product was purified by column chromatography ($\text{CH}_3\text{C}_6\text{H}_5$ – $\text{C}_2\text{H}_5\text{OH}$, 200:3) to give **8** (0.77 g, 73%); m.p. 136–138°C; $[\alpha]_{\text{D}}^{25} + 89.8^\circ$ ($c = 0.93$, CHCl_3); $^1\text{H NMR } \delta$ 7.97 (d, $J = 8.83$ Hz, 2 H), 6.97 (d, $J = 8.83$ Hz, 2 H), 6.06 (m, 1 H), 5.50–5.22 (m, 10 H), 5.22–5.08 (m, 6 H), 4.90 (dd, $J_1 = 9.61$ Hz, $J_2 = 3.28$ Hz, 1 H), 4.70 (dd, $J_1 = 9.61$ Hz, $J_2 = 3.28$ Hz, 6 H), 4.59 (d, $J = 5.22$ Hz, 2 H), 4.17–3.64 (m, 28 H), 2.17–1.75 (m, 39 H), 0.90 (s, 63 H), 0.06 (s, 42 H); $^{13}\text{C NMR } \delta$ 171.3, 171.2, 171.1, 171.0, 170.0, 169.8, 169.5, 166.5, 133.1, 132.8, 122.1, 118.5, 114.9, 100.0, 96.8, 96.6, 77.7, 75.8, 75.7, 75.6, 72.6, 72.3, 72.2, 72.1, 71.9, 71.8, 71.7, 69.6, 69.3, 62.4, 62.3, 62.2, 26.3, 21.4, 21.2, 18.3, –4.5, –4.7, –4.8. Analysis for $\text{C}_{120}\text{H}_{202}\text{O}_{50}\text{Si}_7$: calculated: C, 54.56; H, 7.71; found: C, 54.36; H, 7.70.

2.7. 2^A-O-(p-Allyloxybenzoyl)heptakis(3-O-acetyl)-2^B,2^C,2^D,2^E,2^F,2^G-hexa-O-acetyl- β -cyclodextrin (9) (Fig. 3)

A solution of **8** (0.70 g, 0.27 mmol) in 15 ml of CH_2Cl_2 was stirred with $\text{BF}_3\text{-OEt}_2$ (0.32 g, 2.2 mmol) at room temperature for 6 h. The mixture was diluted with CH_2Cl_2 and poured into ice-water. The organic layer was separated, washed with water, aqueous NaHCO_3 and water, and then dried and concentrated. Column chromatography (CHCl_3 – CH_3OH , 7:1, then 4:1) of the residue gave **9** (0.38 g, 78%); m.p. 178–179°C; $[\alpha]_{\text{D}}^{25} + 102.8^\circ$ ($c = 1.07$, CHCl_3); $^1\text{H NMR } \delta$ 7.95 (d, $J = 8.72$ Hz, 2 H), 6.95 (d, $J = 8.72$ Hz, 2 H), 6.03 (m, 1 H), 5.89–5.50 (m, 10 H), 5.50–5.17 (m, 6 H), 5.17–4.62 (m, 14 H), 4.57 (d, $J = 5.24$ Hz, 2 H), 4.40–3.40 (m, 28 H), 2.30–1.80 (m, 39 H); $^{13}\text{C NMR } \delta$ 171.3, 171.2, 171.1, 169.8, 169.7, 166.5, 133.1, 133.0, 122.1, 118.6, 114.9, 97.4, 97.3, 97.2, 77.7, 73.0, 72.9, 72.8, 72.7, 72.5, 72.4, 72.3, 72.2, 72.1, 72.0, 71.9, 71.8, 71.7, 71.6, 71.5, 71.4, 71.3, 71.2, 71.1, 71.0, 70.8, 69.3, 61.2, 21.3, 21.2. Analysis for $\text{C}_{78}\text{H}_{104}\text{O}_{50}$: calculated: C, 50.87; H, 5.69; found: C, 50.96; H, 5.71.

2.8. 2^A-O-(p-Allyloxybenzoyl)heptakis(3-O-acetyl-6-O-methyl)-2^B,2^C,2^D,2^E,2^F,2^G-hexa-O-acetyl- β -cyclodextrin (10) (Fig. 3)

A mixture of **9** (0.38 g, 0.21 mmol), methyl triflate (0.49 ml, 4.3 mmol) and 2,6-di(*tert.*-butyl)-4-methylpyridine (1.2 g, 5.8 mmol) in 6 ml of CH_2Cl_2 was heated in a sealed tube at 80°C for 2.5 h and cooled. CH_3OH (6 ml) was added, and the mixture was stirred at room temperature for 1 h, and concentrated. A solution of the residue in CHCl_3 was washed successively with water, cold 3% HCl , aqueous NaHCO_3 and water, and then dried and concentrated. The product was subjected to column chromatography (CHCl_3 – CH_3OH , 20:1) to give **10** (0.19 g, 50%); m.p. 127–128°C; $[\alpha]_{\text{D}}^{25} + 100.2^\circ$ ($c = 1.85$, CHCl_3); $^1\text{H NMR } \delta$ 7.95 (d, $J = 8.78$ Hz, 2 H), 6.94 (d, $J = 8.78$ Hz, 2 H), 6.02 (m, 1 H), 5.62–5.19 (m, 10 H), 5.19–5.00 (m, 6 H), 4.95 (dd, $J_1 = 9.67$ Hz, $J_2 = 3.32$ Hz, 1 H), 4.78 (dd, $J_1 = 9.67$ Hz, $J_2 = 3.32$ Hz, 6 H), 4.57 (d, $J = 5.22$ Hz, 2 H), 4.10–3.70 (m, 21 H), 3.65–3.43 (m, 7 H), 3.38 (s, 21 H), 2.15–1.70 (m, 39 H); $^{13}\text{C NMR } \delta$ 171.2, 171.1, 170.1, 169.8, 169.5, 166.4, 133.0, 132.8, 121.2, 118.5, 114.9, 97.6, 96.9, 76.5, 76.2, 75.7, 71.7, 71.3, 71.1, 70.9, 69.3, 59.6, 21.3, 21.1. Analysis for $\text{C}_{85}\text{H}_{118}\text{O}_{50}$: calculated: C, 52.63; H, 6.13; found: C, 52.45; H, 6.34.

2.9. 2^A-O-(p-Allyloxybenzoyl)heptakis[6-O-(*tert.*-butyl)dimethylsilyl-3-O-methyl]-2^B,2^C,2^D,2^E,2^F,2^G-hexa-O-methyl- β -cyclodextrin (11) (Fig. 3)

A mixture of **6** (0.80 g, 0.38 mmol), 2,6-di(*tert.*-butyl)-4-methylpyridine (2.6 g, 12.5 mmol) and methyl triflate (1.6 g, 10 mmol) in 6 ml of CH_2Cl_2 was stirred in a capped PTFE tube at 80°C for 2.5 h. After being cooled, 10 ml of CH_3OH was added, and the mixture was stirred at room temperature for 1 h. The solvent was removed under a reduced pressure to yield a solid mixture, which was dissolved in CH_2Cl_2 . The organic solution was washed successively with 3% cold HCl , 5% aqueous NaHCO_3 and water, and then dried and concentrated. Crude

product was chromatographed ($C_6H_{14}-CH_3CO_2C_2H_5-C_2H_5OH$, 80:20:1) to give 0.65 g (75%) of **11**; m.p. 136–138°C; $[\alpha]_D^{25} + 97.5^\circ$ ($c = 2.68$, $CHCl_3$); 1H NMR δ 8.08 (d, $J = 8.67$ Hz, 2 H), 6.87 (d, $J = 8.67$ Hz, 2 H), 6.04 (m, 1 H), 5.49–5.10 (m, 9 H), 4.92 (dd, $J_1 = 3.28$ Hz, $J_2 = 9.72$ Hz, 1 H), 4.57 (d, $J = 5.26$ Hz, 2 H), 4.23–3.30 (m, 74 H), 3.05 (dd, $J_1 = 3.28$ Hz, $J_2 = 9.72$ Hz, 6 H), 0.88 (s, 63 H), 0.05 (s, 42 H); ^{13}C NMR δ 166.1, 133.1, 132.4, 123.4, 118.5, 114.6, 98.7, 98.6, 98.5, 98.2, 97.6, 82.9, 82.7, 82.6, 82.4, 82.3, 80.8, 79.4, 79.3, 79.2, 78.9, 78.7, 77.0, 72.3, 72.7, 72.6, 69.3, 62.7, 62.1, 62.9, 61.8, 61.3, 59.2, 59.0, 58.9, 58.8, 26.4, 18.8, -4.4, -4.5, -4.7, -4.8. Analysis for $C_{107}H_{202}O_{37}Si_7$: calculated: C, 56.43; H, 8.94; found: C, 56.53; H, 9.01.

2.10. 2^A-O-[p-(tert.-Butyl)benzoyl]heptakis[6-O-(tert.-butyl)dimethylsilyl-3-O-methyl]-2^B,2^C,2^D,2^E,2^F,2^G-hexa-O-methyl- β -cyclodextrin (12**) (Fig. 3)**

Compound **12** was prepared as **11** above from 2.0 g (1.0 mmol) of **7**, 3.8 g (18.3 mmol) of 2,6-di(tert.-butyl)-4-methylpyridine and 2.43 g (14.8 mmol) of methyl triflate to produce 1.72 g (80%) of **12**; m.p. 148–150°C; $[\alpha]_D^{25} + 93.0^\circ$ ($c = 2.11$, $CHCl_3$); 1H NMR δ 8.06 (d, $J = 8.83$ Hz, 2 H), 7.40 (d, $J = 8.83$ Hz, 2 H), 5.47 (d, $J = 3.32$ Hz, 1 H), 5.30–5.10 (m, 6 H), 4.97 (dd, $J_1 = 3.32$ Hz, $J_2 = 9.65$ Hz, 1 H), 4.29–3.30 (m, 74 H), 3.15–2.92 (m, 6 H), 1.34 (s, 9 H), 0.89 (s, 63 H), 0.07 (s, 42 H); ^{13}C NMR δ 166.2, 130.2, 128.0, 125.6, 98.7, 98.6, 98.4, 98.0, 82.6, 82.5, 82.3, 80.8, 79.5, 79.4, 79.2, 76.9, 74.2, 72.7, 72.6, 72.5, 62.7, 62.2, 62.0, 61.8, 61.3, 59.4, 59.1, 58.9, 58.6, 35.6, 31.6, 26.4, 18.8, -4.4, -4.5, -4.6, -4.8. Analysis for $C_{108}H_{206}O_{36}Si_7$: calculated: C, 56.96; H, 9.12; found: C, 57.16; H, 8.95.

2.11. 2^A-O-(p-Allyloxybenzoyl)heptakis(3-O-methyl)-2^B,2^C,2^D,2^E,2^F,2^G-hexa-O-methyl- β -cyclodextrin (13**) (Fig. 3)**

A solution of **11** (0.62 g, 0.27 mmol) in 100 ml of CH_3OH was refluxed with NH_4F (0.71 g, 19.1

mmol) for 24 h and evaporated to dryness. A solution of the residue in $CHCl_3$ was washed with water twice, dried and concentrated. Crude product was subjected to column chromatography ($CHCl_3-CH_3OH$, 8:1) to yield 0.34 g (85%) of **13**; m.p. 175–176°C; $[\alpha]_D^{25} + 156.2^\circ$ ($c = 1.15$, $CHCl_3$); 1H NMR δ 8.05 (d, $J = 8.63$ Hz, 2 H), 6.91 (d, $J = 8.63$ Hz, 2 H), 6.04 (m, 1 H), 5.50–5.25 (m, 3 H), 5.20–5.00 (m, 6 H), 4.89 (dd, $J_1 = 3.29$ Hz, $J_2 = 9.56$ Hz, 1 H), 4.72 (s, 7 H, OH), 4.57 (d, $J = 5.29$ Hz, 2 H), 4.12–2.95 (m, 80 H); ^{13}C NMR δ 166.3, 133.0, 132.4, 123.1, 118.6, 114.8, 99.1, 99.0, 82.5, 82.4, 82.1, 80.8, 77.7, 74.5, 73.0, 72.9, 72.8, 69.6, 69.3, 62.0, 61.8, 61.7, 61.4, 59.2, 59.0, 58.9. Analysis for $C_{65}H_{104}O_{37}$: calculated: C, 52.84; H, 7.09; found: C, 52.87; H, 7.00.

2.12. 2^A-O-[p-(tert.-Butyl)benzoyl]heptakis(3-O-methyl)-2^B,2^C,2^D,2^E,2^F,2^G-hexa-O-methyl- β -cyclodextrin (14**) (Fig. 3)**

Cyclodextrin derivative **14** was prepared as **13** above from 0.88 g (0.39 mmol) of **12** and 0.61 g (16.2 mmol) of NH_4F to give 0.53 g (93%) of **14**; m.p. 197–199°C; $[\alpha]_D^{25} + 150.3^\circ$ ($c = 1.54$, $CHCl_3$); 1H NMR δ 8.02 (d, $J = 8.57$ Hz, 2 H), 7.42 (d, $J = 8.57$ Hz, 2 H), 5.30 (d, $J = 3.31$ Hz, 1 H), 5.25–4.98 (m, 6 H), 4.89 (dd, $J_1 = 3.31$ Hz, $J_2 = 9.65$ Hz, 1 H), 4.73 (broad s, 7 H, OH), 4.12–3.29 (m, 74 H), 3.29–3.03 (m, 6 H), 1.33 (s, 9 H); ^{13}C NMR δ 166.6, 130.3, 127.7, 125.8, 99.4, 99.2, 99.1, 82.5, 82.4, 82.2, 82.0, 81.9, 81.0, 80.8, 79.8, 77.7, 73.1, 73.0, 72.9, 72.8, 72.7, 62.1, 61.9, 61.7, 61.5, 58.8, 35.6, 31.6. Analysis for $C_{66}H_{108}O_{36}$: calculated: C, 53.64; H, 7.37; found: C, 53.63; H, 7.42.

2.13. 2^A-O-(p-Allyloxybenzoyl)heptakis(3,6-di-O-methyl)-2^B,2^C,2^D,2^E,2^F,2^G-hexa-O-methyl- β -cyclodextrin (15**) (Fig. 3)**

Permethylated monoalkenyl- β -cyclodextrin **15** was prepared as above for **10** from 0.19 g (0.13 mmol) of **13**, 0.37 g (1.80 mmol) of 2,6-di(tert.-butyl)-4-methylpyridine and 0.22 g (1.35 mmol) of methyl triflate to give **15** (0.10 g, 59%); m.p. 107–109°C; $[\alpha]_D^{25} + 130.7^\circ$ ($c = 0.99$, $CHCl_3$); 1H

NMR δ 8.10 (d, $J = 8.90$ Hz, 2 H), 6.90 (d, $J = 8.90$ Hz, 2 H), 6.04 (m, 1 H), 5.48–5.21 (m, 3 H), 5.18–5.05 (m, 6 H), 4.93 (dd, $J_1 = 3.30$ Hz, $J_2 = 9.62$ Hz, 1 H), 4.57 (d, $J = 5.24$ Hz, 2 H), 4.00–3.20 (m, 95 H), 3.24–3.05 (m, 6 H); ^{13}C NMR δ 166.3, 133.0, 132.5, 123.2, 118.6, 114.7, 99.5, 99.4, 99.2, 98.4, 82.5, 82.3, 82.0, 81.0, 80.9, 80.5, 80.0, 79.0, 74.4, 72.0, 71.8, 71.5, 71.3, 69.3, 62.0, 61.8, 61.6, 61.5, 59.4, 59.1, 59.0, 58.8. Analysis for $\text{C}_{72}\text{H}_{118}\text{O}_{37}$: calculated: C, 54.88; H, 7.55; found: C, 55.13; H, 7.63.

2.14. 2^A-O-[p-(tert.-Butyl)benzoyl]heptakis(3,6-di-O-methyl)-2^B,2^C,2^D,2^E,2^F,2^G-hexa-O-methyl- β -cyclodextrin (16) (Fig. 3)

A compound **16** was prepared as above for **10** from 1.00 g (0.68 mmol) of **14**, 1.94 g (9.46 mmol) of 2,6-di(tert.-butyl)-4-methylpyridine and 1.17 g (7.10 mmol) of methyl triflate to give 0.88 g (82%) of **16**; m.p. 132–134°C; $[\alpha]_{\text{D}}^{25} + 142.7^\circ$ ($c = 1.52$, CHCl_3); ^1H NMR δ 8.10 (d, $J = 8.71$ Hz, 2 H), 7.43 (d, $J = 8.71$ Hz, 2 H), 5.34 (d, $J = 3.31$ Hz, 1 H), 5.22–5.08 (m, 6 H), 5.00 (dd, $J_1 = 3.31$ Hz, $J_2 = 9.64$ Hz, 1 H), 4.03–3.30 (m, 95 H), 3.26–3.06 (m, 6 H), 1.35 (s, 9 H); ^{13}C NMR δ 166.6, 130.3, 127.8, 125.7, 99.5, 99.4, 99.1, 98.2, 82.5, 82.2, 82.1, 81.9, 81.2, 80.9, 80.8, 80.5, 79.9, 79.0, 77.6, 74.5, 71.8, 71.4, 71.3, 62.0, 61.8, 61.6, 61.5, 59.4, 59.1, 59.0, 58.9, 35.5, 31.6. Analysis for $\text{C}_{73}\text{H}_{122}\text{O}_{36}$: calculated: C, 55.64; H, 7.80; found: C, 55.45; H, 7.75.

2.15. Heptakis(3,6-di-O-methyl)-2^A,2^B,2^C,2^D,2^E,2^F-hexa-O-methyl- β -cyclodextrin (17) (Fig. 3)

A solution of **16** (0.50 g, 0.32 mmol) in diethyl ether (7 ml) was refluxed with LiAlH_4 (0.058 g, 1.53 mmol) for 24 h. Moist ether was added to decompose the excess LiAlH_4 and the mixture was concentrated. The residue was partitioned between CHCl_3 and water, and the organic layer was separated and washed with water two more times. After being dried and concentrated, the residue was subjected to column chromatog-

raphy (CHCl_3 – CH_3OH , 80:1) to give 0.39 g (87%) of **17**; m.p. 105–107°C; $[\alpha]_{\text{D}}^{25} + 145.0^\circ$ ($c = 0.36$, CHCl_3); ^1H NMR δ 5.20–5.06 (m, 6 H), 4.89 (d, $J = 3.27$ Hz, 1 H), 4.34 (d, $J = 7.13$ Hz, 1 H, OH), 3.95–3.31 (m, 96 H), 3.27–3.10 (m, 6 H); ^{13}C NMR δ 102.4, 100.1, 99.9, 99.8, 99.6, 99.3, 99.1, 84.5, 83.4, 82.9, 82.6, 82.5, 82.4, 82.2, 81.6, 81.3, 81.2, 81.1, 80.7, 80.5, 79.1, 74.6, 72.3, 72.0, 71.8, 71.4, 71.3, 70.7, 62.4, 61.9, 61.8, 61.7, 61.3, 59.5, 59.3, 59.2, 59.0, 58.8, 58.7. Analysis for $\text{C}_{62}\text{H}_{110}\text{O}_{35}$: calculated: C, 52.61; H, 7.83; found: C, 52.62; H, 8.00.

2.16. 2^A-O-(p-Allyloxybenzyl)heptakis(3,6-di-O-methyl)-2^B,2^C,2^D,2^E,2^F,2^G-hexa-O-methyl- β -cyclodextrin (18) (Fig. 3)

Compound **17** (0.24 g, 0.17 mmol) in 5 ml of DMF was treated with NaH (0.041 g, 1.7 mmol) at room temperature for 2 h, and then 0.31 g (1.7 mmol) of *p*-allyloxybenzyl chloride were added. The mixture was stirred at room temperature for 24 h, and CH_3OH was added to decompose the excess NaH. The solvent was removed under reduced pressure to produce a slurry which was partitioned between CHCl_3 and water. The organic layer was separated, and washed with water. After being dried and concentrated, the crude product was chromatographed (CHCl_3 – CH_3OH , 80:1) to give 0.17 g (64%) of **18**; m.p. 100–102°C; $[\alpha]_{\text{D}}^{25} + 136.3^\circ$ ($c = 0.60$, CHCl_3); ^1H NMR δ 7.33 (d, $J = 8.83$ Hz, 2 H), 6.85 (d, $J = 8.83$ Hz, 2 H), 6.05 (m, 1 H), 5.32 (m, 2 H), 5.20–5.05 (m, 6 H), 4.93 (d, $J = 3.31$ Hz, 1 H), 4.64 (s, 2 H), 4.51 (d, $J = 5.27$ Hz, 2 H), 3.94–3.26 (m, 95 H), 3.19 (dd, $J_1 = 3.31$ Hz, $J_2 = 9.65$ Hz, 7 H); ^{13}C NMR δ 133.8, 131.9, 131.5, 129.8, 118.0, 114.9, 114.8, 99.8, 99.4, 82.5, 82.3, 82.2, 80.9, 80.8, 80.6, 80.4, 80.0, 72.7, 72.1, 72.0, 71.8, 71.7, 71.6, 71.4, 71.3, 69.6, 69.3, 62.0, 61.9, 59.4, 59.1, 59.0, 58.9. Analysis for $\text{C}_{72}\text{H}_{120}\text{O}_{36}$: calculated: C, 55.37; H, 7.75; found: C, 55.15; H, 7.84.

2.17. Preparation of copolymer 19

A mixture of 1.64 g (5.50 mmol) of 1, 1, 3, 3, 5, 5, 7, 7-octamethylcyclotetrasiloxane

(D₄), 0.13 g (0.56 mmol) of 1,3,5,7-tetramethylcyclotetrasiloxane (D'₄), 0.24 g (0.89 mmol) of dimethoxyditolylsilane and 0.022 g (0.13 mmol) of hexamethyldisiloxane was stirred with 4 mg of triflic acid in a 50-ml PTFE centrifuge tube at room temperature for 50 h. This reaction was similar to that reported [9]. This mixture was neutralized with 30 mg of hexamethyldisilazane while being stirred for 5 min. The resulting polymer (*M_r* about 15 000) was dissolved in 10 ml of CH₂Cl₂ and then precipitated by adding 30 ml of CH₃OH. The mixture was centrifuged, and the solvent was decanted. The polymer was again dissolved in CH₂Cl₂ and precipitated by CH₃OH for a total of four more times, and then dried under vacuum for 10 h.

2.18. General procedure for the preparation of β -cyclodextrin-containing methylpolysiloxanes 20–23 (Fig. 4)

A typical synthetic procedure is given for polymer **20**. Alkene **4** (0.15 g, 0.094 mmol), hydromethylpolysiloxane **19** (0.084 g, 0.094 mmol of Si–H) and 5 g of toluene were placed in a 50-ml PTFE centrifuge tube. Parafilm was placed around the cap to keep out moisture. The mixture was heated in an oil bath at 85–90°C for 72 h, and the solvent was evaporated. A solution of the residue in CH₂Cl₂ (10 ml) was washed with 10 ml of CH₃OH and 10 ml of water. The mixture was centrifuged and the water–CH₃OH layer was removed. This process was repeated three more times. The solvent was evaporated and the residue was dried under vacuum at 60°C for 20 h to give 0.20 (84%) of **20**. The proton NMR spectrum of **20** was consistent with the structure shown in Fig. 4. The other polymers were prepared in a like manner.

2.19. Preparation of open tubular chromatographic columns

Open tubular columns were prepared using cyano-deactivated [10] fused-silica capillaries obtained from Dionex (Sunnyvale, CA, USA). The GC and the SFC columns were 320 and 50 μ m

I.D., respectively. All four stationary phases were used to prepare a total of eight columns: four 15 m long GC columns and four 10 m long SFC columns. The static coating technique [11] was employed for column preparation. An *n*-pentane–methylene chloride (1:1) mixture was used as the coating solvent. Appropriate coating solution concentrations for the preparation of GC and SFC columns were calculated as described [12]. The coating was carried out at 40°C. For GC and SFC columns, the vacuum was equivalent to 200 and 10 μ mHg (1 mmHg = 133.322 Pa), respectively.

After coating, the columns were purged with nitrogen for 30 min and then cross-linked using azo-*tert*-butane (ATB) as a free radical initiator [13]. For cross-linking, the coated stationary phase film was saturated with ATB vapor for 30 min. The columns were then sealed at both ends using an oxyacetylene flame, heated by programming the temperature from 40 to 220°C at a rate of 4°C min⁻¹, and were held at the final temperature for 40 min. Finally, the columns were rinsed with 1 ml of the coating solvent, purged with nitrogen again for 1 h, and conditioned. The conditioning was accomplished by slowly ramping the temperature (1°C min⁻¹) from 40 to 200°C, and holding the column at the final temperature for 2 h. During conditioning, the columns were continuously purged with helium.

3. Results and discussion

3.1. Permethy-substituted 3-*O*-(*p*-allyloxybenzoyl)- β -cyclodextrin (**4**) (Fig. 2)

Heptakis(2,6-di-*O*-methyl)- β -cyclodextrin (**2**) was conveniently obtained from native β -cyclodextrin in a 55% yield as reported [7,8]. The hydroxy groups at the 3-positions of cyclodextrin are the least reactive and resist functionalization, as described by Menger and Dulany [14]. In fact, treatment of **2** with *p*-allyloxybenzoyl chloride and triethylamine (NEt₃) in dry toluene produced no product even at reflux temperature or using *N,N*-dimethylaminopyridine instead of NEt₃. When NaH was used as a base, the

reaction of **2** with *p*-allyloxybenzoyl chloride or *p*-allyloxybenzyl chloride in dry DMF gave mixtures from which the expected product could not be isolated. It was found that treatment of **2** with *p*-allyloxybenzoyl chloride in dry pyridine at 100°C produced 3-O-(*p*-allyloxybenzoyl)heptakis(2,6-di-O-methyl)- β -cyclodextrin (**3**) which was purified by silica gel chromatography. Methylation of **3** with methyl triflate and 2,6-di(*tert.*-butyl)-4-methylpyridine in CH₂Cl₂ gave **4** in an excellent yield.

3.2. Permethyl- or per(methyl/acetyl)-substituted 2-O-alkenyl- β -cyclodextrins (**10**, **15**, **18**) (Fig. 3)

Although selective mono-functionalization of the hydroxy groups at the 2-positions of native β -cyclodextrin was done by other groups [21–23], we preferred using heptakis[6-O-(*tert.*-butyl)dimethylsilyl]- β -cyclodextrin (**5**) [1] as a starting material to make mono-2-O-alkenyl- β -cyclodextrin derivatives. Treatment of **5** with *p*-allyloxybenzoyl chloride or *p*-(*tert.*-butyl)benzoyl chloride and triethylamine in toluene gave 2-O-(*p*-allyloxybenzoyl)heptakis [6-O-(*tert.*-butyl)dimethylsilyl]- β -cyclodextrin (**6**) or 2-O-[*p*-(*tert.*-butyl)benzoyl]heptakis[6-O-(*tert.*-butyl)dimethylsilyl]- β -cyclodextrin (**7**), respectively (see Fig. 3). Acylation of **6** with acetic anhydride in pyridine gave tridecaacetate **8** in a 73% yield. The silyl groups of **8** were removed with BF₃-OEt in CH₂Cl₂ to produce 2^A-O-(*p*-allyloxybenzoyl)heptakis(3-O-acetyl)-2^B, 2^C, 2^D, 2^E, 2^F, 2^G-hexa-O-acetyl- β -cyclodextrin (**9**) in a yield of 78%. Methylation of **9** with methyl triflate and 2,6-di(*tert.*-butyl)-4-methylpyridine in CH₂Cl₂ gave 2^A-O-(*p*-allyloxybenzoyl)heptakis(3-O-acetyl-6-O-methyl)-2^B, 2^C, 2^D, 2^E, 2^F, 2^G-hexa-O-acetyl- β -cyclodextrin (**10**).

Both **6** and **7** were methylated under mild conditions (same as above) to produce permethylated 2^A-O-benzoyl-substituted heptakis[6-O-(*tert.*-butyl)dimethylsilyl]- β -cyclodextrins **11** and **12**, respectively (see Fig. 3). These latter compounds were transformed into heptaols **13** and **14** by treatment with NH₄F in CH₃OH. The

yields of each of the above reactions were excellent. Methylation of **13** and **14** under the mild conditions gave permethylated 2^A-O-(*p*-allyloxybenzoyl)- β -cyclodextrin (**15**) and permethylated 2^A-O-[*p*-(*tert.*-butyl)benzoyl]- β -cyclodextrin (**16**) in good yields. Compound **16** was stable in a hot solution of LiOH in tetrahydrofuran-ethanol-water, but was reduced with LiAlH₄ in diethyl ether to give monoalcohol **17**. Compound **17** was converted to permethylated 2^A-O-(*p*-allyloxy)benzyl- β -cyclodextrin (**18**) in a 64% yield by treatment with NaH and (*p*-allyloxy)benzyl chloride in DMF.

Permethyl-substituted 3^A-O-(*p*-allyloxybenzoyl)- β -cyclodextrin (**4**) was prepared from **2** which has only position 3 on each glucose unit unsubstituted so that, in this case, the allyloxybenzoyl group has to be on position 3. Alkene-substituted cyclodextrins **10**, **15** and **18**, on the other hand, were prepared from **5** which is unsubstituted in positions 2 and 3. Therefore **10**, **15** and **18** could have the allyloxybenzoyl or allyloxybenzyl group in the 2-O or 3-O position. Meier-Augenstein *et al.* [15] reported that the coupling constants for the protons at positions 2

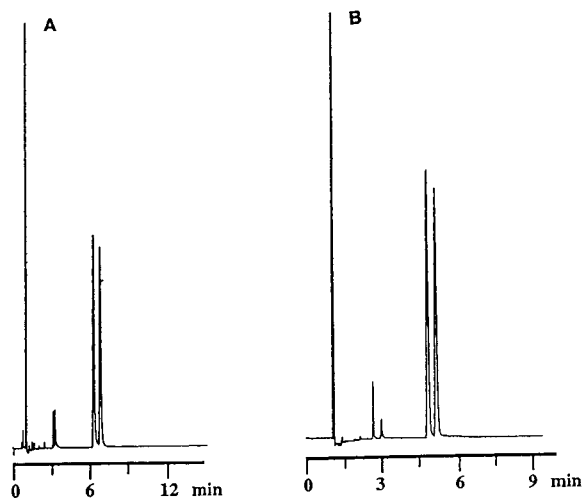


Fig. 5. Gas chromatograms of pantolactone enantiomers obtained on (A) large-rim-tethered (**22**) and (B) small-rim-tethered (polymer made from **1a**) [2] cyclodextrin stationary phases. Conditions: 15 m \times 320 μ m I.D. cyano-deactivated fused-silica columns, 0.25 μ m film thickness; 130°C column temperature; helium carrier gas; split injection (100:1); flame ionization detection.

and 3 of heptakis(2,6-di-O-pentyl)- β -cyclodextrin were $J_{1,2} = 3.7$ Hz, $J_{2,3} = 9.6$ Hz and $J_{3,4} = 9.2$ Hz. We assigned the double doublet at $\delta = 4.90$ ($J_1 = 9.61$ Hz, $J_2 = 3.28$ Hz) in the NMR spectrum of **8** (a precursor to **10**) to the proton at the position 2 of the glucose containing the *p*-allyloxybenzoyl group and the double doublet at $\delta = 4.70$ ($J_1 = 9.61$ Hz, $J_2 = 3.28$ Hz) to the six protons at the other 2-positions containing the acetyl groups. These J values are similar to those reported above for the 2-substituted cyclodextrins [15]. The signal for the protons at the 3-positions of **8** was overlapped by peaks attributable to the protons of the vinyl group. This assignment was also confirmed in the ^1H NMR spectra of **11** and **12** which exhibited similar J values for single proton peaks at $\delta = 4.92$ and 4.97, respectively.

3.3. Preparation and testing of polymers 20–23

In order to have phases that easily coat on the fused-silica columns and that can be cross-linked, hydromethylpolysiloxanes containing tolyl groups were prepared by copolymerizing 10 parts of the cyclic tetramer of dimethylsiloxane, 1 part of the cyclic tetramer of hydromethylsiloxane and 1.6 parts of dimethoxyditolylsilane in a manner similar to that reported [9]. The tolyl substituents were found to be excellent cross-linking agents in polysiloxane systems [16]. The molecular mass of resulting copolymer **19** was 15 000 as determined by the amount of hexamethyldisiloxane, the endcapping reagent, used in the reaction. Persubstituted β -cyclodextrin-bound polymethylsiloxanes **20–23**, shown in Fig. 4, were synthesized by the hydrosilylation of **4**,

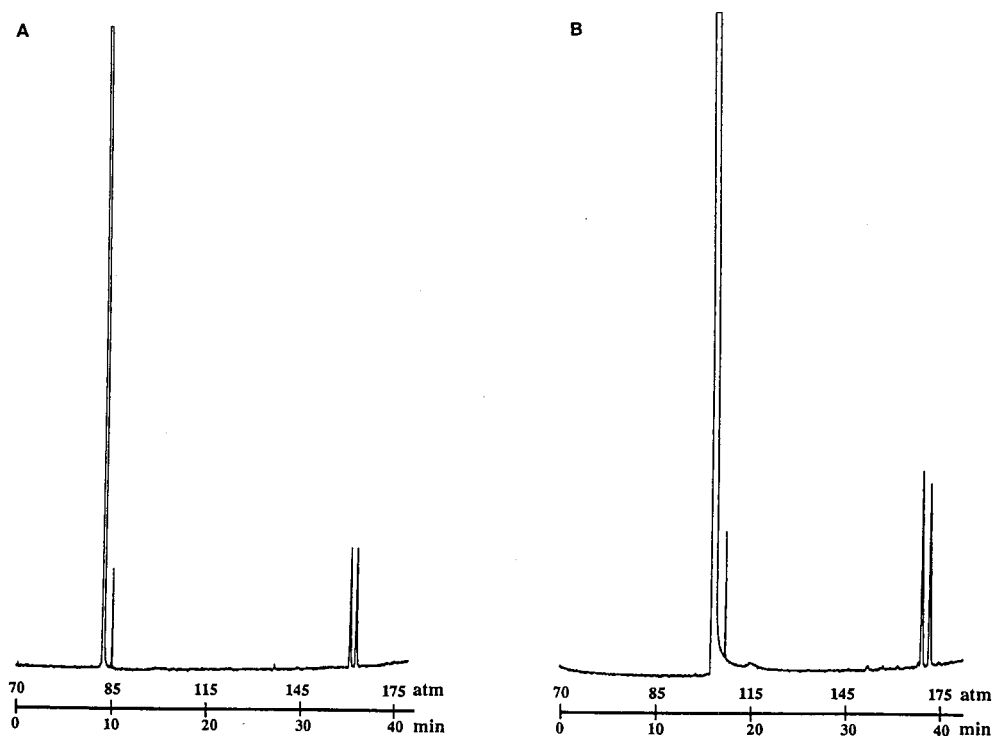


Fig. 6. SFC chromatograms of *tert*-2-phenyl-1-cyclohexanol enantiomers obtained on (A) large-rim-tethered (**23**) and (B) small-rim-tethered (polymer made from **1c**) [2] cyclodextrin stationary phases. Conditions: 10 m \times 50 μm I.D. cyano-deactivated fused-silica columns, 0.20 μm film thickness; 60°C column temperature; pressure program from 70 atm (5 min hold) to 200 atm (1 atm = 101 325 Pa) at a rate of 3 atm min^{-1} ; neat carbon dioxide mobile phase; timed-split injection; flame ionization detection.

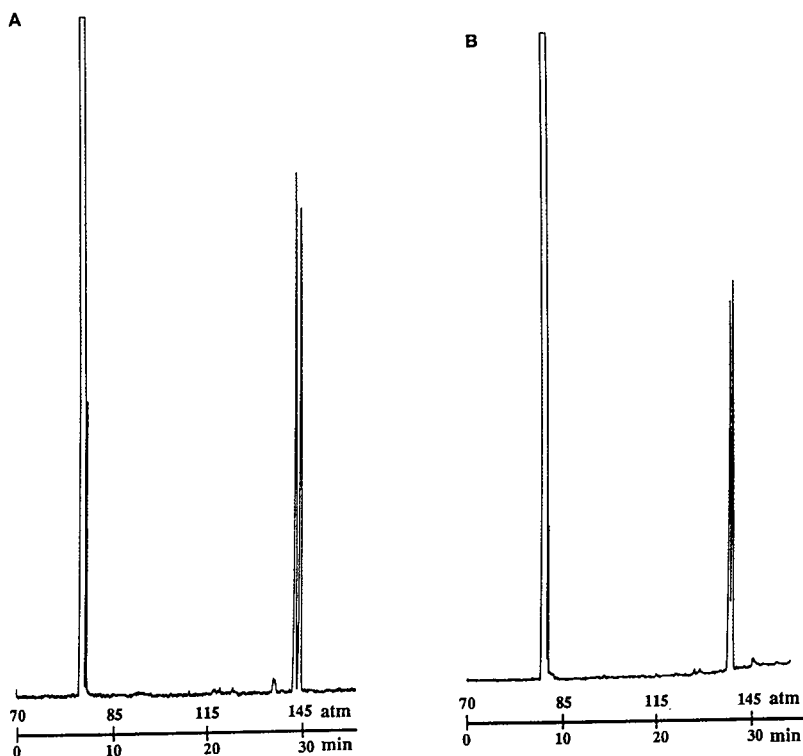


Fig. 7. Comparison of SFC separation of γ -phenyl- γ -butyrolactone enantiomers on (A) large-rim-tethered (**20**) and (B) copolymeric [1] cyclodextrin stationary phases. Conditions as in Fig. 6.

10, **15** and **18** onto copolymer **19** in a manner similar to that previously reported [17]. Equimolar amounts of cyclodextrin and Si–H functional groups on the polymer were used in the hydrosilylation reaction. Assuming that all of the alkene-substituted cyclodextrin reacted with **19**, the resulting polymer would have a ratio of 50 dimethylsiloxanes to 5 methylcyclodextrin-substituted siloxanes to 2 ditolylsiloxanes.

The newly synthesized, large-rim-tethered β -cyclodextrin polysiloxanes were evaluated as stationary phases for open tubular column GC and SFC. Chromatographic efficiencies and chiral selectivities of the new phases were evaluated and compared to analogous parameters of previously reported small-rim-tethered [2] and copolymeric [1] β -cyclodextrin phases.

The columns demonstrated excellent efficiencies and chiral selectivities for a wide variety of

solutes. Efficiency values for the GC columns varied in the range of 3000–3500 theoretical plates/m. The SFC column efficiencies were on the order of 4000–5000 plates/m. These values are comparable to those previously obtained by us for small-rim-tethered β -cyclodextrin phases [2], and are much higher than those recently reported by Schurig and co-workers [18,19]. The highest efficiency reported by those authors in GC was 2300 effective theoretical plates/m; although for more than 70% of the tested solutes, their efficiency values were under 1500 effective plates/m, including as low an efficiency value as 300 effective plates/m for 3-hydroxybutan-2-one. In SFC, column efficiencies on the order of only 2000 theoretical plates/m were reported by those authors, indicating that their SFC column efficiency was barely half of that achieved by us in the present work for large-rim-

tethered β -cyclodextrin phases, as well as for the small-rim-tethered phases reported earlier [2].

The newly synthesized large-rim-tethered cyclodextrin phases exhibited chiral selectivities comparable to those obtained previously on small-rim-tethered analogues. Fig. 5 illustrates this by gas chromatograms of pantolactone enantiomers obtained on (A) large-rim- (**22**) and (B) small-rim-tethered (polymer prepared from **1a**) [2] cyclodextrin phase columns. Analogous results were obtained in SFC. Fig. 6 demonstrates SFC chromatograms of *tert*-2-phenyl-1-cyclohexanol enantiomers obtained on columns using the two types of cyclodextrin phases (**23** for large-rim and polymer prepared from **1c** for small-rim-tethered phases). As can be seen, very similar chromatographic performance (efficiency and selectivity) was obtained on both column types. However, compared to the copolymeric cyclodextrin phases reported earlier [1], both types of pendant cyclodextrin phases demonstrated higher selectivities in SFC for some of the tested chiral compounds. Fig. 7 illustrates this point.

A detailed chromatographic study of the newly synthesized cyclodextrin phases, as well as a comparison of various aspects of their chromatographic performances with other types of cyclodextrin phases will be presented elsewhere [20].

Acknowledgements

This work was supported by a grant from Supelco. We thank Dr. Shawn L. Reese for providing us with starting D_4 .

References

- [1] G.-L. Yi, J.S. Bradshaw, B.E. Rossiter, S.L. Reese, P. Petersson, K.E. Markides and M.L. Lee, *J. Org. Chem.*, 58 (1993) 2561.
- [2] G.-L. Yi, J.S. Bradshaw, B.E. Rossiter, A. Malik, W.-B. Li and M.L. Lee, *J. Org. Chem.*, 58 (1993) 4844.
- [3] P. Fisher, R. Aichholz, U. Bolz, M. Juza and S. Krimmer, *Angew. Chem., Int. Ed. Engl.*, 29 (1990) 427.
- [4] V. Schurig, D. Schmalzing, U. Muhleck, M. Jung, M. Schleimer, P. Mussche, C. Duvekot and J.C. Buyten, *J. High Resolut. Chromatogr.*, 13 (1990) 713.
- [5] V. Schurig, Z. Juvancz, G.J. Nicholson and D. Schmalzing, *J. High Resolut. Chromatogr.*, 14 (1991) 58.
- [6] M. Jung and V. Schurig, *J. Microcol. Sep.*, 5 (1993) 11.
- [7] B. Casu, M. Reggiani, G.G. Gallo and A. Vigevani, *Tetrahedron*, 24 (1968) 803.
- [8] J. Szejtli, A. Liptak, I. Jodal, P. Fugedi, P. Nanasi and A. Neszmelyi, *Starch/Stärke*, 32 (1980) 165.
- [9] J.M. Bayona, B.J. Tarbet, H.-C.K. Chang, C.M. Schregenberger, M. Nishioka, K.E. Markides, J.S. Bradshaw and M.L. Lee, *Int. J. Environ. Anal. Chem.*, 28 (1987) 163.
- [10] K.E. Markides, B.J. Tarbet, C.M. Schregenberger, J.S. Bradshaw, M.L. Lee and K.D. Bartle, *J. High Resolut. Chromatogr. Chromatogr. Commun.*, 8 (1985) 741.
- [11] J. Bouche and M. Verzele, *J. Gas Chromatogr.*, 6 (1968) 501.
- [12] S.R. Sumpter, C.L. Woolley, E.C. Huang, K.E. Markides and M.L. Lee, *J. Chromatogr.*, 517 (1990) 503.
- [13] B.W. Wright, P.A. Peaden, M.L. Lee and T.J. Stark, *J. Chromatogr.*, 248 (1982) 17.
- [14] F.M. Menger and M.A. Dulany, *Tetrahedron Lett.*, 26 (1985) 267.
- [15] W. Meier-Augenstein, B.V. Burger and H.S.C. Spies, *Magn. Reson. Chem.*, 29 (1991) 681.
- [16] B.E. Richter, J.C. Kuei, J.I. Shelton, L.W. Castle, J.S. Bradshaw and M.L. Lee, *J. Chromatogr.*, 279 (1983) 21.
- [17] J.S. Bradshaw, S.K. Aggarwal, B.J. Tarbet, K.E. Markides and M.L. Lee, *J. Chromatogr.*, 405 (1987) 169.
- [18] D. Schmalzing, M. Jung, S. Mayer, J. Rickert and V. Schurig, *J. High Resolut. Chromatogr.*, 15 (1992) 723.
- [19] M. Jung and V. Schurig, *J. High Resolut. Chromatogr.*, 16 (1993) 215.
- [20] A. Malik, H. Yun, G.-L. Yi, J.S. Bradshaw, B.E. Rossiter, K.E. Markides and M.L. Lee, in preparation.
- [21] A. Ueno and R. Breslow, *Tetrahedron Lett.*, 23 (1982) 3451.
- [22] D. Rong and V.T. D'Souza, *Tetrahedron Lett.*, 31 (1990) 4275.
- [23] C.T. Rao, B. Lindberg, J. Lindberg and J. Pitha, *J. Org. Chem.*, 56 (1991) 1327.



ELSEVIER

Journal of Chromatography A, 673 (1994) 231–237

JOURNAL OF
CHROMATOGRAPHY A

Capillary supercritical fluid chromatography–Fourier transform infrared spectroscopy study of triglycerides and the qualitative analysis of normal and “unsaturated” cheeses

Muammer Kaplan, George Davidson*, Martyn Poliakoff

Department of Chemistry, University of Nottingham, University Park, Nottingham NG7 2RD, UK

(First received November 29th, 1993; revised manuscript received February 17th, 1994)

Abstract

Capillary supercritical fluid chromatography (cSFC)–Fourier transform infrared spectroscopy (FT-IR)–flame ionization detection (FID) has been used to examine the separation of a synthetic mixture of saturated triglycerides. A careful study of the on-line FT-IR spectra of the separated components revealed that relative absorption intensities of the infrared peaks corresponding to the antisymmetric CH_2 stretching and carbonyl ($\text{C}=\text{O}$) stretching modes were related to the carbon number of an individual triglyceride.

A comparison of the FT-IR spectra obtained in cSFC–FT-IR–FID separations of a cheese said to be high in unsaturates (“Flora” cheese) and a cheddar cheese showed that the Flora cheese does indeed contain only unsaturated triglycerides. The cheddar cheese contained many more triglyceride components, most of which correspond to saturated species. Comparison with the synthetic saturated triglyceride mixture showed that the speciation of some of the cheddar cheese components can be carried out.

1. Introduction

One of the areas of analytical chemistry where supercritical fluid chromatography (SFC) has already proved to be of considerable value is in the study of food products, particularly fats and oils [1]. These are often mixed materials of some complexity, whose relative involatility and/or thermal lability makes them poor candidates for GC analysis.

Reports by Taylor and coworkers [2,3] have shown that, following SFC, Fourier transform infrared spectroscopic (FT-IR) detection can provide a great deal of structural information on the nature of triglycerides and fatty acids de-

rived, for example, from soya bean oil. In particular, the presence of unsaturation in the hydrocarbon chains gave characteristic infrared absorptions, and it even proved to be possible to identify the geometry associated with specific centres of unsaturation by this means [3].

In our laboratory we have been active in developing an improved on-line capillary SFC (cSFC) system, which has proved to have approximately 25 times greater sensitivity than previous systems, while preserving a linear response to analyte concentration over several orders of magnitude [4]. A number of analytical results using this system have been published, showing that it is compatible with a wide range of analyte types [5–7].

Proot *et al.* [8] have reported a study of

* Corresponding author.

triglyceride separation by SFC and it therefore seemed appropriate to expand the study of triglycerides and related systems by cSFC–FT-IR. In particular, the growing concern with healthy eating habits has led to an enormous growth in the range of food products which are advertised as being “high in unsaturates”. We therefore report a study of a number of saturated triglycerides in a synthetic mixture, in which the possibility of speciation on the basis of infrared intensity measurements is explored, as well as a comparison between the chromatographic and infrared spectroscopic properties of a “natural” cheese (an English cheddar) and a recently-introduced “unsaturated” cheese (marketed in the UK under the “Flora” label).

2. Experimental

The cSFC–FT-IR–flame ionization detection (FID) system used has been described earlier [6,7]. It uses a Brownlee MicroGradient pump (Anachem, Luton, UK) for delivery and pressure programming of the mobile phase. The outlet of the pump was connected via a length of stainless-steel tubing (1.6 mm O.D. \times 0.25 mm I.D.) to the injection valve. This was a Valco C14W two-position switching valve (Anachem) with an internal loop (volume 100 or 200 nl), located on the door of an 8500 GC oven (Perkin-Elmer). The SFC capillary column (Lee Scientific, from Dionex, Camberley, UK) was installed inside the GC oven (maintained at 100 or 120°C in the experiments described in this paper) and connected directly to the valve. Samples (100 nl) were introduced on to the column by direct injection. The column outlet was connected to a 50 cm \times 50 μ m I.D., uncoated, deactivated fused-silica capillary transfer line (S.G.E., Milton Keynes, UK) using a zero dead-volume butt-connector (S.G.E.) which passed through the oven wall and was connected to the FT-IR flow-cell.

The FT-IR flow cells have been described previously [9]. They have volumes of 500 and 980 nl, respectively, and an optical path length of 4.5 mm. The cell being used was placed in the

sample compartment of a 1760-X FT-IR spectrometer (Perkin-Elmer) fitted with a mercury cadmium telluride (MCT) detector. All experiments were carried out with a spectral resolution of 8 cm^{-1} , and the flow-cell maintained at 24°C. After the flow cell a second transfer line was used to return the sample to the GC oven. This transfer line was butt-connected to a frit restrictor (Lee Scientific) which was then interfaced to the FID system of the gas chromatograph. IR data were processed using the standard GC–IR software of the spectrometer, which enabled Gram–Schmidt reconstruction of the IR chromatograms to be carried out.

cSFC–FT-IR studies were carried out on a synthetic mixture of the following triglycerides: tricaprylin (C_8 hydrocarbon chain), trilaurin (C_{12}), trimyristin (C_{14}), tripalmitin (C_{16}), tristearin (C_{18}) and triarachidin (C_{20}). The samples were obtained from Sigma (Poole, UK) and all were used without further purification. The synthetic mixture was prepared as a solution in dichloromethane.

Samples of cheddar and “Flora” cheeses were purchased from a local supermarket, dissolved in dichloromethane to give a saturated solution and filtered to give a clear solution.

The mobile phase used in all of the experiments described in this paper was 99.99% CO_2 (Air Products, Rotherham, UK).

3. Results and discussion

3.1. Triglyceride mixture

Despite the presence of three polar carboxylic groups, the long hydrocarbon chains ensure that triglycerides are soluble in supercritical CO_2 ; and cSFC–FT-IR with CO_2 as the mobile phase has been shown to be a practical proposition [3]. As a preliminary to the investigation of some food samples, we have therefore examined a synthetic mixture of saturated triglycerides, as indicated in the Experimental section above. Fig. 1a shows a Gram–Schmidt reconstructed FT-IR chromatogram of this mixture, showing good separation of the components (the chromato-

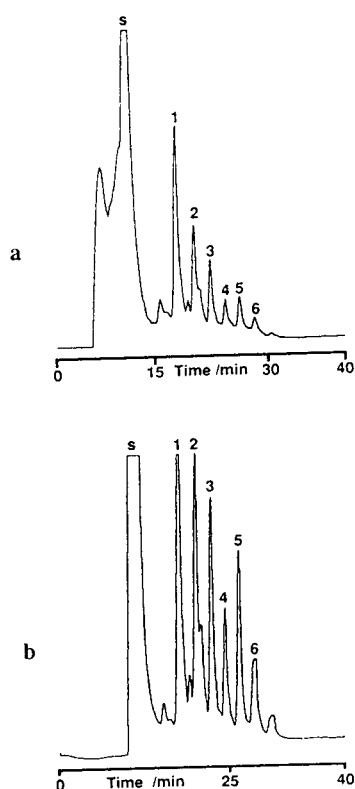


Fig. 1. (a) FT-IR chromatogram of a synthetic mixture of saturated triglycerides, separated by cSFC. Chromatographic conditions: column 10 m \times 100 μ m; stationary phase SB-Phenyl-5; sample size 100 nl; mobile phase CO₂; temperature 100°C; pressure programme 150 bar (5 min isobaric), then ramp to 350 bar at 10 bar/min, and 10 min at 350 bar. Peaks: 1 = tricaprylin; 2 = trilaurin; 3 = trimyristin; 4 = tripalmitin; 5 = tristearin; 6 = triarachidin. (b) FID chromatogram of a synthetic mixture of saturated triglycerides (details as for 1a).

graphic parameters are summarised in the figure caption). In the same run a subsequent FID chromatogram was obtained, which is shown in Fig. 1b. This confirms our earlier results showing that the effect of the FT-IR flow-cell on chromatographic resolution is negligible [10].

The great advantage of FT-IR detection over FID is that it is possible to retrieve a considerable amount of additional structural information about the separated species from the FT-IR spectra (see, e.g., refs. 3 and 6). In Fig. 2a we show the FT-IR spectra corresponding to the peaks labelled 1, 3 and 5 in Fig. 1, *i.e.* tricaprylin (C₈ hydrocarbon chains), trimyristin (C₁₄) and

tristearin (C₁₈). All show an excellent signal-to-noise ratio, and a number of bands characteristic of the fatty acid chains, *i.e.* CH₂ antisymmetric stretch (ν_{as} CH₂) near 2930 cm⁻¹, CH₂ symmetric stretch (ν_s CH₂) near 2865 cm⁻¹, ester C=O stretch (ν C=O) at 1748 cm⁻¹, CH₂ symmetric (scissors) deformation (δ_s CH₂) near 1465 cm⁻¹ and ester C–O stretch (ν C–O) near 1165 cm⁻¹. Note that for tricaprylin, with the shortest hydrocarbon chain and hence the largest proportion of terminal CH₃ groups, the antisymmetric CH₃ stretch (ν_{as} CH₃) is clearly resolved (2966 cm⁻¹). Fig. 2b shows the C–H stretching region for peaks 1 (tricaprylin), 2 (trilaurin), 3 (trimyristin) and 5 (tristearin), in which the CH₃ stretching component (*i.e.* the highest wavenumber band) becomes steadily weaker as the chain length increases. All of these assignments are in good agreement with literature values for solid and conventional solution samples of long-chain esters [11].

As our aim is the individual speciation of the separated analytes, it is necessary to examine the spectra for differences. With the exception of the observation of a CH₃ stretch for tricaprylin, the spectra, however, seem at first sight to be regrettably similar. The wavenumber of the carbonyl (C=O) stretch is invariable, and no clear trends appear in the positions of the other well-defined bands, the CH₂ stretches, *i.e.* for tricaprylin 2929 and 2868 cm⁻¹ for ν_{as} and ν_s respectively, trimyristin 2935, 2862 cm⁻¹ and tristearin 2934, 2862 cm⁻¹. On the other hand, closer investigation of the spectra does reveal significant differences in the relative intensities of some of the bands. This is particularly noticeable for the carbonyl and ν_{as} CH₂ stretches. Each of the triglycerides contains just three carbonyl groups, but differing numbers of CH₂ units in the hydrocarbon chains. In agreement with this, there is a definite increase in the intensity of ν_{as} CH₂ compared to ν C=O as the carbon number of the triglyceride increases (ν C=O is an effective internal intensity standard). The question that must be addressed in the context of speciation is whether this relationship is sufficiently quantitative to allow identification of individual compounds.

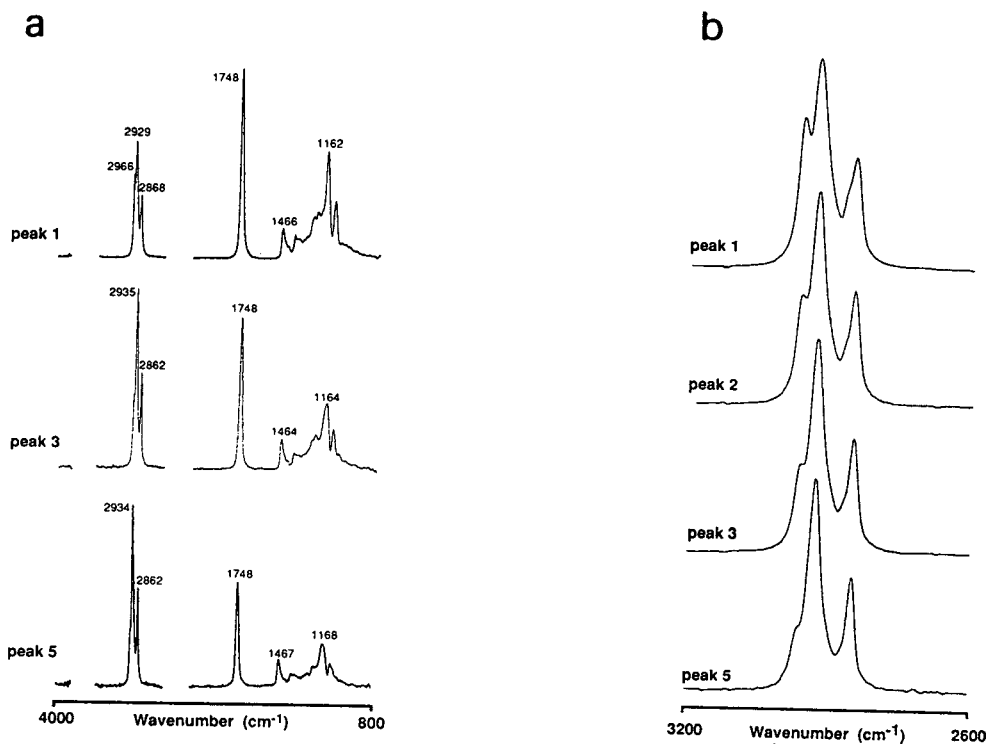


Fig. 2. (a) On-line FT-IR spectra of selected triglycerides from Fig. 1. (i) Tricaprylin (peak 1); (ii) trimyristin (peak 3); (iii) tristearin (peak 5). (b) C-H stretching regions of the FT-IR spectra of (i) tricapyrillin; (ii) trilaurin; (iii) trimyristin; (iv) tristearin.

Fig. 3 shows a plot of the triglyceride carbon number (the number of carbon atoms in each hydrocarbon chain) against the ratio of the intensities of the antisymmetric CH₂ stretch and the C=O stretch, the values of which are listed in Table 1. The intensities were simply measured in terms of peak heights as peak area measurements are subject to considerable uncertainty due to the presence of overlapping bands in the CH₂ stretching region.

It will be seen that there is a relationship between the carbon number (n) and the intensity ratio ($\nu_{\text{as}}\text{CH}_2/\nu\text{C=O}$) (I) which gives an excellent fit ($R = 1.0$) to the empirical equation

$$I = -0.5664 + 0.1400n$$

Thus a simple measurement of peak heights can

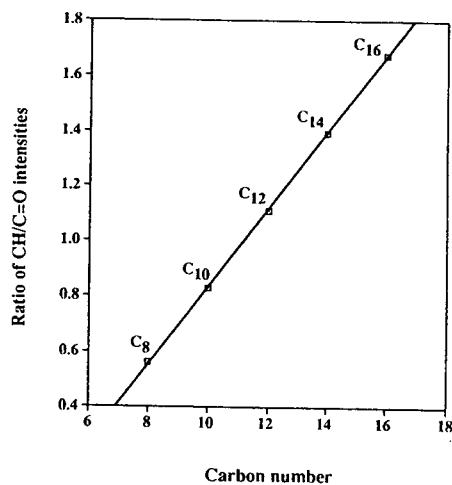


Fig. 3. Plot of intensity ratio, $\nu_{\text{as}}\text{CH}_2/\nu\text{C=O}$, versus carbon number for some saturated triglycerides.

Table 1

Values of the relative intensities (I) of $\nu_{\text{as}}\text{CH}_2$ and $\nu\text{C}=\text{O}$ for saturated triglycerides with different hydrocarbon chain lengths (n)

$I[\nu_{\text{as}}(\text{CH}_2)/\nu(\text{C}=\text{O})]$	n
0.559	8
0.830	10
1.108	12
1.395	14
1.676	16

be used to identify individual saturated triglycerides from what appear to be very similar infrared spectra.

3.2. "Natural" and "unsaturated" cheeses

Current thinking stresses the need for a healthy diet, and an important aspect of this is concerned with the proportions of saturated and unsaturated (mono- and polyunsaturated) fats consumed. Hence it is important to know which triglycerides are present in any foodstuff, and their degrees of unsaturation. In recent times a cheese has come on to the market which claims to be high in unsaturated and low in saturated fats. We have therefore subjected this "Flora" cheese to on-line cSFC–FTIR–FID analysis, and compared it with a conventional, cheddar, cheese.

Fig. 4 shows the cSFC–FTIR chromatograms of the Flora and cheddar cheeses before subtraction of the sloping baseline caused by the increasing CO_2 absorption at higher pressures, and Fig. 5 the FID chromatograms of these cheeses. Both pairs of chromatograms show quite clearly that there is a very marked difference in constitution between the two samples, with a much larger number of components in the "natural" material, and also a wider range of retention times.

In order to probe the degree of unsaturation of the two samples it is of course necessary to record their FT-IR spectra. In Fig. 6 we show the spectra corresponding to peaks 1 and 3 of Fig. 4a. The lower-wavenumber region is very similar in each case, and also very similar to the

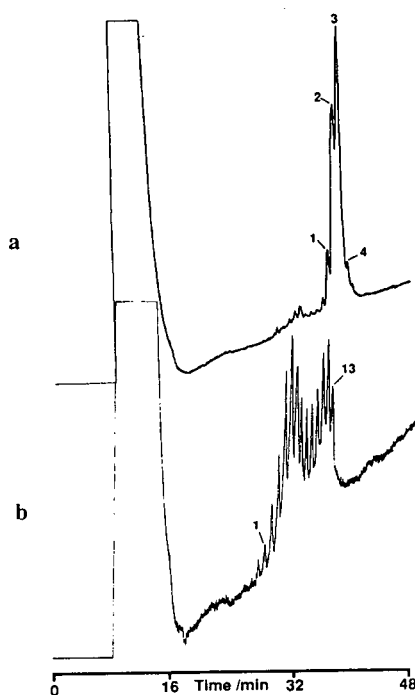


Fig. 4. (a) On-line cSFC–FT-IR chromatogram of "Flora" cheese. Chromatographic conditions: column $10 \times 50 \mu\text{m}$; stationary phase SB-Phenyl-5; sample size 200 nl; temperature 120°C ; pressure programme 90 bar (10 min isobaric) followed by ramp to 400 bar at 10 bar/min. (b) On-line cSFC–FT-IR chromatogram of cheddar cheese (details as for a). Peak nos. referred to in later figures.

FT-IR spectra obtained for the saturated triglycerides (see above). The presence of $\nu\text{C}=\text{O}$ at 1749 cm^{-1} confirms that these are indeed tri-

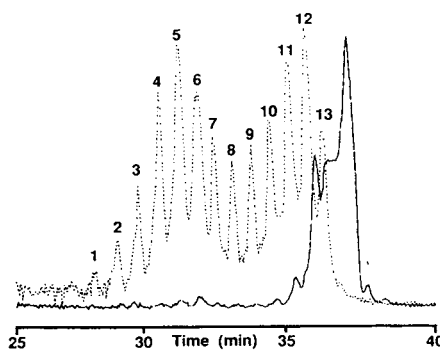


Fig. 5. Comparison of cSFC–FID chromatograms of Flora (solid line) and cheddar cheeses (dotted line) (details as in Fig. 4). Peak nos. referred to in later figures.

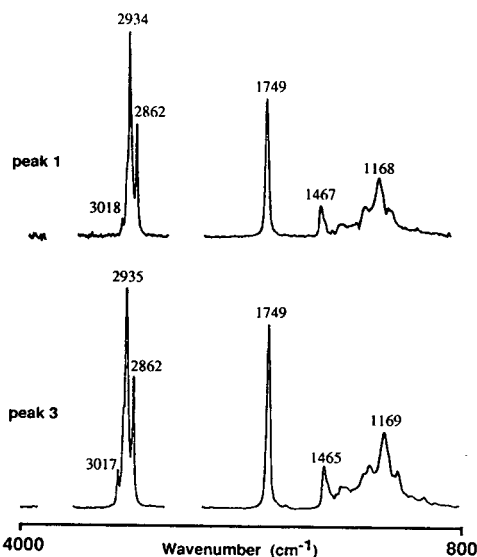


Fig. 6. On-line FT-IR spectra corresponding to selected peaks from the cSFC-FT-IR chromatogram of Flora cheese. (a) Peak 1 (Fig. 4); (b) peak 3 (Fig. 4).

glycerides, rather than, for example, fatty acids, for which $\nu_{\text{C=O}}$ is above 1760 cm^{-1} [3].

Inspection of the C-H stretching region, however, does reveal a significant difference compared to the saturated triglycerides. In addition to $\nu_{\text{s}}\text{CH}_2$ (2862 cm^{-1}) and $\nu_{\text{as}}\text{CH}_2$ (2935 cm^{-1}) a feature is seen above 3000 cm^{-1} . Calvey *et al.* [3] have reported on the FT-IR spectrum of the unsaturated triglyceride, trilinolein, with two double bonds per chain, in the *cis,cis* configuration, and a characteristic $\nu(\text{=C-H})$ band at $3016\text{--}3018\text{ cm}^{-1}$ (compared to a value of $3010\text{--}3012\text{ cm}^{-1}$ for singly, *cis*, unsaturated chains). Thus the triglycerides in Flora cheese appear to contain at least two unsaturated units per hydrocarbon chain, in agreement with advertising claims made for this product.

The difference between Flora and cheddar cheeses is highlighted by Fig. 7, where the C-H stretching regions in the FT-IR spectra, corresponding to peak 3 in Fig. 4a of Flora (Fig. 7b) and to peak in 4 in Fig. 5 of cheddar (Fig. 7a), are compared. Two observations can be made on these spectra. First, it can be suggested that the hydrocarbon chain lengths are relatively modest, as the CH_3 antisymmetric stretches are clearly

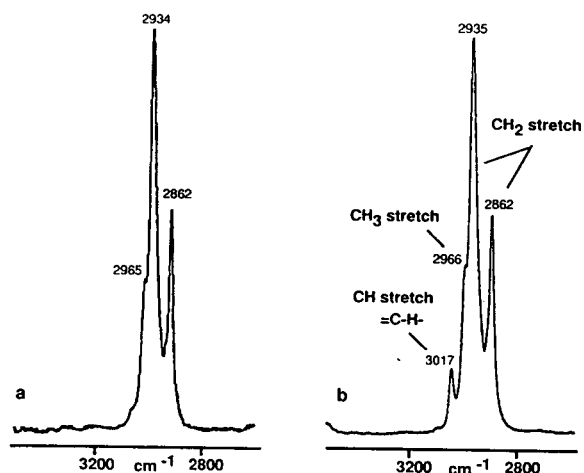


Fig. 7. C-H stretching region of the FT-IR spectra corresponding to (a) peak 4 of cheddar (Fig. 5) and (b) peak 3 of Flora (Fig. 4).

visible as high-wavenumber shoulders (2965 cm^{-1}) on the $\nu_{\text{as}}(\text{CH}_2)$ peak near 2935 cm^{-1} . Second, it is clear that this triglyceride from the cheddar cheese is completely saturated, while peak 3 for Flora (Fig. 7b), as was the case for peaks 1 and 3 (Fig. 6), contains at least two units of unsaturation per hydrocarbon chain.

Fig. 8 shows FT-IR spectra corresponding to two of the components of the cheddar cheese.

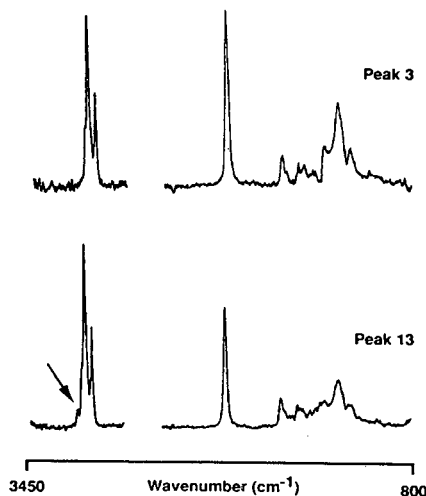


Fig. 8. On-line FT-IR spectra corresponding to selected peaks from the cSFC-FT-IR chromatogram of cheddar cheese. (a) Peak 3 (Fig. 5); (b) peak 13 (Fig. 5).

The early-eluting peak 3 shows no absorption above 3000 cm^{-1} , and is therefore a saturated triglyceride (characteristic $\nu\text{C}=\text{O}$ band at 1748 cm^{-1}), and comparison of the relative peak heights for $\nu_{\text{as}}\text{CH}_2$ and $\nu\text{C}=\text{O}$ shows that it is most likely to be trilaurin (see Fig. 3). The late-eluting component (peak 13) is an unsaturated triglyceride, whose FT-IR spectrum is very similar to that of the species corresponding to peak 1 of the Flora cheese.

Thus, cSFC-FT-IR can, even in the absence of any complementary spectroscopic detection, provide a considerable amount of information as to the chemical constitution of cheeses, with the possibility of individual speciation in some cases.

4. Conclusions

cSFC-FT-IR has been confirmed as an excellent technique for the analysis of fats and oils, and especially triglycerides. Despite the apparent similarity of the FT-IR spectra of saturated triglycerides, careful comparison of diagnostic peak intensities can give information as to their individual identities.

The identification of unsaturation in triglycerides is a straightforward process, and further work is in progress to extend the possibilities of specific triglyceride identification to unsaturated species. In the example studied in this paper, it became clear that at least one advertising claim could be substantiated scientifically!

Despite the successes of FT-IR alone as a detection system, it will clearly be advantageous to obtain more detailed information about the molecular masses and structures of analytes, as can be done by the addition of a mass-spectrometric detector after the FT-IR flow-cell. Preliminary results [12] show that the resultant "multiply-hyphenated" system can be constructed, and that it will be an extremely powerful analytical tool.

5. Acknowledgements

We are grateful to Perkin-Elmer Ltd. (especially Dr. H. Mould and Dr. M.A. Ford) and to British Petroleum (especially Professor D. Gerard and Mr. T. Lynch) for their support, and to Marmara University, Turkey (for financial support to M.K.). We also thank Dr. M.A. Healy, Dr. T.J. Jenkins, Mr. M.R. Simmonds, Dr. D. Dye, Mr. K. Stanley, Mr. J.M. Whalley and Mr. J.G. Gamble for helpful discussions and technical assistance.

6. References

- [1] T.L. Chester, J.D. Pinkston and D.E. Raynie, *Anal. Chem.*, 64 (1992) 153R.
- [2] E.M. Calvey, S.W. Page and L.T. Taylor, *Proc. SPIE-Int. Soc. Opt. Eng.*, 1145 (1989) 540.
- [3] E.M. Calvey, R.E. McDonald, S.W. Page, M.M. Mosoba and L.T. Taylor, *J. Agric. Food Chem.*, 39 (1991) 542.
- [4] T.J. Jenkins, M. Kaplan, G. Davidson, M.A. Healy and M. Poliakoff, *J. Chromatogr.*, 626 (1992) 53.
- [5] M.A. Healy, T.J. Jenkins and M. Poliakoff, *Trends Anal. Chem.*, 10 (1986) 147.
- [6] T.J. Jenkins, M. Kaplan, M.R. Simmonds, G. Davidson, M.A. Healy and M. Poliakoff, *Analyst*, 116 (1991) 1305.
- [7] T.J. Jenkins, G. Davidson, M.A. Healy and M. Poliakoff, *J. High Resolut. Chromatogr.*, 15 (1992) 819.
- [8] M. Proot, P. Sandra, E. Geeraert, *J. High Resolut. Chromatogr. Chromatogr. Commun.*, 9 (1986) 189.
- [9] T.J. Jenkins, *Ph.D. Thesis*, University of Nottingham, Nottingham, 1991.
- [10] T.J. Jenkins, M. Kaplan and G. Davidson, *J. High Resolut. Chromatogr.*, 17 (1994) 160.
- [11] L.J. Bellamy, *The Infrared Spectra of Complex Molecules*, Chapman & Hall, London, 3rd ed., 1975.
- [12] M. Carrott, M. Kaplan, S. Bajic and G. Davidson, unpublished results.

Correlation between zone velocity and current in automated single capillary isotachopheresis–zone electrophoresis

N.J. Reinhoud, U.R. Tjaden*, J. van der Greef

Division of Analytical Chemistry, Leiden/Amsterdam Center for Drug Research, Leiden University, P.O. Box 9502, 2300 RA Leiden, Netherlands

(First received November 5th, 1993; revised manuscript received March 8th, 1994)

Abstract

In single capillary isotachopheresis–zone electrophoresis (ITP–CZE) the sample zone velocity is varying with its position in the capillary during the focusing step. When the voltage is kept constant, the current changes to the same extent. Correlation between the current and the sample zone velocity can therefore be used to calculate the velocity of the hydrodynamic flow that is needed to counterbalance the sample zone velocity. Measured data are in agreement with calculations implying that current monitoring can be used in an automated feedback system to regulate the hydrodynamic flow velocity during the focusing step. Conditions are described where automated anionic single capillary ITP–CZE can be performed without application of a hydrodynamic counterflow, extending its applicability to any commercially available CZE system.

Correlation between the ITP current and the sample zone position in the capillary was used to determine the moment for automatic switching from ITP to CZE. The reproducibility of the corresponding CZE migration times is investigated in addition to the effect of the remaining ITP terminator zone length on the CZE separation. A remaining terminator zone length of 10% of the total capillary length still resulted in an acceptable CZE performance.

1. Introduction

Capillary electrophoresis in combination with trace enrichment procedures has been proven to be a powerful analytical technique capable of highly efficient separations at low analyte concentrations [1,2]. Several methods of lowering determination limits in capillary zone electrophoresis (CZE) have been described [3]. Classical off-line sample pretreatment and preconcentration techniques, such as liquid–liquid extraction or solid-phase isolation, have been used in a

number of bioassays. Although these procedures can be laborious and time consuming they offer flexibility [4]. On-line sample pretreatment offers the possibility of automation but has some restrictions with respect to the following step in the analytical method [5].

Electrophoretic analyte focusing procedures are a convenient way of lowering the determination limits that are typical for zone electrophoretic separations. Several modes have been described and successfully applied. A common feature of procedures such as stacking and sample self stacking or transient isotachopheretic (ITP) preconcentration, is that the analyte is concentrated at the boundary over which a

* Corresponding author.

difference in the electric field strength exists [3,6].

The combination of ITP with CZE has been successfully applied by several groups in a dual-capillary mode. In this mode the sample ions are transferred from the ITP system to the CZE capillary. In the single capillary mode as described by Reinhoud *et al.* [7,8] the process of ITP and CZE takes place in the same capillary, only the buffer vials are switched. Large sample volumes are injected, typically 10–90% of the total capillary volume. A hydrodynamic counterflow is used during the focusing step to keep the sample zones inside the capillary. The discontinuous ITP buffer is removed before the CZE step is started resulting in highly efficient separations. The method is automated, reproducible and takes place in a commercially available CZE apparatus without any modifications of the hardware. Determination limits are at least a factor hundred better than for conventional CZE. Similar results have been obtained in combination with electrospray mass spectrometry of β -agonists [9].

In this paper an equation is derived giving the correlation between the current and the sample zone velocity during the focusing step in single capillary ITP–CZE. With this linear relationship the pressure needed to counterbalance the sample zone velocity can be calculated. The position of the sample zone in the capillary is calculated from the current, compared with experimental data and applied in automated ITP–CZE procedures. The reproducibility is investigated for ITP–CZE using current monitoring for automated switching from the ITP to the CZE mode.

2. Theory

The coupling of ITP with CZE using a single capillary setup has been described for both anions and cations [7,8]. In both cases either the leading or terminating buffer can be used as background electrolyte for CZE, resulting in four modes of ITP–CZE. The focusing step is started after injection of a large sample zone in terminator buffer, typically 30–90% of the total

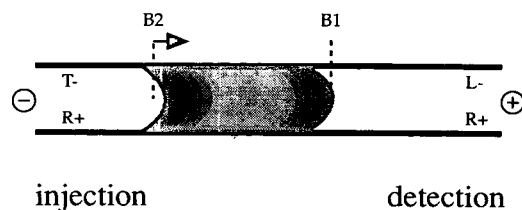


Fig. 1. Schematic representation of an anionic sample zone in the focusing step of ITP–CZE. The sample is solved in terminator buffer (T⁻, R⁺). The leading buffer (L⁻, R⁺) is also used as background electrolyte in the CZE step. The hydrodynamic flow velocity counterbalances the electroosmotic and electrophoretic velocities of a sample zone at the front boundary (B1). The rear boundary (B2) migrates to B1 resulting in a concentration of the analyte.

capillary length. A counterflow is used to keep the sample zones in the capillary during the focusing process (Fig. 1). The front of the sample zone which forms a boundary with the leading buffer, is kept at a fixed position in the capillary by balancing the electrophoretic leading ion velocity with the hydrodynamic velocity. The rear boundary of the analyte zone is migrating in the direction of the front boundary resulting in a concentration of the analyte. After focusing the discontinuous buffer is removed isotachophoretically by either increasing or decreasing the hydrodynamic counterflow depending on the ITP–CZE mode that is used.

2.1. Theoretical model

For the calculation of the zone velocity during the focusing step an isotachophoretic state is assumed. This assumption has been made to enable calculations of the local electric field strengths and the electrophoretic and electroosmotic velocities. In the isotachophoretic state the velocities of all ions are the same with exception of the counter ion velocity [10]. For the analyte ions during the focusing step this assumption is not true, only when the focusing is completed they migrate with the same velocity as the leading and terminating ions. However, when low analyte concentrations in terminator buffer (*i.e.* <0.1% of the terminator buffer concentration) are considered the contribution to

the local electric field strength and conductivity in the terminator zone is negligible. Therefore, the velocity of the leading ions can be calculated without consideration of the migration of sample ions.

The terminator buffer is prepared at the isotachophoretic concentration. This concentration is given by:

$$\bar{c}_T = \frac{m_T}{m_L} \cdot \frac{m_L + m_R}{m_T + m_R} \cdot \bar{c}_L \quad (1)$$

where m_i is the absolute value of the ionic mobility of i . The subscripts L, T and R refer to the leading, terminating and counter ions, respectively. Because in buffer systems weak electrolytes are involved the analytical concentration of an analyte A is notated as $\bar{c}_A([HA] + [A^-])$ and the ionic concentration is notated as $c_A([A^-])$. Analogous, the mobility of the fully ionized analyte A is written as m_A and the effective mobility as \bar{m}_A . The relationship between the ionic and effective mobility is then given by $c_A m_A = \bar{c}_A \bar{m}_A$. An anionic system with univalent buffer ions will be considered, consisting of only one type of cations and anions (i.e. L^- and R^+ , T^- and R^+). The leading buffer is also used as CZE background electrolyte.

In our model the temperature in the leading and terminating zone is considered to be the same and constant. Most of the considered parameters are dependent on temperature. This means that the model is only applicable for systems where the Joule heat is efficiently dissipated. When the terminator zone is removed from the capillary, the local electrical field strength in the terminator zone increases considerably resulting in an increased heat development. Therefore, at a small terminating buffer zone length a deviation of the measured velocities from the calculated velocities may occur. However, in ITP-CZE usually large injection volumes are applied. After the focusing step, when the terminator buffer is removed, the accurate magnitude of the velocity is usually no longer relevant. In the Results and Discussion section the assumption of a constant axial temperature is verified.

2.2. The hydrodynamic counterflow

The counterflow to keep the boundary of the sample zone with the leading buffer zone on a fixed position in the capillary (Fig. 1) is given by:

$$v_L + v_{hd} = 0 \quad (2)$$

where v_L is the velocity of the leading ions and v_{hd} is the hydrodynamic flow velocity in the opposite direction. The velocity of the leading ions is given by the sum of the electrophoretic velocity ($v_{el,L}$) and the bulk electroosmotic velocity (v_{eof})

$$v_L = v_{el,L} + v_{eof} \quad (3)$$

The electrophoretic velocity of the leading ions is given by

$$v_{el,L} = \bar{m}_L E_L \quad (4)$$

where \bar{m}_L is the effective electrophoretic mobility of the leading ions and E_L is the electric field strength in the leading buffer zone.

The electroosmotic velocity is weighted over the fraction of capillary filled with leading buffer (x) and with terminating buffer ($1-x$) [6]

$$v_{eof} = xv_{eof,L} + (1-x)v_{eof,T} \quad (5)$$

where v_{eof} is the bulk electroosmotic velocity, $v_{eof,L}$ is the electroosmotic velocity in the leading zone and $v_{eof,T}$ is the electroosmotic velocity in the terminating zone. Combination of Eqs. 5 and 3 gives for the velocity of the leading ions

$$v_L = xv_{eof,L} + (1-x)v_{eof,T} + v_{el,L} \quad (6)$$

The hydrodynamic flow velocity caused by a pressure difference over a capillary is given by the Poiseuille equation:

$$v_{hd} = \frac{d^2}{32\eta L_0} \cdot \Delta p \quad (7)$$

where L_0 is the total capillary length, η is the viscosity ($9.93 \cdot 10^{-4} \text{ kg m}^{-1} \text{ s}^{-1}$), d the capillary diameter and Δp the pressure difference. Combination of Eqs. 2, 6 and 7 gives the pressure difference that results in a hydrodynamic velocity that counterbalances the velocity of the boundary between the leading and analyte zone

$$\Delta p = \frac{32\eta L_0}{d^2} \cdot [xv_{\text{eof,L}} + (1-x)v_{\text{eof,T}} + v_{\text{el,L}}] \quad (8)$$

where the electrophoretic velocity ($v_{\text{el,L}}$) has a negative value for anions. The fraction of the capillary that is filled with leading buffer (x) depends on the injected volume and changes when the focusing procedure proceeds. When the capillary is filled for 75% with sample in terminating buffer, the value of x is 0.25. This fraction will increase to 1.0 when the terminating buffer is removed from the capillary.

From Eq. 3 it can be seen that when the electroosmotic velocity is smaller than the velocity of the leading ions ($v_{\text{el,L}} + v_{\text{eof}} > 0$) the direction of the leading zone velocity reverses. Therefore, the counterflow velocity balancing the leading zone velocity (Eq. 1) is also reversed. This means that in stead of an increased pressure a reduced pressure is needed for complete removal of the anionic ITP buffer. The four ITP-CZE procedures as described previously [8] can all be performed in absence as well as in presence of electroosmotic flow using the appropriate pressure difference given by Eq. 8.

When the electrophoretic mobility is approximately the same as the electroosmotic mobility, there will be one value of x for which the leading zone velocity (v_{L}) is zero. Without applying a hydrodynamic flow, the boundary of the sample zone and leading zone will migrate in the electric field until this particular leading zone length is reached and the velocity is zero. When all parameters are kept constant, the position of this boundary will not change in time. When the position of this boundary is close to the capillary inlet, the ITP step can be stopped and the CZE step can be started without removing the remaining terminator zone. For untreated fused silica with an electroosmotic mobility of the buffer of $ca. 60 \cdot 10^{-9} \text{ m}^2 \text{ V}^{-1} \text{ s}^{-1}$ this may be the case when chlorate ($m = 63 \cdot 10^{-9} \text{ m}^2 \text{ V}^{-1} \text{ s}^{-1}$) or chloride ($m = 75 \cdot 10^{-9} \text{ m}^2 \text{ V}^{-1} \text{ s}^{-1}$) is used as leading ion.

2.3. Determination of parameters

In the isotachophoretic steady state the electric field strength in the leading buffer zone (E_{L})

is by definition lower than in the terminating buffer zone (E_{T}). The local electric field strength depends on the total electric field applied over the capillary (E_0), the conductivities of the buffers and the length over which the capillary is filled with leading or terminating buffer. The total electric field strength is given by the running voltage (V_0) divided by the total capillary length (L_0). The electric field strength in the leading zone is given by [6]

$$E_{\text{L}} = \frac{\gamma E_0}{[\gamma x + (1-x)]} \quad (9)$$

and in the terminating zone

$$E_{\text{T}} = \frac{E_0}{[\gamma x + (1-x)]} \quad (10)$$

where γ is the conductivity ratio of the terminating and the leading zone ($\kappa_{\text{T}}/\kappa_{\text{L}}$) and x is the fraction of the capillary that is filled with leading buffer (L_{L}/L_0). The fraction that is filled with terminator buffer ($1-x$) is equal to L_{T}/L_0 . When the sample is solved in terminator buffer at the isotachophoretic concentration (Eq. 1) the length of the injection zone is considered to be L_{T} .

The conductivity (κ_i in S m^{-1}) can be measured in a capillary filled with buffer i using Eq. 11:

$$\kappa_i = \frac{I}{\pi r^2 E} \quad (11)$$

where I is the electric current and r is the capillary radius. Alternatively, when the electrophoretic mobilities are known, the conductivity for weak univalent electrolytes can be calculated by [11]

$$\kappa_i = F\bar{c}_{\text{A}}(\bar{m}_{\text{A}} + \alpha_{\text{A}}m_{\text{R}}) \quad (12)$$

where F is the Faraday constant (96485 C mol^{-1}) and α_{A} the mole fraction of A that is in the ionic form. In case of univalent buffer ions the conductivity ratio γ is given by

$$\frac{\kappa_{\text{T}}}{\kappa_{\text{L}}} = \frac{\bar{c}_{\text{T}}(\bar{m}_{\text{T}} + \alpha_{\text{T}}m_{\text{R}})}{\bar{c}_{\text{L}}(\bar{m}_{\text{L}} + \alpha_{\text{L}}m_{\text{R}})} \quad (13)$$

The concentration \bar{c}_{T} is calculated via the ITP equation (Eq. 1). The ionic mobility m_{R} is

assumed to be the same in the leading and terminating zone. Although the ionic mobility depends on the ionic strength which differs in the leading and terminating zone, for the conductivity ratio this is negligible.

The electroosmotic flow velocities are calculated using

$$v_{\text{eof,L}} = m_{\text{eof,L}} E_L \quad (14)$$

and

$$v_{\text{eof,T}} = m_{\text{eof,T}} E_T \quad (15)$$

where m_{eof} is the electroosmotic mobility ($\text{m}^2 \text{V}^{-1} \text{s}^{-1}$). The bulk electroosmotic mobility is the same in both zones; however, local differences in the electroosmotic mobility in the leading and terminating zone exists. The electroosmotic mobility decreases as the ionic strength of the buffer increases. Because of a lower buffer concentration in the terminator zone, the electroosmotic mobility will be higher than in the leading buffer zone. The local difference in flow-rate with respect to the bulk flow-rate, is compensated for by a convective flow in the buffer zones. The electroosmotic velocity ($v_{\text{eof,L}}$) can be measured in the CZE mode, when the leading buffer is used as background electrolyte. The electroosmotic velocity of the terminator zone $v_{\text{eof,T}}$ can be measured in the capillary filled with terminating buffer, using the buffer concentration calculated using the ITP equation (Eq. 1).

From Eqs. 9 and 10 it follows that the electric field strength is considerably influenced by the length of the leading zone, which results in varying electrophoretic and electroosmotic velocities during the focusing procedure. Substituting Eqs. 9, 10, 14 and 15 in Eq. 8 gives the full impact of the fractional leading zone length (x) on the pressure difference.

$$\Delta p = \frac{32\eta L_0}{d^2} \cdot \frac{\gamma E_0}{[\gamma x + (1-x)]} \cdot \left[xm_{\text{eof,L}} + \frac{(1-x)}{\gamma} \cdot m_{\text{eof,T}} + \bar{m}_L \right] \quad (16)$$

where the effective mobility of the leading ions (\bar{m}_L) has a negative value for anions. Both Eqs. 16 and 8 can be used to calculate the pressure difference that results in a hydrodynamic flow

that counterbalances the velocity of the boundary between the leading and analyte zone. Eq. 16 gives insight in all the parameters that are affecting the pressure difference.

When the conductivities of the leading and terminating buffer are measured or calculated (Eq. 12), the conductivity ratio γ (Eq. 13) can be calculated. Via experimentally determined electrophoretic and electroosmotic mobilities the corresponding velocities can be calculated using Eqs. 4, 14 and 15. The total velocity of the boundary of the leading buffer zone with the sample zone (v_L) is then calculated with Eq. 6. The pressure that results in a hydrodynamic flow velocity that counterbalances v_L is then given by Eq. 8.

When it is not possible to apply a pressure during the focusing procedure, a height difference can be used. The calculated pressure difference can be converted to a height difference using

$$\Delta h = \Delta p / \rho g \quad (17)$$

where Δp is the pressure difference (bar), ρ is the buffer density (1000 kg m^{-3}) and g is the gravitational force (9.8 m s^{-2}). A pressure difference of 20 mbar corresponds to a height difference of approximately 20 cm. This conversion is independent of the capillary diameter.

2.4. Current monitoring

When a constant voltage is applied during the focusing step, and the leading buffer is used as background electrolyte in the CZE step, the current will increase as more leading buffer enters the capillary. Just before a complete removal of the terminator buffer the ITP is stopped and the CZE is started. Monitoring of the current can be used to determine the moment for automated switching from ITP to CZE.

The total current in an ITP process is determined by Ohm's Law as the ratio of the applied voltage and the electrical resistance of the liquid in the capillary. The total resistance in the ITP capillary is given by the sum of the resistances of the leading, terminating and sample zones. For the ITP of low concentrations of analyte the contribution of the sample zones to

the total resistance of the capillary will be negligible so that

$$I = V_0 / (R_L + R_T) \quad (18)$$

The electrical resistance of zone i (R_i) depends on the capillary radius (r), the length (L_i) and the conductivity (κ_i) of the zone.

$$R_i = L_i / (\pi r^2 \kappa_i) \quad (19)$$

Substituting Eq. 19 in Eq. 18 gives

$$I = \frac{V_0 \pi r^2}{\left(\frac{L_L}{\kappa_L} + \frac{L_T}{\kappa_T} \right)} \quad (20)$$

When the conductivities are known the variation of current during the focusing step can be calculated using Eq. 20 for a given leading and terminating zone length. The current after removal of the terminator zone in single capillary ITP-CZE is given by Eq. 20 for $L_T = 0$, *i.e.* when the capillary is filled with leading buffer only. In practice always a small zone of terminator will remain in the capillary when switching from ITP to CZE.

In ITP the composition of the leading zone also determines the composition of the terminating zone. Thus when the composition of the leading zone is known and the mobilities of the leading and terminating ions and of the counter ions are known, the change in current can be calculated. The conductivity in a zone is given by the sum of the product of concentration, mobility and charge of all ionic species. Combining Eqs. 12 and 20 for a system with univalent ions gives

$$I = \frac{V_0 \pi r^2 F}{\left[\frac{L_L}{\bar{c}_L(\bar{m}_L + \alpha_L m_R)} + \frac{L_T}{\bar{c}_T(\bar{m}_T + \alpha_T m_R)} \right]} \quad (21)$$

When in single capillary ITP-CZE a given remaining zone length of the terminator buffer is allowed, the corresponding ITP current is then calculated using Eq. 20. This is the threshold of the current that can be used to program the CZE apparatus to switch automatically from the ITP step to the CZE step. Although Eq. 21 gives a better insight in all parameters that are affecting

the change in current, for precise determination of the current profile during the ITP step it is advisable to use Eq. 20 in conjunction with conductivity measurements of the leading and terminating buffers.

2.5. Counterflow and current

The hydrodynamic flow velocity needed to counterbalance the sample zone velocity depends on the position of the sample zones in the capillary (Eq. 16). This position can be calculated from the current (Eqs. 20 and 21). Combining these equations makes it possible to calculate the hydrodynamic flow velocity for a given current. The current is measured during the analysis and will be constant as long as the sample zones are not moving. Using Eq. 20, $L_L = xL_0$ and $L_T = (1-x)L_0$, the relative leading zone length x can be written as

$$x = \frac{\pi r^2 E_0 \kappa_T}{I(\gamma - 1)} - \frac{1}{(\gamma - 1)} \quad (22)$$

Substituting the expression for the current density $I/(\pi r^2) = E_L \kappa_L$ (Eq. 11) in Eq. 9 gives

$$\frac{\gamma E_0}{[\gamma x + (1-x)]} = \frac{I}{\pi r^2 \kappa_L} \quad (23)$$

Substituting Eqs. 22 and 23 in Eq. 16 results in the linear equation

$$\Delta p = a + bI \quad (24)$$

which gives the pressure difference for a given current. The slope b and intercept a are given by

$$a = \frac{32\eta V_0}{d^2} \cdot \left[\frac{\kappa_T m_{\text{eof,L}} - \kappa_L m_{\text{eof,T}}}{\kappa_T - \kappa_L} \right] \quad (25)$$

$$b = \frac{128\eta L_0}{d^4 \kappa_L \pi} \cdot \left[\frac{1}{\gamma} \cdot \left(1 + \frac{1}{\gamma - 1} \right) \cdot m_{\text{eof,T}} - \left(\frac{1}{\gamma - 1} \right) \cdot m_{\text{eof,L}} + \bar{m}_L \right] \quad (26)$$

where the effective mobility of the leading ions (\bar{m}_L) has a negative value for anions. Eq. 24 implies that with current monitoring not only the

moment to switch from ITP to CZE can be determined, but also the pressure needed in single capillary ITP–CZE.

2.6. The focusing step

An important aspect in the focusing step is the focusing time of the analytes. The time to focus the injection zone is given by the sample zone length divided by the total velocity of the slowest analyte ion in the ITP separation window, $t = L_{inj}/v_{A,f}$. The subscript f refers to focusing conditions. The total velocity of the analyte ions under focusing conditions is given by

$$v_{A,f} = xv_{eof,L} + (1-x)v_{eof,T} + v_{el,A} + v_{hd} \quad (27)$$

where $v_{el,A}$ is the electrophoretic velocity of the slowest analyte A. Because A is migrating in the terminator zone, the electrophoretic velocity of A can be written as $v_{el,A} = \bar{m}_A E_T$. The velocity of the terminating ions under focusing conditions can be written as

$$v_{T,f} = xv_{eof,L} + (1-x)v_{eof,T} + v_{el,T} + v_{hd} = 0 \quad (28)$$

Assuming ITP conditions the terminator ion velocity is counterbalanced by the hydrodynamic velocity, $v_L = v_T = -v_{hd}$. Combining this with Eqs. 27 and 28 gives for the analyte velocity under focusing conditions

$$v_{A,f} = v_{el,A} - v_{el,T} = (\bar{m}_A - \bar{m}_T)E_T \quad (29)$$

The focusing time is then given by

$$t = L_{inj}/[(\bar{m}_A - \bar{m}_T)E_T] \quad (30)$$

The focusing time is thus independent from the electroosmotic and hydrodynamic velocity. When the effective electrophoretic mobilities of the analyte and the terminator ion are similar the focusing time will increase to infinity.

In practice the focusing step and the isotachophoretic removal of the terminator buffer can be combined thus reducing the analysis time. The focusing step is started at the appropriate pressure, given by Eq. 8 and after a few minutes the pressure is lowered. As a result the terminating zone length decreases slowly and the

electrical field strength E_T increases. This can be repeated several times, thus increasing E_T and reducing the focusing time.

The described focusing procedure as illustrated in Fig. 1 offers several alternatives. In stead of counterbalancing the sample zone boundary with the leading buffer (the front boundary) the boundary of the slowest sample ion with the terminator zone (rear boundary) can be counterbalanced. Analogous to Eq. 8 the pressure needed to induce an appropriate counterflow is given by

$$\Delta p = \frac{32\eta L_0}{d^2} \cdot [xv_{eof,L} + (1-x)v_{eof,T} + v_{el,A}] \quad (31)$$

where $v_{el,A}$ is given by the effective electrophoretic mobility of the slowest analyte A and the electric field strength in the terminator zone (Eq. 4).

Solving the sample in leading buffer is another option. When the boundary of the terminator buffer with the sample zone in leading buffer (rear boundary) is counterbalanced (using Eq. 8), the focusing time is given analogous to Eq. 30 by

$$t = L_{inj}/[(\bar{m}_L - \bar{m}_A)E_L] \quad (32)$$

In most cases it is unlikely that this will reduce the analysis time because the electrical field strength in the leading buffer is always lower than in the terminating buffer. However, when the effective electrophoretic mobility of the analyte and the terminator ion are similar the focusing time can be reduced by solving the sample in leading buffer.

Another possibility in reducing the focusing time is focusing under unsteady state conditions by solving the sample in a lower terminator concentration than given by Eq. 1 which results in an increased E_T . However, under unsteady state conditions care must be taken that no analyte is lost.

2.7. Composition of the sample

For the calculation of the velocities at the start of the focusing procedure, it is assumed that

low-concentrations analyte are solved in terminating buffer. When the terminating buffer is at the ITP concentration (Eq. 1) the sample zone length is considered to be L_T . The conductivity of the sample is considered to be the same as the terminating buffer. In that case all equations can be used immediately from the start of the focusing procedure. Another advantage of working under these well defined conditions is that the velocities of analyte ions are known and by using the appropriate counterflow no loss of analyte occurs.

When the sample is solved in a matrix other than the terminator buffer or when high concentrations of matrix constituents are present in the sample, the applicability of the derived equations is limited to the ITP steady state. Only the zone velocity at the start of the focusing step can be calculated with the sample zone conductivity. The focusing step then proceeds under unsteady state conditions. The sample zone velocity is not only changing with its position in the capillary but also because of local changes in electric field strength as a result of the migration of matrix ions. Under unsteady state conditions the possibility exists that analyte ions migrate out of the capillary. A full discussion on unsteady state migration is given by Foret *et al.* [12].

One way to overcome incompatibility of the sample matrix with the ITP conditions is a sample pretreatment where an excess of matrix components is removed and the analytes are transferred to a well defined matrix. In trace analysis (nanomolar sample concentration range and lower) of analytes in complex matrix it is unlikely that ITP-CZE or CE in general can be used without an additional pretreatment step. An additional sample pretreatment usually improves the performance of ITP-CZE with respect to reproducibility, selectivity and ITP focusing time [7,8].

3. Experimental

3.1. Chemicals

Acetic acid (HAc) was from Merck (Darmstadt, Germany). Fluorescein (F) and tri-

ethanolamine (TEtOHA) (97%) were purchased from Janssen Chimica (Beerse, Belgium). Fluoresceinisothiocyanate isomer I (FITC) was from Aldrich Chemie (Steinheim, Germany). The food colorant brilliant acid green (E142) was from Morton (Amersfoort, Netherlands). Hydroxypropylmethylcellulose (HPMC) and 4-(2-hydroxyethyl)-1-piperazineethanesulphonic acid (HEPES) came from Sigma (St. Louis, MO, USA). The viscosity of a 2% aqueous HPMC solution is 4000 cP. In all experiments deionised water was used (Milli-Q system; Millipore, Bedford, MA, USA).

3.2. Conditions used in calculations

Zone velocity, current and counterflow (Figs. 2, 3 and 6) are calculated for an untreated fused-silica capillary of 500 mm \times 100 μ m I.D. An electroosmotic mobility of $60.0 \cdot 10^{-9} \text{ m}^2 \text{ V}^{-1} \text{ s}^{-1}$ is used for the leading buffer and $70.5 \cdot 10^{-9} \text{ m}^2 \text{ V}^{-1} \text{ s}^{-1}$ for the terminating buffer. The leading buffer consisted of 10 mM HAc set at pH 8.0 with TEtOHA and is also used as CZE background electrolyte. In the ITP step 7.25 mM HEPES at pH 8.0 is used as terminating buffer. The effective and ionic electrophoretic mobilities used in calculations are -42.0 and $-42.0 \cdot 10^{-9} \text{ m}^2 \text{ V}^{-1} \text{ s}^{-1}$ for acetate, -16.5 and $-22.0 \cdot 10^{-9} \text{ m}^2 \text{ V}^{-1} \text{ s}^{-1}$ for HEPES and 11.0 and $30.1 \cdot 10^{-9} \text{ m}^2 \text{ V}^{-1} \text{ s}^{-1}$ for TEtOHA. The ITP took place at a voltage of 10 kV. The calculated conductivities are 0.070 and 0.027 S m^{-1} in respectively the leading and the terminating zone. The equations used for calculation of these parameters were given in the Theory section.

In most commercially available apparatus the pressure is applied at the capillary inlet. An increased pressure at the inlet is always considered a positive pressure and the resulting hydrodynamic flow has therefore a positive sign. A reduced pressure at the inlet results in a hydrodynamic flow in the opposite direction and has, according to our notation a negative sign.

During the ITP of anions the cathode is at the capillary inlet (Fig. 1), therefore the sign of the electrophoretic velocity of an anion A ($v_{el,A}$) in the direction of the anode is positive, analogous to the sign of a hydrodynamic flow. The sign of

the electroosmotic velocity (v_{eof}) in the direction of the cathode is negative for the same reason. The total velocity of the anion (v_A) in cases where the electroosmotic velocity predominates, is thus negative.

3.3. Experimental conditions

The conditions in Figs. 4 and 5 were similar to the conditions as given above with exception of the following. The capillary (520 mm \times 0.100 mm I.D.; SGE, Ringwood, Australia) was pre-treated by standing overnight with a solution of 0.05% HPMC and as a result the electrophoretic mobilities were 30 and $35 \cdot 10^{-9} \text{ m}^2 \text{ V}^{-1} \text{ s}^{-1}$ in the leading and the terminating zone, respectively. The effective mobility of acetate was $-39.7 \cdot 10^{-9} \text{ m}^2 \text{ V}^{-1} \text{ s}^{-1}$ which value was also used as the ionic mobility. A voltage of 15 kV was used and the currents were 13.1 and 6.0 μA for the leading and terminating buffer, respectively. Corresponding conductivities of 0.058 and 0.0265 S m^{-1} were used in calculations in Figs. 4 and 5.

For the counterflow and current monitoring experiments the food colorant brilliant acid green (E142) was used as visible test compound. For the reproducibility measurements and the variation of the terminator zone length (Fig. 7) fluoresceins were used with laser-induced fluorescence (LIF) detection. The LIF detection system has been described in detail elsewhere [7]. A programmable injection system for capillary electrophoresis (PRINCE; Lauerlabs, Emmen, Netherlands) equipped with a reversible polarity power supply and possibility for pressurized and electrokinetic injection was used for the automated ITP–CZE procedures.

3.4. Analyte focusing

The analyte focusing procedure consists of five steps [7,8]. In step 1 the injection takes place hydrodynamically at a pressure of 100 mbar. In the focusing step (step 2), the analyte focusing is started by applying a voltage in conjunction with a hydrodynamic pressure. The hydrodynamic pressure is used to prevent the sample zone from leaving the capillary. After 5–20 min of focusing, depending on the injected zone length, the

focusing is completed. Step 3 is the ITP removal of the terminator buffer zone from the capillary. A voltage of 20 kV is applied without a hydrodynamic pressure. At the time that the sample zone is approaching the capillary inlet the terminator buffer vial is replaced for a vial containing the CZE background electrolyte (step 4), the voltage is reversed and the CZE run is started (step 5).

The current was monitored for precise timing of the moment to switch from the ITP to the CZE mode. When a constant voltage is applied the current increases as long as the terminating zone length decreases. The CZE equipment could be programmed so that at a defined threshold of the current the switching took place automatically. In principle, all terminating ions and sample ions with mobilities below that of the terminating ion, including the counter ions, are removed by the described procedure.

4. Results and discussion

Eq. 16 gives insight in all parameters that are affecting the zone velocity and the linear related counterbalancing pressure difference in the focusing and ITP step. Several of these parameters will now be discussed and compared with experimental data. Then the applicability of current monitoring for automated switching from ITP to CZE will be investigated in addition to the effect of the terminator zone length on the CZE performance.

4.1. Parameters affecting the sample zone velocity

In Fig. 2 the leading zone velocity is given for several electroosmotic flow-rates. As can be seen from Eq. 3 for a high electroosmotic flow-rate the zone velocity is always negative. However, when the electroosmotic mobility is similar or lower than the electrophoretic mobility the velocity v_L increases or becomes positive (increases in the opposite direction). As an example an injection zone length of 60% of the total capillary length will be considered. The leading zone velocity is counterbalanced so that the rear

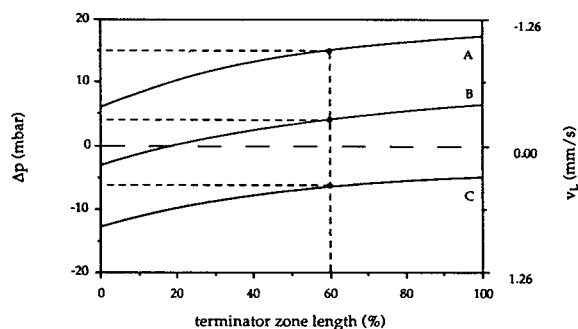


Fig. 2. The effect of the electroosmotic flow-rate on the leading zone velocity and the counterbalancing pressure in ITP-CZE. The lines are calculated values for an electroosmotic mobility in the leading zone of 60.0 (A), 30.0 (B) and 1.0 (C) $\cdot 10^{-9} \text{ m}^2 \text{ V}^{-1} \text{ s}^{-1}$. All further parameters are given in the Experimental section.

boundary is moving to the fixed front boundary. As already mentioned in the Theory section several alternatives are possible.

Under conditions as illustrated in Fig. 2 line A, the focusing procedure is started at a pressure of 15 mbar (for conditions see the Experimental section). The front boundary of the sample zone is then focused at 60% terminator zone length. When the focusing step is completed the pressure is reduced to zero and the analyte zones migrate to the cathode. The analyte zones remain focused because of the ITP conditions and the terminator zone is removed from the capillary. The velocity of the sample zone as a function of the terminator zone length is described by line A. Just before complete removal of the terminator zone the voltage is reversed and the CZE is started.

For a similar injection under the conditions in Fig. 2 line B, the focusing procedure is started at a pressure of 4 mbar. After the focusing step the pressure is reduced to zero and the analyte zones will move to the point of 18% terminator zone length. At this point the electrophoretic mobility of the leading ions is counterbalanced by the electroosmotic mobility of the bulk. A reduced pressure (*i.e.* $\Delta p < -4$ mbar) is needed to remove the remaining terminator zone from the capillary.

Under the conditions in Fig. 2 line C, the focusing procedure is started at a pressure of -7

mbar to focus the analyte front boundary at 60% terminator zone length. After focusing the pressure is reduced (*i.e.* $\Delta p < -14$ mbar) to remove the remaining terminator zone from the capillary. All constants and variables used for Fig. 2 are given in the Experimental section.

Another parameter that is affecting the counterflow needed in the focusing procedure is the electric field strength. Increasing the electric field strength linearly increases all velocities (Eqs. 4, 9, 10, 14 and 15) and shortens the focusing time in ITP-CZE. As a result a linear increase of the counterflow velocity is needed. When the focusing voltage is doubled, a doubling of the pressure is needed to counterbalance the leading zone velocity. The time to complete the focusing will be reduced by a factor two (Eqs. 30 and 32).

High electric field strengths are not always favourable with respect to zone broadening. Increasing the electric field strength will increase the heat generation in the capillary, especially in the terminator zone where the electrical resistance is higher. When the terminator zone is almost removed from the capillary the electric field strength in the terminator zone increases to E_0/γ (Eq. 10, $x = 1$). At the same time, at a constant voltage the current through the capillary increases as more leading buffer is entering the capillary. The power in the terminator zone (W_T) increases with $W_T = V_T I$ resulting in a corresponding increase in heat development. Furthermore, the laminar flow profile that exists because of a mismatch of the electroosmotic velocities in the leading and the terminating zone [6] will be increased at higher electric field strengths. This is usually compensated for by the self-correcting properties of the ITP zones [7,8,10] but at high electric field strengths problems may arise. In order to avoid zone distortion or even disruption of the electrical current, it is might be necessary to reduce the voltage when the length of the terminating zone is getting smaller.

The ratio of mobility of the leading and terminator ions is important for the focusing time (Eqs. 30 and 32). When a zwitterionic buffer is used as terminator buffer a low conductivity can be obtained, resulting in a small value

of γ . The electroosmotic velocities in the leading and terminator zone change with the local electric field strengths E_T and E_L (Eqs. 9, 10, 14 and 15). A lower conductivity of the terminating zone results in an increase in E_T , especially at small terminator zone length. This results in a reduction of the focusing time. However, as mentioned, a high electrical field strength may lead to excessive heat development in the terminating zone.

The sample zone velocity is independent from the capillary diameter. However, the pressure (and height) difference is inversely dependent on the square of the capillary diameter. Capillaries with smaller inner diameters have better heat-dissipating properties and therefore higher electric field strengths are allowed. Because of a decreased loadability and detectability at small inner diameters an optimum can be found with respect to electric field strength, analysis time, capillary diameter and determination limits.

4.2. Single capillary ITP-CZE without a hydrodynamic counterflow

During the ITP step the electric field strength in the terminator (E_T) and leading buffer zone (E_L) and the corresponding zone velocities can be calculated. From Eqs. 9 and 10 it follows that when x (relative leading zone length) approaches unity, the terminating electric field strength increases to E_0/γ and the electric field strength in the leading zone increases to E_0 . For the focusing step this means that during the removal of the terminating zone the electric field strength and the corresponding electrophoretic and electroosmotic velocities in the leading and the terminating zones increase. For anionic separations the electroosmotic and electrophoretic velocities increase in opposite directions. Under certain conditions the possibility exists that at a certain terminator length the electrophoretic velocity is counterbalanced by the electroosmotic velocity, without application of a pressure.

In Fig. 3A the calculated electrophoretic and electroosmotic velocities during the focusing procedure are shown for a given position in the capillary. Although the local electroosmotic ve-

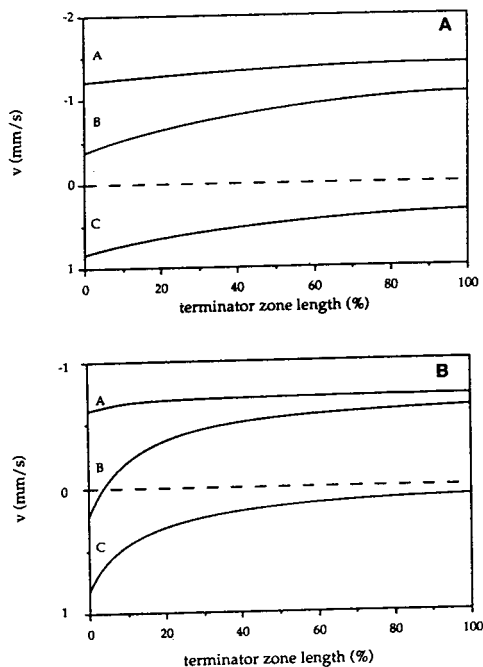


Fig. 3. (A) Variation in the bulk electroosmotic (line A, v_{eof}) and the electrophoretic (line C, $v_{e1,L}$) flow velocity for a given position in the capillary. The total sample zone velocity (line B, v_L) decreases during the removal of the terminator zone. All further parameters are given in the Experimental section. (B) The same velocities as in (A) were calculated for an electroosmotic and electrophoretic mobility of respectively 30 and $-42 \cdot 10^{-9} \text{ m}^2 \text{ V}^{-1} \text{ s}^{-1}$ and a γ of 0.1 . At 4% terminator zone length the electrophoretic velocity is counterbalanced by the electroosmotic velocity. This implies that in principle anionic ITP-CZE can be carried out without a hydrodynamic counterflow.

locities in the leading ($v_{eof,L}$) and terminating zone ($v_{eof,T}$) vary during the focusing procedure, the bulk electroosmotic flow velocity (v_{eof} , line A) is more or less constant. The electrophoretic velocity ($v_{e1,L}$, line C) of the anionic leading ions increases in the opposite direction (gets more positive). This means that the total sample zone velocity (v_L , line B) reduces as the terminating buffer is removed from the capillary using a constant voltage.

When the electroosmotic mobility in the leading zone is approximately equal to the electrophoretic mobility of the leading ions, there is one value of x where the zone velocity is zero. A

reduced pressure is necessary to remove the remaining terminator buffer. The sample zone velocity will be reversed as the terminator zone length is getting smaller. Under these conditions (*i.e.* $-m_L \approx m_{\text{eof,L}}$) in principle the complete ITP-CZE procedure can be carried out without the application of a hydrodynamic counterflow.

Under the conditions in Fig. 3B the leading zone velocity is zero at 4% terminator zone length. This means that when ITP-CZE is carried out without application of a counterflow the sample zones will be focused at 4% terminator zone length. Under these conditions the velocity of the front boundary of the sample zone is not counterbalanced by a hydrodynamic flow. As a result the terminator zone length containing the analyte ions is reduced to 4% already during the focusing step. As mentioned in the Theory section, this means that a loss of analyte may occur. Therefore the sample should be solved in leading buffer so that the rear boundary of the sample zone is the boundary between leading and terminating buffer. During focusing this boundary moves to the 4% position and remains there. The front boundary will migrate to the rear boundary without loss of analyte. The boundary velocity and the focusing time are then given by Eqs. 6 and 32, respectively. After the focusing step the CZE can be started without the additional step of the removal of the terminator buffer, providing that the 4% zone does not disturb the CZE separation. Fine tuning of the leading ion velocity with respect to the electroosmotic flow velocity is one way of optimizing such an ITP-CZE procedure. This broadens the applicability of automated anionic single capillary ITP-CZE to all commercially available systems that are not capable of fine adjustment of a pressure.

4.3. Verification of sample zone velocity

To verify the derived Eq. 16 a counterflow experiment was carried out using height differences for focusing a zone of coloured dye on a fixed position in the capillary. The height difference was measured at two points, where the sample zone was slowly moving forward and

where the sample zone was slowly moving backward. The mean value was considered the height difference where the sample zone velocity was zero. At height differences close to zero, where the direction of the sample zone velocity reversed, it was not possible to obtain reliable results. A hysteresis in the zone velocity was observed when counterbalancing it with a hydrodynamic velocity. Different results were obtained depending from which direction the height difference was changed. At height differences of 5 cm or more the data became reproducible. In Fig. 4A the calculated line and measured data points are shown. The deviation of the measured data points from the calculated line may be due to temperature effects which

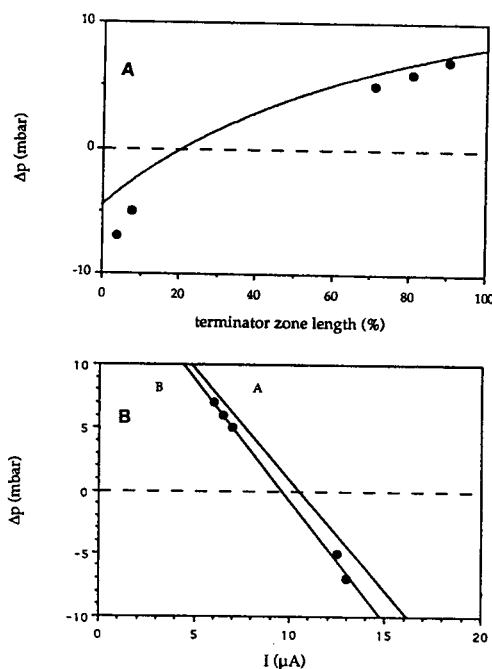


Fig. 4. (A) Calculated counterbalancing pressure difference in ITP-CZE (line) and the measured data points at several positions in the capillary. A negative pressure difference was needed for complete removal of the terminator buffer from the capillary. All parameters are given in the Experimental section. (B) For several positions of a sample zone in the capillary the running current was plotted against the counterbalancing pressure. Calculated (line A) and measured (line B) data result in straight lines as predicted by Eq. 24. The same data points as in (A) are used.

become more pronounced at small terminator zone lengths.

In Fig. 4B the calculated current is plotted against the pressure difference needed for a proper counterflow which is a straight line (Eq. 24). The same data points as in Fig. 4A are used in Fig. 4B. The regression line of the calculated data was $p = 18.4 - 1.76I$, the line of the measured data was $p = 18.5 - 1.92I$. The measured intercept is approximately similar to the calculated intercept. The calculated slope however is 9% below the value of the measured slope. Using the regression line for $p = 0$ the current at zero sample zone velocity (*i.e.* $-v_{el,L} = v_{eof}$) is calculated. For the calculated line this was at $10.5 \mu\text{A}$, for the measured data this was $9.63 \mu\text{A}$.

Fig. 4B demonstrates that relatively small differences in the used parameters may result in considerable differences in the calculated and the actually needed pressure, especially near the point of reversal of the pressure. However, it should be kept in mind that current monitoring will be a convenient tool in compensating for these differences. Only when the appropriate pressure is applied under ITP conditions the current will be constant. In the Experimental section all parameters and those used for calculations are given.

4.4. Temperature effects

One of the assumptions in the described model is that the temperature in the leading and terminating zone is the same and constant. For ITP this is by definition not true because the electrical field strength in the leading buffer is lower than in the terminating zone. However, in systems with efficient dissipation of the Joule heat the effects of axial temperature differences will be negligible. The temperature inside the capillary can be calculated using [13]

$$T = T_a + \frac{E^2 \kappa d_1^2}{8} \cdot \left[\frac{1}{k_1} \ln \left(\frac{d_2}{d_1} \right) + \frac{1}{k_2} \ln \left(\frac{d_3}{d_2} \right) + \frac{2}{hd_3} \right] \quad (33)$$

where d_1 , d_2 and d_3 are the inside capillary diameter, the outside fused-silica diameter and the outside polyimide diameter, respectively. T_a is the working temperature and h is the heat-transfer coefficient to the surroundings. The thermal conductivities k_1 and k_2 are respectively $1.5 \text{ W m}^{-1} \text{ K}^{-1}$ for silica and $0.16 \text{ W m}^{-1} \text{ K}^{-1}$ for polyimide. For example, the temperature in the leading and terminating zone is calculated for a terminating zone length of 60% and 10% of the total capillary length under conditions as described for Fig. 2.

When the capillary is filled for 60% with sample in terminating buffer, the temperatures inside the leading and terminating zones are 293.3 and 293.8 K, respectively ($T_a = 293$, $E_L = 10.4 \text{ kV m}^{-1}$, $E_T = 26.4 \text{ kV m}^{-1}$, $\kappa_L = 0.070 \text{ S m}^{-1}$, $\kappa_T = 0.027 \text{ S m}^{-1}$, $d_1 = 100 \mu\text{m}$, $d_2 = 340 \mu\text{m}$, $d_3 = 355 \mu\text{m}$, $h = 180 \text{ W m}^{-2} \text{ K}^{-1}$, for other conditions see the Experimental section). The viscosity and electrophoretic mobility decrease 2.6% per degree K, which means a difference of 1.3% in viscosity and mobility is expected under these conditions. The effects on the calculated counterbalancing pressure will be negligible.

After the focusing step the terminator buffer is removed from the capillary. When the length of the terminating zone is 10% of the total capillary length the temperatures inside the leading and terminating zones are 293.8 and 295.1 K, respectively ($E_L = 17.3 \text{ kV m}^{-1}$, $E_T = 44.1 \text{ kV m}^{-1}$). When the running voltage is reduced to 6 kV ($E_0 = 12 \text{ kV m}^{-1}$) the temperatures in the leading and terminating zones become 293.3 and 293.8 K, respectively ($T_a = 293$, $E_L = 10.4 \text{ kV m}^{-1}$, $E_T = 26.5 \text{ kV m}^{-1}$). As the terminating zone gets smaller the temperature will increase. In our experience, the corresponding decrease in viscosity does not interfere with automated ITP-CZE procedures.

4.5. Current monitoring

The calculated change in current (Eq. 20) is in good agreement with the measured data (Fig. 5). The change in current at constant voltage during the focusing procedure is calculated for several other conductivities of the terminator buffer

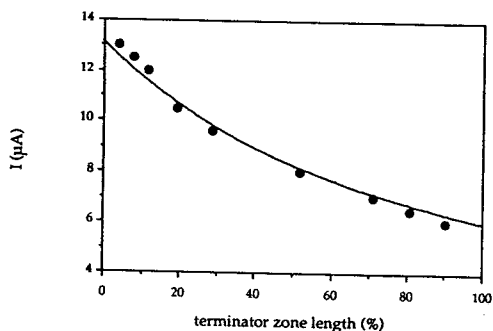


Fig. 5. Calculated change in current at a constant voltage during the focusing step in ITP-CZE (line) and the measured data points at several positions in the capillary. All parameters are given in the Experimental section.

(Fig. 6). The larger the difference in conductivity, the larger the change in current. In practice large differences in conductivity will make automated switching from ITP to CZE using current monitoring easier.

When the zone length of terminator buffer is 5% of the total capillary length, the current is at 95% of I_0 for a conductivity ratio of 0.48 (line A), where I_0 is the maximum current when the capillary is completely filled with leading buffer. For the same terminator zone length the current is at 50% of I_0 for a conductivity ratio of 0.048 (line C). In practice this means that at large

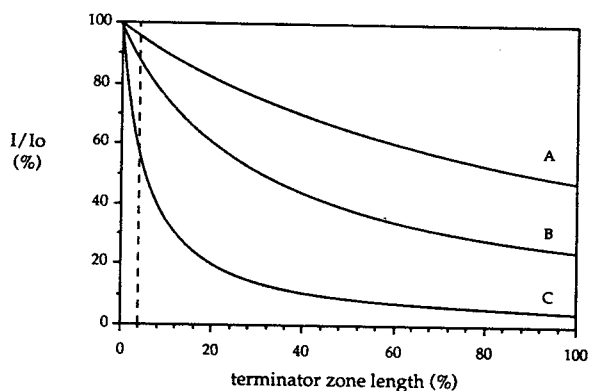


Fig. 6. The calculated change in current at a constant voltage during the focusing step in ITP-CZE. A conductivity ratio of terminating and leading buffer (γ) of 0.48 (A), 0.24 (B) and 0.048 (C) is used for calculation. The conductivity of the leading buffer (κ_L) was kept constant. The ionic mobility of the terminator ions was $-22.0 \cdot 10^{-9} \text{ m}^2 \text{ V}^{-1} \text{ s}^{-1}$. All other parameters are given in the Experimental section.

differences in conductivities smaller terminator zone length will remain after automated switching from ITP to CZE. However, in case of similar conductivities of leading and terminator buffer, somewhat larger remaining terminator zone lengths are allowed. The effect on zone broadening in the CZE step caused by conductivity differences will consequently be less.

In Fig. 7 the effect of the length of the remaining terminator zone on the CZE separation is shown. When the current at the moment of switching is lower than 92% of I_0 zone broadening occurs. The corresponding remaining terminating zone length is 10% of the total

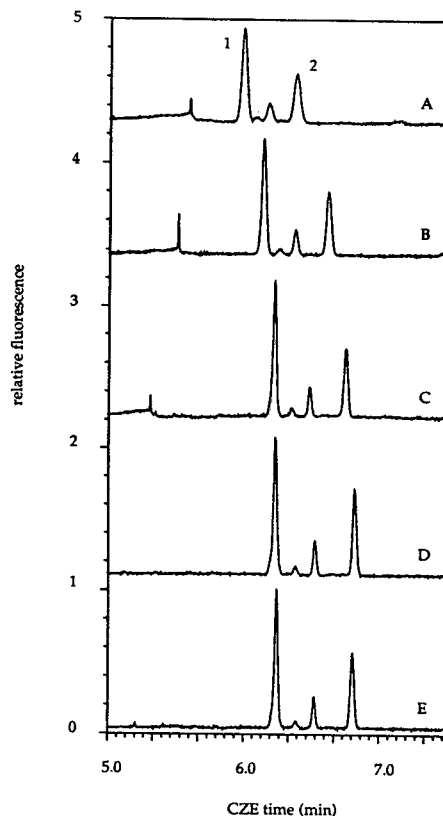


Fig. 7. The effect of the remaining terminator buffer zone length on the CZE separation of FITC (1) and F (2) in ITP-CZE. Other peaks are unknown degradation products of FITC. Automated switching using current monitoring was used at 88.2% (A), 90.9% (B), 93.6% (C), 96.3% (D) and 99.0% (E) of the maximum current I_0 . Because of a decrease in the migration length in CZE a decreased migration time is notable as the remaining terminating zone gets larger.

capillary length. Although the 10% seems like an overload of the CZE, the effect on the peak shape is relatively small. Because of the conductivity ratio of 0.48 the disturbance of the homogeneity of the electric field by the remaining terminator zone is limited. A larger difference in conductivity would result in more peak broadening, but the consequently smaller conductivity ratio would make precise switching with small remaining terminator zones easier (Fig. 6, line C: $\gamma = 0.048$).

The reproducibility of CZE migration times in ITP–CZE with automated switching using current monitoring was investigated for six ITP–CZE runs. The current was programmed at 99% of I_0 at the switching time. The R.S.D. in migration times was 1.4%. This is approximately three times higher in comparison with CZE in a bioassay of anthracyclines where a R.S.D. of the migration times of 0.5% has been reported by our group [4].

5. Conclusions

Equations have been derived giving the zone velocity and the current for a given terminator zone length in single capillary ITP–CZE. Monitoring the current offers the possibility to calculate the hydrodynamic flow velocity that is needed to counterbalance the leading zone velocity. It is therefore expected that current monitoring can be used in an automated feedback mechanism to control the applied pressure. Correlation between current and the position of the sample zones in the capillary can be used for automated switching from ITP to CZE. This

results in reproducible CZE migration times and will make the implementation of automated focusing procedures in bioassays easier.

Under certain conditions ITP–CZE separations can be carried out even without the application of a hydrodynamic counterflow. This extends the applicability of this procedure to equipment that is not capable of applying a hydrodynamic pressure during the focusing step.

References

- [1] W.G. Kuhr, *Anal. Chem.*, 62 (1990) 403R.
- [2] W.G. Kuhr and C.A. Monnig, *Anal. Chem.*, 64 (1992) 389R.
- [3] M. Albin, P.D. Grossman and S.E. Moring, *Anal. Chem.*, 65 (1993) A489.
- [4] N.J. Reinhoud, U.R. Tjaden, H. Irth and J. van der Greef, *J. Chromatogr.*, 574 (1992) 327.
- [5] A.J.J. Debets, M. Mazereeuw, W.H. Voogt, D.J. Vaniperen, H. Lingeman, K.P. Hupe and U.A.Th. Brinkman, *J. Chromatogr.*, 608 (1992) 151.
- [6] R.L. Chien and D.S. Burgi, *Anal. Chem.*, 64 (1992) A489.
- [7] N.J. Reinhoud, U.R. Tjaden and J. van der Greef, *J. Chromatogr.*, 641 (1993) 155.
- [8] N.J. Reinhoud, U.R. Tjaden and J. van der Greef, *J. Chromatogr. A*, 653 (1993) 303.
- [9] M.H. Lamoree, N.J. Reinhoud, U.R. Tjaden, W.M.A. Niessen and J. van der Greef, *Biol. Mass. Spectrom.*, in press.
- [10] P. Boček, M. Deml, P. Gebauer and V. Dolnik, in B.J. Radola (Editor), *Analytical Isotachopheresis (Electrophoresis Library, Vol. 1)*, VCH, Weinheim, 1988, pp. 17–51.
- [11] V. Sustacek, F. Foret and P. Boček, *J. Chromatogr.*, 545 (1991) 239.
- [12] F. Foret and P. Boček, in A. Chrambach, M.J. Dunn and B.J. Radola (Editors), *Advances in Electrophoresis*, Vol. 3, VCH, Weinheim, 1989, pp. 271–347.
- [13] E. Grushka, R.M. McCormick and J.J. Kirkland, *Anal. Chem.*, 61 (1989) 241.

Automated on-capillary isotachophoretic reaction cell for fluorescence derivatization of small sample volumes at low concentrations followed by capillary zone electrophoresis

N.J. Reinhoud, U.R. Tjaden*, J. van der Greef

Division of Analytical Chemistry, Leiden/Amsterdam Center for Drug Research, Leiden University, P.O. Box 9502, 2300 RA Leiden, Netherlands

(First received January 6th, 1994; revised manuscript received March 7th, 1994)

Abstract

An automated on-line reaction cell is described combining the concentrating properties of isotachopheresis (ITP), the separation efficiency in capillary zone electrophoresis (CZE) and the detection sensitivity of laser-induced fluorescence (LIF) detection. The applicability of the reaction cell is demonstrated for an automated derivatization procedure of glutathione and several amino acids with *o*-phthalaldehyde (OPA) and naphthalene-2,3-dicarboxaldehyde. Nanolitre analyte, at nanomolar concentration level, were concentrated and derivatized in capillary ITP. The derivatives were analyzed by CZE with LIF detection. The entire procedure was automated and took place in the same capillary using single capillary ITP–CZE. Furthermore, an easy applicable on-capillary OPA derivatization is described for CZE without ITP step.

1. Introduction

The on-line coupling of capillary zone electrophoresis (CZE) with other analytical separation techniques has resulted in increased selectivity and separation power. Improvements in detection techniques has resulted in detection of extremely low amounts of analyte [1–3]. In combination with electrophoretic stacking or isotachophoretic preconcentration methods the corresponding determination limits are impressive [4].

Small injection volumes, typically in the nanolitre range, are characteristic for CZE. However, in most analytical sample pretreatment procedures the smallest volumes that can

be handled are in the microlitre range. This implies that in most cases more than 99% of the sample is wasted. In situations where analytes are chemically modified before analysis a more efficient use of reagents is achieved by reduction of the reaction cell volume. This is especially relevant in cases where expensive reagents are involved such as enzymes or antibodies. The reaction cell described in this paper has at least a factor 100 lower reagent consumption compared to a conventional 100- μ l reaction vial. The applicability of the reaction cell is demonstrated for a fluorescence introducing derivatization reaction.

The use of on-line fluorescence derivatization procedures puts several demands on the analytical method. Fluorophoric derivatization reagents, where the reagent shows fluorescent

* Corresponding author.

properties similar to that of the derivatization product, are difficult to apply in an on-line procedure because the reagent has to be separated from the derivative before detection takes place. Therefore, fluorophoric derivatization reagents are usually applied in the pre-column mode, sometimes in combination with an additional step for removal of the excess of reagent. Fluorogenic reagents, where the reagent does not have fluorescent properties similar to that of the derivatization product, are considerably easier to apply in on-line procedures [5–7].

Several applications of CZE with laser-induced fluorescence (LIF) detection and pre-column derivatization have been described [1–3,7]. Recently, Houben *et al.* [8] described an automated derivatization procedure for absorbance detection of amino acids. Combination of CZE with an on-capillary enzyme reactor has been described by Avila and Whitesides [9]. Chang and Yeung [10] described an on-column protein digestion with pepsin followed by CZE with native LIF detection.

In this paper the applicability of the capillary reaction cell is demonstrated for an automated on-capillary derivatization of low concentrations of analyte in single capillary isotachopheresis (ITP)–CZE. The analyte is concentrated in the focusing step, derivatized in the ITP step and analyzed in the CZE step. The method takes place in a commercially available CZE system without any hardware modifications. In previous papers we have described automated procedures for ITP–CZE in a single capillary for cationic and anionic separations [11–13]. Furthermore, an on-capillary *o*-phthalaldehyde (OPA) derivatization is described for CZE without an ITP step of amines at higher analyte concentrations.

2. Theory

2.1. Derivatization reactions

The OPA reagent in combination with a nucleophile such as β -mercaptoethanol (ME) forms N-substituted 1-alkyl-isoindole derivatives. The derivative is formed within 1 min and slowly

decomposes (Fig. 1A). Therefore, it is important that the reaction times are kept constant. This makes the OPA reagent only suitable for pre-capillary derivatization if the procedure is automated so that the derivatization times are kept constant as is the case in the described on-capillary derivatization methods. Derivatization of peptides with the OPA reagent is only possible if the peptide contains lysine, due to the high reactivity of the ϵ -amine function [14,15].

The naphthalene-2,3-dicarboxaldehyde (NDA) reagent in presence of a nucleophile such as cyanide forms stable derivatives with primary amines, including the terminal amine function of peptides. As a result of the formation of side products and the derivatization time needed (10

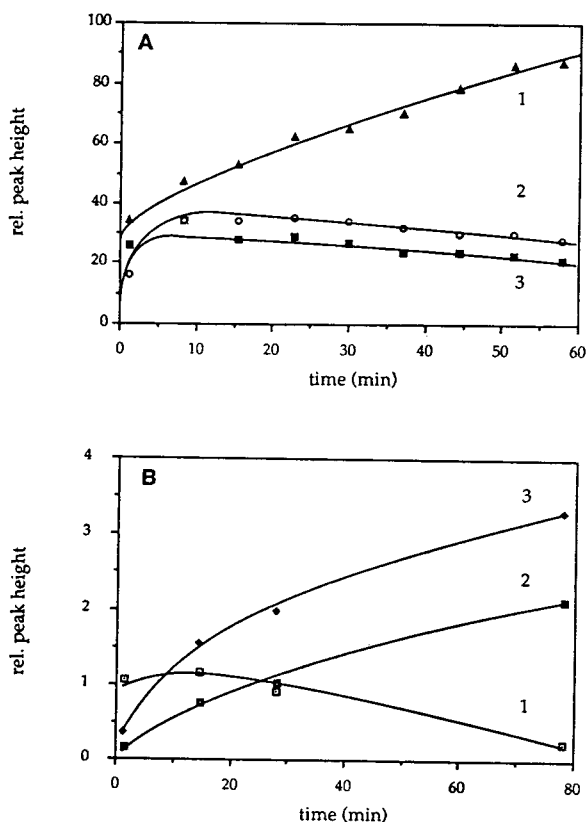


Fig. 1. Relative peak height measured at different times after derivatization of GSH (1), Asp (2) and Glu (3) with (A) OPA–ME and (B) NDA–CN reagent. Concentrations analyte were respectively 100, 100 and 200 ng/ml for the OPA derivatization and 1.0 μ M each for the NDA derivatization.

min for peptides, Fig. 1B) it is mainly used as pre-capillary derivatization reagent. NDA in combination with ME forms a less stable product but in combination with fast reaction times (1 min for peptides) it is suitable as post-capillary derivatization reagent [16].

OPA and NDA are also used in derivatization procedures for electrochemical detection [17], for NDA derivatives a selective peroxyoxalate chemiluminescence detection procedure has been described [18]. Certain analytes such as histidine [19], histamine [19], spermidine [20], serotonin [21] and glutathione [22,23] react with OPA without addition of a nucleophile which increases the selectivity of the derivatization reaction considerably.

2.2. ITP–CZE

CZE has become an important separation technique complementary to high-performance liquid chromatography (HPLC). One of the challenges in the application of CZE separations in the analysis of biological samples is to reach for relevant determination limits. Electrophoretic analyte focusing techniques provide a way to increase the loadability and concentration detection sensitivity in CZE. The coupling of ITP with CZE has been described by several authors [4]. Improvements in determination limits by a factor of 1000 have been reported.

In ITP a discontinuous buffer is used and only anions or cations can be analyzed in one run. In anionic separations the capillary and the anode vial are filled with leading buffer. The leading buffer contains anions with a mobility higher than the mobility of the analyte ions. The cathode vial is filled with terminating ions which have the lowest mobility. The pH is set with the buffering counterions. In the steady state, when the analytes are separated, they migrate as consecutive zones ordered by their electrophoretic mobilities. A characteristic of ITP is its concentrating property. The concentrations of analyte ions are adapted to the concentration of the leading ions according to the Kohlraush regulation function (see ref. 13). The analyte

concentrating property makes the technique attractive as preconcentration technique for CZE.

2.3. On-capillary reactions in ITP–CZE

An on-capillary reaction cell in ITP–CZE puts several demands on the system that is used. The reagent is added to the ITP buffer, therefore it should not be reactive to buffer components and the buffers should be of a high purity. In case of reactions with primary amines the number of buffers that can be used is limited. When the reagent is ionic, care must be taken that the ITP conditions are not disturbed and that mixing of the reagent with sample zones takes place. The analyte is derivatized under ITP conditions. To maintain sharp analyte zones the analyte and derivative should be within the ITP separation window. These conditions are all fulfilled with the OPA and NDA derivatization of primary amines.

The combination of single capillary ITP–CZE and an on-capillary reaction offers several advantages. Reaction conditions such as the temperature can be chosen easily, most of the commercially available CZE equipment offers the possibility of temperature control. The reaction time can be chosen as long as necessary. We already demonstrated that the ITP time does not influence the efficiency in single capillary ITP–CZE [11]. When the analyte zone is concentrated and fixed on a certain position in the capillary it stays there until the hydrodynamic pressure is reduced. In an automated ITP–CZE procedure the reaction time will be constant which is important in case of instable reaction products.

Using single capillary ITP–CZE adds an interesting feature to reaction kinetics. Not only the initial concentrations of reactants can be set but also the supply of fresh reagent can be varied while the analyte concentration is kept constant. In principle only the length of the underivatized analyte zone will reduce under ITP conditions until the derivatization is complete. The mixing of the reacting species is done in a very controlled way. The velocity of the neutral reagent is precisely known and can be manipulated by the applied electrical field strength during the

ITP step. The velocity of the analyte is zero and because of the concentrating properties of ITP the analyte concentration will be high resulting in favourable reaction kinetics. The excess of reagent will automatically be removed before the CZE is started. All reaction products that are outside the separation window with a mobility lower than the terminator ions, are discarded during the ITP step. Another aspect is that in ITP–CZE using narrow-bore capillaries, reactions in picolitre volumes can be carried out.

2.4. The reagent molar mass flow

One of the attractive features of the on-capillary ITP reaction cell is the possibility of controlling the reagent molar mass flow in the analyte zone. The reagent molar mass flow is calculated by deriving an equation for the velocity of neutrals during the ITP step. A simple buffer system is assumed, consisting of only one type of univalent cations and anions (i.e. L^- and R^+ , T^- and R^+ for leading and terminating buffer).

In single capillary ITP–CZE a hydrodynamic pressure is applied during the focusing and ITP step to keep the front boundary of the sample zone (Fig. 2, B1) on a fixed position in the capillary. The hydrodynamic flow velocity counter balances the velocity of the leading ions so that the total velocity of the leading ions is zero. In the focusing step the terminating boundary of the sample zone (B2) migrates towards B1 resulting in a concentration of the analytes until the ITP state is reached. Under ITP conditions the velocities of all anions are the same. This distinguishes the focusing step from the ITP step.

The molar mass flow of a neutral reagent in the ITP step (J in mol/s) is determined by the reagent velocity, the cross-sectional area of the capillary and the reagent concentration and is given by

$$J = v\pi r^2 c \quad (1)$$

where v is the velocity of the neutral reagent under ITP conditions with a counterbalancing pressure, c is the reagent concentration and r is the capillary radius.

When the velocity of the leading ions is

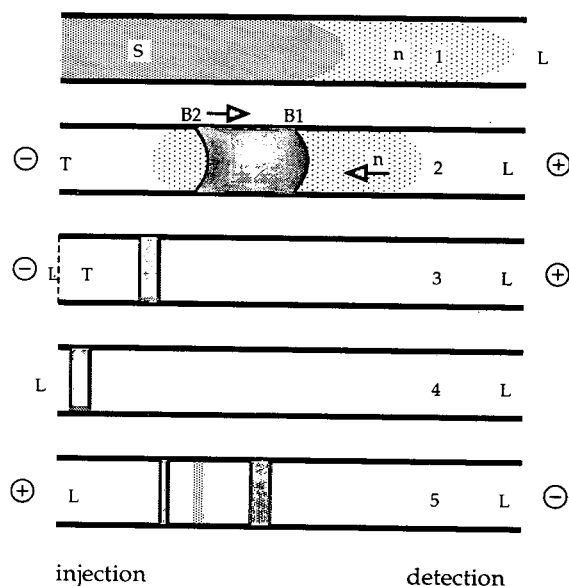


Fig. 2. Schematic representation of the on-capillary derivatization during the ITP step in single capillary ITP–CZE. In step 1 the neutral reagent (n , in leading buffer) is injected before the sample (S , in terminating buffer). In the focusing step 2 electrophoretic and hydrodynamic velocities are balanced so that the boundary B1 is kept on a fixed position in the capillary. Boundary B2 moves to boundary B1. The neutral derivatization reagent is moving through the sample zones into the direction of the cathode and the derivatization takes place. The reagent is supplied by injection as a zone with a defined length or continuously supplied by addition to the leading buffer vial. See Experimental for further explanation.

counterbalanced by a pressure-induced flow, the electrophoretic velocity of the leading ions will be zero. Fig. 3 gives a schematic vector representation of the velocities during electrophoresis. Under ITP conditions the velocity of the neutrals is determined by the hydrodynamic and electroosmotic velocity. During electrophoresis a leading anion with an electrophoretic velocity (vector 1) will migrate to the cathode with a total velocity (vector 3) due to a high electroosmotic velocity (vector 2). Neutrals are carried with the electroosmotic flow and have a velocity (vector 2). When a counterbalancing pressure is applied (vector 4), the velocity of the anion (vector 3) is reduced to zero. Under these conditions the velocity of the neutrals (vector 5) is also reduced. The velocity of neutrals under conditions

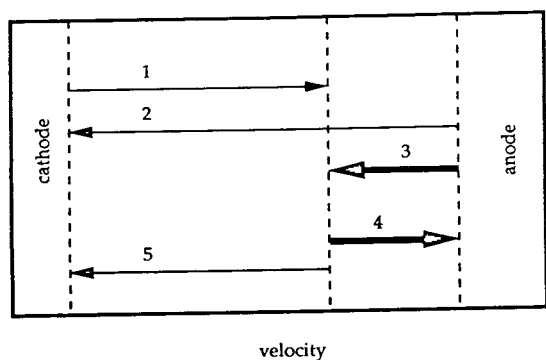


Fig. 3. Velocities during electrophoresis (1–3) and during electrophoresis under ITP conditions (4,5). The vectors represent the electrophoretic velocity of the leading ions (1), the velocity of the electroosmotic flow (2), the net velocity of the leading ion (3) which is the sum of 1 and 2, the velocity of the counterbalancing hydrodynamic flow (4) and the velocity of the neutrals in presence of the counterbalancing hydrodynamic flow during the ITP step (5). For further explanation see Theory.

with a counterbalancing pressure (vector 5) is the same as the electrophoretic velocity of the leading anions without a counterbalancing pressure (vector 1), in the opposite direction.

The velocity of the neutrals is then given by [13]

$$v = -v_{el,L} \quad (2)$$

where $v_{el,L}$ is the electrophoretic velocity of the leading ions under ITP conditions without a counterbalancing pressure.

The supply of reagent can be manipulated by the electric field strength. Using $v_{el,L} = \bar{m}_L E_L$, the reagent molar mass flow is given by

$$J = \bar{m}_L E_L \pi r^2 c \quad (3)$$

where \bar{m}_L is the effective electrophoretic mobility of the leading ions and E_L is the electrical field strength in the leading buffer zone. Analogous to Eq. 3 the molar mass flow in the terminator zone is given by $J = \bar{m}_T E_T \pi r^2 c$. In the ITP steady state the electrical field strength in the leading buffer zone (E_L) is by definition lower than in the terminating buffer zone (E_T). In ITP it holds that $E_T \bar{m}_T = E_L \bar{m}_L$ which means that the molar mass flow of the neutral reagent in the terminator zone is the same as in the leading buffer

zone. In a similar way it can be shown that in ITP the molar mass flow in the sample zones is the same as in the leading buffer zone.

The capillary reaction cell is not only restricted to neutrals. Charged reagents can be used as long as the focusing and ITP process are not disturbed. In case of anionic separations cationic reagents or anionic reagents with a low electrophoretic mobility can be used as well. Ampholytic reagents (enzymes, antibodies) can be used at a pH near the isoelectric point where the net charge is zero. For on-capillary NDA derivatization of amino acids cyanide is used which has a small anionic charge at the working pH (pK_a of cyanide is 9.5). When a counterion is used as a reagent the velocity and concentration in the leading and terminating zone can be calculated using the well known moving boundary equation.

3. Experimental

Untreated fused-silica capillaries (SGE, Ringwood, Australia) were used. A programmable injection system for capillary electrophoresis (PRINCE; Lauerlabs, Emmen, Netherlands) equipped with a reversible polarity power supply and possibility for pressurised and electrokinetic injection was used for the analyte focusing process. The LIF detection system has been described previously [11]. Excitation of OPA derivatives took place at 351.1 and 363.8 nm and for emission a 450-nm bandpass filter (10 nm bandwidth, type 53830; Oriel, Stratford, CT, USA) was used. The NDA derivatives were detected using the 457.9-nm laser line for excitation and a 515-nm long-pass filter (Oriel) for emission.

3.1. Chemicals

Sodium cacodylate, triethanolamine (TEtOHA) (97%) and 4-(2-hydroxyethyl)-1-piperazineethanesulphonic acid (HEPES) were purchased from Janssen Chimica (Beerse, Belgium). Hydroxypropylmethylcellulose (HPMC) with a viscosity for a 2% aqueous HPMC solution of 4000 cP, came from Sigma (St. Louis,

MO, USA). Acetic acid (HAc), sodium borate, phosphoric acid, barium hydroxide, potassium cyanide (KCN), glutamic acid (Glu), aspartic acid (Asp), arginine (Arg), lysine (Lys), tryptophan (Trp), phenylalanine (Phe), threonine (Thr), serine (Ser), 3,4-dihydroxyphenylalanine (Dopa) and bromophenol blue were from Merck (Darmstadt, Germany). OPA and ME were from Aldrich Chemie (Steinheim, Germany). NDA came from Molecular Probes (Eugene, OR, USA). In all experiments deionised water was used (Milli-Q system; Millipore, Bradford, MA, USA).

3.2. Analyte focusing with on-capillary derivatization

The ITP–CZE procedures were used as described previously [11,12], with exception of the first step (Fig. 2). In step 1 the capillary is filled with leading buffer containing the derivatization reagent. Then the injection of sample takes place hydrodynamically at a pressure of 100 mbar. In step 2 the analyte focusing starts by applying a voltage in conjunction with a hydrodynamic pressure. After 5–20 min of focusing and derivatization, depending on the injected volume, a voltage of –20 kV is applied without a hydrodynamic pressure (step 3). The zone of terminating buffer is removed isotachophoretically out of the capillary. At the time that the sample zone is approaching the capillary inlet the terminator buffer vial is replaced for a vial containing the CZE background electrolyte (step 4), the voltage is reversed and the CZE run is started (step 5).

The current is monitored for precise timing of the moment to switch from ITP to CZE. When a constant voltage is applied the current increases as long as the terminating ions leave the capillary. The CZE equipment can be programmed so that at a defined threshold of the current the switching takes place automatically. In principle all ions with mobilities below that of the terminating ion, including the counter ions, are removed by the described procedure.

3.3. ITP–CZE buffer systems

System I

The leading buffer consisted of 10 mM HAc set at pH 8.0 with TEOHA and was also used as CZE background electrolyte. The terminating buffer was 10 mM HEPES set at pH 8.0 with TEOHA. The capillary dimensions were 590 × 0.100 mm, detection took place at 520 mm from the inlet.

System II

The leading buffer was a 10 mM sodium phosphate buffer at pH 9.4 and was also used as CZE background electrolyte. To the leading buffer 0.05% (w/v) of HPMC was added. The terminating buffer consisted of 10 mM sodium cacodylate set at pH 9.4 with Ba(OH)₂ and contained 0.05% HPMC (w/v). The capillary dimensions were 700 × 0.100 mm, detection took place at 600 mm from the inlet.

System III

The CZE buffer consisted of a 40 mM borate buffer at pH 9.5 and contained 0.1 mg/ml OPA and 0.1% (v/v) ME. In initial experiments 1.0 mg/ml OPA was used. The capillary dimensions were 730 × 0.075 mm, detection took place at 665 mm from the inlet.

3.4. Derivatization

Pre-column OPA derivatives were made by 1:1 addition of the analyte in leading buffer to an OPA solution of 1 mg/ml in leading buffer containing 0.1% ME. The NDA derivatives were made by 1:1 addition of the analyte in leading buffer to a NDA solution of 2 mM in leading buffer containing 1 mM potassium cyanide. The NDA reagent was diluted from a stock solution of 100 mM in MeOH and mixed with KCN in leading buffer just before the derivatization was started.

For on-capillary derivatization reactions in ITP–CZE the reagent was added to the leading buffer. The OPA reagent was used at a concentration of 0.1 mg/ml and 0.01% ME and was

added to the leading buffer vial. This buffer vial was used during the entire ITP–CZE procedure. The NDA and KCN concentrations were 0.1 mM. The NDA reagent was supplied by injecting a zone of leading buffer containing the derivatization reagent before sample injection for immediate start of the derivatization during the focusing step. For NDA derivatization with continuous supply of reagent only during the ITP step the leading buffer vial was switched after the focusing step for a leading buffer vial containing the NDA reagent. Glutathion is unstable under alkaline conditions and was added to the terminator buffer just before injection.

4. Results and discussion

Several aspects of the on-capillary reaction cell are investigated. The linearity and reproducibility of the method is investigated for the selective derivatization of glutathion (GSH) with NDA at nanomolar analyte concentration levels. Supplying the reagent immediately after analyte injection is compared with supplying the reagent from the leading buffer vial after the focusing step, during the ITP step. A less selective and more widely applicable derivatization procedure of amino acids with NDA in conjunction with CN is investigated.

The loadability and linearity over a large concentration range is investigated for the OPA–ME derivatization in ITP–CZE of some amino acids. Finally, the linearity and efficiency of a rapid on-capillary derivatization of amino acids in CZE without ITP step is investigated.

4.1. On-capillary ITP derivatization with NDA

In Fig. 4 the electropherograms are shown of the on-capillary reaction of GSH with NDA at nanomolar concentration level. System I is used for ITP–CZE (see Experimental). The capillary is filled for 13.5% with leading buffer containing NDA, followed by a 27% injection of terminator buffer containing GSH. The focusing step took place at a voltage of –10 kV, in the CZE step 25

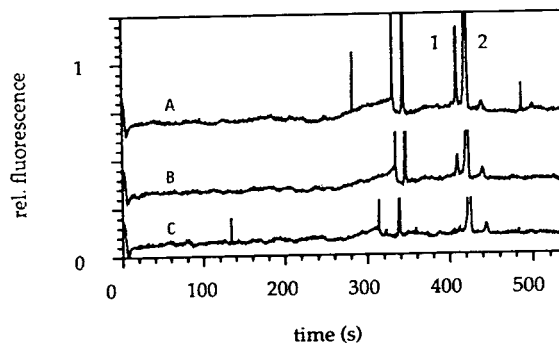


Fig. 4. On-capillary NDA derivatization and ITP–CZE of 3.0 (A) and 1.0 (B) nM GSH (1) and the blank (C). Peak 2 is the internal standard fluorescein. Other peaks are system peaks.

kV is used. The electrical field strength in the leading buffer zone under ITP conditions is –12 kV/m (for calculation see ref. 13, conductivity ratio leading and terminating buffer is 0.39, fractional leading zone length 0.73). When an effective electrophoretic mobility of acetate of $-42 \cdot 10^{-9} \text{ m}^2 \text{ V}^{-1} \text{ s}^{-1}$ is assumed, the velocity of the neutral NDA is 0.5 mm/s (Eq. 2). The reagent molar mass flow is $3.92 \cdot 10^{-13} \text{ mol/s}$ under these conditions (Eq. 3, $c = 0.1 \text{ mM}$, $v = 0.5 \text{ mm/s}$). The time for the NDA zone to leave the capillary is 372 s.

The linearity of the reaction of NDA with GSH is investigated at concentrations just above the detection limit from 1 to 11 nM (Table 1). The correlation is considerably improved by

Table 1

Unweighted linear regression data of the on-capillary derivatization in ITP–CZE of GSH with NDA in the range 1–11 nM

	$a \pm \text{S.D.}$	$b \pm \text{S.D.}$	r
Height	248 ± 152	151 ± 22	0.960
Height ratio	0.18 ± 0.10	0.20 ± 0.015	0.989
Area ratio	-0.022 ± 0.084	0.17 ± 0.012	0.990

Six calibration points were used with concentration intervals of 2 nM. Analyte injection volumes of 1.25 μl were used corresponding to 27% of the capillary volume. The intercept a and the slope b are given with the standard deviation. The correlation coefficient is r .

using fluorescein as internal standard. The relative standard deviation in CZE migration times of the ITP–CZE derivatization procedure is 1.4% ($n = 5$).

When in the ITP–CZE procedure, the capillary is filled with leading buffer containing the neutral reagent, the derivatization starts immediately after injection of the analyte. For the considered derivatization reaction this is convenient because it reduces the total analysis time. However, in cases where precise control of the reaction parameters are needed, the starting time of the reaction should be better defined. Therefore, the possibility of performing a derivatization reaction under ITP conditions was demonstrated in Fig. 5. The same ITP–CZE buffers are used as in Fig. 4 except that the capillary was filled with leading buffer without NDA reagent. The underivatized GSH was focused for 10 min and then the leading buffer vial was replaced for a leading buffer vial containing the reagent. The GSH is kept isotachophoretically at a fixed position in the capillary and the velocity of the neutral NDA reagent is 1.0 mm/s at an ITP voltage of -20 kV ($E_L = -24$ kV/m). After 10 min of derivatization under ITP conditions the CZE is started. The remaining NDA reagent migrates with the velocity of the electroosmotic flow which is seen as an increase in the

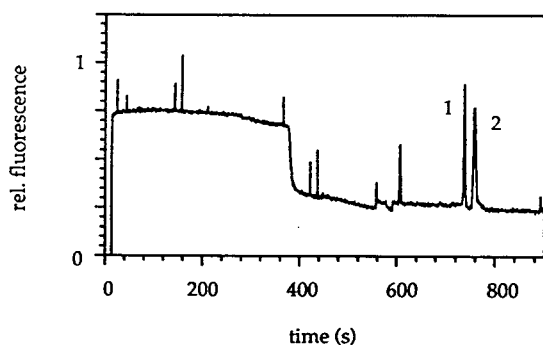


Fig. 5. ITP–CZE of 5 nM GSH (1) with NDA reagent in the leading buffer vial. Derivatization of GSH occurred after focusing during the ITP step. The remaining NDA reagent caused an increased background in the CZE step. Peak 2 is fluorescein.

baseline until $t = 400$ s. At 750 s the derivative of GSH appears.

This example illustrates the flexibility of the on-capillary reaction cell. The analyte zones are kept isotachophoretically between the leading and terminating buffer. Using a hydrodynamic counter flow the position of the analyte zones along the capillary is fixed. By switching buffer vials cationic or neutral reagents can be supplied; as long as the ITP conditions are not disturbed the analyte zones remain concentrated. The reaction speed can be increased with the reagent molar mass flow. This can be done by choosing a leading ion with a high electrophoretic mobility, by increasing the electrical field strength during ITP or by using higher reagent concentrations (Eq. 3).

4.2. On-capillary ITP derivatization with NDA–CN

In the derivatization reaction of amines with NDA in presence of CN stable cyanobenz[*f*]isindole (CBI) adducts are formed. However, also several side products are formed, even when no amine-containing analyte is present [18]. The on-capillary derivatization and ITP–CZE analysis of GSH, Glu and Asp is demonstrated in Fig. 6. At low analyte concentrations the analysis is hindered by background peaks. Most of the background peaks appeared also in the blank

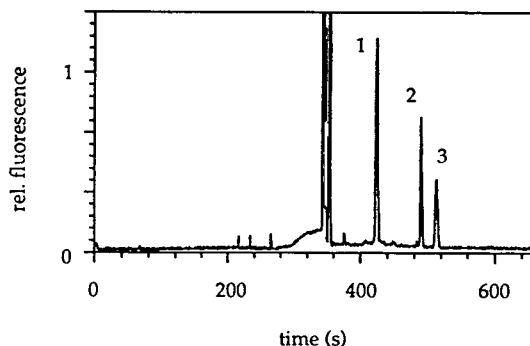


Fig. 6. On-capillary NDA–CN derivatization and ITP–CZE of 50 nM GSH (1), Glu (2) and Asp (3). Other peaks are system peaks.

Table 2
Unweighted linear regression data of the on-capillary derivatization in ITP-CZE of Glu and Asp with OPA-ME in the range 50–2000 ng/ml

	$a \pm \text{S.D.}$	$b \pm \text{S.D.}$	r
Glu (height)	150 ± 160	3.4 ± 0.17	0.995
Asp (height)	-31 ± 100	4.4 ± 0.11	0.999
Glu (area)	137 ± 1700	36 ± 1.6	0.997
Asp (area)	-19 ± 1500	54 ± 1.6	0.998

Six calibration points were used with concentrations 50, 100, 200, 500, 1000 and 2000 ng/ml. Analyte injection volumes of 0.53 μl were used corresponding to 9.6% of the capillary volume.

electropherogram and were formed at the moment that KCN and NDA were mixed. Therefore, quantitative analysis with NDA-CN derivatization is difficult at low analyte concentration levels.

4.3. On-capillary ITP derivatization with OPA-ME

The linearity in on-capillary ITP-CZE derivatization is investigated for the reaction of OPA-ME with Glu and Asp in the range 50–2000 ng/ml. Although an internal standard was not used all correlation coefficients were higher than 0.99 (Table 2).

The determination limit of Glu and Asp is 40 pg/ml based on 10 times the signal-to-noise ratio (Fig. 7A). The noise is calculated as one fifth of the peak-to-peak noise, measured at a high sensitivity. The determination limit of Glu and Asp in CZE with conventional pre-capillary derivatization is 7 ng/ml (Fig. 7B). In both cases a derivatization time of approximately 10 min is used. The improvement in the determination limit by a factor of 175 is mainly due to the concentrating ITP step. The analyte loadability

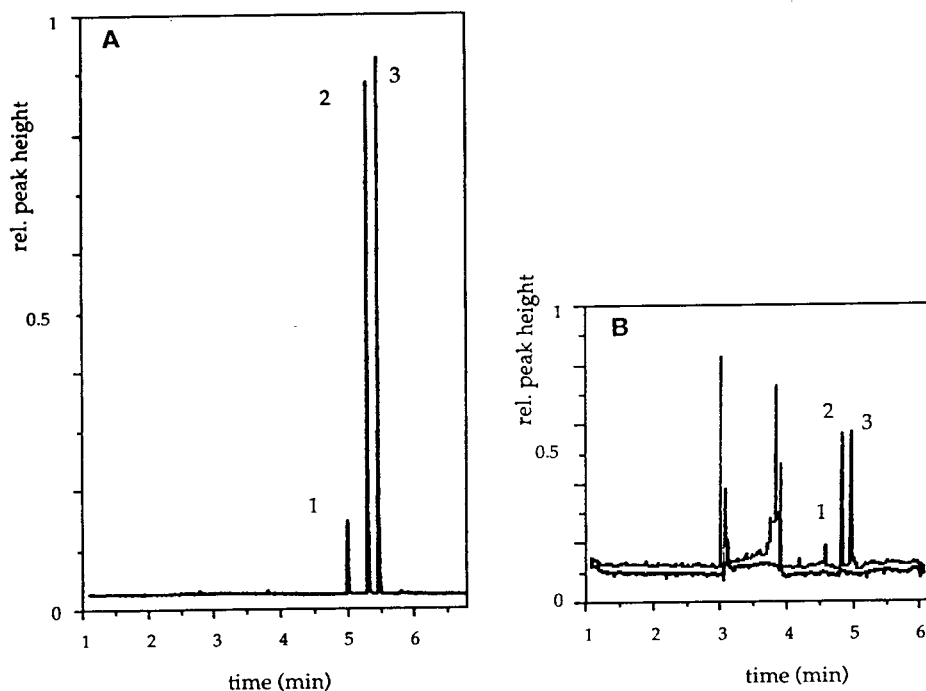


Fig. 7. Derivatization of 100 ng/ml GSH (1), Glu (2) and Asp (3) with OPA-ME with (A) on-capillary derivatization using ITP-CZE and with (B) CZE with conventional off-line derivatization. Injection volumes are (A) 1800 nl and (B) 13 nl. Improvement in S/N ratio in (A) is mainly due to the high loadability and the ITP concentration step.

in ITP–CZE is increased by a factor 135 in comparison with CZE. In CZE several system peaks resulting from the OPA reagent are visible between 3–4 min (Fig. 7B). In ITP–CZE these side products migrate outside the ITP window and do not appear in the electropherogram (Fig. 7A).

In Fig. 8 the effect of the loadability on the peak height is shown. The increase in peak height is linear with the loadability until the injection zone length is 60% of the total capillary length. At higher injection volumes, longer ITP and focusing times are used and degradation of the derivatives results in a decreased signal. The zone width is the same at all injection volumes. Similar results have been obtained in ITP–CZE of these amino acids with pre-capillary derivatization [11].

At high sensitivity determinations precautions are taken to avoid memory effects. Because ITP–CZE takes place without waste of buffers, in principle all injected analytes maintain within the separation system until all buffers are refreshed. In conventional CZE this is not a problem because all analyte ions are migrating in the same direction from injection to detection. However, in ITP–CZE the voltage is reversed in the ITP step which makes it in principle possible for analyte ions to be concentrated several times within the ITP window resulting in an increase of the background signal. In practice this means that the capillary is flushed between runs and

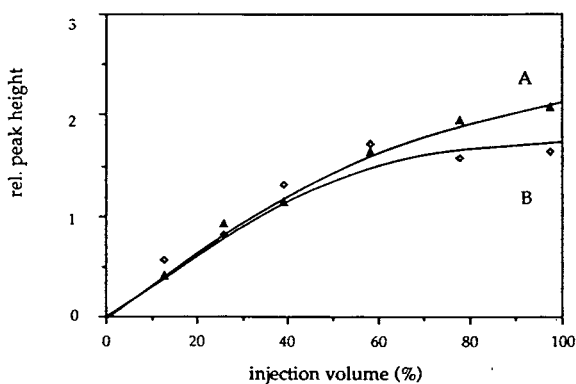


Fig. 8. Loadability in on-capillary derivatization of 100 ng/ml Glu (A) and Asp (B) with OPA–ME using ITP–CZE.

that the buffers are refreshed several times a day.

4.4. On-capillary derivatization for CZE

In cases where the analyte concentrations are high enough the ITP step is not always necessary. In Fig. 9B and C an on-capillary OPA derivatization method for CZE without ITP step is demonstrated. Simply by adding the OPA reagent to the background electrolyte (system III, see Experimental), a nanolitre (or picolitre, if smaller-I.D. capillaries are used) reaction cell is created.

This is demonstrated in Fig. 9B. A mixture of underivatized amino acids was electrokinetically injected and the CZE was started within 20 s. Plate numbers in this on-capillary derivatization procedure (Fig. 9B) were varying from $1.5 \cdot 10^5$ to $2.5 \cdot 10^5$. This was approximately 15% lower than in CZE with conventional off-line derivatization (Fig. 9A). This indicates that the OPA derivatization takes place before the electrophoresis is started. Otherwise zone broadening would occur because of small differences in electrophoretic mobility of the amino acids and the OPA derivatives of the amino acids.

The reaction times are easily kept constant in automated CZE procedures and can be increased if necessary, without zone broadening. In Fig. 9C the time between injection and the start of the CZE was 10 min. Plate numbers are the same as in Fig. 9B. The fluorescence background signal increased by a factor 2 after addition of 1 g/l OPA and 0.1% (v/v) ME to the background electrolyte. The detection limit for Phe was 10 ng/ml based on a *S/N* ratio of 3. This was 5 ng/ml for CZE with conventional off-line derivatization of Phe under similar CZE conditions. When a ten times lower reagent concentration is used in the electrophoresis buffer the derivatization reaction still takes place and the increase in fluorescence background is less than 20% compared to buffer only. Fluorescent reaction products, including contaminants in the buffer, decompose in time. Therefore, the OPA reagent was mixed with the electrophoresis buffer a day before use.

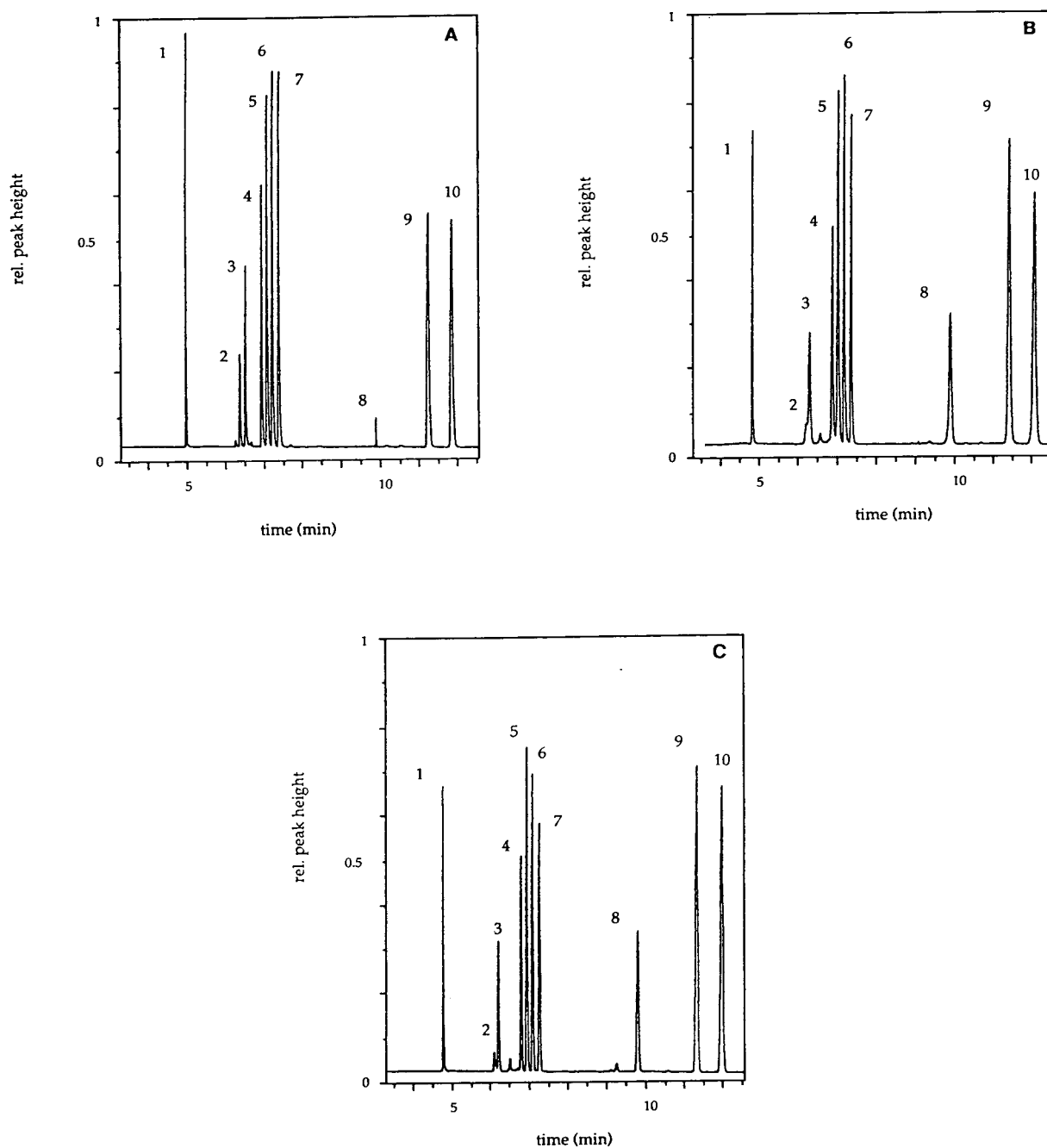


Fig. 9. On-capillary derivatization using CZE without ITP step. Separation of Arg (1), Lys (2, 3), Trp (4), Phe (5), Thr (6), Ser (7), L-Dopa (8), Glu (9) and Asp (10). (A) CZE after 10 min off-line derivatization compared with (B) on-capillary derivatization using CZE immediately started after injection or (C) started 10 min after electrokinetic injection. All concentrations were 5 $\mu\text{g/ml}$ except Lys (50 $\mu\text{g/ml}$), Asp and Glu (12 $\mu\text{g/ml}$).

Table 3

Unweighted linear regression data of the on-capillary derivatization in CZE of amino acids with OPA–ME in the range 0.040–240 $\mu\text{g/ml}$

	$a \pm \text{S.D.}$	$b \pm \text{S.D.}$	
Arg	202 \pm 149	0.149 \pm 0.002	0.9996
Lys	205 \pm 125	0.0048 \pm 0.00015	0.997
Trp	118 \pm 68	0.0746 \pm 0.0007	0.9997
Phe	130 \pm 73	0.128 \pm 0.0008	0.9999
Thr	150 \pm 94	0.121 \pm 0.0009	0.9998
Ser	–169 \pm 245	0.145 \pm 0.003	0.9990
Glu	–251 \pm 321	0.039 \pm 0.002	0.997
Asp	–161 \pm 215	0.030 \pm 0.001	0.997

Seven calibration points were used with concentrations 0.040, 0.200, 0.800, 4.00, 20.0, 80.0 and 240 $\mu\text{g/ml}$. Electrokinetic injection was applied at 3 kV for 3 s, corresponding to 5–15 nl injection volume depending on the analyte mobility.

The linearity of the on-capillary derivatization method for CZE was studied in the range of 0.040–240 $\mu\text{g/ml}$ for eight amino acids. All correlation coefficients are higher than 0.99 (Table 3).

5. Conclusions

An on-capillary reaction cell is described for nanolitre volumes at nanomolar concentration levels. When reactions with expensive reagents are involved the costs are reduced with the reduction of the reaction cell volume. The applicability is demonstrated for on-capillary fluorescence derivatization reactions. Requirements for the ITP reaction cell are described, including the equations necessary to calculate the electrophoretic supply of a neutral reagent.

The described procedure combines the concentrating properties of ITP, the separation efficiency of CZE and the detection sensitivity of LIF. The method is automated and quantitative at nanomolar concentration level for the reaction of GSH with NDA. Depending on the concentration of analyte and the required determination limit a choice can be made for on-capil-

lary OPA–ME derivatization with or without ITP step before CZE.

References

- [1] R.A. Wallingford and A.G. Ewing, *Adv. Chromatogr.*, 29 (1989) 1.
- [2] W.G. Kuhr, *Anal. Chem.*, 62 (1990) 403R.
- [3] W.G. Kuhr and C.A. Monnig, *Anal. Chem.*, 64 (1992) 389R.
- [4] M. Albin, P.D. Grossman and S.E. Moring, *Anal. Chem.*, 65 (1993) A489.
- [5] Y. Ohkura and H. Nohta, *Adv. Chromatogr.*, 29 (1989) 221–258.
- [6] J.A.P. Meulendijk and W.J.M. Underberg, in H. Lingeman and W.J.M. Underberg (Editors), *Detection Oriented Derivatization Techniques in Liquid Chromatography (Chromatographic Science Series, Vol. 48)*, Marcel Dekker, New York, 1990, Ch. 7.
- [7] M. Albin, R. Weinberger, E. Sapp and S. Moring, *Anal. Chem.*, 63 (1991) 417.
- [8] R.J.H. Houben, H. Gielen and S. van der Wal, *J. Chromatogr.*, 634 (1993) 317.
- [9] L.Z. Avila and G.M. Whitesides, *J. Org. Chem.*, 58 (1993) 5508.
- [10] H.T. Chang, E.S. Yeung, *Anal. Chem.*, 65 (1993) 2947.
- [11] N.J. Reinhoud, U.R. Tjaden and J. van der Greef, *J. Chromatogr.*, 641 (1993) 155.
- [12] N.J. Reinhoud, U.R. Tjaden and J. van der Greef, *J. Chromatogr. A*, 653 (1993) 303.
- [13] N.J. Reinhoud, U.R. Tjaden and J. van der Greef, *J. Chromatogr. A*, 673 (1994) 239.
- [14] L.A. Sternson, J.F. Stobaugh, J. Reid and P. deMontigny, *J. Pharm. Biomed. Anal.*, 6 (1988) 657.
- [15] R.F. Chen, C. Scott and E. Trepman, *Biochim. Biophys. Acta*, 576 (1979) 440.
- [16] K.J. Dave, J.F. Stobaugh, T.M. Rossi and C.M. Riley, *J. Pharm. Biomed. Anal.*, 10 (1992) 965.
- [17] M.A. Nussbaum, J.E. Przedwiecki, D.U. Staerk, S.M. Lunte and C.M. Riley, *Anal. Chem.*, 64 (1992) 1259.
- [18] P. Kwakman, *Ph.D. Thesis*, Free University, Amsterdam, 1991.
- [19] T. Yoshimura, T. Kamataki and T. Miura, *Anal. Biochem.*, 188 (1990) 132.
- [20] R. Håkanson and A.L. Rönnerberg, *Anal. Biochem.*, 54 (1973) 353.
- [21] R.P. Maickel and F.P. Miller, *Anal. Chem.*, 38 (1966) 1937.
- [22] V.H. Cohn and J.L. Lyle, *Anal. Biochem.*, 14 (1966) 434.
- [23] P.J. Hissin and R. Hilf, *Anal. Biochem.*, 74 (1976) 214.



ELSEVIER

Journal of Chromatography A, 673 (1994) 267–274

JOURNAL OF
CHROMATOGRAPHY A

Capillary electrophoresis of some tetracycline antibiotics

S. Croubels*^a, W. Baeyens^b, C. Dewaele^c, C. Van Peteghem^a

^aLaboratory of Food Analysis, Faculty of Pharmaceutical Sciences, University of Ghent, Harelbekestraat 72, B-9000 Ghent, Belgium

^bLaboratory of Drug Analysis, Faculty of Pharmaceutical Sciences, University of Ghent, Harelbekestraat 72, B-9000 Ghent, Belgium

^cBio-Rad RSL, Begoniastraat 5, B-9810 Nazareth, Belgium

(First received December 7th, 1993; revised manuscript received March 22nd, 1994)

Abstract

Data on the separation of tetracycline antibiotics by capillary electrophoresis are rather limited and have not been reported for micellar electrokinetic capillary chromatographic separation (MECC). In the present study, the separation of tetracycline, oxytetracycline and chlortetracycline by capillary zone electrophoresis and MECC was investigated. Adding non-ionic surfactants such as Triton X-100 to a 0.2 M phosphate migration buffer of pH 2.2 greatly improved separation. The use of mixed micelles enlarged the variety of the micellar phases, *e.g.* a combination of Tween 20 and Tween 80 provided a similar separation pattern. The addition of β -cyclodextrin to a Triton X-100 and Brij-35 surfactant combination did not result in an improved separation. A Triton X-100 and Brij-35 combination could separate tetracycline and its degradation products 4-epitetracycline (ETC), anhydrotetracycline and 4-epianhydrotetracycline. This enabled us to identify ETC in a commercial tetracycline sample.

1. Introduction

Tetracycline antibiotics are an important class of therapeutic compounds as they represent a key component in the strategy used to control bacterial infections in both humans and animals. Although many high-performance liquid chromatographic (HPLC) methods for the analysis of antibiotics have been reported and reviewed [1,2], the use of capillary electrophoresis (CE) has gained considerable importance in recent years. This topic was recently reviewed by Bobbitt and Ng [1] and Grossman and Colburn [3]. This includes reports by Nishi and co-workers [4–6] using micellar electrokinetic capillary

chromatography (MECC) to separate both penicillin and cephalosporin antibiotics, Tsikas *et al.* [7] using capillary isotachophoretic chromatography to separate penicillin and cephalosporin antibiotics and their precursors, and Ackermans and co-workers using capillary zone electrophoresis (CZE) to separate aminoglycoside antibiotics [8] and eleven sulphonamides [9]. Most of the reported studies usually involve only one family of the antibiotics. Yeo *et al.* [10] reported the CZE separation of six selected antibiotics of different types, including chlortetracycline.

For further enhancement of selectivity, cyclodextrins [11,12] and organic solvents [12–14] can be added to the electrophoretic media. The inclusion complexing properties of cyclodextrins have been discussed in detail, espe-

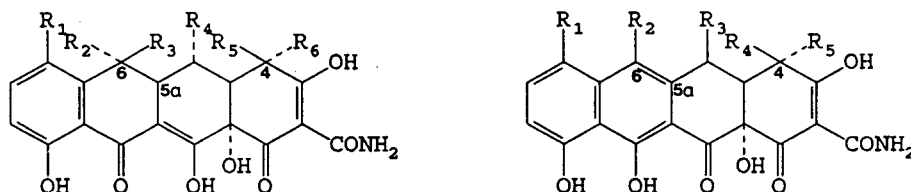
* Corresponding author.

cially their applications to perform chiral separations [15]. Interactions between additives and solutes may cause the latter to migrate at different velocities owing to differences in the magnitude of solute–additive associations. Nevertheless, none of these additives have been applied to the CE separation of tetracyclines. To our knowledge, only one CZE method has been published for the separation of tetracycline and its degradation products [16]. By this method, complete baseline separation of tetracycline and its degradation products was achieved using EDTA as an additive in a phosphate buffer solution (pH 3.9). In view of this, attempts were made to establish the optimum conditions for CZE separation of three widely used tetracyclines: tetracycline (TC), oxytetracycline (OTC) and chlortetracycline (CTC).

One aspect of current interest is the addition of micelles to the electrophoretic buffer to perform a chromatography-like separation [17], which was first described by Terabe *et al.* [18] in

1984 as micellar electrokinetic chromatography. Nevertheless, this MECC was not mentioned before for tetracycline antibiotics. The present study was undertaken to determine the CZE and MECC behaviour of TC, OTC and CTC. Indeed, the separation of TC, OTC and CTC by MECC provided a better resolving power than CZE due to the interaction or partition of the analytes with the micellar phase [19].

In Fig. 1 the structural formulae of the investigated tetracycline antibiotics and tetracycline degradation products are given. At pH values lower than 2, especially upon heating, a dehydration reaction at C5a–C6 leads to the formation of anhydrotetracycline (ATC). In aqueous solutions at pH 2–6 a reversible epimerization reaction at C4 takes place to form 4-epitetracycline (ETC) and 4-epianhydrotetracycline (EATC), respectively [20]. The separation of TC and its degradation products was similarly studied by MECC in the present investigation. ETC could be detected in a commercial tetracycline sample.



Compound	R ₁	R ₂	R ₃	R ₄	R ₅	R ₆	Compound	R ₁	R ₂	R ₃	R ₄	R ₅
TC	H	CH ₃	OH	H	H	N(CH ₃) ₂	ATC	H	CH ₃	H	H	N(CH ₃) ₂
OTC	H	CH ₃	OH	OH	H	N(CH ₃) ₂	EATC	H	CH ₃	H	N(CH ₃) ₂	H
CTC	Cl	CH ₃	OH	H	H	N(CH ₃) ₂						
ETC	H	CH ₃	OH	H	N(CH ₃) ₂	H						

Fig. 1. Structural formulae of some representative tetracycline antibiotics: tetracycline (TC), oxytetracycline (OTC), chlortetracycline (CTC) and tetracycline degradation products 4-epitetracycline (ETC), anhydrotetracycline (ATC) and 4-epianhydrotetracycline (EATC).

Its presence could be confirmed applying a validated HPLC method for purity control of tetracycline samples [21].

2. Experimental

2.1. Instrumentation

CE analysis

CE was performed on a HPE 100 high-performance CE instrument from Bio-Rad (Nazareth, Belgium), equipped with a variable-wavelength UV detector. Commercial cartridges (Bio-Rad) containing coated fused-silica columns of 20 cm × 25 μm I.D. were used. Sample solutions were injected into the capillary on the anodic side by electromigration for 10 s at 12 kV. A constant-voltage mode was applied for the separation of the analytical solutions. For detection, the absorbance was measured at 265 nm, and the signal from the detector was processed with a Shimadzu (Kyoto, Japan) Chromatopac C-R3A integrator system.

HPLC analysis

HPLC was performed on a Varian (Walnut Creek, CA, USA) 9010 solvent-delivery system with a 20-μl loop, coupled with a Hewlett-Packard (Waldbronn, Germany) Series 1050 multiple-wavelength detector. A Shimadzu CTO-6A column oven was used to maintain column temperature at 60°C. The chromatograms were recorded and integrated on a Hewlett-Packard (Grenoble, France) Vectra QS/16S integrator.

2.2. Chemicals

CE analysis

CTC hydrochloride, ETC hydrochloride, EATC hydrochloride and ATC hydrochloride were purchased from Janssen Chimica (Beerse, Belgium). TC hydrochloride and OTC were kindly provided by Pfizer (Brussels, Belgium). EDTA and sodium dodecyl sulphate (SDS) were obtained from Merck (Darmstadt, Germany). Cetyltrimethylammonium bromide was pur-

chased from UCB (Drogenbos, Belgium). Sodium taurocholate, sodium deoxycholate, β-cyclodextrin (β-CD) and Triton X-100 were obtained from Janssen Chimica. Polyoxyethylene (20) sorbitan monooleate (Polysorbate 80, Tween 80) was from Laboratoria Flandria (Zwijnaarde, Belgium), polyoxyethylene sorbitan monolaurate (Tween 20) was from Sigma (St. Louis, MO, USA) and polyoxyethylene dodecyl ether (Brij-35) was from Merck-Schuchardt (Munich, Germany).

All other reagents and solvents, of analytical-reagent grade, were purchased from Janssen Chimica or from Merck. Distilled deionized water was used to prepare solutions for CE purposes.

HPLC analysis

The reference TC·HCl sample, which was certified to contain 98.1% of the hydrochloride salt, was available from Janssen Chimica. Dipotassium hydrogenphosphate and 2-methyl-2-propanol were from Merck, tetrabutylammonium hydrogensulphate was from Janssen Chimica. HPLC-grade water was from Labscan (Dublin, Ireland). Sample solutions were stored protected from light not more than 12 h at about 5°C.

2.3. Procedures

CZE analysis

An aqueous solution of TC, OTC and CTC each at a concentration of 20 μg ml⁻¹ was prepared daily and subjected to CZE and MECC.

Phosphate buffers in the pH range 1.6–2.2 and concentrations between 0.01 and 0.2 M were composed of sodium dihydrogenphosphate solutions with the pH adjusted using a 85% phosphoric acid solution. Other phosphate buffers with pH values of 6.0 (0.05 M) and 9.0 (0.2 M) consisted of disodium hydrogenphosphate solutions adjusted to pH using a 4 M sodium hydroxide solution.

The effect of buffer additives on the separation of TC, OTC and CTC in the CZE mode

was studied with addition of EDTA, organic modifiers and β -CD. EDTA was added in a concentration of 0.005 M to a 0.05 M phosphate buffer (pH 6.0). The addition of acetonitrile and methanol to a 0.1 M phosphate buffer system (pH 2.2) at concentrations of 30 and 10% (v/v), respectively, was studied. The effect of the addition of β -CD in a concentration range between 0.5 and 20 mM to the same buffer system was also tested.

MECC analysis

Anionic micelle systems consisted of a 12 mM sodium deoxycholate solution in a phosphate running buffer 0.2 M (pH 9.0), 17 mM sodium taurocholate solution in a phosphate running buffer 0.05 M (pH 6.0) and 40 mM SDS in the same buffer system.

The cationic micelle system tested was a 10 mM cetyltrimethylammonium bromide solution in a 0.1 M phosphate running buffer (pH 2.2).

In this investigation, all non-ionic surfactants were added to a 0.2 M phosphate running buffer of pH 2.2 and their concentration values are expressed as % (m/m). The effect of serial dilutions of the investigated micelle systems in the same migration buffer (1:2) was studied.

For the separation of TC, OTC and CTC a micelle system containing 0.48% Triton X-100 was applied. Also a mixed micelle system containing a mixture of Tween 20 (0.52%) and Tween 80 (0.56%) was applicable. The addition of β -CD (10 mM) to another mixed micelle system which combined Triton X-100 (0.48%) and Brij-35 (0.16%) was also tested.

For the separation of TC and its degradation products a combination of Brij-35 (0.035%) and Triton X-100 (0.10%) was applied.

HPLC analysis

HPLC was carried out as described by Hendrix *et al.* [21]. The column used was a PRP-1 column (25 cm \times 4.6 mm I.D., 10 μ m spherical 75 Å poly(styrene–divinylbenzene) particles, Hamilton, Reno, USA). The mobile phase contained 8.5% (m/v) of 2-methyl-2-propanol, 10% (v/v) of a 3.5% (m/v) dipotassium hydrogen-

phosphate solution adjusted to pH 9.0, 20% (v/v) of a 1.0% (m/v) tetrabutylammonium hydrogensulphate solution adjusted to pH 9.0, 1% (v/v) of a 4.0% (m/v) EDTA solution adjusted to pH 9.0 and the volume was made up to 100% (v/v) with water. Dilute phosphoric acid (10%, m/m) or dilute sodium hydroxide solution (8.5%, m/m) were used to adjust the solutions to the required pH. The mobile phase was degassed by ultrasonication. The flow-rate was set at 1.0 ml min⁻¹.

A solution containing 1.0 mg ml⁻¹ of the TC sample (Pfizer) in 0.01 M hydrochloric acid was prepared.

3. Results and discussion

3.1. CZE separation of TC, OTC and CTC: choice of parameters

Several electrophoretic parameters were considered and their influence on the overall performance of the separation studied. The results can be summarized as follows.

Influence of migration buffer pH

The pK_a values relevant to acid–base equilibrium in aqueous solution of the tetracycline antibiotics are agreed to be approximately 3.3, 7.5 and 9.3 [20]. At buffer pH values below the value of the isoelectric point at pH 5.5, the positively charged tetracyclines migrate towards the cathode. In order to fully utilize the electrophoretic mobility differences as a result of this ionization, an acid buffer of pH 2.2, using phosphate as the buffering ion, was chosen.

Influence of migration buffer concentration

It has been shown that the ionic strength of the buffer has significant effects on solute mobilities and separation efficiency [22]. In general, the migration times of the tetracyclines increased with increasing buffer concentration. A phosphate buffer concentration of 0.2 M was finally chosen as the most suitable.

Influence of running voltage

During the separation a constant voltage mode was applied and migration occurred under rather constant currents of about 12 μA . Running voltages in the range 4–12 kV were tested. As expected, decreasing migration times were obtained with increasing applied voltages but varying the voltage did not influence the selectivity. A running voltage of 12 kV was chosen for further experiments, because this was the maximum value allowed by the instrument and this significantly shortened the migration times.

3.2. Effect of buffer additives on the separation of TC, OTC and CTC

Since CZE experiments did not provide baseline separation, the effect of buffer additives was investigated. Zhang *et al.* [16] added 0.005 M EDTA to a 0.02 M CZE migrating phosphate buffer (pH 3.9) to improve the resolution between TC and its degradation products ETC, ATC and EATC. To avoid solubility problems of EDTA at pH 2.2, a similar addition of EDTA to a phosphate buffer pH 6.0 was tested. Organic modifiers as acetonitrile and methanol were added to the running buffer as well, as was β -CD based on its extensive application in various CZE systems [11,12]. None of the additions provided improved resolution.

3.3. MECC separation

Separation of TC, OTC and CTC

MECC has the advantage that changing the micellar phase is very easy, requiring only that the capillary be rinsed and filled with the micellar solution. In practice, the applicability of a surfactant to MECC will mainly depend on its solubility and its critical micellar concentration (CMC) [22]. Anionic and cationic micelle systems are the most commonly employed micellar phases, though non-ionic surfactants are employed as well. SDS, sodium deoxycholate and sodium taurocholate added to a phosphate running buffer, did not improve the separation, neither did cetyltrimethylammonium bromide. However, when introducing non-ionic surfactants distinct effects upon the separation could be observed. Fig. 2 illustrates the striking effect of Triton X-100 on the separation of a solution of TC, OTC and CTC. Initially, resolution increased strongly with decreasing surfactant concentration but then levelled off at a maximum value. During migration, the micelles can interact with the tetracyclines in a chromatographic manner, possible through hydrophobic interactions with the alkyl chain. The more hydrophobic compounds interact more strongly with the micelle and are "retained" longer.

Also surfactant combinations were tested for

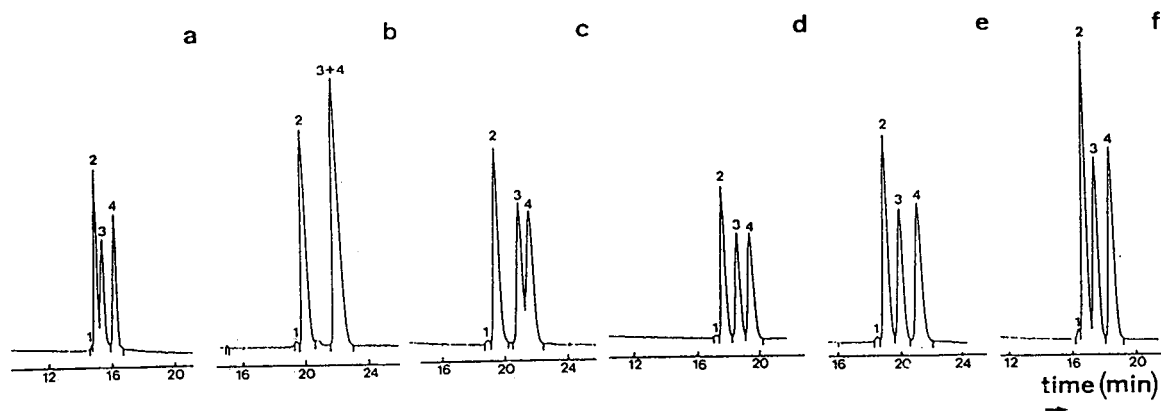


Fig. 2. Effect of Triton X-100 concentration on the MECC separation of a solution of 20 $\mu\text{g ml}^{-1}$ TC, OTC and CTC each. Experimental conditions: 20 cm \times 25 μm I.D. coated column; 0.2 M phosphate migration buffer of pH 2.2; running voltage: 12 kV; 12 kV 10 s injection conditions; detection: 265 nm. Peaks: 1 = ETC; 2 = TC; 3 = CTC; 4 = OTC. Concentration Triton X-100 (% m/m) included in the migration buffer: (a) 0%, (b) 0.48%, (c) 0.24%, (d) 0.12%, (e) 0.06%, (f) 0.03%.

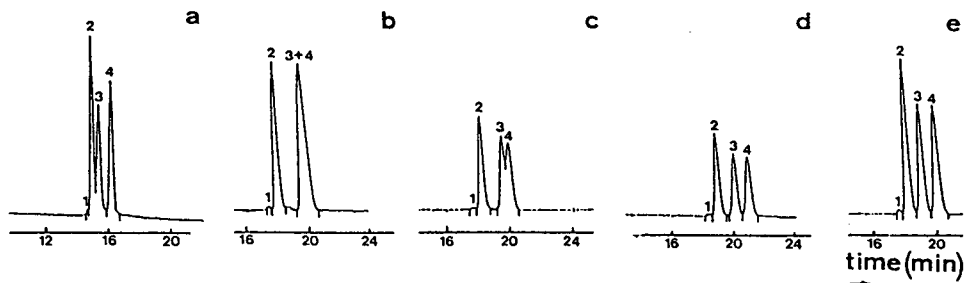


Fig. 3. Effect of a Tween 20 and Tween 80 combination on the separation of a solution of $20 \mu\text{g ml}^{-1}$ TC, OTC and CTC each. Experimental conditions and peaks as in Fig. 2. Concentration Tween 20 and Tween 80 (% m/m) included in the migration buffer: (a) 0%, (b) 0.52% Tween 20 and 0.56% Tween 80, (c) 0.26% Tween 20 and 0.28% Tween 80, (d) 0.13% Tween 20 and 0.14% Tween 80, (e) 0.065% Tween 20 and 0.07% Tween 80.

further enhancement of selectivity. The effect of a Tween 20 and Tween 80 combination is shown in Fig. 3, but analogue separations as in Fig. 2 can be noted.

Addition of β -CD to a surfactant combination did not effect selectivity and similar separation patterns were observed.

Separation of TC and its degradation products

As the electropherograms showed a peak co-eluting with the TC peak, the question raised whether this compound was either a degradation product created during the electrophoretic run or

was already present in the commercial TC sample.

Therefore, a separation of a standard mixture of TC and its degradation products ETC, ATC and EATC was needed to check the migration behaviour of the degradation products. This separation was performed using a similar combination of non-ionic micelles as for the separation of TC, OTC and CTC. The MECC system combined Triton X-100 and Brij-35 added to a 0.2 M phosphate buffer of pH 2.2 (Fig. 4). As can be seen, peak shapes of ATC and EATC are not optimal, but allow anyhow confirmation of their presence or absence in the sample. Further

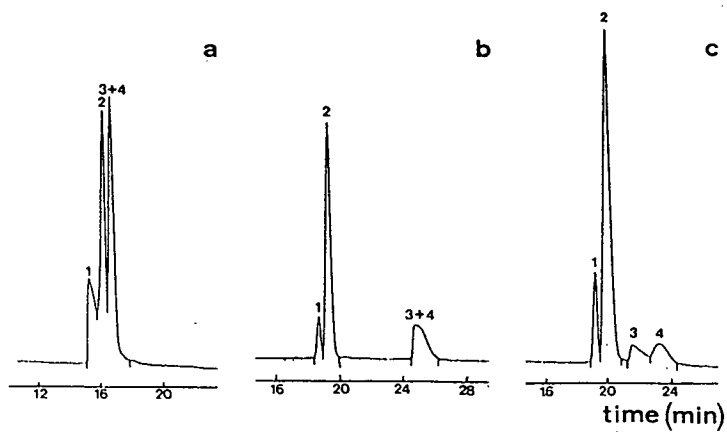


Fig. 4. Effect of a Triton X-100 and Brij-35 combination on the separation of a standard mixture of TC and its degradation products ETC, EATC and ATC. Concentration TC $30 \mu\text{g ml}^{-1}$; ETC, ATC and EATC: (a) $10 \mu\text{g ml}^{-1}$, (b and c) $2 \mu\text{g ml}^{-1}$. Experimental conditions as in Fig. 2. Peaks: 1 = ETC; 2 = TC; 3 = EATC; 4 = ATC. Concentration Triton X-100 and Brij-35 (% m/m) included in the migration buffer: (a) 0%, (b) 0.10% Triton X-100 and 0.035% Brij-35, (c) 0.05% Triton X-100 and 0.017% Brij-35.

experiments are required to optimize the MECC separation pattern of the decomposition products. The mentioned co-eluting peak could be identified as ETC after standard addition.

HPLC confirmation of ETC presence

Under conditions of acid pH (pH 2–6) and heating (Joule effect in the capillary [23]), TC can degrade to ETC [20].

Possible degradation of TC to ETC during the CE analysis providing erroneous results was examined with the same TC sample using another separation technique. Therefore a method reported for the analysis of TC by liquid chromatography on poly(styrene–divinylbenzene) was applied [21]. A chromatogram ob-

tained from the TC sample is given in Fig. 5. The relative amounts of ETC found by the HPLC method corresponded well with those found by MECC, so the MECC separation method proved to be a non-destructive method.

4. Conclusions

The present findings demonstrate the power of MECC for the separation of TC, OTC and CTC as their cations using an acid running buffer solution. Adding non-ionic surfactants such as Triton X-100, Brij-35, Tween 20 and Tween 80 to the running buffer solution provided improved separation. A MECC buffer system combining

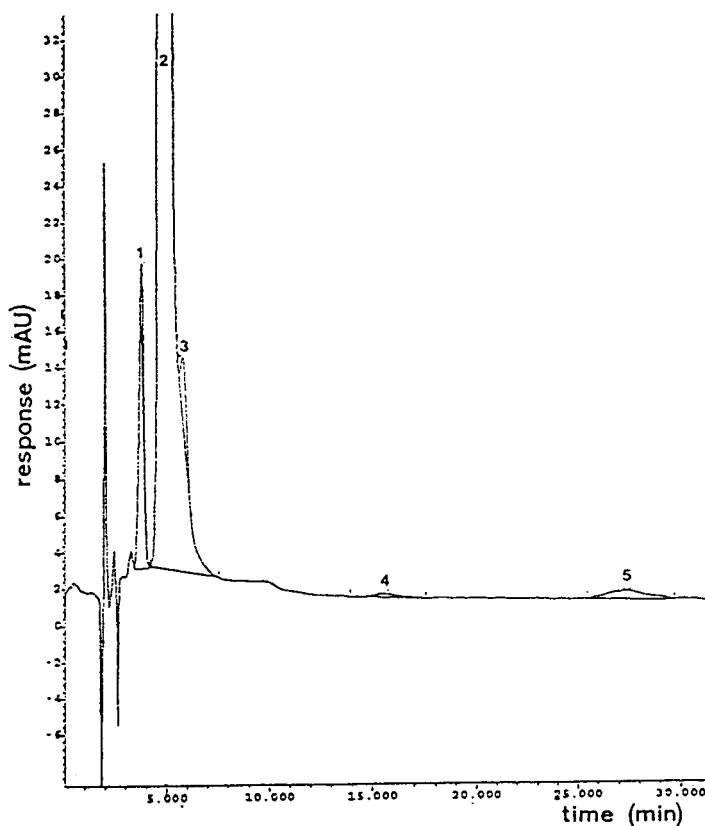


Fig. 5. HPLC chromatogram of a TC sample. Conditions: column: PRP-1 column; mobile phase: 2-methyl-2-propanol (8.5%, m/v), 3.5% (m/v) dipotassium hydrogenphosphate pH 9.0 (10 ml), 1.0% (m/v) tetrabutylammonium hydrogensulphate pH 9.0 (20 ml), 4.0% (m/v) EDTA pH 9.0 (1 ml), water (up to 100 ml); temperature: 60°C; injection loop: 20 μ l; flow-rate: 1 ml min^{-1} ; detection: 254 nm. Peaks: 1 = ETC; 2 = TC; 3 = 2-acetyl-2-decarboxamidotetracycline (ADTC); 4 = EATC; 5 = ATC.

Triton X-100 and Brij-35 was suitable for the separation of TC, ETC, ATC and EATC.

The separation of these tetracycline antibiotics by MECC could be achieved in less than half an hour requiring only small volumes of analyte solutions and limited quantities of electrolytes and additives.

Acknowledgements

S.C. is Research Assistant of the National Fund for Scientific Research (Belgium). The authors thank Miss A. Van Overbeke for running the HPLC experiments and Dr. H. Pintens from Pfizer (Brussels) for the generous gifts of TC and OTC samples.

References

- [1] D.R. Bobbitt and K.W. Ng, *J. Chromatogr.*, 624 (1992) 153.
- [2] S.A. Barker and C.C. Walker, *J. Chromatogr.*, 624 (1992) 195.
- [3] P.D. Grossman and J.C. Colburn, *Capillary Electrophoresis — Theory and Practice*, Academic Press, San Diego, CA, 1992.
- [4] H. Nishi, N. Tsumagari, T. Kakimoto and S. Terabe, *J. Chromatogr.*, 477 (1989) 259.
- [5] H. Nishi, N. Tsumagari and S. Terabe, *Anal. Chem.*, 61 (1989) 2434.
- [6] H. Nishi, T. Fukuyama and M. Matsuo, *J. Chromatogr.*, 515 (1990) 245.
- [7] D. Tsikas, A. Hofrichter and G. Brunner, *Chromatographia*, 30 (1990) 657.
- [8] M.T. Ackermans, F.M. Everaerts and J.L. Beckers, *J. Chromatogr.*, 606 (1992) 229.
- [9] M.T. Ackermans, J.L. Beckers, F.M. Everaerts, H. Hoogland and M.J.H. Tomassen, *J. Chromatogr.*, 596 (1992) 101.
- [10] S.K. Yeo, H.K. Lee and S.F.Y. Li, *J. Chromatogr.*, 585 (1991) 133.
- [11] T.E. Peterson, *J. Chromatogr.*, 630 (1993) 353.
- [12] D.N. Heiger, *High Performance Capillary Electrophoresis: An Introduction*, Hewlett-Packard, Waldbronn, 1992.
- [13] S. Honda, A. Taga, K. Kakehi, S. Koda and Y. Okamoto, *J. Chromatogr.*, 590 (1992) 364.
- [14] G.M. Janini, K.C. Chan, J.A. Barnes, G.M. Muschik and H.J. Issaq, presented at the *5th International Symposium on High Performance Capillary Electrophoresis*, Orlando, FL, January 25–28, 1993.
- [15] P. Jandik and G. Bonn, *Capillary Electrophoresis of Small Molecules and Ions*, VCH, New York, 1993.
- [16] C.-X. Zhang, Z.-P. Sun, D.-K. Ling and Y.J. Zhang, *J. Chromatogr.*, 627 (1992) 281.
- [17] J. Vindevogel and P. Sandra, *Introduction to Micellar Electrokinetic Chromatography*, Hüthig, Heidelberg, 1992.
- [18] S. Terabe, K. Otsuka, K. Ichikawa, A. Tsuchiya and T. Ando, *Anal. Chem.*, 56 (1984) 113.
- [19] Y.J. Yao, H.K. Lee and S.F.Y. Li, *J. Chromatogr.*, 637 (1993) 195.
- [20] L.A. Mitscher, *The Chemistry of the Tetracycline Antibiotics*, Marcel Dekker, New York, 1978.
- [21] C. Hendrix, E. Roets, J. Crommen, J. De Beer, E. Porqueras, W. Van den Bossche and J. Hoogmartens, *J. Liq. Chromatogr.*, 16 (1993) 3321.
- [22] S.F.Y. Li, *Capillary Electrophoresis — Principles, Practice and Applications (Journal of Chromatography Library, Vol. 52)*, Elsevier, Amsterdam, 1992.
- [23] H.-T. Chang and E.S. Yung, *J. Chromatogr.*, 632 (1993) 149.



ELSEVIER

Journal of Chromatography A, 673 (1994) 275–285

JOURNAL OF
CHROMATOGRAPHY A

Determination of alkali and alkaline earth metals in real samples by capillary ion analysis

Qing Yang, M. Jimidar, T.P. Hamoir, J. Smeyers-Verbeke, D.L. Massart*

Farmaceutisch Instituut, Vrije Universiteit Brussel, Laarbeeklaan 103, B-1090 Brussels, Belgium

(First received October 20th, 1993; revised manuscript received March 8th, 1994)

Abstract

Imidazole–H₂SO₄ background electrolyte was used to perform capillary ion analysis with indirect UV detection. Baseline separation of K, Na, Ca, Mg and Mn was achieved and the resolution could be enhanced by decreasing the pH of the electrolyte buffer. The electromigration dispersion for Na was smaller in the imidazole–H₂SO₄ buffer than in the background electrolyte containing UVCat1 (a UV-absorbing amine) and 2-hydroxyisobutyric acid. This therefore resulted in less Na peak broadening. As a consequence, large amounts of Na could be separated efficiently without interference with the other analyte cations. The method was validated for the quantitative analysis of pharmaceutical electrolyte solutions and beverages, and compared with flame atomic spectrometry for evaluation.

1. Introduction

Koberda *et al.* [1] tried to develop a capillary electrophoresis (CE) method to analyse parenteral electrolyte solutions quantitatively for Na, K, Ca and Mg simultaneously. Using UVCat1–2-hydroxyisobutyric acid (HIBA) as the background electrolyte (BGE), they found that Na, present in much higher concentrations than other ions, caused overlap between Na and the rest of the analyte cations. They therefore maximized the resolution by increasing the concentration of the complexing agent HIBA. Although they obtained an enhanced resolution, an increase in buffer conductivity and running current resulted in a significant increase in baseline noise and a marked decrease in the analyte peak response. Nevertheless, their method could not deal with

the analysis of parenteral solutions owing to the presence of very high levels of Na.

The overlap is considered to result from the electromigration dispersion which causes a broad peak. The higher the concentration of the sample component in its zone, the more pronounced in this dispersion and therefore the broader is the peak [2]. There are two ways to suppress the electromigration broadening. The first is to keep the solute concentrations sufficiently lower than the concentration of BGE. This, however, will produce a negative effect on the sensitivity as a reduced amount of analyte is used. Another possibility is based on the selection of a co-ion with a mobility close to that of the analytes. In such a case the electromigration broadening of the analyte zones during the migration is negligible even if the concentration of solutes reaches the concentration of BGE.

Beck and Engelhardt [3] proposed a new

* Corresponding author.

background electrolyte system, imidazole– H_2SO_4 , for the determination of alkali and alkaline earth metal cations by capillary ion analysis (CIA). In this buffer, positively charged imidazole ion was reported to have a mobility of $0.44 \text{ cm}^2 \text{ kV}^{-1} \text{ s}^{-1}$, which is close to the mobility of Na ($0.48 \text{ cm}^2 \text{ kV}^{-1} \text{ s}^{-1}$). It was also found experimentally that Na had the highest separation efficiency in the pH range of 3–6. Although Beck and Engelhardt [3] applied this method to the quantitative analysis of mineral waters, so far work on the CIA of cations has mostly been focused on qualitative detection.

The main aim of this work was to investigate the applicability of CIA, by adapting Beck and Engelhardt's method, to the quantitative analysis of real complex mixtures. For this reason, a comparison with a well established metal analysis method, flame atomic spectrometry (FAS), was carried out in terms of sensitivity, limit of detection, linearity, accuracy and precision.

2. Experimental

2.1. Instrumentation

The CE instrument was a Waters Quanta 4000 capillary electrophoresis system with a twenty-sample carousel, a positive power supply and a zinc lamp detector (214 nm). Accusep fused-silica capillaries, $75 \mu\text{m}$ I.D. and 60 cm total length, were used in all analyses. A positive voltage of 20 kV was applied. The detector time constant was 0.3 s. The samples were introduced into the capillary by 20- or 30-s hydrostatic injections from a height of 10 cm, which corresponds to an injection volume of about 40 nl [4]. The electropherograms were recorded and treated with a Waters Model 810 data workstation equipped with a W51-watch-dog interface. Absolute peak areas (microvolts multiplied by seconds) were used in all calculations.

A Perkin-Elmer Model 373 flame atomic absorption spectrometer was used for the determination of Ca and Mg in the absorption mode (FAAS) and for Na and K in the emission mode (FAES). For Ca determinations, 1% (w/v) La

was added to both standards and samples to eliminate possible interference from phosphate.

2.2. Temperature control for experiments

Temperature control was achieved by locating the instrument in a room with air conditioning where the temperature was set at 21.5°C . A temperature probe was inserted into the compartment where the capillary was situated in order to monitor the temperature inside the compartment. Within one day the temperature difference inside the compartment, as monitored by the temperature probe, was about 0.5°C at the end of all experiments.

2.3. Capillary preparation and cleaning

Every morning the capillary was cleaned and prepared according to the following procedure: washing for 2 min with 0.5 M KOH, for 5 min with Milli-Q-purified water and for 2 min with the BGE. Finally, the capillary was conditioned with the BGE for at least 15 min. At the end of the day the whole cleaning procedure was repeated, then the capillary was dried by sucking air through it for 5 min to prevent the formation of a gel layer inside the capillary overnight [5].

2.4. Reagents and standards

Water used for the preparation of all solutions was obtained from a Milli-Q water purification system (Millipore, Bedford, MA, USA) and contained no detectable analyte cations. Standards containing Na, K, Mg, Ca and Mn were prepared by mixing and diluting different Titrisol concentrates of $1000 \mu\text{g/ml}$ of these elements (Merck, Darmstadt, Germany). H_2SO_4 was of Suprapur grade and imidazole was of analytical-reagent grade (Merck). BGE containing 5 mM imidazole was prepared by dissolving 0.034 g of imidazole in a 100-ml plastic volumetric flask and then the pH was adjusted by titration first with 5 M and then 0.5 M H_2SO_4 . The solution was kept in a refrigerator. Just before use it was filtered through a $0.45\text{-}\mu\text{m}$ syringe filter (Millipore, Molsheim, France).

2.5. Samples

Pharmaceutical NaCl, KH_2PO_4 , $\text{MgSO}_4 \cdot 7\text{H}_2\text{O}$, calcium gluconate used for the preparation of a simulated concentrate and multiple electrolyte solutions for parenteral use were commercially available. Glucose, mixtures of various amino acids, intralipid and a mixture of trace elements Zn, Cu, Fe, Cr, Se, Mn, F and I, used for preparing real multiple electrolyte solutions were also commercially available. They were used in the hospital to prepare the electrolyte solutions for parenteral use. In this work, two test solutions (1 and 2) were obtained from the hospital and diluted 100-fold (1 ml in 100 ml) with Milli-Q-purified water for quantitative analysis.

The simulated electrolyte concentrate was prepared in the laboratory by mixing the aforementioned four electrolyte salts. The prepared electrolyte contained 178.4 $\mu\text{g/ml}$ of Na, 468.5 $\mu\text{g/ml}$ of K, 180.6 $\mu\text{g/ml}$ of Ca and 43.9 $\mu\text{g/ml}$ of Mg. In order to obtain the solutions at two concentration levels for each cation, the concentrated solution was diluted 25-fold (1 ml in 25 ml) and 50-fold (1 ml in 50 ml), respectively.

Apple juice and orange juice samples were purchased at a local supermarket and diluted 50-fold for Na, Ca and Mg determinations and 100-fold for K determination. Because pulp was present in the orange juice, the diluted orange juice was filtered through a 0.45- μm syringe filter.

3. Results and discussion

3.1. Effect of pH of the background electrolyte

A decrease in the pH of BGE results in an increase in the difference of the migration times between two neighbouring cations, Δt (min): changing pH affects the selectivity. When the pH decreases from 6 to 3, Δt increases from 0.4 to 0.8 for the K–Na pair, from 0.1 to 0.3 for the Na–Ca pair, from 0.08 to 0.1 for the Ca–Mg pair and from 0.07 to 0.15 for the Mg–Mn pair.

The pH effect could result from the following

factors. First, the electroosmosis flow (EOF) decreases with a decrease in pH owing to a reduced dissociation of surface silanol groups. The effect of the EOF on the selectivity of separation can be derived from the following equation for Δt :

$$\Delta t = \frac{l}{E} \cdot \frac{\mu_1 - \mu_2}{(\mu_1 + \mu_{\text{eof}})(\mu_2 + \mu_{\text{eof}})} \quad (\mu_1 > \mu_2) \quad (1)$$

where μ_1 and μ_2 are the electrophoretic mobilities of two neighbouring cations and μ_{eof} is the electroosmotic mobility, l is the distance from the injector to the detector and E is the electric field strength. When l and E are kept constant, decreasing the pH of the electrolyte buffer will decrease μ_{eof} and therefore increase Δt , except when $\mu_1 = \mu_2$. In that case another separation mechanism such as complexation and/or solvation must be included to maximize the resolution [6].

Second, when basic imidazole is neutralized by H_2SO_4 , the ionic strength of the BGE increases owing to the addition of SO_4^{2-} , which results in a decreased μ_{eof} and electrophoretic mobilities of the analyte cations. Issaq *et al.* [7] have theoretically and experimentally confirmed that as the buffer concentration is increased, the μ_{eof} and ionic electrophoretic mobilities μ_1 and μ_2 are both reduced. The migration times of the solutes increase and the resolution improves with increasing concentration of the electrolyte buffer.

Vindevogel and Sandra [8] found that adjusting the pH of the buffer has two effects, namely a pure pH effect and an ionic strength effect. The two effects can be either cooperative or contradictory with respect to the influence on the EOF. In a strong acid–weak base type of electrolyte buffer as in our case, the pH effect and the ionic strength effect are cooperative, therefore resulting in a strong pH dependence of the EOF. Fig. 1 shows a plot of the number of theoretical plates (N) as a function of pH. The number of theoretical plates was calculated using the expression [7]

$$N = 5.545 \left(\frac{t_m}{W_{1/2}} \right)^2 \quad (2)$$

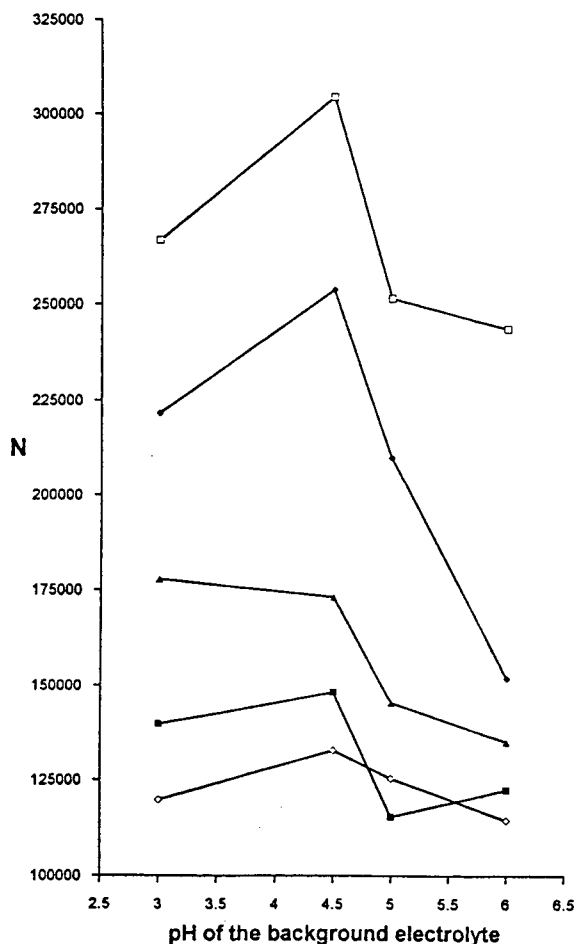


Fig. 1. Dependence of the number of theoretical plates (N) on the pH of the BGE. BGE, 5 mM imidazole- H_2SO_4 ; applied voltage, +20 kV; hydrostatic injection, 30 s from 10 cm. K, Na, Ca, Mg and Mn concentrations, 1 $\mu g/ml$ each. ■ = K; □ = Na; ◆ = Ca; ◇ = Mg; ▲ = Mn.

where t_m is the migration time of the corresponding cation and $W_{1/2}$ is the peak width at half-height. With increasing pH, N for K, Na, Ca and Mg first increases and reaches a maximum at pH 4.5 and then decreases when the pH is increased further. Therefore, at pH 4.5, the largest peak height and consequently the highest detectability for these cations are obtained. The measurement of N is affected by the asymmetry of the peak and the asymmetry changes with pH. It is well known that the form of peaks in

indirect detection is influenced by many parameters, but the theory of indirect detection and its influence on peak form are not well established and need further research. Na has the highest N value, about 300 000, because its electrophoretic mobility is close to that of ionic imidazole. The order of N as such $Na > Ca > Mn > K > Mg$ can be explained by the order of the electrophoretic mobilities of these cations except for Mg. The exception is possibly due to the fact that Mg has a much higher displacement ratio than the other ions. This causes a higher peak and a larger peak width at half-height. As described in Eq. 2, the peak width is adversely proportional to N . To avoid this influence one should consider the use of peaks with equal height.

Fig. 2 is a plot of resolution (R_s) as a function

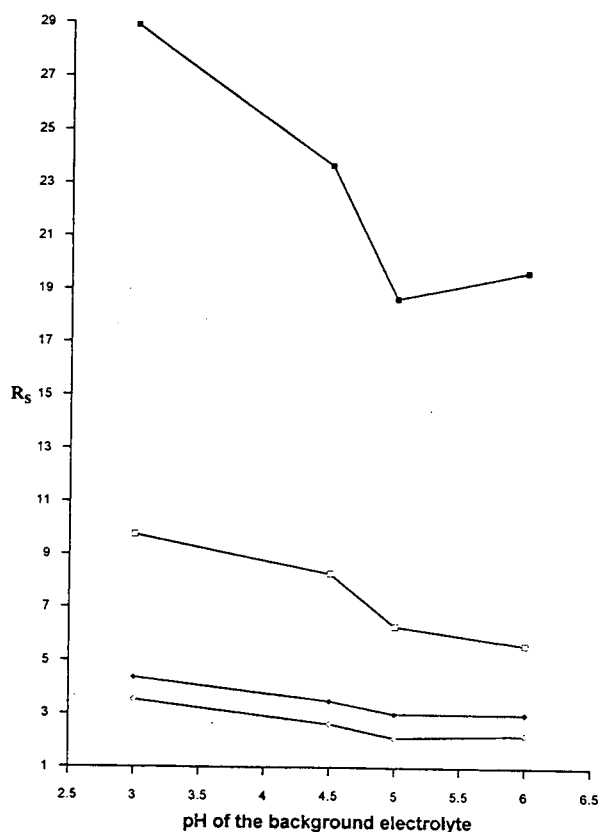


Fig. 2. Dependence of resolution (R_s) on the pH of the BGE. Experimental conditions as in Fig. 1. □ = K-Na; ◆ = Ca-Na; ◇ = Ca-Mg; ◇ = Mg-Mn.

of pH. R_s is calculated by the following equation [7]:

$$R_s = 1.177 \cdot \frac{(t_{m_2} - t_{m_1})}{(W_{1/2})_1 + (W_{1/2})_2} \quad (3)$$

The effect of pH on R_s is largest for the K–Na and Na–Ca pairs and is less pronounced for the Ca–Mg and Mg–Mn pairs. Hence, decreasing the pH of the BGE improves the separation.

Fig. 3a and b show the electropherograms of 1 $\mu\text{g}/\text{ml}$ each of K, Ca, Mg, Mn and 20 $\mu\text{g}/\text{ml}$ of Na at pH 4.5 and 3.0. The resolution is enhanced

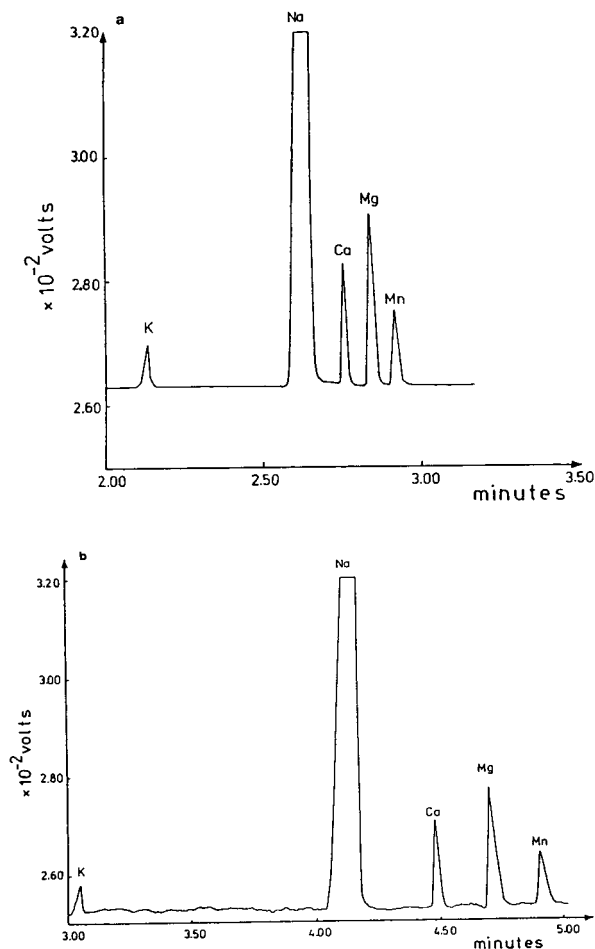


Fig. 3. Separation of 1 $\mu\text{g}/\text{ml}$ each of K, Ca, Mg and Mn and 20 $\mu\text{g}/\text{ml}$ of Na at (a) pH 4.5 and (b) pH 3.0. Experimental conditions as in Fig. 1.

when the pH changes from 4.5 to 3.0. Even at pH 4.5 as much as 20 $\mu\text{g}/\text{ml}$ of Na do not cause any overlap with the rest of the cations and baseline separation is achieved. At pH 3.0 even 40 $\mu\text{g}/\text{ml}$ of Na are well separated from K, Ca and Mg. With UVCat1–HIBA BGE, however, even 10 $\mu\text{g}/\text{ml}$ of Na led to very broad Na peaks [1]. Hence the electromigration dispersion for Na is smaller in the imidazole– H_2SO_4 BGE than in the UVCat1–HIBA BGE.

In Fig. 4, a decrease in pH results in an increase in peak area, although it is less pronounced for K. The increased peak responses are caused by a decreased migration velocity of the sample zone through the detector because peak area is inversely related to the migration velocity [9]. At pH 3.0 the largest peak response,

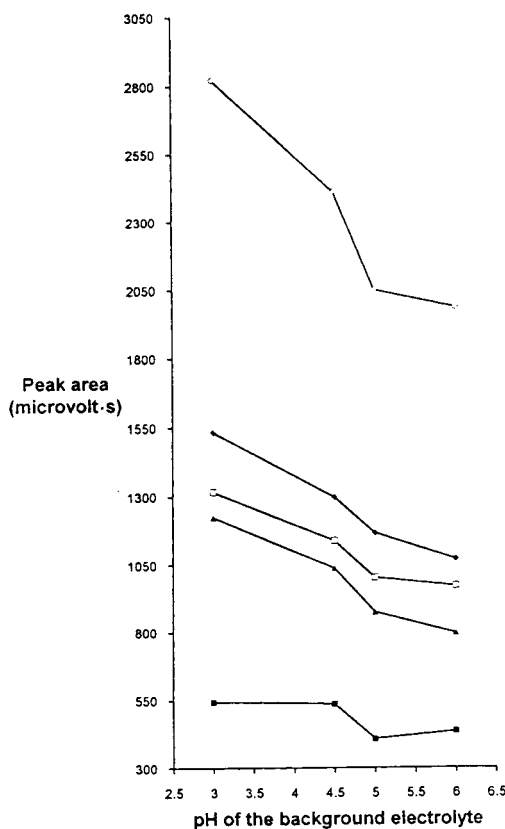


Fig. 4. Dependence of peak areas on the pH of the BGE. Experimental conditions and symbols as in Fig. 1.

and consequently the highest sensitivity, are obtained for all the cations.

3.2. Effect of applied voltage

The relationship between the number of theoretical plates (N) and the applied voltage is as follows [7]:

$$N = \frac{\mu V}{2D} \quad (4)$$

where V is the applied voltage and D is the diffusion coefficient of the solute. N increases with increasing applied voltage and maximum separation efficiency is attained at the highest possible applied voltage. In practice there is a limit to the voltage that can be applied [7].

Fig. 5 shows a plot of the number of theoretical plates (N) for K, Na, Ca, Mg and Mn as a function of applied voltage. N first increases with increased voltage, reaches a plateau at a certain voltage and then drops as the applied voltage is increased further. This is in agreement with the observation of Issaq *et al.* [7] and was explained as the result of increased temperature and the formation of a radial temperature gradient inside the capillary. The higher temperatures result in increased buffer conductivity, solute diffusion coefficient and double-layer thickness and decreased buffer density and viscosity [10]. The net effect of these changes is an increase in solute mobility and a decrease in efficiency. As observed here, the voltage where N reaches a maximum value varies among the cations: 20 kV for K and Ca, 25 kV for Na and 15 kV for Mn. For Mg a larger N was observed at 10 kV. This may be due to the ratio of the electrophoretic mobility, μ , to the diffusion coefficient, D , being a solute-dependent parameter. The mechanism is not clearly understood. It is also observed that the number of theoretical plates is significantly higher for Na and Ca than for K, Mg and Mn, and again Na has the highest N , about 310 000. The explanation is the same as above.

Fig. 6 shows a plot of the resolution as a function of applied voltage. The resolution between K and Na and that between Na and Ca are much higher than the others. A change in the

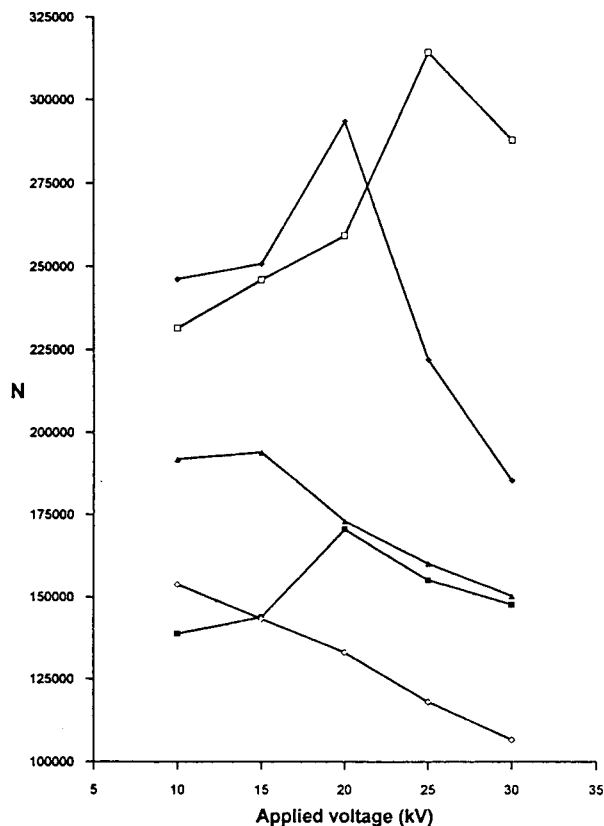


Fig. 5. Effect of applied voltage on the number of theoretical plates (N). BGE, 5 mM imidazole- H_2SO_4 (pH = 4.5); hydrostatic injection, 20 s from 10 cm. K, Na, Ca, Mg and Mn concentrations, 1 $\mu\text{g}/\text{ml}$ each. Symbols as in Fig. 1.

applied voltage has a slight effect on the resolution, as the resolutions between the neighbouring cation pairs change by less than 1 unit when the applied voltage changes from 10 to 30 kV. From the above considerations, a positive voltage of 20 kV was selected for all further experiments.

3.3. Validation of the method

Limit of detection (LOD)

With hydrostatic injection for 30 s, at pH 4.5 the LOD was found to be 100 $\mu\text{g}/\text{l}$ for K, Na, Ca and Mn and 50 $\mu\text{g}/\text{l}$ for Mg, based on three times the baseline noise. With the UVCat1-HIBA BGE [11] the LOD was 135 $\mu\text{g}/\text{l}$ for K,

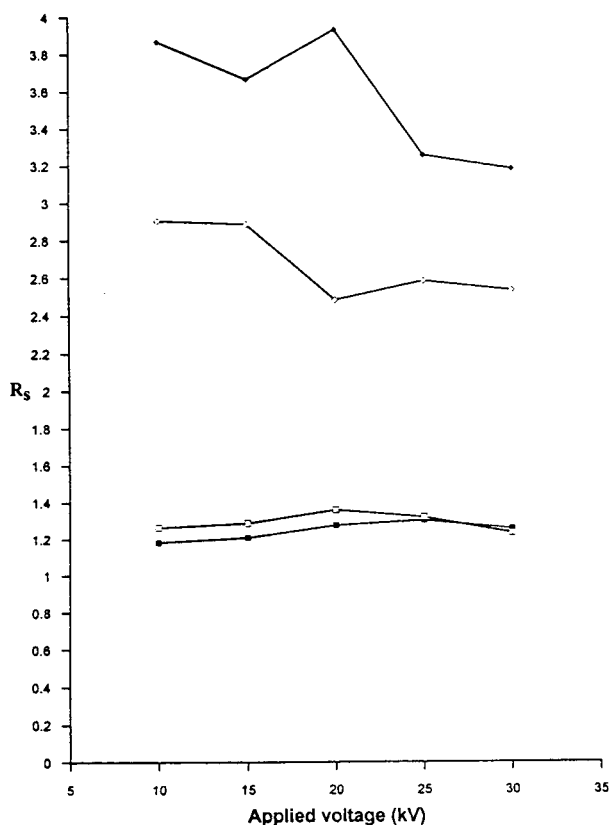


Fig. 6. Effect of applied voltage on the resolution (R_s). Experimental conditions as in Fig. 5. Symbols as in Fig. 2.

110 $\mu\text{g/l}$ for Ca, 100 $\mu\text{g/l}$ for Na, 60 $\mu\text{g/l}$ for Mg and 120 $\mu\text{g/l}$ for Mn. It is concluded that comparable LODs are obtained.

With FAAS, the LOD was 1 $\mu\text{g/l}$ for Ca, 0.1 $\mu\text{g/l}$ for Mg and 1 $\mu\text{g/l}$ for Mn, and using FAES, 3 $\mu\text{g/l}$ for K and 0.1 $\mu\text{g/l}$ for Na [12]. In relative amounts (concentrations) CIA is much less sensitive. However, considering that at least 100 times more sample is needed in FAS than in CIA (in our experiment about a 40-nl sample volume), the minimum detectable absolute amounts are similar.

Linearity of the calibration line

Standard solutions containing 0.5, 1, 3, 5, 7, 10 and 20 $\mu\text{g/ml}$ each of K, Na, Ca, Mg and Mn were prepared. Four injections were performed at each concentration level. Analytical calibra-

tion lines were calculated based on the measurement of the absolute peak areas. Analysis of variance (ANOVA) for lack of fit was used to check the linearity of the calibration lines estimated by the least-squares linear model. The regression equations are $y = 995x + 123$ (K), $y = 2367x + 104$ (Na), $y = 2569x + 245$ (Ca), $y = 4723x + 283$ (Mg) and $y = 2124x + 139$ (Mn), where x = concentration in $\mu\text{g/ml}$ and y = peak area. In all instances, the calculated F value is smaller than the theoretical value, so that the null hypothesis is accepted, that is there is no lack-of-fit: the calibration lines are straight. At pH 3.0 the calibration lines were linear up to 20 $\mu\text{g/ml}$ for K, Na, Ca and 10 $\mu\text{g/ml}$ for Mg and Mn. At high concentrations peak distortion occurred owing to overloading, which caused insufficient selectivity of separation, so that the calibrations were no longer useful. At pH 4.5 the calibration line for Mn was linear only up to 6 $\mu\text{g/ml}$ owing to the insufficient separation between Mn and Mg. In addition, the estimated calibration lines were subjected to statistical evaluation to determine whether or not the intercepts are different from zero [13]. No significant difference was found.

In FAS, owing to the restriction of the Lambert–Beer law, the calibration is linear up to 2 $\mu\text{g/ml}$ for K, 1 $\mu\text{g/ml}$ for Na, 0.5 $\mu\text{g/ml}$ for Mg, 5 $\mu\text{g/ml}$ for Ca and 3 $\mu\text{g/ml}$ for Mn [14]. In this respect CIA is superior.

Precision and accuracy and analysis of multiple electrolyte solutions

The precision of the proposed method was evaluated within day (repeatability) and from day to day (reproducibility). The repeatability was determined first by analysing the two 25- and 50-fold dilutions of the simulated multiple electrolyte concentrate. For each dilution six replicate determinations was carried out. The concentrations were calculated from the same calibration line measured on the same day. Subsequently analysis was performed over 6 days to determine the reproducibility. Each day a new calibration line was measured. The results are given in Table 1. The relative standard deviations (R.S.D.) for the repeatability and repro-

Table 1
Repeatability and reproducibility

	Metal	Calculated ($\mu\text{g/ml}$)	Found ^a ($\mu\text{g/ml}$)	R.S.D. ^b (%)	Recovery ^c (%)
<i>Repeatability</i>					
<i>(n = 6)</i>					
50-fold dilution	K	9.4	9.4	3.2	100
	Na	3.6	3.5	2.2	98
	Ca	3.6	3.5	3.2	96
	Mg	0.9	0.8	2.4	95
25-fold dilution	K	18.7	19.1	2.5	102
	Na	7.1	7.3	1.2	102
	Ca	7.2	7.6	1.5	105
	Mg	1.8	1.8	2.3	103
<i>Reproducibility</i>					
<i>(n = 6 days)</i>					
50-fold dilution	K	9.4	9.6	2.4	102
	Na	3.6	3.6	2.9	99
	Ca	3.6	3.6	5.5	98
	Mg	0.9	0.8	5.4	93
25-fold dilution	K	18.7	18.8	3.4	101
	Na	7.1	7.2	4.9	101
	Ca	7.2	7.1	4.2	98
	Mg	1.8	1.7	3.0	98

Experimental conditions: BGE, 5 mM imidazole–H₂SO₄ (pH 4.5); applied voltage, +20 kV; hydrostatic injection, 30 s from 10 cm.

^a Mean.

^b Relative standard deviation.

^c Result from CIA/calculated value.

ducibility are less than 3 and 6%, respectively. The recoveries range from 93 to 105%. One can conclude that reliable results can be obtained by CIA without the use of an internal standard.

In order to evaluate the precision of the method for real samples, the repeatability was determined for two real electrolyte solutions (see Section 2.5) and the reproducibility for one of them. The data are given in Table 2, where the R.S.D. values indicate that the repeatability is less than 3%. The repeatability for FAS is better than that for CIA. The R.S.D. values for the reproducibility in CIA are less than 4%.

Baseline separation for K, Na, Ca and Mg in a 100-fold dilution of the multiple electrolyte solu-

tion was achieved in the presence of amino acids and glucose. The concentrations of the four cations obtained by CIA and FAS are given in Table 2. The concentrations of K, Na and Mg obtained from both methods are comparable. With CIA, the Ca concentrations are slightly lower than those measured with FAAS. Probably some sample components such as amino acids interact with Ca, causing the deviation [15]. A similar observation was also made by Swaile and Sepaniak [16] in the detection of Zn in blood and was attributed to protein binding. Matrix interferences in CIA are therefore possible and the accurate determination of an element requires a single ionic form. The use of digestion

Table 2
Analysis of real multiple electrolyte solutions for parenteral use

Metal	Found by CIA ($\mu\text{g/ml}$) ^a (n = 6)	Repeatability ^b (%) (n = 6)	Reproducibility ^b (%) (n = 6 days)	Found by FAS ^a ($\mu\text{g/ml}$) (n = 6)	FAS Repeatability ^b (%) (n = 6)
<i>Solution 1</i>					
K	4.4	1.9		4.4	1.2
Na	5.1	0.4		5.3	0.4
Ca	3.1	3.3		3.5	0.3
Mg	0.5	2.5		0.5	0.0
<i>Solution 2</i>					
K	4.4	2.7	2.7	4.4	0.2
Na	2.6	0.9	2.2	2.6	0.4
Ca	1.8	2.2	2.9	2.0	0.3
Mg	0.4	3.3	4.3	0.4	1.0

Experimental conditions: BGE, 5 mM imidazole-H₂SO₄ (pH 4.5); applied voltage, +20 kV; hydrostatic injection, 30 s from 10 cm.

^a Mean. The results are given as the concentrations of the 100-fold dilutions of original samples obtained from the hospital.

^b R.S.D.

to destroy the matrix, extraction to separate the analyte ions from the matrix or perhaps the use of a stronger complexing reagent might solve the problem.

Analysis of beverages

To avoid clogging and contamination of the capillary, diluted orange juice was filtered before analysis. In order to be sure that no analyte elements were left inside the filter membrane and no contamination caused by the filtration, the results obtained with and without the treatment were compared. No significant difference was found.

Baseline separation of K, Na, Ca and Mg was obtained for apple and orange juice. Fig. 7 shows an electropherogram of a 50-fold dilution of orange juice. The repeatability and reproducibility were determined for orange juice and apple juice (Table 3). The repeatability shows R.S.D. values less than 5%. For FAS the repeatability is less than 2%. The R.S.D. values for the reproducibility in CIA are less than 6% for both juices.

The results obtained with CIA and FAS are given in Table 3. The concentrations of K, Na, Ca and Mg obtained by both methods agree well

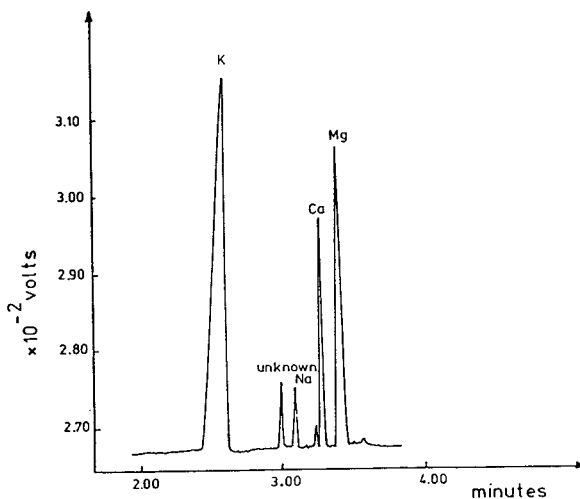


Fig. 7. Separation of a 50-fold dilution of orange juice. BGE, 5 mM imidazole-H₂SO₄ (pH 4.5); applied voltage, +20 kV; hydrostatic injection, 30 s from 10 cm.

Table 3
Analysis of orange juice and apple juice

Metal	Found by CIA ^a ($\mu\text{g/ml}$) ($n = 6$)	Repeatability ^b (%) ($n = 6$)	Reproducibility ^b (%) ($n = 6$ days)	Found by FAS ^a ($\mu\text{g/ml}$) ($n = 6$)	FAS Repeatability ^b (%) ($n = 6$)
<i>Apple juice</i>					
K	20.0	2.5	5.3	18.1	1.8
Na	0.5	3.1	5.5	0.5	1.4
Ca	2.3	1.6	1.2	2.5	1.9
Mg	1.1	3.6	5.5	1.1	1.9
<i>Orange juice</i>					
K	36.8	1.6	4.4	36.6	0.6
Na	0.7	0.7	5.4	0.7	1.1
Ca	2.7	1.4	3.9	2.8	1.3
Mg	2.3	3.4	2.0	2.4	0.2

Experimental conditions: BGE, 5 mM imidazole–H₂SO₄ (pH 4.5); applied voltage, +20 kV; hydrostatic injection, 30 s from 10 cm.

^a Mean. The results are given as the concentrations of the 50-fold dilutions of commercial juices.

^b R.S.D.

but the repeatability of FAS is better than that of CIA.

4. Conclusions

Imidazole was found to be suitable for performing indirect detection of inorganic cations by CIA. With the imidazole–H₂SO₄ BGE, Na shows smaller peak broadening, so that high concentrations of Na present in samples do not interfere with the other cations. The CIA method can be used in the separation of metal cations in complex samples.

The accuracy and precision of CIA with hydrostatic injection are acceptable but that of FAS is better. A wider linear range is obtained in CIA than in FAS. As expected, the limit of detection for CIA is poorer than that for FAS. As in most analytical techniques, matrix effects arise in CIA. The CE method is comparatively more susceptible to matrix interferences and a sample pretreatment may be necessary. However, it is possible in CIA to detect different elements simultaneously, but this is not the case in FAS, thus making the new approach very attractive. CIA may therefore be a promising technique for process analysis.

Acknowledgements

The authors thank Mrs. Anita Vander Straeten for technical assistance and DPWB for financial assistance. Mrs. Betty De Belder of the pharmacy of AZ-VUB is also acknowledged for preparing the pharmaceutical samples.

References

- [1] M. Koberda, M. Konkowski, P. Youngberg, W.R. Jones and A. Weston, *J. Chromatogr.*, 602 (1992) 235.
- [2] F. Foret, S. Fanali, L. Ossicini and P. Boček, *J. Chromatogr.*, 470 (1989) 299.
- [3] W. Beck and H. Engelhardt, *Chromatographia*, 33 (1992) 313.
- [4] J.D. Olechno, J.M.Y. Tso, J. Thayer and A. Wainright, *Int. Lab.*, May (1991) 42.
- [5] C. Schwer and E. Kennedlew, *Anal. Chem.*, 63 (1991) 1801.
- [6] Q. Yang, J. Smeyers-Verbeke and D.L. Massart, *J. Chromatogr. A*, submitted for publication.
- [7] H.J. Issaq, I.J. Aamna, G.M. Muschik and G.M. Janini, *Chromatographia*, 32 (1991) 155.
- [8] J. Vindevogel and P. Sandra, *J. Chromatogr.*, 541 (1991) 483.
- [9] D.K. Altria, *LC·GC*, 6 (1993) 164.
- [10] R.J. Wieme, *A Laboratory Handbook of Chromatography and Electrophoretic Methods*, Van Nostrand Reinhold, New York, 1975.

- [11] A. Weston, P.R. Brown, P. Jandik, A.L. Heckenberg and W.R. Jones, *J. Chromatogr.*, 608 (1992) 395.
- [12] B. Welz, *Atomic Absorption Spectrometry*, VCH, Weinheim, 1985.
- [13] J.C. Miller and J.N. Miller, *Statistics for Analytical Chemistry*, Ellis Horwood, Chichester, 1984.
- [14] *Instructions for Model 372 and Model 373 Atomic Absorption Spectrophotometers*, Perkin-Elmer, Norwalk, CT, 1977.
- [15] O.A. Shpigun and Yu.A. Zolotov, *Ion Chromatography in Water Analysis*, Ellis Horwood, Chichester, 1988.
- [16] D.F. Swaile and M.J. Sepaniak, *Anal. Chem.*, 63 (1991) 179.

Short Communication
1-Thio- β -D-galactose as a chiral derivatization agent for the
resolution of D,L-amino acid enantiomers

Alexandr Jegorov^{*,a}, Jan Tříška^b, Tomáš Trnka^c

^aGalena Co., Research Unit, Branišovská 31, 370 05 České Budějovice, Czech Republic

^bAcademy of Sciences of the Czech Republic, Branišovská 31, 370 05 České Budějovice, Czech Republic

^cDepartment of Organic Chemistry, Charles University, Albertov 6, 128 40 Prague, Czech Republic

(Received January 13th, 1994)

Abstract

o-Phthaldialdehyde in combination with 1-thio- β -D-galactose is a powerful chiral reagent for the precolumn derivatization of primary amino acids. The diastereomers formed can be efficiently resolved on conventional reversed-phase columns. Comparison of 1-thio- β -D-galactose with 1-thio- β -D-glucose revealed that even the change of the configuration of the remote OH group on the sugar moiety influences the resolution of D,L-amino acid derivatives.

1. Introduction

Fungi and bacteria produce biologically active compounds in which D-amino acids are sometimes present. The slow racemization of L-amino acids in biological material leads to D-amino acids. These acids also form undesirable side-products, for example, in peptide synthesis. In all instances an appropriate analytical method is necessary to control the enantiomeric purity of either natural or synthetic products. A number of methods have been developed for this purpose, based on chiral stationary phases which are usually designed to resolve a group of enantiomers [1]. A different approach consists in the use of chiral derivatization agents, the target reaction of which produces diastereomers which can be resolved on conventional columns; sever-

al such reagents have already been described for the determination of D,L-amino acids [2–5]. Sugars represent a natural source of easily accessible chiral compounds, the derivatives of which retain their chirality and might be used, therefore, as suitable derivatization agents. The derivatization of D,L-amino acids with the sodium salt of 1-thio- β -D-glucose has been described [6]. The aim of this work was to evaluate the effect on chiral recognition of changing the OH group configuration on the C-4 atom of the sugar moiety.

2. Experimental

2.1. Instrumentation and chromatographic conditions

A Varian Vista 5500 liquid chromatographic

* Corresponding author.

system equipped with a Rheodyne Model 7126 injection valve, a DS 604 data station and a Fluorichrom filter fluorescence detector was used. The excitation wavelength was 360 nm and the emission wavelength was a bandpass above 420 nm. The analytical columns were LiChrosorb RP-8 (5 μm) (250 \times 4 mm I.D.) from Merck (Darmstadt, Germany) and a Separon SGX C8 (5 μm) (150 \times 3 mm I.D.) glass column from Tessek (Prague, Czech Republic). A back-pressure terminator (Varian, Sunnyvale, CA, USA), set at 0.6 MPa, was used to prevent the formation of bubbles.

Solvent A was 0.05 M sodium acetate adjusted to pH 6.10 with acetic acid and solvent B was 0.1 M sodium acetate (pH 7.60)–methanol (1:9). Both solvents were carefully degassed prior to use. Isocratic elution with solvent A was carried out for 8 min, then a 47-min linear gradient to 45% A and 55% B was applied, followed by a column wash with a linear gradient to 100% B in 5 min. A constant flow-rate of 1.20 ml/min was maintained during the analysis. The column was thermostated at 35°C. Stability studies were performed with a Bio-Rad (Richmond, CA, USA) AS-100 HRLC automatic sampling system and a Hypersil ODS (60 \times 4.6 mm I.D.) column from Hewlett-Packard (Amstelveen, Netherlands) under isocratic conditions.

2.2. Chemicals and derivatization procedure

The sodium salts of 1-thio- β -D-galactose and 1-thio- β -D-glucose were prepared as described previously [7,8]; *o*-phthaldialdehyde (Calbiochem, Los Angeles, CA, USA), amino acids (Calbiochem or Sigma, St. Louis, MO, USA), methanol, boric acid, potassium hydroxide and sodium acetate (Lachema, Brno, Czech Republic) were used.

Stock solutions were prepared weekly with 50 mg of sodium salts of thiosugars in 1 ml of water, 50 mg of *o*-phthaldialdehyde (OPA) in 1.25 ml of methanol and amino acids (4 mM in water). Borate buffer was prepared by dissolving 0.50 g of boric acid in 19 ml of water and adjusting the pH to 9.30 (8.20 or 10.40) with potassium hydroxide solution (45 g of potassium hydroxide

in 100 ml of water). A 10- μl sample of the amino acid solution, 100 μl of the borate buffer, 50 μl of the thiosugar solution and 50 μl of the OPA solution (thiosugar/OPA = 2.2) were added consecutively to a small glass vessel with Hamilton syringes, and the mixture was thoroughly stirred. After 60 s a 10- μl aliquot was analysed.

2.3. Absorbance and fluorescence measurements

The derivatives for the absorbance measurements were obtained from the chromatographic fractions containing the desired enantiomers. A volume of the eluate corresponding to the peak of the each separated stereoisomer of the 1-isoindolyl-(1-thio- β -D-glycoside) was placed manually into a small vial and measured with a Varian DMS 300 double-beam UV–Vis spectrophotometer. The reference solutions were appropriate mixtures of solvents A and B. The fluorescence spectra were measured employing a Hewlett-Packard Model 1090 liquid chromatograph connected with an HP 1046 fluorescence detector. The excitation wavelength was set at 360 nm and the emission wavelength at 420 nm.

3. Results and discussion

Amino acids bearing primary amino groups form highly fluorescent compounds after derivatization with OPA in the presence of a thiol. By analogy with the reaction of mercaptoethanol [9] or glutathione [10], 1-isoindolyl-(1-thioglycosides) are assumed to be formed in the course of the reaction of amino acids, OPA and thiosugars. The reactions occurred rapidly and quantitatively at ambient temperature, reaching their maximum fluorescence within 1 min (Fig. 1). Our experience indicated that repeated injections of basic buffers may quickly cause the column performance to deteriorate. Therefore, the use of buffers with pH above 9.5 should be avoided or the derivatization mixture should be diluted with acidic buffer before injection. Similarly as with OPA–2-mercaptoethanol derivatives [11–14], thiosugar-substituted isoindoles were un-

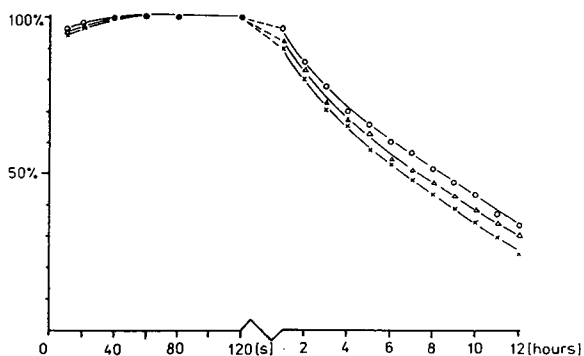


Fig. 1. Fluorescence response of OPA-1-thio- β -D-galactose derivatization as a function of reaction time and pH ($\times = 8.2$; $\Delta = 9.3$; $\circ = 10.0$) and stability of the selected derivative in borate buffer at 20°C (mixture: 10 μ l of 4 mM L-alanine, 200 μ l of borate buffer, 50 μ l of thiosugar solution, 50 μ l of OPA solution). The ordinate (relative %) refers to the area of the chromatographic peak obtained by the analysis of the reaction mixture injected after 60 s (100%). Conditions: Hypersil ODS (3 μ m) column (60 \times 4.6 mm I.D.); isocratic elution with 0.05 M sodium acetate (pH 6.3)–methanol (65:35, v/v); flow-rate, 0.5 ml/min.

stable. The stability of these isoindoles was found to decrease with decreasing pH.

The detection limit for L-Ala, based on a signal-to-noise ratio of 2, was less than 10 pmol. The relative standard deviations of the retention times with OPA-1-thio- β -D-glucose were 0.72% (Ala), 0.48% (Val) and 0.65% (Leu) for eleven analyses of insect haemolymph [15] within 2 days. The average relative deviations for various thiosugar derivatives were less than 5% for between-day assays and less than 3% for within-day assays, which shows that the present method is highly reproducible. The determination of amino acids is relatively easy when large samples are available (>100 pmol). Problems associated with the analysis increase with diminishing sample size and are largely due to impurities in the OPA reagent, old samples of thiosugar solutions and the chemical instability of the isoindoles in the solution.

The successful separation diastereomeric isoindoles on a conventional reversed-phase column has been reported with 2,3,4,6-tetra-O-acetyl-1-thio- β -D-glucose [2] and 1-thio- β -D-glucose [6]. In the same way, OPA-1-thio- β -D-galactose can be used as a chiral derivatization reagent. Fig. 2a

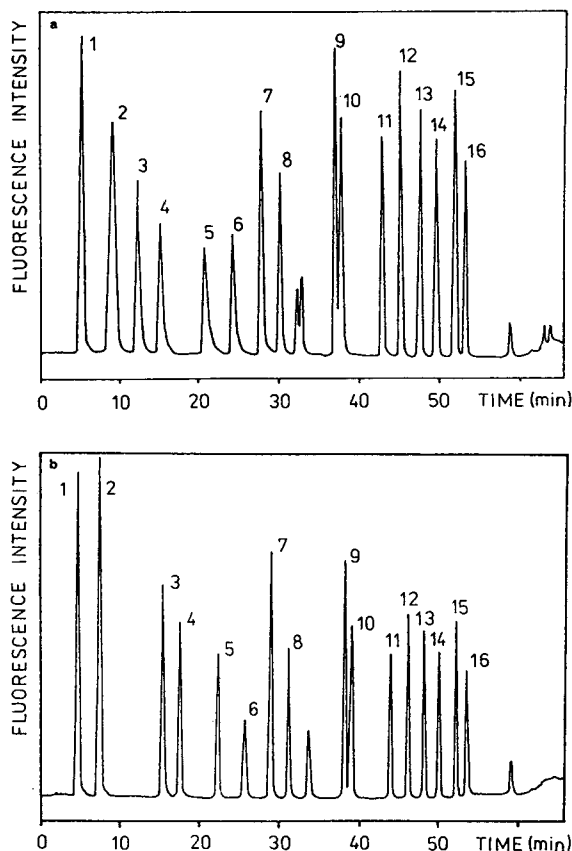


Fig. 2. Separation of amino acids enantiomers after derivatization with OPA-1-thio- β -D-galactose reagent. Conditions: mobile phase A, 0.05 M sodium acetate buffer (pH 6.10); B, 0.1 M sodium acetate (pH 7.60)–methanol (1:9, v/v); columns: (a) Merck LiChrosorb RP-8 (5 μ m) (250 mm \times 4 mm I.D.), isocratic elution, 100% A for 8 min, linear gradient to 45% A in 55 min and 0% A in 60 min, flow-rate 1 ml/min; (b) Tessek Separon SGX C₈ (5 μ m) (150 \times 3 mm I.D.), linear gradient elution from 100% A at 0 min to 30% A at 55 min, flow-rate 0.5 ml/min. Peaks: 1 = D,L-Asp; 2 = D,L-Glu; 3, 4 = L-, D-Ser; 5, 6 = L-, D-Tre; 7, 8 = L-, D-Ala; 9, 10 = L-, D- α -amino-*n*-butyric acid; 11, 12 = D-, L-Val; 13, 14 = L-, D-Phe; 15, 16 = L-, D-Leu. Each peak represents 2 nmol.

shows the separation of some amino acid enantiomers, the resolutions and elution orders for which are given in Table 1, in comparison with those obtained with 1-thio- β -D-glucose. The type of RP column is not critical to achieve the resolution of amino acid enantiomers, but because a methanol–buffer mixture causes a

Table 1
Resolution and retention times of various diastereomeric OPA–thiosugar derivatives

Amino acid	Derivatization reagent					
	1-Thio- β -D-glucose			1-Thio- β -D-galactose		
	t_r (min)		Resolution	t_r (min)		Resolution
	L-	D-		L-	D-	
Asp	5.3	4.9	0.64	4.6		0
Glu	11.3	12.6	1.24	8.9		0
Ser	16.0	18.4	2.18	12.1	15.2	3.29
Tre	23.3	26.6	5.20	20.7	24.2	4.13
Ala	30.1	32.7	4.35	27.7	30.1	4.48
Arg	31.5	32.0	0.76	29.9	30.3	0.58
Tyr	38.4	38.8	0.25	37.1	37.8	0.85
α -n-Abu	38.7	39.7	1.74	37.0	37.8	1.33
Val	46.6	45.1	2.84	45.4	43.0	4.28
Nva	46.4	47.5	1.76	44.9	45.9	1.73
Trp	46.6	47.5	1.52	45.1	46.8	3.19
Phe	48.8	50.4	3.03	47.6	49.6	3.53
Ile	52.8	51.6	1.62	52.2	51.8	1.75
Leu	53.0	53.9	1.75	51.8	53.1	2.31
Nle	53.1	54.0	1.73	52.2	53.1	1.67
Lys		56.9	0	55.5	54.2	2.61

For chromatographic conditions, see Experimental. $t_0 = 1.15$ min (NaNO_3); resolution = $1.177(t_2 - t_1)/[w_{1/2(1)} + w_{1/2(2)}]$.

relatively high back-pressure, the use of short columns is preferred. Particularly good resolution was obtained with 150×3 mm I.D. columns and a slightly modified gradient programme (Fig. 2b).

The enantiomers of most primary amino acids were baseline resolved. Some separations might be further improved by changing the pH of the buffer, because the capacity factors of some derivatives, e.g., Asp, Glu and Arg, are pH dependent. Generally, the 1-thio- β -D-galactose derivatives were slightly less hydrophobic and were eluted earlier than the 1-thio- β -D-glucose derivatives. Although the thiosugars differ only in the configuration of the OH group on the C-4 atom, i.e., on the remote hydroxy group with respect to the bond of the isoindole moiety, this influences the resolution of some D,L-amino acid enantiomers. As is evident from this comparison, “long-range” interactions between the amino acid residue and the sugar moiety take place, and the change in configuration of the OH group

may alter the mechanism of resolution. This effect was illustrated by the different resolutions of Lys, Asp and Glu. In addition, it is well known that no reagent has general applicability, and the potential advantage of 1-thio- β -D-galactose as a chiral reagent consists in the improved resolution of some enantiomeric pairs, e.g., Ser, Val or Trp. The method can possibly be applied also to the routine determination of amino acids in biological fluids or peptide hydrolysates, as most L-amino acids are baseline separated [15]. In analysis, derivatives of biogenic amines and urea were eluted later than amino acids, whereas amino sugars, e.g., galactosamine or glucosamine, were eluted between Ser and Tre and thus can be determined simultaneously.

The D- and L-derivatives of amino acids usually exhibited a slightly different fluorescence response. 1-Thio- β -D-galactose and 1-thio- β -D-glucose and most L-amino acids formed derivatives the chromatographic peaks of which had about 5–20% greater areas whether or not they

were eluted first or second from the enantiomeric pair (Fig. 2). To elucidate this difference, D,L-enantiomers of Asp, Ser, Arg, Tyr, Trp and Phe were chosen as different types of amino acids for UV absorbance and fluorescence measurements of their corresponding 1-isoindolyl-(1-thioglycoside) derivatives (Fig. 3). In addition to small differences caused by the substituents themselves, all derivatives exhibited in the range 200–400 nm broad maxima at 333 nm with a shoulder at 347 nm, which is in accordance with data published for other isoindoles [9]. The fluorescence characteristics of the derivatives were measured with the excitation wavelength set at 360 nm. The emission spectra thus obtained were very similar in shape to those of UV spectra, with a broad maximum at 420 nm. This indicates the significance of the isoindolyl ring system for the course of both UV and fluorescence spectra and minimal influence of the

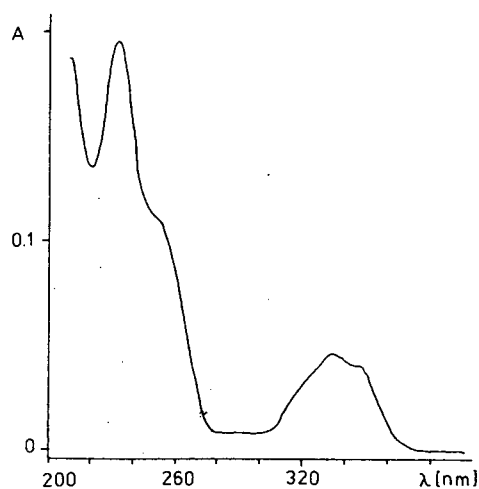


Fig. 3. UV spectrum of 1-isoindolyl-(1-thio- β -D-galactoside) derivative with L-phenylalanine.

substituents. The small differences in the fluorescence intensities of the D,L-derivatives, therefore, probably originate from the different local arrangements of substituents around the isoindolyl moiety in individual diastereomers. This effect is in fact the same as that of changing the solvent on the fluorescence intensity.

References

- [1] R. Däppen, H. Arm and V.R. Meyer, *J. Chromatogr.*, 373 (1986) 1.
- [2] S. Einarsson, S. Folestad and B. Josefsson, *J. Liq. Chromatogr.*, 10 (1987) 1589.
- [3] R.H. Buck and K. Krummen, *J. Chromatogr.*, 387 (1987) 255.
- [4] M.R. Euerby, L.Z. Partridge and W.A. Gibbons, *J. Chromatogr.*, 483 (1989) 239.
- [5] H. Nishi, K. Ishii, K. Taku, R. Shimizu and N. Tsumagari, *Chromatographia*, 27 (1989) 301.
- [6] A. Jegorov, J. Triska, T. Trnka and M. Černý, *J. Chromatogr.*, 434 (1988) 417.
- [7] M. Černý, J. Staněk and J. Pacák, *Monatsh. Chem.*, 94 (1963) 290.
- [8] M. Černý and J. Pacák, *Collect. Czech. Chem. Commun.*, 26 (1961) 2084.
- [9] S.S. Simons and D.F. Johnson, *J. Org. Chem.*, 43 (1978) 2886.
- [10] G. Morineau, M. Azoulay and F. Frappier, *J. Chromatogr.*, 467 (1989) 209.
- [11] B.N. Jones, in E. Shively (Editor), *Methods of Protein Microcharacterization*, Humana Press, Clifton, NJ, 1986, Ch. 5, p. 121.
- [12] J.C. Hodgkin, P.Y. Howard, D.M. Ball, C. Cloete and L. De Jager, *J. Chromatogr. Sci.*, 21 (1983) 503.
- [13] W.A. Jacobs, *J. Chromatogr.*, 392 (1987) 435.
- [14] B.J. Micallef, B.J. Shelp and R.O. Ball, *J. Liq. Chromatogr.*, 12 (1989) 1281.
- [15] R. Hanzal and A. Jegorov, *Comp. Biochem. Physiol. A*, 100 (1991) 957.



ELSEVIER

Journal of Chromatography A, 673 (1994) 291–294

JOURNAL OF
CHROMATOGRAPHY A

Short Communication

Simultaneous determination of cobalt and nickel by reversed-phase high-performance liquid chromatography with diethyldithiocarbamic acid[☆]

V. González Rodríguez, J.M. Castro Romero*, J.M. Fernández Solís,
J. Pérez Iglesias, H.M. Seco Lago

Department of Analytical Chemistry, University School Polytechnic of Ferrol, University of La Coruña, 15405 Ferrol, Spain

(First received December 6th, 1993; revised manuscript received February 27th, 1994)

Abstract

The reagent diethyldithiocarbamic acid has been examined for the high-performance liquid chromatographic separation of cobalt(II) and nickel(II) chelates on reversed-phase HPLC columns (150 × 3.9 mm) packed with Nova-Pak C₁₈, 4 μm. The metal-diethyldithiocarbamic chelates were preconcentrated by solvent extraction. An aliquot of sample containing copper, cobalt and nickel in a mixture was transferred to a well-stoppered test tube to which was added reagent [diethyldithiocarbamic acid 0.5% in ethanol–water (1:1), pH 10] and 10 ml organic solvent (diethyl ether). After shaking with mechanical shaker for 5 min, the organic layer was separated and 0.1 ml transferred to another tube containing methanol (1 ml). The methanolic solution (15 μl) was injected, on the reversed-phase HPLC column. The complexes are eluted with methanol–water (75:25) at a flow-rate of 0.5 ml min⁻¹. The detection is carried out with a UV detector at 260 nm. The method shows several advantages: short analysis time, minimized sample preparation, minimized effect of interfering ions, a low detection limit (50 ppb for nickel and 5 ppb for cobalt) and good reproducibility, making it suitable for many types of samples, including alloys.

1. Introduction

The analysis of single or multiple metal ions in trace amounts in environmental matrices is a general problem. As a result many methods for the preconcentration of metal ions have been described [1,2]. Of these, solvent extraction has been, until recently, the most popular method.

Liquid–liquid extraction is a simple and convenient approach in separation science and it is one of the most frequently used sample pre-treatment techniques in the determination of trace metals. In previous steps complexes of metal ions can be obtained, to increase the sensitivity [3]. Diethyldithiocarbamic acid is a widely used organic chelating reagent. Most of the chelates formed by this reagent are coloured and can be extracted into a variety of organic solvents.

A wide variety of techniques have been described for the determination of metal chelates. Spectroscopic methods are by far the most popu-

* Corresponding author.

[☆] Presented at the 22nd Annual Meeting of the Spanish Chromatography Group, Barcelona, October 20–22, 1993.

lar but this traditional method requires that the complexing agent is available in highly pure form and of sufficiently high solubility in the liquid medium used in the investigation. In addition, the absorption wavelengths of the ligand and complex will be very difficult to measure accurately. Liquid chromatography may be able to make up for this deficiency. These complexes of metal ions can be separated by high-performance liquid chromatography (HPLC) [4–7]. Khuhawar and Soomro [5] have examined the reagent bis(acetyl-pivalylmethane)ethylenediamine for the HPLC separation of metal chelates with UV detection. A HPLC technique for the determination of metals as their 8-hydroxyquinolinate complexes using spectrophotometric detection at 400 nm is described by Ryan and Meaney [6].

Presently the application of reversed-phase (RP) HPLC to the determination of metal chelates is a promising alternative approach for overcoming the lack of selectivity of the chelating reagents. HPLC has attractive advantages such as high sensitivity, selectivity and simultaneous detection capability.

In this paper, a new simultaneous determination of cobalt(II) and nickel(II) by RP-HPLC is described, with previous solvent extraction with diethyl ether and diethyldithiocarbamic acid as reagent. Separation of chelates and ligand was carried out by RP-HPLC using UV detection.

2. Experimental

2.1. Chromatographic instrumentation

The liquid chromatographic system consisted of a Waters Model 501 pump, a Waters 486 UV-Vis spectrophotometric detector, a Waters Model U6K universal liquid chromatograph injector, and a Waters 746 data module integrator. The column used was a Waters Nova-Pak C₁₈ (150 × 3.9 mm) filled with dimethyloctadecylsilyl-bonded amorphous silica (particle size 4 μm).

2.2. Materials

All the chemicals used were of analytical-reagent grade. Methanol was supplied by Merck. The water was purified using a Milli-Q system (Millipore). Analytical-reagent grade sodium diethyldithiocarbamate (trihydrate) (Merck) was used. All metal salt solutions were prepared by dilution of the 1000 ppm stock standard solutions (Merck atomic absorption grade).

2.3. Sample preparation

An aliquot of sample containing cobalt and nickel in a mixture was transferred to a well-stoppered test tube to which was added reagent [diethyldithiocarbamic acid 0.5% in ethanol-water (1:1), pH 10] and 10 ml organic solvent (diethyl ether). After shaking with a mechanical shaker for 5 min, the organic layer was separated and 0.1 ml transferred to another tube containing methanol (1 ml).

2.4. Chromatographic procedures

The eluent used was methanol-water (75:25). The flow-rate of the eluent was 0.5 ml min⁻¹ (3000 p.s.i.; 1 p.s.i. = 6894.76 Pa). It was monitored at 260 nm. The methanolic solution of the sample (15 μl) was injected on the RP-HPLC column.

3. Results and discussion

3.1. Chromatographic separation

Among the metal ions tested, the diethyldithiocarbamic chelates of cobalt(II) and nickel(II) yielded good peaks on the chromatogram, as shown in Fig. 1. Complete separation between chelate reagent and the two chelates was obtained. The Ni(II) chelate is eluted first and the cobalt(II) chelate is eluted second.

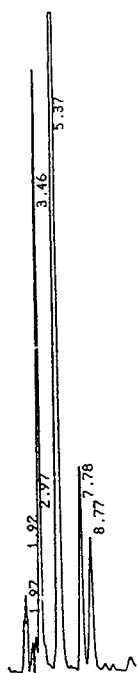


Fig. 1. HPLC separation of diethyldithiocarbamic acid chelates of Ni(II) (1 ppm) and Co(II) (0.1 ppm). Column, Nova-Pak C₁₈ (150 × 3.9 mm); eluent, methanol–water (75:25); flow-rate 0.5 ml min⁻¹; detection wavelength, 260 nm; injection volume, 15 μl. Peaks: solvent (*t_R* 3.46 min); reagent (5.37 min); Ni(II) (7.78 min); Co(II) (8.77 min).

The effects of variation in chelate reagent concentration, pH, temperature, interferences and the reproducibility were investigated for the extraction of 0.1 ppm of cobalt and 1 ppm of nickel.

3.2. Influence of diethyldithiocarbamic acid concentration

The influence of diethyldithiocarbamic acid concentration on the chelates is shown in Fig. 2. To form the chelate are necessary 2 ml of chelating reagent. This amount allows an extraction of cobalt(II) and nickel(II) quantitatively and reproducibly. The composition of the chelates was 1:2 (metal:ligand).

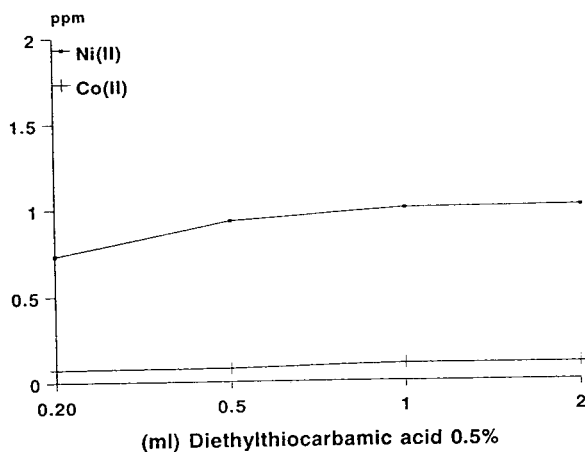


Fig. 2. Influence of diethyldithiocarbamic acid concentration on the extraction of chelates. Other conditions as in Fig. 1.

3.3. Influence of the pH, temperature and stability

The extraction capacity of the chelate were investigated in the pH range 1.6–10.2. Chelates of cobalt(II) and nickel(II) in acidic or in basic solution are extracted in a similar way. But the peak of nickel(II) chelates showed irregular interferences in the pH range 1.5–6.0. For analytical purposes the optimum working range is pH 6.5–10.

With increasing temperature the amount of detected metal ions decreases, mainly nickel(II) chelates (Fig. 3).

The detector response to freshly prepared and “aged” standard solutions of the metal chelates was similar for periods up to 4 h. Concentration values for cobalt(II) and nickel(II) chelates remained constant.

3.4. Calibration and detection limits; reproducibility

A linear calibration was obtained from injections of 0.01–1 ppm for cobalt(II) and 0.1–5 ppm for nickel(II):

$$\text{Ni(II)}: y = 2.0 \cdot 10^5 x - 1.5 \cdot 10^4; r = 0.9997$$

Table 1
Reproducibility

	Ni(II) (1 ppm)	Co(II) (0.1 ppm)	Ni(II) (5 ppm)	Co(II) (0.5 ppm)
	198848	152205	996782	882115
	191879	151169	988993	955453
	207724	157520	1164932	924668
	187730	158266	1046346	924550
	195130	148623	1148486	961243
	177638	142858	1072428	923219
	187531	149359	1082664	927743
Mean	198354	151429	1071519	928427
R.S.D. (%)	5.0	3.5	6.4	2.7

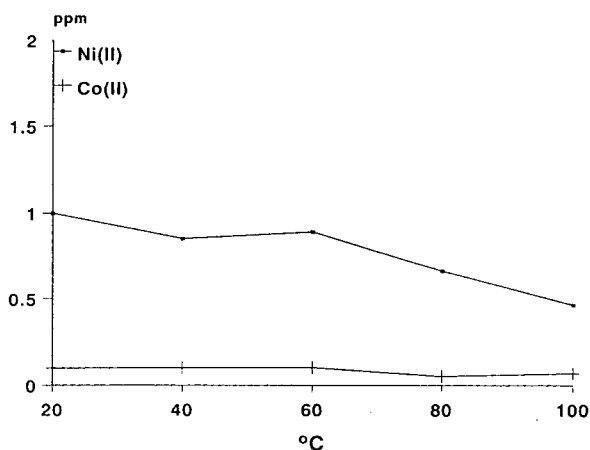


Fig. 3. Influence of temperature on the extraction of chelates. Other conditions as in Fig. 1.

$$\text{Co(II)}: y = 1.5 \cdot 10^6 x - 7.5 \cdot 10^3; r = 0.9999$$

The detection limits (signal-to-noise ratio 3) were 5 ppb for cobalt(II) and 50 ppb for nickel(II).

These values demonstrate the reproducibility of the method. Data are shown in Table 1.

3.5. Interferences

The effect of foreign species on the determination of Co(II) and Ni(II) was studied. A level of 10 ppm of Zn(II), Cd(II), Mg(II), Mn(II), Li(I), Hg(II) and Na(I) is tolerated in the determination. However, the determination of Co(II) and Ni(II) is interfered by a level of 10

ppm of Se(IV), Ba(II), Be(II), Ca(II), Sr(II), K(I) and Ag(I).

4. Conclusions

Trace enrichment of metal ions using solvent extraction is an effective tool for the enhancement of sensitivity and selectivity when applied to the analysis of trace metals as their diethyldithiocarbamate complexes.

The method shows several advantages: short analysis time, simultaneous determination minimizes analysis time, and it decreases the time spent in sample preparation, minimized effect of interfering ions, and a good reproducibility.

References

- [1] M. Valcárcel and A. Gómez (Editors), *Técnicas Analíticas de Separación*, Reverté, Barcelona, 1988, pp. 1–51.
- [2] J.P. Brunette and M.J.F. Leroy, *Analisis Mag.*, 20 (1992) M30.
- [3] F. Bermejo, in H.A. Flaschka and A.J. Barnard (Editors), *Chelates in Analytical Chemistry*, Vol. 5, Marcel Dekker, New York, 1976, pp 1–33.
- [4] G. Bazylak and J. Maslowska, *Analisis*, 20 (1992) 611.
- [5] M.Y. Khuhawar and A.I. Soomro, *Talanta*, 39 (1992) 609.
- [6] E. Ryan and M. Meaney, *Analyst*, 117 (1992) 1435.
- [7] N. Uehara, K. Morimoto and Y. Shijo, *Analyst*, 117 (1992) 977.



ELSEVIER

Journal of Chromatography A, 673 (1994) 295–298

JOURNAL OF
CHROMATOGRAPHY A

Short Communication

Capillary gas chromatography method for the analysis of the *trans* isomers of ceralure, a medfly attractant

Albert B. DeMilo*, J. David Warthen, Jr., Barbara A. Leonhardt
US Department of Agriculture, ARS, PSI, Insect Chemical Ecology Laboratory, Beltsville, MD 20705, USA

(First received February 2nd, 1994; revised manuscript received April 6th, 1994)

Abstract

A capillary GC method has been developed to analyze laboratory or commercial samples of the medfly attractant ceralure [ethyl 4- (and 5-)iodo-*trans*-2-methylcyclohexane-1-carboxylate]. The method utilizes a specially prepared fused-silica column with a bonded phenyl-methyl polysiloxane liquid phase. Baseline separation was achieved for three of the four *trans*-ceralure isomers. Difficulties encountered with other columns investigated are also discussed.

1. Introduction

Ceralure [ethyl 4- (and 5-)iodo-*trans*-2-methylcyclohexane-1-carboxylate] is a potent and persistent synthetic attractant for the Mediterranean fruit fly, *Ceratitis capitata* (Wiedemann) [1–3], commonly referred to as the medfly. The medfly, a worldwide pest, feeds on 253 varieties of fruit, nuts and vegetables [4] and if established in California, the total yearly recurrent costs for crop damage are estimated to be as much as US\$ 756 089 000 [5]. Early warning systems to detect medfly infestations involve traps baited with the synthetic attractant trimedlure [TML, 1,1-dimethylethyl 4- (and 5-)chloro-*trans*-2-methylcyclohexane-1-carboxylate] [6]. Although TML has proven extremely useful in the medfly surveillance program, research to discover attractants

with unusual properties that may lead to novel detection and/or control techniques, still continues. The highly persistent nature of ceralure (an iodo analogue of TML) combined with its inherent activity has stimulated considerable interest in this attractant and, as a result, large-scale field trials were recently initiated to exploit these properties.

Methods used to synthesize TML [6] and ceralure [1,2] result in mixtures containing a preponderance (90–95%) of the four *trans* isomers A, B₁, B₂ and C (see Fig. 1) [7]. The *trans* refers to the configurational relationship of the methyl and ester moieties on the cyclohexane ring and descriptors A, B₁, B₂ and C refer to relative order of gas chromatographic (GC) retention times arbitrarily assigned for TML [8]. The remainder (5–10%) of the synthetic mixture is usually comprised of the four *cis* isomers [*i.e.*, for TML 1,1-dimethylethyl *cis*- and *trans*-4- (and

* Corresponding author.

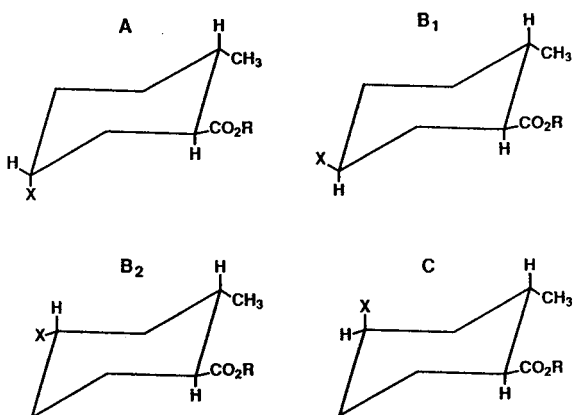


Fig. 1. Structures of the *trans* isomers of ceralure and trimedlure. Ceralure: X = I, R = ethyl; trimedlure: X = Cl, R = 1,1-dimethylethyl.

5-)chloro-*cis*-2-methylcyclohexane-1-carboxylate] [6]. Medfly attractancy to TML or ceralure is correlated with orientation (*i.e.*, position, configuration) of the halogen, methyl and ester moieties. For example, while the C isomer [7,9] is the most attractive isomer in TML (specifically the 1*S*,2*S*,4*R*-enantiomer [10,11]), the B₁ isomer is the most attractive in ceralure [2,12,13].

Since the relative distribution of the four *trans* isomers in ceralure is influenced by variations in synthetic procedures [2], an accurate method to detect and quantify these isomers is indispensable to the optimization of the synthesis procedure and the success of pest management programs using this attractant. High-performance liquid chromatography (HPLC) was used on a semi-preparative scale to separate the four *trans* isomers [14]; isomers B₁ and B₂ were separated directly, while isomers A and C were separated as their *tert*-butyl esters and then subsequently converted to their corresponding ethyl esters. A GC method using a packed-column was also reported [14] for *trans*-ceralure isomers but retention times were too close to effect an accurate analysis. We wish to report here an efficient capillary GC method to determine the *trans* isomer content of ceralure mixtures.

2. Experimental

2.1. Materials and sample preparation

The ceralure standard, >50% in B₁ and B₂ isomers, was synthesized from predominantly (90–95%) *trans*-6-methyl-3-cyclohexenecarboxylic acid (Albany International, Columbus, OH, USA) according to published procedures [2]. Distillation afforded a pale-yellow liquid, b.p. 81°C (0.15 mmHg; 1 mmHg = 133.322 Pa), *n*_D(25°C) 1.5130. The standard was stored in an amber-colored vial over copper wire.

Ceralure B₁ (ethyl *cis*-5-iodo-*trans*-2-methylcyclohexane-1-carboxylate) and ceralure B₂ (ethyl *trans*-4-iodo-*trans*-2-methylcyclohexane-1-carboxylate) were obtained by semi-preparative HPLC [14]. Ceralure A (ethyl *trans*-5-iodo-*trans*-2-methylcyclohexane-1-carboxylate) and ceralure C (ethyl *cis*-4-iodo-*trans*-2-methylcyclohexane-1-carboxylate) were obtained by converting their corresponding *tert*-butyl ester isomers [14] to free acids, then to acid chlorides and finally to the desired ethyl esters. A technical grade amber-colored sample of ceralure [*n*_D(25°C) 1.5165] was obtained from AgriSense/Biosys (Fresno, CA, USA).

Samples for analyses were prepared by dissolving 1 μl of a standard or test material in 100 μl of acetone (Fisher A19-4); 0.25 μl of pure isomer standard or 1 μl of ceralure standard or test material was injected into the column.

2.2. Capillary gas chromatography

Samples were analyzed on a Shimadzu GC-9A chromatograph (Columbia, MD, USA), equipped with a flame ionization detector and Shimadzu C-R4A data processor. The column was a specially prepared SPB-608 column (Supelco, Bellefonte, PA, USA); 60 m × 0.25 mm I.D. × 0.25 μm film. The stationary phase is a proprietary blend of bonded methyl and phenyl polysiloxanes. GC conditions were: column temperature 180°C (isothermal), injector/detector temperature 220°C and carrier gas (helium) head pressure 2.0 kg/cm² (19.4 cm/s linear velocity at

180°C). Samples were injected in the split mode (1:100).

2.3. GC–MS analyses

Electron impact (EI) spectra were recorded on a Hewlett-Packard 5971A mass spectrometer equipped with the identical specially prepared SPB-608 column. GC conditions for the mass spectrometer were identical to those described for the GC analysis of ceralure.

3. Results and discussion

Ceralure's reported [14] instability during capillary GC analysis was not unexpected since many iodo compounds are susceptible to various photolytic, hydrolytic, thermolytic or oxidative decomposition processes. Although TML has been successfully analyzed by capillary GC on a Carbowax 20M column [15], attempts to analyze ceralure on a 60-m Supelcowax-10 (Supelco) column were unsuccessful. Ceralure isomers eluting from this column, although well resolved, showed signs of decomposing (A and C mostly). Similar results were observed with a 60-m dicyanopropyl polysiloxane SPB-2340 (Supelco) column.

Decomposition by these polar columns did not appear to be thermally induced (*i.e.*, excessive column/injector temperatures) but rather seemed to be caused by build up of column contaminants. This hypothesis was supported by the facts that decomposition increased with increased column use and was eliminated (or substantially reduced) by washing poorly performing columns with polar solvents.

Although non-polar methyl polysiloxane columns failed to resolve the ceralure isomers, medium-polarity columns were substantially more effective. For example, near-baseline separation and good peak symmetry were achieved by either a 60-m SPB-35 (Supelco) or a 15-m DB-17 (Durabond) column. Optimum results, however, were obtained with a specially prepared 60-m phenyl-methyl polysiloxane SPB-608 column operated at isothermal conditions. Fig. 2

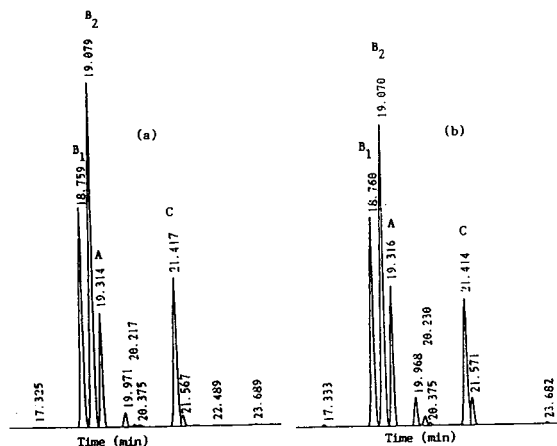


Fig. 2. GC traces of ceralure standard (a) and commercial ceralure (b). B₁, B₂, A and C identify specific isomers.

shows typical GC traces on the SPB-608 column for a ceralure standard and commercial sample. Retention times (min) for the isomers, in order of elution, were B₁ (18.76), B₂ (19.08), A (19.31) and C (21.42). GC profiles in Fig. 2 show acceptable peak symmetry and except for ceralure C (small peak overlap at 21.57 min), isomers were baseline resolved. Percentages of the B₁, B₂, A and C isomers (based on total *trans* isomer content) for the ceralure standard were 27.10, 41.53, 12.44 and 18.92%, respectively and for the commercial sample were 26.83, 38.57, 16.39 and 18.21%, respectively. Interestingly, baseline separation of the four *trans* and four *cis* isomers of TML was also achieved on the SPB-608 column (isothermal conditions, 155°C); the order of elution for *trans* isomers was identical to that observed for ceralure.

GC–EI–MS data were obtained for the four *trans* isomers in the commercial sample. As expected, the B₁, B₂, A and C isomers gave nearly identical fragmentation patterns. Intensities of molecular ions (M⁺ 296) were extremely low making it difficult to identify these ions over background noise. Mass-to-charge ratios (*m/z*) and corresponding relative intensities of fragmentation ions for the B₁ isomer follow: 251 (5.5%), 169 (41.0%), 128 (5.5%), 123 (11.1%), 95 (100%), 81 (7.1%), 67 (9.5%), 55 (11.9%).

GC–MS spectra for minor components eluting at 19.97 and 21.57 min (Fig. 2) were nearly identical to those obtained for the *trans* isomers, suggesting that these compounds are *cis* isomers.

In summary, a capillary GC method has been developed to analyze the principal isomers of ceralure. The method is reproducible and requires less than 30 min for completion. Over 100 ceralure samples have been analyzed on the SPB-608 column with no apparent signs of column deterioration or performance problems. Research is in progress to fully define the elution characteristics of the four *cis* isomers of ceralure on this column.

Acknowledgements

We are deeply appreciative to Supelco for providing the specially prepared SPB-608 column used in this research. We especially thank Sterley B. Cole and David Martinec (Supelco) for technical guidance and for providing preliminary data on ceralure on the SPB-608 and other columns. We thank Victor Levi and Samuel Spencer for technical assistance and Frank Rankin (Dow Corning Ltd.) for helpful discussions. We also thank Robert Shackelford (Hewlett-Packard) for providing GC–MS spectra of ceralure.

Names of products in this paper are included for the benefit of the reader and do not imply endorsement or preferential treatment by the US Department of Agriculture.

References

- [1] T.P. McGovern and R.T. Cunningham, presented at the *National Conference of the Entomological Society of America, Boston, MA, Nov. 29–Dec. 3, 1987*, paper 1283.
- [2] T.P. McGovern and R.T. Cunningham, *US Pat.*, 4 764 366 (August 16, 1988).
- [3] A.B. DeMilo, R.T. Cunningham and T.P. McGovern, *J. Econ. Entomol.*, submitted for publication.
- [4] K.S. Hagen, W.W. Allen and R.L. Tassan, *Calif. Agr.*, 35 (1981) 5.
- [5] R.V. Dowell, *Hortscience*, 18 (1983) 39.
- [6] T.P. McGovern and M. Beroza, *J. Org. Chem.*, 31 (1966) 1472.
- [7] T.P. McGovern, R.T. Cunningham and B.A. Leonhardt, *J. Econ. Entomol.*, 79 (1986) 98.
- [8] M. Beroza and R. Sarmiento, *J. Assoc. Off. Agric. Chem.*, 47 (1964) 41.
- [9] T.P. McGovern, M. Beroza, K. Ohinata, D. Miyashita and L.F. Steiner, *J. Econ. Entomol.*, 59 (1966) 1450.
- [10] P.E. Sonnet, T.P. McGovern and R.T. Cunningham, *J. Org. Chem.*, 49 (1984) 4639.
- [11] R.E. Doolittle, R.T. Cunningham, T.P. McGovern and P.E. Sonnet, *J. Chem. Ecol.*, 17 (1991) 475.
- [12] J.D. Warthen, Jr., R.T. Cunningham, A.B. DeMilo and S. Spencer, *J. Chem. Ecol.*, 20 (1994) 569.
- [13] R.T. Cunningham, unpublished results.
- [14] J.D. Warthen, Jr. and T.P. McGovern, *Chromatographia*, 29 (1990) 135.
- [15] B.A. Leonhardt, T.P. McGovern and J.R. Plimmer, *J. High Resolut. Chromatogr. Chromatogr. Commun.*, 5 (1982) 430.



ELSEVIER

Journal of Chromatography A, 673 (1994) 299–302

JOURNAL OF
CHROMATOGRAPHY A

Short Communication

Capillary electrophoresis coupled on-line with flame photometric detection

C.E. Sanger-van de Griend^a, Ch.E. Kientz^{*a}, U.A.Th. Brinkman^b

^aTNO Prins Maurits Laboratory, P.O. Box 45, 2280 AA Rijswijk, Netherlands

^bDepartment of Analytical Chemistry, Free University, De Boelelaan 1083, 1081 HV Amsterdam, Netherlands

(First received February 14th, 1994; revised manuscript received April 14th, 1994)

Abstract

Preliminary work indicates that capillary electrophoresis can be coupled on-line with a gas chromatographic detector such as a flame photometric detector. A test mixture containing low-nanogram amounts of three organophosphorus compounds has successfully been analysed.

1. Introduction

In analytical chemistry, the determination of more polar, and also ionic non-volatile or high-molecular-mass compounds often is a serious problem. Recent developments in the field of analytical chemistry favour the use of liquid-based separation techniques such as liquid chromatography (LC) and capillary electrophoresis (CE). However, a serious drawback is the lack of detectors that can match the sensitivity and selectivity of gas chromatographic (GC) detectors such as, for example, thermionic (TID) (N, P-selective) and flame photometric (FPD) (S, P-selective) detection systems. When using conventional (non-selective) LC detectors, off-line or on-line sample clean-up and/or trace enrichment are generally necessary. Besides, the compounds of interest do not always possess suitable

chromophores or fluorophores; that is, detection will create manifest problems. Solving these problems by combining LC and CE with GC-type detectors is an interesting alternative.

In recent years, we have extensively studied the on-line coupling of micro-column liquid chromatography (μ LC) and flame-based GC detectors for the trace-level determination of non-volatile compounds such as substituted phosphoric and phosphonic acids [1–6]. As a sequel to this work, we have now attempted to use the same interface for the direct on-line coupling of CE and FPD. The present paper describes the first results of this work, with methylphosphonic acid (MPA), which is the final breakdown product of several highly toxic chemical warfare agents, and two related compounds as test solutes. MPA does not have a chromophoric group and can therefore not be determined by UV detection. The coupling of CE with FPD will make it possible to separate and selectively detect phosphorus-containing compounds such as MPA.

* Corresponding author.

2. Experimental

2.1. Materials

Analytical-grade hexane, ethanol, acetic acid, phosphoric acid (PA) and 25% ammonia solution were purchased from Merck (Darmstadt, Germany). Analytical-reagent grade ammonium acetate was obtained from Aldrich-Chemie (Steinheim, Germany). MPA and triethyl phosphate (TEP) were synthesized at the Prins Maurits Laboratory.

All solvents and solutions were filtered prior to use over 0.45- μm pore size filter disks from Millipore (Bedford, MA, USA).

2.2. Instrumentation

For the CE-FPD set-up, a Prince CE system (Lauerlabs, Emmen, Netherlands) and an FPD system Model 380 (Fisons, Milan, Italy) were used. A Valco valve from VICI (Schenkon, Switzerland) was used. Fused-silica capillaries of different diameters were obtained from Polymicro Technologies (Phoenix, AZ, USA). A Knurl-Lok III polyether ether ketone (PEEK) tee and PTFE tubing of different diameters were obtained from Alltech (Deerfield, IL, USA). The on-line coupling of the separation and detection parts of the system is discussed below.

3. Results and discussion

The main difference between μLC and CE when coupled with a GC-type detector is that the former is a pressure-driven system and the latter an electroosmotically driven one. With a CE system care must be taken to avoid pressure differences in the separation part of the set-up. Furthermore, the electric field should be decoupled after the electrophoresis capillary in such a way, that no gases formed due to electrochemical reactions will enter the separation and/or the detection system and disturb either the electrical field or the introduction of the liquid into the detector.

Considering the above, the experimental set-

ups of Fig. 1 were built. The CE system of Fig. 1A was grounded via a piece of 0.3 mm I.D. \times 1/16 in. O.D. (1 in. = 2.54 cm) PTFE tubing that had been treated under high pressure with hexane, which slowly penetrates the tubing wall, and washed with ethanol and water. Coupling of the make-up flow to the interface was made via a modified Valco injection valve. The make-up liquid was pure water.

The CE system of Fig. 1B was grounded via the make-up liquid, which was 1% acetic acid. Care was taken that the first contact of the make-up liquid with metal would be in the bulk

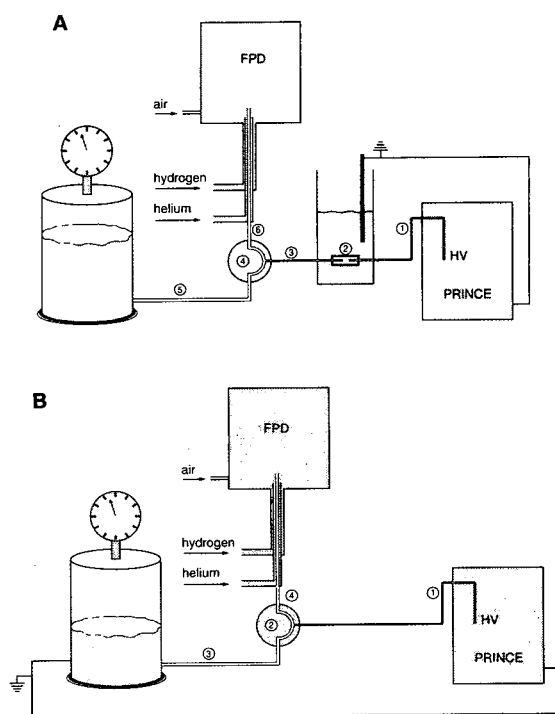


Fig. 1. Experimental CE-FPD set-ups. (A) 1 = Electrophoresis capillary, 75 cm \times 75 μm I.D. fused-silica capillary; 2 = modified PTFE tubing; 3 = coupling capillary, 5 cm \times 75 μm I.D. fused-silica capillary; 4 = modified Valco injection valve; 5 = hydrostatic make-up flow (pressure: 250 mbar); 6 = interface capillary, 35 cm \times 100 μm I.D. fused-silica capillary. (B) 1 = Electrophoresis capillary, 75 cm \times 75 μm I.D. fused-silica capillary; 2 = Knurl-Lok III PEEK tee; 3 = hydrostatic make-up flow, 0.8 mm I.D. PTFE tubing (pressure: 300 mbar); 4 = interface capillary, 40 cm \times 100 μm I.D. fused-silica capillary. Hydrogen flow-rate, 600 ml/min; air flow-rate, 300 ml/min; helium flow-rate, 40 ml/min. All capillary outlets in set-ups A and B were at the same height.

liquid, so that any gas bubbles formed would not enter the make-up tubing and disturb the electric field.

For both set-ups the make-up flow was induced by a hydrostatic pressure in order to have a constant, and relatively low, pressure rather than a constant flow at the end of the CE capillary. The pressure can then be counterbalanced at the inlet of the capillary. The required pressure was calculated from the length and diameter of the interface capillary by means of Poiseuille's law for laminar capillary flow, for a make-up flow-rate of *ca.* 10 $\mu\text{l}/\text{min}$. During injection, no make-up pressure was applied.

As regards the grounding via the modified PTFE tubing, its efficiency was tested by comparing the electric current through the electrophoresis capillary at the same electric field with and without the modified PTFE tubing inserted. This showed the tubing to be permeable for the electric current. When a solution of MPA was injected into the coupled CE-FPD system, the same peak height was registered as for an injection into the system without the modified PTFE tubing. In other words, no significant loss of analyte occurred due to sorption into and/or permeation through the modified tubing. We do realise that the performance of this grounding device has to be studied in more detail. However, for preliminary work where frequent modification of a system is required, it has the distinct advantage of being inexpensive and easy to exchange.

Both experimental set-ups could be used successfully. As an example, Fig. 2 shows the electropherogram of an on-line CE-FPD analysis performed using the set-up shown in Fig. 1B: a 15-nl injection was made of a mixture of 0.4 mg/ml TEP, 0.8 mg/ml MPA and 1.3 mg/ml PA in water, with 0.05 M ammonium acetate (adjusted to pH 9.3) as eluent. Obviously, the coupling is successful and a limit of detection of, *e.g.*, 1–2 ng MPA can be achieved. Actually, the experimental plate height of this test solute is $2 \cdot 10^4$ as against a theoretical plate height of $4 \cdot 10^5$ ($D = 1 \cdot 10^{-9} \text{ m}^2 \text{ s}^{-1}$). The rather large difference may well be due to the use of a liquid junction instead of a coaxial coupling of the CE

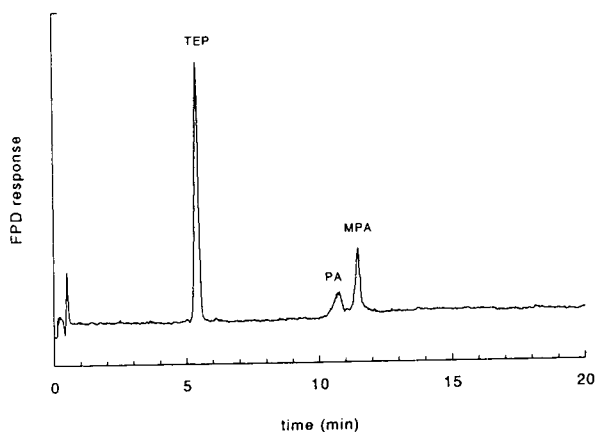


Fig. 2. CE-FPD analysis of a test mixture containing 0.8 mg/ml MPA, 0.4 mg/ml TEP and 1.3 mg/ml PA, injection 0.05 min at 50 mbar (15 nl); electrophoresis eluent: 0.05 M ammonium acetate adjusted to pH 9.3; 20 kV; 25°C; 300 mbar.

eluent with the make-up flow to the interface capillary [7]. Besides, a commercially available tee was used, which introduced a relatively large dead volume. Furthermore the electrophoretic conditions were not optimized for these compounds. It is to be expected therefore that the rather poor concentration sensitivity can be distinctly improved by optimizing these parameters and by minimizing band broadening due to dead volume. In addition, preconcentration techniques already developed for CE can be used (*e.g.* refs. 8 and 9). Further work will therefore be devoted to designing a coaxial coupling of the CE eluent and the make-up flow.

Finally, the liquid introduction into the detector is currently under investigation. By improving this introduction, *e.g.* by using electrospray introduction or inductive heating [10], the detector performance should be improved as a result of a reduction of the detector noise.

4. Conclusions

Our first attempts show that the on-line coupling of CE and FPD can be carried out using principles similar to those of μLC -FPD. This is a rather rewarding result because the use of CE

with its high separation efficiency in combination with the selective and sensitive detection provided by FPD is of distinct interest as an alternative method of analysis for polar and non-volatile phosphorus-containing ionic compounds that can not be determined by UV detection.

References

- [1] Ch.E. Kientz, A. Verweij, G.J. de Jong and U.A.Th. Brinkman, *J. Chromatogr.*, 626 (1992) 59.
- [2] Ch.E. Kientz, A. Verweij, G.J. de Jong and U.A.Th. Brinkman, *J. Chromatogr.*, 626 (1992) 70.
- [3] Ch.E. Kientz, J.P. Langenberg, G.J. de Jong and U.A.Th. Brinkman, *J. High Resolut. Chromatogr. Chromatogr. Commun.*, 7 (1991) 460.
- [4] Ch.E. Kientz, A. Verweij, G.J. de Jong and U.A.Th. Brinkman, *J. High Resolut. Chromatogr.*, 12 (1989) 793.
- [5] Ch.E. Kientz, A. Verweij, G.J. de Jong and U.A.Th. Brinkman, *J. Microcol. Sep.*, 4 (1992) 465.
- [6] Ch.E. Kientz, A. Verweij, G.J. de Jong and U.A.Th. Brinkman, *J. Microcol. Sep.*, 4 (1992) 476.
- [7] S. Pleasance, P. Thibault and J. Kelly, *J. Chromatogr.*, 591 (1992) 325.
- [8] R.-L. Chien and D.S. Burgi, *Anal. Chem.*, 64 (1992) 1046.
- [9] D.S. Stegehuis, H. Irth, U.R. Tjaden and J. van der Greef, *J. Chromatogr.*, 538 (1991) 393.
- [10] C.E. Sanger-van de Griend, Ch.E. Kientz and U.A.Th. Brinkman, presented at *EUROANALYSIS VIII, Edinburgh, September 5–11, 1993*, poster.



ELSEVIER

Journal of Chromatography A, 673 (1994) 303

JOURNAL OF
CHROMATOGRAPHY A

Erratum

corrected 3 Oct. 94/AP

Method to determine resveratrol and pterostilbene in grape berries and wines using high-performance liquid chromatography and highly sensitive fluorimetric detection [*Journal of Chromatography A*, 663 (1994) 191–197]

R. Pezet, V. Pont, P. Cuenat

Page 197, Table 1: mmol l⁻¹ should read μmol l⁻¹.

Author Index

- Baddoo, P.A., see Sen, N.P. 673(1994)77
- Baeyens, W., see Croubels, S. 673(1994)267
- Barceló, D., see Puig, D. 673(1994)55
- Blomberg, L.G., see Hägglund, I. 673(1994)93
- Bradshaw, J.S., see Yi, G. 673(1994)219
- Brinkman, U.A.Th., see Sängers-van de Griend, C.E. 673(1994)299
- Broto-Puig, F., see Codina, G. 673(1994)21
- Brown, R.J., see Konecny, P. 673(1994)45
- Buszewski, B., Jaroniec, M. and Gilpin, R.K.
Studies of physicochemical and chromatographic properties of mixed amino-alkylamide bonded phases 673(1994)11
- Campos, A., see Porcar, I. 673(1994)65
- Castro Romero, J.M., see González Rodríguez, V. 673(1994)291
- Claude, S.G., see Hägglund, I. 673(1994)93
- Cloux, R., see Reddy, K.S. 673(1994)181
- Codina, G., Vaquero, M.T., Comellas, L. and Broto-Puig, F.
Comparison of various extraction and clean-up methods for the determination of polycyclic aromatic hydrocarbons in sewage sludge-amended soils 673(1994)21
- Comellas, L., see Codina, G. 673(1994)21
- Croubels, S., Baeyens, W., Dewaele, C. and Van Peteghem, C.
Capillary electrophoresis of some tetracycline antibiotics 673(1994)267
- Davidson, G., see Kaplan, M. 673(1994)231
- DeMilo, A.B., Warthen, Jr., J.D. and Leonhardt, B.A.
Capillary gas chromatography method for the analysis of the *trans* isomers of ceralure, a medfly attractant 673(1994)295
- Dewaele, C., see Croubels, S. 673(1994)267
- Domb, A.J.
Quantitative analysis of mixtures of symmetric and mixed anhydrides 673(1994)31
- Dross, K., Sonntag, C. and Mannhold, R.
Determination of the hydrophobicity parameter R_{Mw} by reversed-phase thin-layer chromatography 673(1994)113
- Farooqui, A.A., Yang, H.-C. and Horrocks, L.A.
Purification of lipases, phospholipases and kinases by heparin-Sepharose chromatography (Review) 673(1994)149
- Fernández Solís, J.M., see González Rodríguez, V. 673(1994)291
- Fleet, G.H., see Zhao, J. 673(1994)167
- Foulkes, M., see Jones, P. 673(1994)173
- García, R., see Porcar, I. 673(1994)65
- Garrido, J.L. and Medina, I.
One-step conversion of fatty acids into their 2-alkenyl-4,4-dimethylloxazoline derivatives directly from total lipids 673(1994)101
- Gilpin, R.K., see Buszewski, B. 673(1994)11
- González Rodríguez, V., Castro Romero, J.M., Fernández Solís, J.M., Pérez Iglesias, J. and Seco Lago, H.M.
Simultaneous determination of cobalt and nickel by reversed-phase high-performance liquid chromatography with diethyldithiocarbamic acid 673(1994)291
- Grainger, J., see Liu, Z. 673(1994)125
- Hägglund, I., Blomberg, L.G., Janák, K., Claude, S.G. and Tabacchi, R.
Silicone gum of OV-225 type for open-tubular gas chromatography 673(1994)93
- Hamoir, T.P., see Yang, Q. 673(1994)275
- Hamoir, T. and Massart, D.L.
Retention prediction for β -adrenergic blocking drugs in normal-phase liquid chromatography 673(1994)1
- Hirota, T., Minato, K., Ishii, K., Nishimura, N. and Sato, T.
High-performance liquid chromatographic determination of the enantiomers of carnitine and acetylcarnitine on a chiral stationary phase 673(1994)37
- Horrocks, L.A., see Farooqui, A.A. 673(1994)149
- Ishii, K., see Hirota, T. 673(1994)37
- Ivanov, A.E. and Zubov, V.P.
Adsorption and separation of proteins on composite anion exchangers with poly(N-diethylamino-ethylacrylamide) bonded phases 673(1994)159
- Janák, K., see Hägglund, I. 673(1994)93
- Jaroniec, M., see Buszewski, B. 673(1994)11
- Jegorov, A., Triska, J. and Trnka, T.
1-Thio- β -D-galactose as a chiral derivatization agent for the resolution of D,L-amino acid enantiomers 673(1994)286
- Jimidar, M., see Yang, Q. 673(1994)275
- Jones, P., Foulkes, M. and Paull, B.
Determination of barium and strontium in calcium-containing matrices using high-performance chelation ion chromatography 673(1994)173
- Kapadia, G.J., Oguntimein, B. and Shukla, Y.N.
High-speed counter-current chromatographic separation of biflavonoids from *Garcinia kola* seeds 673(1994)142
- Kaplan, M., Davidson, G. and Poliakoff, M.
Capillary supercritical fluid chromatography-Fourier transform infrared spectroscopy study of triglycerides and the qualitative analysis of normal and "unsaturated" cheeses 673(1994)231
- Khalifaoui, B. and Newsham, D.M.T.
Determination of infinite dilution activity coefficients and second virial coefficients using gas-liquid chromatography. I. The dilute mixtures of water and unsaturated chlorinated hydrocarbons and of water and benzene 673(1994)85
- Kientz, Ch.E., see Sängers-van de Griend, C.E. 673(1994)299

- Konecny, P., Brown, R.J. and Scouten, W.H.
Chromatographic purification of immunoglobulin G from bovine milk whey 673(1994)45
- Kováts, E., see Reddy, K.S. 673(1994)181
- Lee, M.L., see Yi, G. 673(1994)219
- Leonhardt, B.A., see DeMilo, A.B. 673(1994)295
- Li, W., see Yi, G. 673(1994)219
- Liu, Z., Sam, P., Sirimanne, S.R., McClure, P.C., Grainger, J. and Patterson, Jr., D.G.
Field-amplified sample stacking in micellar electrokinetic chromatography for on-column sample concentration of neutral molecules 673(1994)125
- Malik, A., see Yi, G. 673(1994)219
- Mannhold, R., see Dross, K. 673(1994)113
- Massart, D.L., see Hamoir, T. 673(1994)1
- Massart, D.L., see Yang, Q. 673(1994)275
- McClure, P.C., see Liu, Z. 673(1994)125
- Medina, I., see Garrido, J.L. 673(1994)101
- Minato, K., see Hirota, T. 673(1994)37
- Newsham, D.M.T., see Khalfaoui, B. 673(1994)85
- Nishimura, N., see Hirota, T. 673(1994)37
- Oguntimein, B., see Kapadia, G.J. 673(1994)142
- Ou, Q., see Wan, H. 673(1994)107
- Patterson, Jr., D.G., see Liu, Z. 673(1994)125
- Paull, B., see Jones, P. 673(1994)173
- Pérez Iglesias, J., see González Rodríguez, V. 673(1994)291
- Poliakoff, M., see Kaplan, M. 673(1994)231
- Porcar, I., García, R., Campos, A. and Soria, V.
Size-exclusion chromatographic and viscometric study of polymer solutions containing nicotine or silicic acid 673(1994)65
- Puig, D. and Barceló, D.
Comparative study of various size-exclusion chromatographic columns for the clean-up of selected pesticides in soil samples 673(1994)55
- Reddy, K.S., Cloux, R. and Kováts, E.
Pair-wise interactions by gas chromatography. IV. Interaction free enthalpies of solutes with trifluoromethyl-substituted alkanes 673(1994)181
- Reinhold, N.J., Tjaden, U.R. and Van der Greef, J.
Automated on-capillary isotachophoretic reaction cell for fluorescence derivatization of small sample volumes at low concentrations followed by capillary zone electrophoresis 673(1994)255
- Reinhold, N.J., Tjaden, U.R. and van der Greef, J.
Correlation between zone velocity and current in automated single capillary isotachopheresis-zone electrophoresis 673(1994)239
- Rossiter, B.E., see Yi, G. 673(1994)219
- Roston, D.A., see Sun, J.J. 673(1994)211
- Sam, P., see Liu, Z. 673(1994)125
- Sänger-van de Griend, C.E., Kientz, Ch.E. and Brinkman, U.A.Th.
Capillary electrophoresis coupled on-line with flame photometric detection 673(1994)299
- Sato, T., see Hirota, T. 673(1994)37
- Scouten, W.H., see Konecny, P. 673(1994)45
- Seaman, S.W., see Sen, N.P. 673(1994)77
- Seco Lago, H.M., see González Rodríguez, V. 673(1994)291
- Sellergren, B.
Imprinted dispersion polymers: a new class of easily accessible affinity stationary phases 673(1994)133
- Sen, N.P., Baddoo, P.A. and Seaman, S.W.
Rapid and sensitive determination of nitrite in foods and biological materials by flow injection or high-performance liquid chromatography with chemiluminescence detection 673(1994)77
- Shukla, Y.N., see Kapadia, G.J. 673(1994)142
- Sirimanne, S.R., see Liu, Z. 673(1994)125
- Smeyers-Verbeke, J., see Yang, Q. 673(1994)275
- Sonntag, C., see Dross, K. 673(1994)113
- Soria, V., see Porcar, I. 673(1994)65
- Sun, J.J. and Roston, D.A.
Matrix effects during standard addition quantitation of a trace volatile impurity in a drug substance sample 673(1994)211
- Tabacchi, R., see Häggglund, I. 673(1994)93
- Tjaden, U.R., see Reinhold, N.J. 673(1994)239
- Tjaden, U.R., see Reinhold, N.J. 673(1994)255
- Todd, B., see Zhao, J. 673(1994)167
- Tríska, J., see Jegorov, A. 673(1994)286
- Trnka, T., see Jegorov, A. 673(1994)286
- Van Peteghem, C., see Croubels, S. 673(1994)267
- Van der Greef, J., see Reinhold, N.J. 673(1994)239
- Van der Greef, J., see Reinhold, N.J. 673(1994)255
- Vaquero, M.T., see Codina, G. 673(1994)21
- Wan, H., Zhou, X. and Ou, Q.
Gas chromatographic separation of amino acid enantiomers and their recognition mechanism on a 2,6-di-O-butyl-3-O-trifluoroacetylated- γ -cyclodextrin capillary column 673(1994)107
- Warthen, Jr., J.D., see DeMilo, A.B. 673(1994)295
- Yang, H.-C., see Farooqui, A.A. 673(1994)149
- Yang, Q., Jimidar, M., Hamoir, T.P., Smeyers-Verbeke, J. and Massart, D.L.
Determination of alkali and alkaline earth metals in real samples by capillary ion analysis 673(1994)275
- Yi, G., Bradshaw, J.S., Rossiter, B.E., Malik, A., Li, W., Yun, H. and Lee, M.L.
Large-rim-tethered permethyl-substituted β -cyclodextrin polysiloxanes for use as chiral stationary phases in open tubular column chromatography 673(1994)219
- Yun, H., see Yi, G. 673(1994)219
- Zhao, J., Todd, B. and Fleet, G.H.
Separation of ribonucleotides, ribonucleosides, deoxyribonucleotides, deoxyribonucleosides and bases by reversed-phase high-performance liquid chromatography 673(1994)167
- Zhou, X., see Wan, H. 673(1994)107
- Zubov, V.P., see Ivanov, A.E. 673(1994)159

PUBLICATION SCHEDULE FOR THE 1994 SUBSCRIPTION

Journal of Chromatography A and *Journal of Chromatography B: Biomedical Applications*

MONTH	1993	J	F	M	A	M	J	
Journal of Chromatography A	652-657	658/1 658/2 659/1 659/2	660/1 + 2 661/1 + 2 662/1 662/2	663/1 663/2 664/1	664/2 665/1 665/2 666/1 + 2 667/1 + 2	668/1 668/2 669/1 + 2	670/1 + 2 671/1 + 2 672/1	The publication schedule for further issues will be published later.
Bibliography Section				681/1			681/2	
Journal of Chromatography B: Biomedical Applications		652/1	652/2 653/1	653/2 654/1	654/2 655/1	655/2	656/1 656/2	

INFORMATION FOR AUTHORS

(Detailed *Instructions to Authors* were published in *J. Chromatogr. A*, Vol. 657, pp. 463-469. A free reprint can be obtained by application to the publisher, Elsevier Science B.V., P.O. Box 330, 1000 AH Amsterdam, Netherlands.)

Types of Contributions. The following types of papers are published: Regular research papers (full-length papers), Review articles, Short Communications and Discussions. Short Communications are usually descriptions of short investigations, or they can report minor technical improvements of previously published procedures; they reflect the same quality of research as full-length papers, but should preferably not exceed five printed pages. Discussions (one or two pages) should explain, amplify, correct or otherwise comment substantively upon an article recently published in the journal. For Review articles, see inside front cover under Submission of Papers.

Submission. Every paper must be accompanied by a letter from the senior author, stating that he/she is submitting the paper for publication in the *Journal of Chromatography A* or *B*.

Manuscripts. Manuscripts should be typed in **double spacing** on consecutively numbered pages of uniform size. The manuscript should be preceded by a sheet of manuscript paper carrying the title of the paper and the name and full postal address of the person to whom the proofs are to be sent. As a rule, papers should be divided into sections, headed by a caption (*e.g.*, Abstract, Introduction, Experimental, Results, Discussion, etc.) All illustrations, photographs, tables, etc., should be on separate sheets.

Abstract. All articles should have an abstract of 50-100 words which clearly and briefly indicates what is new, different and significant. No references should be given.

Introduction. Every paper must have a concise introduction mentioning what has been done before on the topic described, and stating clearly what is new in the paper now submitted.

Experimental conditions should preferably be given on a *separate* sheet, headed "Conditions". These conditions will, if appropriate, be printed in a block, directly following the heading "Experimental".

Illustrations. The figures should be submitted in a form suitable for reproduction, drawn in Indian ink on drawing or tracing paper. Each illustration should have a caption, all the *captions* being typed (with double spacing) together on a *separate sheet*. If structures are given in the text, the original drawings should be provided. Coloured illustrations are reproduced at the author's expense, the cost being determined by the number of pages and by the number of colours needed. The written permission of the author and publisher must be obtained for the use of any figure already published. Its source must be indicated in the legend.

References. References should be numbered in the order in which they are cited in the text, and listed in numerical sequence on a separate sheet at the end of the article. Please check a recent issue for the layout of the reference list. Abbreviations for the titles of journals should follow the system used by *Chemical Abstracts*. Articles not yet published should be given as "in press" (journal should be specified), "submitted for publication" (journal should be specified), "in preparation" or "personal communication".

Vols. 1-651 of the *Journal of Chromatography*; *Journal of Chromatography, Biomedical Applications* and *Journal of Chromatography, Symposium Volumes* should be cited as *J. Chromatogr.* From Vol. 652 on, *Journal of Chromatography A* (incl. Symposium Volumes) should be cited as *J. Chromatogr. A* and *Journal of Chromatography B: Biomedical Applications* as *J. Chromatogr. B*.

Dispatch. Before sending the manuscript to the Editor please check that the envelope contains four copies of the paper complete with references, captions and figures. One of the sets of figures must be the originals suitable for direct reproduction. Please also ensure that permission to publish has been obtained from your institute.

Proofs. One set of proofs will be sent to the author to be carefully checked for printer's errors. Corrections must be restricted to instances in which the proof is at variance with the manuscript.

Reprints. Fifty reprints will be supplied free of charge. Additional reprints can be ordered by the authors. An order form containing price quotations will be sent to the authors together with the proofs of their article.

Advertisements. The Editors of the journal accept no responsibility for the contents of the advertisements. Advertisement rates are available on request. Advertising orders and enquiries can be sent to the Advertising Manager, Elsevier Science B.V., Advertising Department, P.O. Box 211, 1000 AE Amsterdam, Netherlands; courier shipments to: Van de Sande Bakhuyzenstraat 4, 1061 AG Amsterdam, Netherlands; Tel. (+31-20) 515 3220/515 3222, Telefax (+31-20) 6833 041, Telex 16479 els vi nl. UK: T.G. Scott & Son Ltd., Tim Blake, Portland House, 21 Narborough Road, Cosby, Leics, LE9 5TA, UK; Tel. (+44-533) 753 333, Telefax (+44-533) 750 522. USA and Canada: Weston Media Associates, Daniel S. Lipner, P.O. Box 1110, Greens Farms, CT 06436-1110, USA; Tel. (+1-203) 261 2500, Telefax (+1-203) 261 0101.

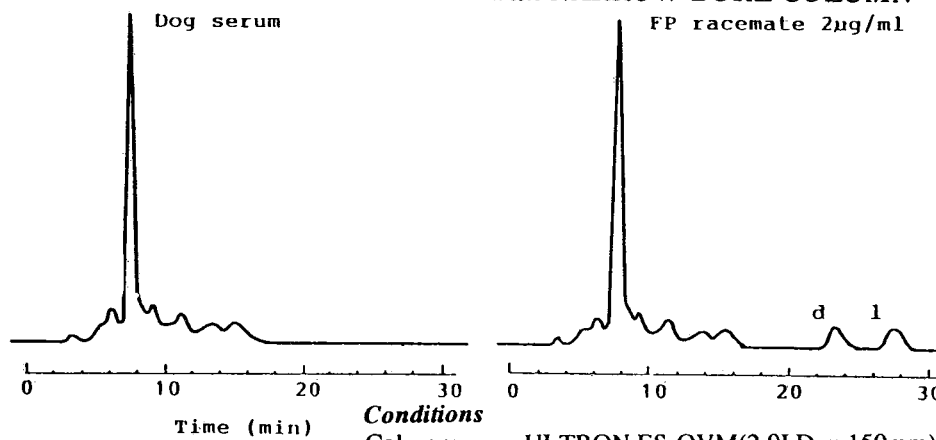
Ovomucoid Bonded Column for Direct Chiral Separation

ULTRON ES-OVM

Narrow-Bore Column (2.0 I.D. x 150 mm) for Trace Analyses
Analytical Column (4.6 I.D. , 6.0 I.D. x 150 mm) for Regular Analyses
Semi-Preparative Column (20.0 I.D. x 250 mm) for Preparative Separation

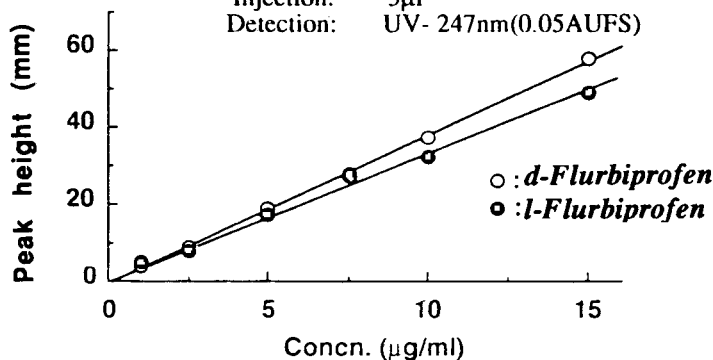
Analysis of Trace FLURBIPROFEN in Metabolite

with NARROW-BORE COLUMN



Conditions

Column: ULTRON ES-OVM(2.0I.D. x 150mm)
Mobile Phase: 20mMPhosphate Buffer(pH=3.0)/CH₃CN
=100/15
Flow Rate: 0.1ml/min
Temperature: 25°C
Injection: 5µl
Detection: UV- 247nm(0.05AUFS)



Calibration Curve for Each Enantiomer of Flurbiprofen

SHINWA CHEMICAL INDUSTRIES, LTD.

50 Kagekatsu-cho, Fushimi-ku, Kyoto 612, JAPAN
Phone:+81-75-621-2360 Fax:+81-75-602-2660

In the United States and Europe, please contact:

Rockland Technologies, Inc.

538 First State Boulevard, Newport, DE 19804, U.S.A.

Phone: 302-633-5880 Fax: 302-633-5893

This product is licenced by Eisai Co., Ltd.